

5-2008

High-solids saccharification and viscosity studies in a scraped surface bio-reactor.

Rajesh Kumar Dasari 1983-
University of Louisville

Follow this and additional works at: <http://ir.library.louisville.edu/etd>

Recommended Citation

Dasari, Rajesh Kumar 1983-, "High-solids saccharification and viscosity studies in a scraped surface bio-reactor." (2008). *Electronic Theses and Dissertations*. Paper 313.
<https://doi.org/10.18297/etd/313>

This Master's Thesis is brought to you for free and open access by ThinkIR: The University of Louisville's Institutional Repository. It has been accepted for inclusion in Electronic Theses and Dissertations by an authorized administrator of ThinkIR: The University of Louisville's Institutional Repository. This title appears here courtesy of the author, who has retained all other copyrights. For more information, please contact thinkir@louisville.edu.

**HIGH-SOLIDS SACCHARIFICATION AND VISCOSITY STUDIES IN A
SCRAPED SURFACE BIO-REACTOR**

By

Rajesh Kumar Dasari

B.Tech., Osmania University, India, 2004

A Dissertation Submitted to the Faculty of the Graduate School of the University of
Louisville in Partial Fulfillment of the Requirements for the Degree of

Doctor of Philosophy

Department of Chemical Engineering

University of Louisville

Louisville, KY

May 2008

Copyright 2008 by Rajesh Kumar Dasari

All rights reserved

HIGH-SOLIDS SACCHARIFICATION AND VISCOSITY STUDIES IN A
SCRAPES SURFACE BIO-REACTOR

By

Rajesh Kumar Dasari
B.Tech., Osmania University, India, 2004

A Dissertation Approved on

3/27/2008

By the following Dissertation Committee:

Dissertation Director

DEDICATION

This dissertation is dedicated to my beloved wife

Mrs. Saritha Dasari

and my respected parents

Mr. & Mrs. Nandagopal Dasari

who have given me an invaluable support, priceless suggestions and an unexhausted helping hand.

ACKNOWLEDGEMENTS

I would like to thank my major professor, Dr. R. Eric Berson, for his guidance and patience. I would also like to thank the other committee members, Dr. Gerold A. Willing, Dr. Ellen G. Brehob, Dr. James C. Watters and Dr. David J. Schultz for their comments and assistance over the past three years. I also take this opportunity to thank my best friend Surendar Reddy Venna for his valuable support and help during the final stages of my dissertation.

ABSTRACT

HIGH-SOLIDS SACCHARIFICATION AND VISCOSITY STUDIES IN A SCRAPED SURFACE BIO-REACTOR

Rajesh Kumar Dasari

May 10, 2008

High solids processing of biomass slurries provides the following benefits: maximized product concentration in the fermentable sugar stream, reduced water usage, and reduced reactor size. However, high solids processing poses mixing and heat transfer problems above about 15% for pretreated corn stover solids due to their high viscosities. Also, highly viscous slurries require high power consumption in conventional stirred tanks since they must be run at high rotational speeds to maintain proper mixing. An 8 liter scraped surface bio-reactor (SSBR) is employed here that is designed to efficiently handle high solids loadings for enzymatic saccharification of pretreated corn stover (PCS) while maintaining power requirements on the order of low viscous liquids in conventional stirred tanks.

The determination of the rheological behavior of biomass slurries is vital for process design at industrial scale. The viscosities of biomass slurries are seen here to be a function of initial solids concentration and initial biomass particle size. An extensive study has been conducted to investigate the effect of solids loading and viscosity on the rates and extent of enzymatic hydrolysis reactions. For batch testing with 25% (highest

loading studied) initial PCS solids concentration, about 10% more glucose is released in the SSBR than in the shake flask after 168 hours of the saccharification reaction. The role of the viscosity of biomass slurries in power consumption of the reactor is presented. A semi-batch approach is employed to maintain lower slurry viscosity and, therefore, improved glucose release rates and reduced power consumption when operating with higher solids content. A processing efficiency is defined as sugar released per unit energy input. The 20% semi-batch saccharification test efficiency is about 27% higher than the 20% batch saccharification test efficiency.

The settling of biomass particles presents a serious problem for measuring the viscosity of the slurries. Maintaining homogeneity by uniformly suspending all the particles is necessary for accurate viscosity measurements. Therefore, a new viscosity measuring technique has been developed here that incorporates the uniform suspension speed (USS) for particles in the viscometer cup that can be applied to any type of particulate suspension. The USS has been determined experimentally and computationally by a Computational Fluid Dynamics (CFD) model developed here that is well validated by experimental results. The wet density of PCS solids, which is not reported in the literature, is determined from the CFD model to be $1100 \pm 50 \text{ kg/m}^3$ based on the volume fraction distribution of solids at 305 rpm, the USS of a 5% solids slurry.

TABLE OF CONTENTS

	PAGE
ACKNOWLEDGEMENTS.....	IV
ABSTRACT.....	V
CHAPTER I.....	1
INTRODUCTION.....	1
Background.....	1
Current problem.....	3
Objectives.....	4
CHAPTER II.....	6
LITERATURE REVIEW.....	6
Ethanol Properties.....	7
Biomass Sources.....	8
Ethanol Impact on Environment.....	11
Energy Content of Ethanol.....	12
Physical Constituents of Biomass.....	13
Biomass Conversion Process.....	14
Pretreatment of Biomass	17
Enzymatic Hydrolysis (Saccharification)	19
Cellulase Synergism.....	21
Product Inhibition.....	22

Enzyme Deactivation.....	23
Fermentation.....	23
High Solid Processing	25
Viscosity & Power Correlation.....	26
Rheology of Biomass Slurries.....	29
Viscosity Measuring Techniques.....	31
Just Suspended Speed (JSS) & Uniform Suspension Speed (USS)	32
CUTTING EDGE TECHNOLOGIES.....	34
COMPUTATIONAL FLUID DYNAMICS (CFD)	36
FLUENT.....	38
Multiphase Model.....	40
Eulerian Model.....	41
Volume Fractions.....	43
Post Processing.....	44
CFD Modeling of Solid Suspension in a Mixing Tank.....	44
CHAPTER III.....	46
EXPERIMENTAL PLAN.....	46
Effect of Initial Particle Size on Saccharification Rates and Rheology of Sawdust Slurries.....	46
Effect of Solids Loading on Saccharification Rate and Power Consumption in a Bench-Scale.....	47
Technique to Measure Viscosity of Solid Suspensions.....	50
CFD Simulations of Flow in the Viscometer Cup.....	52

CHAPTER IV.....	53
EFFECT OF SUBSTRATE PARTICLE SIZE ON SACCHARIFICATION RATES AND RHEOLOGY OF SAWDUST SLURRIES.....	53
MATERIALS AND METHODS.....	53
Cellulose Substrate and Enzyme	53
Saccharification Procedure.....	54
Sampling and Sugar Measurement.....	54
Calculation of Glucose yield.....	55
Viscosity Measurements.....	56
RESULTS & DISCUSSION.....	58
The Effect of Substrate Particle Size on Saccharification Rate.....	59
Initial Viscosity Measurements Prior to Reaction.....	63
Discrete Viscosity Measurements During the Saccharification Reaction.....	70
Continuous Viscosity Measurements During the Saccharification Reaction.....	72
CHAPTER V.....	77
SACCHARIFICATION USING THE SCRAPED SURFACE BIO-REACTOR.....	77
MATERIALS AND METHODS.....	77
Cellulose Substrate and Enzyme.....	77
Saccharification Procedure.....	78
Sampling and Sugar Measurement.....	78
Viscosity Measurements.....	79
Reactor and Torque Sensor Assembly.....	81
RESULTS AND DISCUSSION.....	84

Saccharification of PCS Slurries in the SSBR.....	84
Effect of Initial Solids Loading on Enzymatic Saccharification.....	85
Saccharification with Batch Loading.....	85
Rheology of PCS Slurries.....	91
Rheology of PCS Slurries During Batch Saccharification.....	93
Power Consumption in the SSBR.....	103
Power Consumption in the SSBR during Batch Saccharification.....	107
Efficiency of the SSBR During Batch Saccharification.....	109
Saccharification in Semi-Batch Model.....	112
Rheology of PCS Slurries and Power Consumption in the SSBR during Semi-Batch Saccharification.....	114
Efficiency of the SSBR During Semi-Batch Saccharification.....	127
Other Semi-Batch Saccharification Tests.....	128
CHAPTER VI.....	137
TECHNIQUE TO MEASURE VISCOSITY OF SOLID SUSPENSIONS.....	137
MATERIALS AND METHODS.....	137
Determination of Just Suspended Speed and Uniform Suspension Speed.....	137
RESULTS & DISCUSSION.....	139
Determination of JSS and USS for PCS Slurries.....	139
Effect of Premixing on Viscosity Measurements.....	141
Determination of Time to Reach Steady State Viscosity for PCS Slurries.....	142
Viscosity Measurements for PCS Slurries with Premixing at Various Shear Rates...	147
CHAPTER VII.....	152

CFD SIMULATIONS OF SOLIDS SUSPENSIONS IN A VISCOMETER CUP..	152
CFD Simulation Problem Set-Up.....	152
Eulerian Multiphase Model.....	157
RESULTS AND DISCUSSION.....	168
Determination of Wet Density of PCS Solids.....	168
CHAPTER VIII.....	181
Conclusions and Recommendations.....	181
REFERENCES.....	186
APPENDIX – A.....	206
APPENDIX – B.....	218
APPENDIX – C.....	237
APPENDIX – D.....	239
CURRICULUM VITAE.....	242

LIST OF TABLES

TABLE	PAGE
1. World Primary Energy Consumption (Quadrillion Btu).....	6
2. Renewable Energy Targets in the World.....	7
3. Important Physical Properties of Ethanol.....	8
4. Composition of Various Lignocellulosic Raw Materials.....	9
5. Effect of Various Pretreatment Methods on the Chemical Composition and Chemical/Physical Structure of Lignocellulosic Biomass.....	20
6. Saccharification Experiments for Tests with Sawdust as Substrate.....	49
7. Experiments for Viscosity Measurements During Saccharification Tests With Sawdust as Substrate.....	49
8. Design of Experiments for Batch Tests with Corn Stover as Substrate.....	50
9. Design of Experiments for Semi-batch Tests with Corn Stover as Substrate.....	50
10. Various PCS Solids Concentrations and Shear Rates of the Premixing Tests.....	51
11. The effect of initial particle size on glucose production with 10 % initial solids concentration.....	61

12. Power Law Model Parameters for Sawdust Slurries With 13% Initial Solids at ‘0’ Hour for Various Particle Size Ranges.....	65
13. Power Law Model Parameters for Sawdust Slurries With 10% Initial Solids at ‘0’ Hour for Various Particle Size Ranges.....	65
14. Power Law Model Parameters for Sawdust Slurries With 13% Initial Solids ($33 \mu\text{m} < x \leq 75 \mu\text{m}$) Concentration at Various Times of Enzymatic Saccharification.....	73
15. Glucose release during the First 8 Hours of Saccharification as a Percentage of the Actual Amount That is Released in 72 Hours.....	88
16. Power Law Parameters for Viscosity Data of PCS Slurries with Various Initial Solids Concentrations at ‘0’ Hour.....	92
17. Power Law Parameters for Viscosity Data During Enzymatic Saccharification of 10% PCS Solids in the SSBR.....	96
18. Power Law Parameters for Viscosity Data During Enzymatic Saccharification of 10% PCS Solids in the Shake Flask.....	96
19a. Power Law Parameters for Viscosity Data During Enzymatic Saccharification of 25% PCS Solids in the SSBR.....	98
19b. Power Law Parameters for Viscosity Data During Enzymatic Saccharification of 25% PCS Solids In the Shake Flask.....	100
20a. Power Law Parameters for Viscosity Data During Semi-Batch Saccharification of 20% Equivalent PCS Solids in the SSBR.....	120
20b. Power Law Parameters for Viscosity Data During Semi-Batch Enzymatic Saccharification of 20% Equivalent PCS Solids in the Shake Flask.....	120

21. Glucose Release in Semi-Batch Saccharification after 8 Hours of Final Feeding As Percentage of the Maximum Achievable Glucose in 168 Hours.....	123
22. Efficiency of Saccharification Tests with Various Concentrations of PCS Solids in the SSBR.....	135
23. Efficiency of Saccharification Tests with Various Concentrations of PCS Solids in the SSBR.....	140
24. Time to Reach Steady State Viscosity for PCS Slurries with Various Solids Concentrations at Various Premixing Shear Rates.....	146
A1. Power Law Model Parameters for Sawdust Slurries with 13% Initial Solids ($75 \mu\text{m} < x \leq 104 \mu\text{m}$) Concentration at Various Times of Enzymatic Saccharification.....	214
A2. Power Law Model Parameters for Sawdust Slurries with 13% Initial Solids ($104 \mu\text{m} < x \leq 150 \mu\text{m}$) Concentration at Various Times of Enzymatic Saccharification.....	214
A3. Power Law Model Parameters for Sawdust Slurries with 13% Initial Solids ($150 \mu\text{m} < x \leq 180 \mu\text{m}$) Concentration at Various Times of Enzymatic Saccharification.....	215
A4. Power Law Model Parameters for Sawdust Slurries with 10% Initial Solids ($33 \mu\text{m} < x \leq 75 \mu\text{m}$) Concentration at Various Times of Enzymatic Saccharification.....	215
A5. Power Law Model Parameters for Sawdust Slurries with 10% Initial Solids ($75 \mu\text{m} < x \leq 104 \mu\text{m}$) Concentration at Various Times of Enzymatic Saccharification.....	216
A6. Power Law Model Parameters for Sawdust Slurries with 10% Initial Solids ($104 \mu\text{m} < x \leq 150 \mu\text{m}$) Concentration at Various Times of Enzymatic Saccharification.....	216
A7. Power Law Model Parameters for Sawdust Slurries with 10% Initial Solids ($150 \mu\text{m} < x \leq 180 \mu\text{m}$) Concentration at Various Times of Enzymatic Saccharification.....	217

A8. Power Law Model Parameters for Sawdust Slurries with Various Initial Solids Concentrations at Time '0' Hour for the Particle Size Range $33 \mu\text{m} < x \leq 75 \mu\text{m}$	217
B1. Power Law Parameters for Viscosity Data During Batch Enzymatic Saccharification of 15% Initial PCS Solids in the SSBR.....	222
B2. Power Law Parameters for Viscosity Data During Batch Enzymatic Saccharification of 15% Initial PCS Solids in the Shake Flask.....	223
B3. Power Law Parameters for Viscosity Data During Batch Enzymatic Saccharification of 20% Initial PCS Solids in the SSBR.....	224
B4. Power Law Parameters for Viscosity Data During Batch Enzymatic Saccharification of 20% Initial PCS Solids in the Shake Flask.....	226
B5. Power Law Parameters for Viscosity Data During Semi-Batch Enzymatic Saccharification of 25% Equivalent Final PCS Solids in the Shake Flask.....	229
B6. Power Law Parameters for Viscosity Data During Semi-Batch Enzymatic Saccharification of 25% Equivalent Final PCS Solids in the SSBR.....	229
B7. Power Law Parameters for Viscosity Data During Semi-Batch Enzymatic Saccharification of 30% Equivalent Final PCS Solids in the Shake Flask.....	232
B8. Power Law Parameters for Viscosity Data During Semi-Batch Enzymatic Saccharification of 30% Equivalent Final PCS Solids in the SSBR.....	232
B9. Power Law Parameters for Viscosity Data During Semi-Batch Enzymatic Saccharification of 25% Equivalent Final PCS Solids in the Shake Flask with Hand-Mixing.....	233

B10. Power Law Parameters for Viscosity Data During Semi-Batch Enzymatic Saccharification of 30% Equivalent Final PCS Solids in the Shake Flask with 2 nd Type Feeding.....	235
B11. Power Law Parameters for Viscosity Data During Semi-Batch Enzymatic Saccharification of 30% Equivalent Final PCS Solids in the SSBR with 2 nd Type Feeding.....	235

LIST OF FIGURES

FIGURE	PAGE
1. Biomass From Left to Right: Corn Stover, Wood Chips, Bagasse, Switchgrass, and Hybrid poplar. (Photos from the National Renewable Energy Laboratory website).....	3
2. Estimated corn stover availability and ethanol production potential as a function of the stover fraction that can be sustainably collected.....	11
3. Linear chains of glucose linked in a crystalline structure to form cellulose.....	14
4. Linear chains of glucose linked in an amorphous structure to form starch.....	15
5. Overall conversion process of biomass to ethanol.....	16
6. The result of biomass pretreatment. The hemicellulose, lignin, and cellulose are separated, making the cellulose fibers more accessible for attack by Enzymes.....	18
7. Rheological behavior of various types of fluids.....	29
8. Schematic of the algorithm for problem solving in CFD.....	38
9. Algorithm of a GAMBIT process.....	40
10. Anton Parr Modular Compact Rheometer.....	57
11. The effect of initial particle size on glucose production with 10 % initial solids concentration.....	60
12. The effect of initial particle size on glucose production with 13 % initial solids concentration.....	61

13. Viscosity vs. shear rate (t = 0 hr, 13% initial solids concentration) and the power law fit.....	66
14. SEM images of sawdust particles. (a) $33\ \mu\text{m} < x \leq 75\ \mu\text{m}$, 3500x magnification. (b) $590\ \mu\text{m} < x \leq 850\ \mu\text{m}$, 35x magnification.....	67
15. Viscosity vs. shear rate for various initial solids concentrations (time = 0 hr, size range = $33\ \mu\text{m} < x \leq 75\ \mu\text{m}$).....	69
16. Viscosity vs. shear rate at different times during enzymatic saccharification (Size range: $33\ \mu\text{m} < x \leq 75\ \mu\text{m}$, 13% initial solids concentration).....	71
17. Continuous viscosity vs. time measurement (13% initial solids concentration, $150\ \mu\text{m} < x \leq 180\ \mu\text{m}$, $10\ \text{s}^{-1}$).....	74
18. Continuous viscosity vs. time measurement (10% initial solids concentration, $33\ \mu\text{m} < x \leq 75\ \mu\text{m}$, $10\ \text{s}^{-1}$).....	75
19. SEM images (1000x magnification) of sawdust particles with the size range $150\ \mu\text{m} < x \leq 180\ \mu\text{m}$ (a) '0' hour (b) '8' hour.....	76
20. Premixing test for 5% and 10% PCS slurries at $160\ \text{s}^{-1}$	80
21. Premixing test for 15, 20 & 25% PCS slurries at $160\ \text{s}^{-1}$	81
22. Scraped Surface Bio-Reactor.....	82
23. Reactor and torque assembly inside the insulation box.....	83
24a. Glucose release during batch enzymatic saccharification in the SSBR with various initial PCS solids concentrations.....	87
24b. Comparison of percent glucose release between the SSBR and the shake flask during enzymatic saccharification with 25% initial PCS solids concentrations.....	88

25. Viscosity vs. shear rate for PCS slurries with various initial solids concentrations at ‘0’ hour.....	92
26. Viscosity changes throughout the saccharification reaction in the SSBR for 10% initial PCS solids concentration.....	94
27. Viscosity changes throughout the saccharification reaction in the shake flask for 10% initial PCS solids concentration.....	95
28. Consistency index throughout the saccharification reaction for 10% initial PCS solids concentration in the SSBR and the shake flask.....	97
29a. Viscosity changes throughout the saccharification reaction in the SSBR for 25% initial PCS solids concentration.....	98
29b. Viscosity changes throughout the saccharification reaction in the shake flask for 25% initial PCS solids concentration.....	99
30. Consistency index vs. reaction time for 25% initial PCS solids concentration for the SSBR and the shake flask.....	100
31. Comparison of power consumption for mixing PCS slurries with various initial solids concentrations in the SSBR at various speeds at ‘0’ hour time of saccharification.....	103
32. Comparison of power consumption for mixing PCS slurries with various initial solids concentrations in the SSBR at various speeds at ‘0’ hour time of saccharification.....	105
33. Specific power consumption in the SSBR during batch enzymatic saccharification of PCS slurries with various initial solids concentrations.....	108
34. Comparison of efficiency for saccharification of PCS slurries with various initial solids concentrations throughout the first 72 hours.....	111

35. Comparison of percent glucose release in the SSBR at 2 rpm between batch and semi-batch enzymatic saccharification with 20% equivalent PCS solids concentration.....	113
36. Comparison of power consumption in the SSBR at 2 rpm between batch and semi-batch operation during enzymatic saccharification with 20% equivalent PCS solids concentration.....	115
37. ‘K’ values in the SSBR at 2 rpm during batch and semi-batch enzymatic saccharification with 20% equivalent PCS solids concentration.....	116
38. Comparison of percent glucose release in the SSBR and the shake flask at 2 rpm during semi-batch enzymatic saccharification with 20% equivalent PCS solids concentration.....	117
39a. Viscosity changes during semi-batch enzymatic saccharification in the SSBR for 20% equivalent PCS solids concentration.....	118
39b. Viscosity changes during semi-batch enzymatic saccharification in the shake flask for 20% equivalent PCS solids concentration.....	119
40. Comparison of percent glucose release between the SSBR and the shake flask during semi-batch saccharification with 25% and 30% final equivalent PCS solids concentrations.....	121
41a. ‘K’ values during semi-batch saccharification in the SSBR and the shake flask with 25% final equivalent PCS solids concentrations.....	124
41b. ‘K’ values during semi-batch saccharification in the SSBR and the shake flask with 30% final equivalent PCS solids concentrations.....	125
42. Specific power consumption during saccharification for 25% and 30% semi-batch and 25% batch tests with PCS solids.....	126

43. Efficiencies during semi-batch saccharification in the SSBR with 20, 25 and 30% equivalent PCS solids concentrations.....	127
44. Comparison of percent glucose release in the shake flask between semi-batch saccharification tests (with and without hand-mixing) with 25% final equivalent PCS solids concentrations.....	129
45. Comparison of percent glucose release between semi-batch saccharification tests with 30% final equivalent PCS solids concentrations for two types of feeding policies.....	131
46. Comparison of changes in ‘K’ values during the semi-batch saccharification with 30% PCS equivalent solids with the second type of feeding policy.....	132
47. Comparison of specific power consumption between the first and second type of feeding during semi-batch saccharification with 30% equivalent solids.....	133
48. Comparison of efficiency during saccharification in the SSBR between the first and second type of feedings with 30% equivalent PCS solids concentrations.....	134
49. Experimental set up for experimental determination of JSS and USS.....	138
50. Premixing test with a 5% PCS slurry.....	143
51. Premixing test with a 7.5% PCS slurry.....	144
52. Premixing test with a 10% PCS slurry.....	145
53. Premixing test with a 15% PCS slurry.	145
54. Premixing test with a 20% PCS slurry.	146
55. Viscosity data for a 5% PCS solids slurry with premixing at various shear rate.....	148
56. Viscosity of a 7.5% PCS solids slurry with premixing at various shear rates.....	149
57. Viscosity of a 10% PCS solids slurry with premixing at various shear rates.....	150
58. Viscosity of a 15% PCS solids slurry with premixing at various shear rates.....	151

59. Viscosity of a 20% PCS solids slurry with premixing at various shear rates.....	151
60a. GAMBIT drawing of the MCR cup and vane impeller (View 1).....	153
60b. GAMBIT drawing of the MCR cup and vane impeller (View 2).....	154
61. Quad:Pave face meshing scheme-example mesh (Fluent Inc., 2006).....	155
62. Sample T-Grid meshing scheme (Fluent Inc., 2006).....	155
63. Meshed geometry of a pie shaped wedge of the viscometer cup and vane impeller.	156
64. Read → Case panel.....	157
65. Grid → Check panel.....	158
66. Display → Views panel.....	158
67. Solver panel.....	159
68. Multiphase model panel.....	159
69. Viscous model panel.....	160
70. Operating conditions panel.....	160
71. Materials panel.....	161
72. Phases panel.....	162
73. Boundary Conditions panel.....	163
74. Solution Controls panel.....	164
75. Residuals panel.....	164
76. Surface Monitors panel.....	165
77. Solution Initialization panel.....	165
78. Patch-Volume Fraction panel.....	166
79. Iteration panel.....	167
80. Write → Case & Data panel.....	167

81. Contours of volume fraction of PCS solids in the slurry at various horizontal cross-sections of the viscometer cup at 305 rpm with 1100 kg/m ³ density.....	170
82. Contours of volume fraction of PCS solids in the slurry along the vertical axis of the viscometer cup at 305 rpm with 1100 kg/m ³ density.....	170
83. Contours of volume fraction of PCS solids in the slurry at various horizontal cross-sections of the viscometer cup at 305 rpm with 1200 kg/m ³ density.....	171
84. Contours of volume fraction of PCS solids in slurry along the vertical axis of the viscometer cup at 305 rpm with 1200 kg/m ³ density.	172
85. Contours of volume fraction of PCS solids in slurry at various horizontal cross-sections of the viscometer cup at 305 rpm with 1300 kg/m ³ density.	172
86. Contours of volume fractions of PCS solids in slurry along the vertical axis of the viscometer cup at 305 rpm with 1300 kg/m ³ density.	173
87. Contours of volume fraction of PCS solids in slurry at various horizontal cross-sections of the viscometer cup at 305 rpm with 1400 kg/m ³ density.	173
88. Contours of volume fraction of PCS solids in slurry along the vertical axis of the viscometer cup at 305 rpm with 1400 kg/m ³ density.	174
89. Contours of volume fraction of PCS solids in the slurry at various horizontal cross-sections of the viscometer cup at 230 rpm.	175.
90. Contours of volume fraction of PCS solids in the slurry along the vertical axis of the viscometer cup at 230 rpm.	175
91. Contours of volume fraction of the PCS solids in slurry at various horizontal cross-sections of the viscometer cup at 270 rpm.	176

92. Contours of volume fraction of PCS solids in the slurry along the vertical axis of the viscometer cup at 270 rpm.....	177
93. Contours of volume fraction of PCS solids in the slurry along the vertical axis of the viscometer cup at 340 rpm.....	178
94. Contours of volume fraction of PCS solids in the slurry along the vertical height of the viscometer cup at 400 rpm.....	179
95. Contours of volume fraction of PCS solids in the slurry along the vertical of the viscometer cup at 450 rpm.....	179
96. Contours of volume fraction of PCS solids in the slurry along the vertical axis of the viscometer cup at 600 rpm.....	180
A1. Viscosity vs. shear rate during enzymatic saccharification (Size range: $75 \mu\text{m} < x \leq 104 \mu\text{m}$, 13% initial solids concentration).....	206
A2. Viscosity vs. shear rate at different times during enzymatic saccharification (Size range: $104 \mu\text{m} < x \leq 150 \mu\text{m}$, 13% initial solids concentration).....	207
A3. Viscosity vs. shear rate at different times during enzymatic saccharification (Size range: $150 \mu\text{m} < x \leq 180 \mu\text{m}$, 13% initial solids concentration).....	208
A4. Viscosity vs. shear rate at different times during enzymatic saccharification (Size range: $33 \mu\text{m} < x \leq 75 \mu\text{m}$, 10% initial solids concentration).....	209
A5. Viscosity vs. shear rate at different times during enzymatic saccharification (Size range: $75 \mu\text{m} < x \leq 104 \mu\text{m}$, 10% initial solids concentration).....	210
A6. Viscosity vs. shear rate at different times during enzymatic saccharification (Size range: $104 \mu\text{m} < x \leq 150 \mu\text{m}$, 10% initial solids concentration).....	211

A7. Viscosity vs. shear rate at different times during enzymatic saccharification (Size range: $150 \mu\text{m} < x \leq 180 \mu\text{m}$, 10% initial solids concentration).....	212
A8. Viscosity vs. shear rate ($t = 0$ hr, 10% initial solids concentration).....	213
B1. Glucose release during batch enzymatic saccharification in the shake flask with various initial PCS solids concentrations.....	218
B2. Comparison of glucose yields between the SSBR and the shake flask during batch enzymatic saccharification with 10% initial PCS solids concentrations.....	219
B3. Comparison of glucose yields between the SSBR and the shake flask during batch enzymatic saccharification with 15% initial PCS solids concentrations.....	220
B4. Comparison of glucose yields between SSBR and shake flask during batch enzymatic saccharification with 20% initial PCS solids concentrations.....	221
B5. Viscosity changes during batch enzymatic saccharification in the SSBR for 15% initial PCS solids concentration.....	222
B6. Viscosity changes during batch enzymatic saccharification in the shake flask for 15% initial PCS solids concentration.....	223
B7. Viscosity changes during batch enzymatic saccharification in the SSBR for 20% initial PCS solids concentration.....	224
B8. Viscosity changes during batch enzymatic saccharification in the shake flask for 20% initial PCS solids concentration.....	225
B9. Viscosity changes during semi-batch enzymatic saccharification in the shake flask for 25% final equivalent PCS solids concentration.....	227
B10. Viscosity changes during semi-batch enzymatic saccharification in the SSBR for 25% final equivalent PCS solids concentration.....	228

B11. Viscosity changes during semi-batch enzymatic saccharification in the shake flask for 30% final equivalent PCS solids concentration.....	230
B12. Viscosity changes during semi-batch enzymatic saccharification in the SSBR for 30% final equivalent PCS solids concentration.....	231
B13. Viscosity changes during semi-batch enzymatic saccharification of 25% equivalent final PCS solids in the shake flask with hand-mixing.....	233
B14. Viscosity changes during semi-batch enzymatic saccharification of 30% equivalent final PCS solids in the shake flask with the 2 nd type of feeding.....	234
B15. Viscosity changes during semi-batch enzymatic saccharification of 30% equivalent final PCS solids in the SSBR with the 2 nd type of feeding.....	236

CHAPTER I

INTRODUCTION

Background:

In the present global situation, the desire and necessity for alternative transportation fuels continues to grow at a rapid pace due to the rapid consumption and depletion of fossil fuel reserves. In addition to reducing foreign oil dependency, bio-fuels from renewable resources offer many benefits including sustainability, reduction of greenhouse gas emissions, regional development of social structure and agriculture, and security of supply (Reijnders, 2006).

The search for the replacement of fossil fuels has been going on over the past few decades. It is estimated that the supply of fossil fuels will be extremely limited 40-50 years from now (Duncan and Youngquist, 1999; Youngquist and Duncan, 2003; Pimentel and others, 2004a). Although there are many other resources available as an alternate, such as wind energy, solar energy, hydrogen etc., biomass is a leading choice right now since the ethanol that is derived from it integrates well with existing infrastructure, such as gas pumps and automobile engines. Ethanol is produced from biomass by a fermentation process where yeast or bacteria metabolize simple sugars into ethanol that can be used as fuel. Mature technologies in the United States use corn as the feedstock from where the sugars are obtained since the high starch content is easily degraded into

simple sugars ready for fermentation. The ethanol which is produced from biomass is called bio-ethanol. Because of the increasing demand for ethanol, corn alone cannot substantially serve as a feedstock. Currently, about 1/5th of the nation's corn crop is being channeled to ethanol production. The price of corn is about 35 percent more in 2008 than it was last year, mainly due to the demand from new ethanol plants. This will lead to an increase in the price of other products produced from corn such as feed for cattle and pigs and sweeteners. The price of dairy products is also expected to grow at a rapid rate because of the increased demand for ethanol. All these factors: higher energy costs, tighter supply, higher milk demand and retail marketing costs, together account for higher milk costs. According to the U.S. Bureau of Labor Statistics, corn demand is making overall food prices to increase by 4% in 2008, as compared to 2% last year (Jensen, 2007).

This has led researchers to search for cheaper sources, such as cellulosic biomass, which happens to be the most plentiful form of biological material on earth. Examples of cellulosic biomass include corn stover (the parts of the corn plant not eaten such as stalks, leaves, and husks), wood chips, bagasse, switchgrass, and fast growing hybrid trees (Figure 1).

Bioethanol is a very eco-friendly fuel that can reduce typical emissions by up to 70% as compared to fossil fuels. Biomass grown for conversion to bioethanol consumes CO₂ for photosynthesis from the atmosphere, which is released when burning the bioethanol and thus resulting in a neutral CO₂ cycle. Bioethanol is available in various blends, most commonly E5, E10, E85, or E100 where the E represents bioethanol and the number stands for the percentage of bioethanol in the blend. For example, E85 is

a blend of 85% bioethanol and 15% gasoline. As an alternate fuel, bioethanol can significantly reduce the United States' dependency on foreign oil.



Figure 1: Biomass. From Left to Right: Corn Stover, Wood Chips, Bagasse, Switchgrass and Hybrid poplar. (Photos from the National Renewable Energy Laboratory Website)

Current Problem:

Despite the advantages of bioethanol as a transportation fuel, efficiently and economically designed processes for producing ethanol from biomass will not be realized until key obstacles are overcome.

- 1) A key bottleneck in the overall conversion process is the enzymatic hydrolysis (saccharification) of cellulose because of the long residence times. For 10% and greater solids concentration, it takes on the order of two weeks to get about 90-95% glucose yield from cellulose. These yields are not even achievable as the solids loading approaches 20% (Dasari, 2007).
- 2) The biomass is processed as a slurry of suspended solids, so it is vital to know the rheological behavior of these slurries for reactor modeling and

process design. Also, the viscosity of the biomass slurry changes during saccharification and how this property changes over time is yet to be characterized.

- 3) Continuous stirred tanks with conventional mixing impellers such as: rushton turbine, marine etc., cannot effectively process slurries with higher solids concentrations. At high solids concentration, the mixing is poor which leads to poor mass transfer, heat transfer, and solids suspension in the reactor.
- 4) The optimum initial solids concentration for the saccharification step is not yet defined. Knowing this will improve the efficiency of the process, both in terms of sugar produced and power consumed, which can be prohibitive on an industrial scale.
- 5) The viscosity of slurries with suspended particles is very challenging to measure. Solid particles tend to settle at the bottom by gravity and so achieving a uniform suspension for the true measurement of viscosity is difficult with currently existing techniques.

Objectives:

The objectives of this research are to:

- 1) Characterize the viscosity of biomass slurries for various initial solids concentrations, and fit the viscosity characteristics to a suitable model.
- 2) Improve slow reaction rates of enzymatic saccharification by mechanically altering the solids, for instance initiate the reaction with smaller particles.

- 3) Track viscosity changes of biomass slurries as the saccharification reaction proceeds for various initial solids concentrations.
- 4) Scale-up the saccharification reaction to a bench-scale reactor. Run enzymatic saccharification reactions in the reactor in batch and fed-batch modes to determine optimum solids loading.
- 5) Use power measurements in the bench-scale reactor to determine a substrate feeding/processing strategy.
- 6) Improve the current viscosity measurement techniques for biomass slurries and solid suspensions in general.

CHAPTER II
LITERATURE REVIEW

Fossil energy reserves are now depleting at a very rapid rate. Table 1 shows the estimated energy consumption in the world (EIA, 2003).

Table 1

World Primary Energy Consumption (Quadrillion Btu)

Sources	History			Projections				
	1990	2000	2001	2005	2010	2015	2020	2025
Oil	135.1	155.9	156.5	164.2	181.7	200.1	219.2	240.7
Natural gas	75	91.4	93.1	103	117.5	137.3	158.5	181.8
Coal	91.6	93.6	95.9	100.7	110.9	119.6	128.1	139
Nuclear	20.3	25.5	26.4	27.8	29.1	30.3	29.9	28.6
Other	26.4	32.8	32.2	37.6	41.5	44.5	47.3	50
Total	348.4	398.9	403.9	433.3	480.6	531.7	583	640.1

The present estimated share of renewable energy out of the total world energy consumption is 8% and is expected to remain unchanged through 2025 (EIA, 2003).

Renewable energy targets in the world are given in Table 2 (Demirbas, 2000a).

Table 2

Renewable Energy Targets in the World

Renewable energy source	1994 [PJ]	2000 [PJ]	2007 [PJ]	2020 [PJ]
Wind energy	2.06	16	33	45
Photovoltaic solar	0.01	1	2	10
Thermal solar	0.16	2	5	10
Geothermal	0	0	0	2
Cold/heat storage	0.02	2	8	15
Heat pumps	0.25	7	50	65
Hydropower	0.90	1	3	3
Biomass and waste	35.2	54	85	120
Total	38.6	83	204	270

where, PJ (peta joule) = 10^{15} joules.

Ethanol Properties:

Ethanol under atmospheric conditions is a volatile, flammable, clear, colorless liquid. Its odor is a pleasant, familiar characteristic, as is its taste when it is suitably diluted with water. The properties of ethanol stem primarily from the presence of its hydroxyl group and the shortness of its carbon chain. Ethanol's hydroxyl group is able to participate in hydrogen bonding, rendering it more viscous and less volatile than less polar organic compounds of similar molecular weight. The polar nature of the hydroxyl

group causes ethanol to dissolve in many ionic compounds, notably sodium and potassium hydroxides, magnesium chloride, calcium chloride, ammonium chloride, ammonium bromide, and sodium bromide (Merck Index). The physical properties of ethanol are listed in Table 3.

Table 3

Important Physical Properties of Ethanol (Skoog, 1996)

Property	Value
Normal boiling point, °C	78.32
Critical temperature, °C	243.1
Density, g/mL	0.7893
Heat of combustion at 25°C, J/g	29676.69
Autoignition temperature, °C	793.0
Flammable limits in air	
Lower, vol%	4.3
Upper, vol%	19.0

Biomass Sources:

Biomass resources available for ethanol production include low-cost residues, by-products, and wastes from other processes such as: pulp and paper mill residues, municipal solid waste, and recycled paper that has been previously recycled (Glassner *et al.* 1998). The dry mass composition of various lignocellulosic materials is shown in Table 4 (Lee, 1997).

Table 4

Composition of Various Lignocellulosic Raw Materials

	Corn stover	Wheat straw	Rice straw	Rice hulls	Bagasse fiber	Cotton in trash	News print	Populus tristis	Douglas fir
Carbohydrate (% of Sugar equivalent)									
Glucose	39	36.6	41	36.1	38.1	20	64.4	40	50
Mannose	0.3	0.8	1.8	3	NA	2.1	16.6	8	12
galactose	0.8	2.4	0.4	0.1	1.1	0.1	NA	NA	1.3
Xylose	14.8	19.2	14.8	14	23.3	4.6	4.6	13	3.4
Arabinose	3.2	2.4	4.5	2.6	2.5	2.3	0.5	2	1.1
Non-carbohydrate (%)									
Lignin	15.1	14.5	9.9	19.4	18.4	17.6	21	20	28.3
Ash	4.3	9.6	12.4	20.1	2.8	14.8	0.4	1	0.2
Protein	4	3	NA	NA	3	3	NA	NA	NA

Biofuel sources are geographically more evenly distributed than are fossil fuels; hence, the sources of energy will mostly remain domestic and provide security of supply. Another advantage of using lignocellulosic raw materials for ethanol production is to minimize the potential conflict between land use for food (and feed) production and energy feedstock production. Lignocellulosic material is less expensive than conventional agricultural feedstock and can be produced with lower input of fertilizers, pesticides, and energy (Hagerdal, 2006).

Amongst all lignocellulosic raw materials, corn stover has attained much attention as a potential resource for bioethanol production for it is the most abundantly available agricultural waste. Kadam (2003) has estimated the amount of corn stover that can be sustainably collected to be 80 -100 million dry tonnes per year and a majority of this would be available to ethanol plants in the near term. The estimated corn stover availability and ethanol production potential as a function of the stover fraction that can be sustainably collected is shown in Figure 2. An amount equal to 19–26 billion L (5–7 billion gallons) of ethanol per year can be produced using corn stover availability of 82 million dry t/yr, depending on which ethanol yield is assumed.

However, corn stover has many competing uses such as: potential feed for dairy cattle (Ayers and Buchele, 1982; Fernandez-Rivera and Klopfenstein, 1989; Adams, 1998), fuel in a boiler furnace (Hitzhusen and Abdallah, 1980; Richey *et al.*, 1982), corn stover-based pulp and paper production (Domier, 1995; Wagner *et al.*, 2000), and substrate for furfural production (Foley and Vander Hoover, 1981; Riera *et al.*, 1991). This would lower the amount of corn stover accessible for ethanol production, thus the

other lignocellulosic raw material resources mentioned earlier are also to be equally considered for ethanol production.

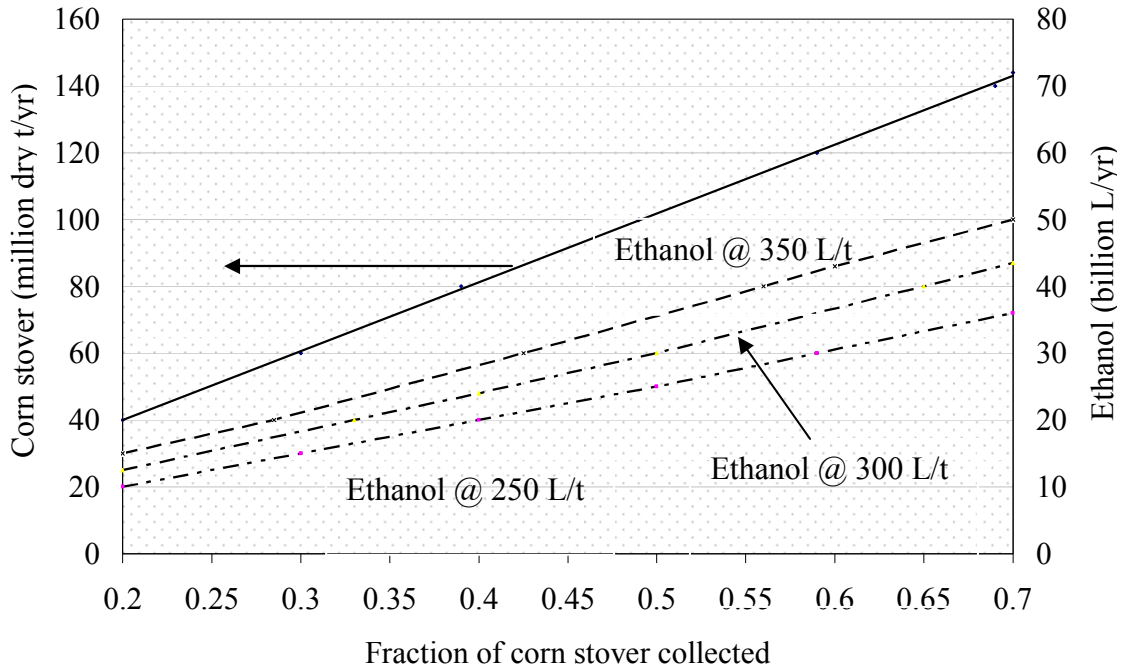


Figure 2. Estimated corn stover availability and ethanol production potential as a function of the stover fraction that can be sustainably collected.

Ethanol Impact on Environment:

Worldwide energy consumption has increased 17 fold in the last century and emissions of CO₂, SO₂ and NO_x from fossil-fuel combustion are primary causes of atmospheric pollution (Ture, 1997). Bioethanol is a very eco-friendly fuel that can reduce the typical emissions of fossil fuel by up to 70%. Many energy production and utilization

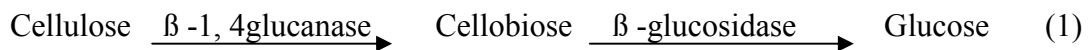
cycles based on cellulosic biomass have near-zero greenhouse gas emissions on a life-cycle basis (Delucchi, 1991; Lynd et. al., 1991 and Wang, 2002). The biomass grown for conversion to bioethanol takes in CO₂ for photosynthesis from the atmosphere, this is released by burning the Bioethanol, thus completing the cycle of CO₂. It is estimated that by using biofuels, the total fossil energy use (coal, oil, and natural gas) and greenhouse gas emissions (fossil CO₂, N₂O, and CH₄) on a life-cycle basis are 102% and 113% lower, respectively (Sheehan et. al, 2004). Besides, ethanol contains 35% oxygen on a weight basis which assists further in complete combustion of fuel which leading to reduced tail pipe emissions. Ethanol is also being used as a substitute for MTBE (methyl-tertiary-butyl-ether), which was the major oxygenate added to fuels until a few years ago when it was determined to be a carcinogenic pollutant in ground water.

Energy Content of Ethanol:

While hard to measure, the cumulative sum of farming, collection, storage, and production of ethanol from biomass may actually result in a net energy loss. Between an estimated 29% and 57% more fossil energy is required for ethanol production than the ethanol fuel produced (Lang, 2005). Furthermore, the energy content (BTUs per gallon) of ethanol is 30% less than that of gasoline, meaning for every mile one gallon of gasoline moves a car, one gallon of ethanol moves that same car 0.7 miles (Sheehan et. al, 2004).

Physical Constituents of Biomass:

Cellulose and hemicellulose, the primary components of biomass, are polysaccharides that can be converted to ethanol once their energy-rich sugars are released. Cellulose is a polymer made up of repeating glucose (a six-carbon saccharide molecule) units tied together by β -glycosidic linkages (Figure 3). The high degree of hydrogen bonding between linear chains of cellulose is highly stable and resistant to chemical attack. In a hydrolysis reaction, which breaks the glycosidic bonds in the presence of water, cellulose is reduced to a cellobiose repeating unit, $C_{12}H_{22}O_{11}$, and ultimately to glucose, $C_6H_{12}O_6$, by enzymes as shown in the following reaction:



Hemicellulose contains mostly five-carbon sugars (primarily xylose and some arabinose) and a few six-carbon sugars (galactose, glucose, and mannose). Hemicellulose is relatively easy to hydrolyze to its constituent sugars compared to cellulose because it is amorphous in nature due to its branched structure.

Lignin is the major non-carbohydrate present in cellulose and is a highly polymeric substance with a complex, cross-linked, polyphenolic structure. It encrusts the cell walls and cements the cells together. Lignin can be thought of as nature's way of protecting the valuable cellulosic material. Lignin is rich in energy, and when separated, can be burned for heat, converted to electricity, or gasified and converted to synthetic fuels by a Fischer-Tropsch (FT) process.

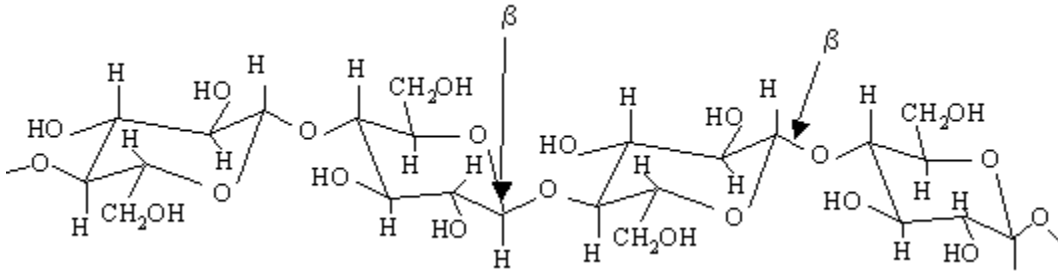


Figure 3. Linear chains of glucose linked in a crystalline structure to form cellulose.

The three polymers, cellulose, hemicellulose and lignin, are assembled into a complex composite. This composite provides plant cell walls with strength and resistance to degradation. So, it is a challenge to use the biomass as a substrate for biofuel production. The conversion of corn to ethanol is a much easier process since the starch is a polysaccharide (repeating units of $C_{12}H_{16}O_5$) composed of long chains of linked α -glucose molecules (Figure 4). The α -1,6 linkages between the chains result in a branched highly amorphous structure, making it more readily attacked by enzyme systems and broken down into glucose.

Biomass Conversion Process:

The process of conversion of a feedstock to ethanol consists of a series of steps, which are shown in Figure 5 as a schematic diagram.

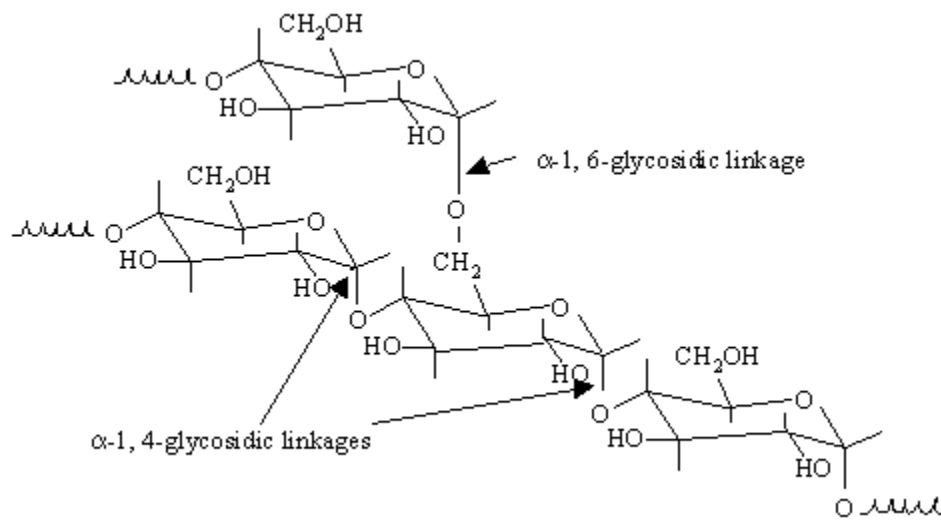


Figure 4. Linear chains of glucose linked in an amorphous structure to form starch.

The raw feedstock is first milled to obtain smaller particle sizes and also to make the material easier to process in the subsequent steps. Hammer mills and knife mills are commonly used for this purpose. The upstream processes (pretreatment, fractionation, and enzymatic hydrolysis) are usually recognized as the major components in the cost (60% of total price) of producing ethanol from biomass (Nguyen and Saddler, 1991). The main factors to be considered in the bioconversion process are: development of a high yield pretreatment procedure, a highly effective enzyme system, better engineering techniques to maximize glucose yield, and microorganisms that can efficiently convert multiple sugars to ethanol.

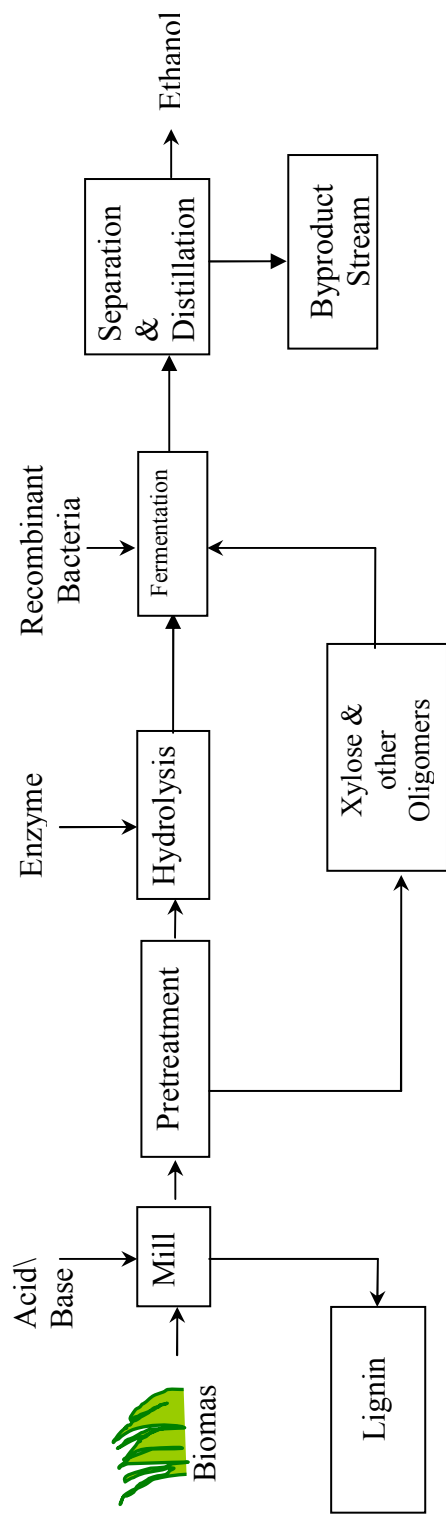


Figure 5. Overall conversion process of biomass to ethanol.

Cellulase production costs have recently been reported in the range of 10 to 20 cents per gallon of ethanol produced (Greer, 2005). If this is true, then the cost of enzymes is no longer a barrier for the commercialization of a biomass-to-ethanol conversion process. Thus, the other aspects of the process require further improvement to make it a commercially viable technique. The individual steps of the biomass to ethanol conversion process are detailed in the following sections.

Pretreatment of Biomass:

The amorphous component of cellulose can be digested more easily by enzymatic attack than the crystalline component. The pretreatment process disrupts the lignin crust, and therefore, removes the physical barrier for enzymatic attack as shown in Figure 6. Also, the external surface area is increased in the process of pretreatment, thereby increasing the accessibility of cellulose to enzymes that convert the carbohydrate polymers into fermentable sugars. A partial hydrolysis occurs during pretreatment because of the severe conditions used such as high temperature and high pressure. Hydrolysis is a process in which the H₂ bonds in the hemicellulose and cellulose fractions are broken down to convert those polymers into their sugar components: pentoses and hexoses. These sugars can then be fermented into bioethanol. Reduction in crystallinity, reduction in lignin content, and an increase in surface area and pore size should be the achievements of an ideal pretreatment process.

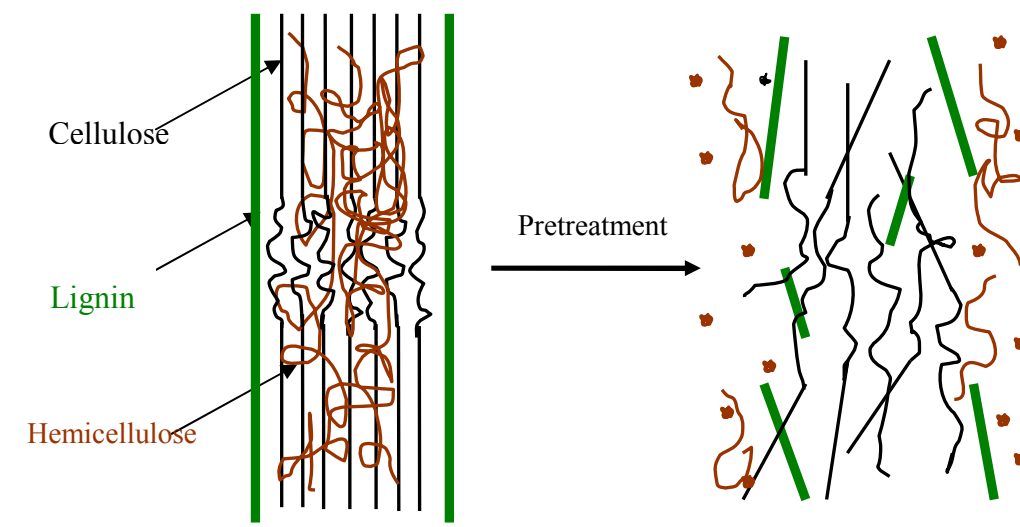


Figure 6. The result of biomass pretreatment. The hemicellulose, lignin, and cellulose are separated, making the cellulose fibers more accessible for attack by enzymes.

There are two types of pretreatment available, i.e. physical and chemical. Mechanical and non-mechanical pretreatments, considered as physical pretreatments, can reduce the particle size and also the crystallinity. Chemical pretreatments are suitable for the structural modifications of lignocellulosics, increasing the pore size and the removal of lignin (Abraham and Kurup, 1997).

The most frequently used and widely known chemical pretreatment methods are dilute-acid pretreatment, steam explosion including acid-catalyzed steam explosion, ammonia fiber explosion, and treatment with organic solvent or alkali (Walsum et al., 1996). In acid-catalyzed pre-treatment, the hemicellulose layer is hydrolyzed, whereas in alkali-catalyzed pretreatment, a part of the lignin is removed and hemicellulose has to be hydrolyzed by the use of hemicellulases (Hagerdal, 2006).

Steam-explosion and dilute-acid pretreatments have been more heavily researched. The advantages of steam explosion over dilute-acid methods are less corrosive operating conditions, it is relatively less expensive and it allows the partial fractionation of the substrate into its cellulose, hemicellulose, and lignin components (Schwald et al., 1989). The advantages of dilute acid hydrolysis over the steam explosion are that it has higher recoveries of hemicellulose sugars and faster reaction rates which facilitate continuous processing (Walsum et al., 1996). The critical factors needed to make this process economically viable are to optimize sugar recovery and cost effective recovery of the acid for recycling (Demirbas, 2006). Rivers (1988) concluded from the indication of his experimental data that each individual lignocellulosic substrate requires a specific pretreatment in order to achieve maximum enzymatic hydrolysis. The effects of various pretreatment methods are summarized in Table 5.

Enzymatic Hydrolysis (Saccharification):

Hydrolysis can be defined as a process of breaking cellulose polymer into its monomer, glucose, in the presence of water. Enzymes are used to assist this process, hence it is called enzymatic hydrolysis. This is the immediate step following pretreatment of biomass. Enzymatic hydrolysis of lignocellulosic material is in general a slow process. Cellulase is used as the biocatalyst for conversion of cellulose to glucose. The kinds of enzymes that can convert the cellulose in biomass to its monomeric sugars are called cellulases and are mostly produced from fungi such as: *Fusarium solani*,

Table 5

Effect of Various Pretreatment Methods on the Chemical Composition and

Chemical/Physical Structure of Lignocellulosic Biomass (Source: Mosier et al, 2005)

	Increases accessible surface area	Decrystallizes cellulose	Removes hemicellulose	Removes lignin	Alters lignin structure
Uncatalyzed steam explosion	*	*	*	-	•
Liquid hot water	*	ND	*	-	•
pH controlled hot water	*	ND	*	-	ND
Flow-through liquid hot water	*	ND	*	•	•
Dilute acid	*	-	*	-	*
Flow-through acid	*	-	*	•	*
AFEX	*	*	•	*	*
ARP	*	*	•	*	*
Lime	*	ND	•	*	*

• - Minor effect, * - Major effect, ND - Not determined.

Clostridium thermocellum, *Trichoderma reesei*, *Trichoderma viride* etc. Any fungal cellulase complex system may consist of four enzymes: endo-1,4- β -glucanase, exo-1,4- β -glucanase (cellobiohydrolase), exo-1,4- β -glucosidase, and cellobiase (β -glucosidase) (Gusakov et al., 1992).

The basic mechanism of enzymatic hydrolysis involves four steps that are as follows:

- Diffusion of enzymes on to the surface of substrate
- Release of glucose from the cellulose polymer
- Release of glucose into bulk solution
- Diffusion of enzymes into bulk solution

The most important structural features affecting the susceptibility of cellulose to enzymatic hydrolysis are surface area and crystallinity. They are directly related to the initial hydrolysis rate (Ramos et al., 1993 and Walker et al., 1991). The crystallinity of lignocellulosics may be altered either upward or downward, but does not appear to have a direct relationship in determining susceptibility of the β -1,4-glucosidic bonds to enzymatic hydrolysis (Rivers, 1988).

Cellulase Synergism:

The complex of cellulase enzyme acts in a synergistic way to hydrolyze lignocelluloses. β -1,4-Glucanase hydrolyses β -1,4-bonds in a cellulose molecule. Endo- β -1,4-glucanase attacks β -1,4-bonds with random action, and exo- β -1,4-glucanase successively removes single glucose units from the nonreducing end of the cellulose chain (Fan et al., 1983). The efficiency of enzymatic hydrolysis of cellulosic material

depends not only on the presence of all cellulase components but also, more importantly, on the appropriate proportional ratio of the various components (Gregg and Saddler, 1996).

Cellulase synergism (a combination of enzymes from the same microorganisms) could achieve higher glucose yields as compared to those achieved by each individual enzyme action (Nidetzky et al., 1994 and Tarantili et al., 1996). Cross-synergism (cellulases from different microorganisms) can more efficiently hydrolyze the cellulose even at high crystallinity than the cellulose synergism (Tarantili, et al., 1996). Converse and Optekar (1993) reported that the degree of synergism goes through a maximum as total enzyme concentration is increased.

Product Inhibition:

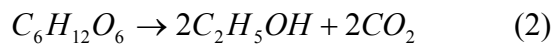
Cellobiose, an intermediate product, and/or glucose inhibit the cellulolytic enzymes. This inhibition is competitive according to (Gregg et al., 1996), non-competitive according to (Holtzaple et al., 1984), and is a combination of both according to (Gusakov and Sinitsyn, 1992). Holtzaple et al. (1990) discovered that all forms of the enzyme species (free, adsorbed and complexed) are subjected to inhibition in the process of cellulose hydrolysis. Ghose and Das (1971) reported that cellobiose competitively inhibits the hydrolysis of cellulose by *T. viride* far more severely than the glucose even at a very low concentration. Gusakov and Sinitsyn (1992) reported that the enzyme/substrate ratio is a very important factor in deciding the extent of inhibition. So, depending on both the absolute enzyme concentration and the enzyme/substrate concentration ratio, different product inhibition patterns may be observed.

Enzyme Deactivation:

The cellulase enzymes undergo deactivation when exposed long enough to fluid shear stress and temperature in the reaction zone. The degree of deactivation varies from less significant to more serious especially when the enzymes are on the liquid surface exposed to air (Reese and Ryu 1980). They suggested that enzyme deactivation at the gas-liquid interface is due to the unfolding of protein molecules at the interface. Since agitation by impellers in a stirred tank continually renews the surface, more and more protein molecules are subjected to the unfolding process, and therefore protein denaturation and deactivation increases over time (Kaya et al., 1994).

Fermentation:

Fermentation is an anaerobic biological process, following enzymatic hydrolysis, in which sugars are converted to alcohol by the action of microorganisms, such as bacteria and yeast. The fermentation process is also defined as a sequence of metabolic reactions whose chief purpose is the production of ATP (adenosine-tri-phosphate) entirely via substrate-level phosphorylation (SLP) reactions (Morris, 1985). The fermentation is performed in a fermentor typically at a temperature of about 30 °C and a pH of about 5. The stoichiometry for conversion of glucose to ethanol is shown in the following equation:

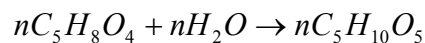


In addition to glucose, hydrolysis produces other six-carbon sugars from cellulose and five-carbon sugars from hemicellulose that are not readily fermented to ethanol by naturally occurring organisms. They can be converted to ethanol by genetically

engineered microorganisms that are currently available. Contrary to sucrose- and starch-based ethanol production, lignocellulose-based production is a mixed-sugar fermentation in the presence of inhibiting compounds – low molecular weight organic acids, furan derivatives, phenolics and inorganic compounds – released and formed during pretreatment and/or hydrolysis of the raw material (Larsson et al., 2000). The lignocellulosic-based fermentation produces a 8-11% (weight basis) concentrated ethanol stream, which can be further concentrated to about 90-95% purity by using multiple distillation columns. Molecular sieves are used to further improve the purity of ethanol. CO₂ is obtained in the ethanol production process as a side product. The residue of distillation can be dried and used as a burning fuel to produce power for the process.

Knowing stoichiometry is vital in order to calculate the theoretical yields during the enzymatic saccharification and the glucose fermentation. The stoichiometric equations for ethanol production are given in the following:

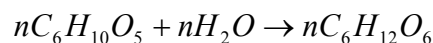
1. Pentosan to Pentose



$$n132_{MWU} + n18_{MWU} \rightarrow n150_{MWU}$$

$$(1gram) + (0.136gram) \rightarrow (1.136gram)$$

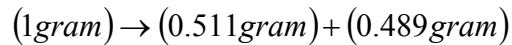
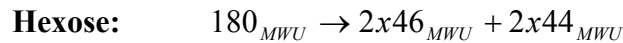
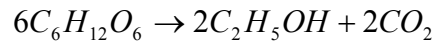
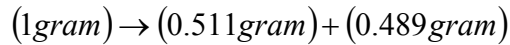
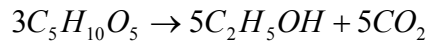
2. Hexosan to Hexose



$$n162_{MWU} + n18_{MWU} \rightarrow n180_{MWU}$$

$$(1gram) + (0.111gram) \rightarrow (1.111gram)$$

3. Pentose and Hexose to Ethanol



The weight yield of pentose from pentosan – xylan and arabinan – is 1.136 grams pentose per gram pentosan. This number results from 150/132, the ratio of the molecular weight of pentose per molecular weight of anhydropentoses that make up pentosans.

The yield of hexose from glucan, mannan, and galactan that are hexans from the cellulose and hemicellulose is 1.111 grams glucose per gram hexosan, the molecular weight ratio of 180/162 for glucose and anhydrohexoses.

The yield of ethanol from fermenting is 0.511 grams per gram of hexose or pentose. The overall theoretical yield for conversion is 0.581 grams ethanol per gram pentosan and 0.568 grams per gram hexosan, just a 2.3% difference.

High Solids Processing:

The enzymatic saccharification step may be the key step for the success of the biomass to ethanol conversion process because the amount of glucose obtained is proportional to the amount of ethanol that can be obtained by fermentation. Therefore, it

is very important to maximize the sugar released during enzymatic saccharification. For economic reasons, it is advantageous to perform the processes with high solids concentrations. Operating costs can be reduced with high-solids processing due to higher concentrations of fermentable sugars in the product stream, less process water and energy usage, reduced disposal and treatment costs due to lower water usage, plus smaller reactor sizes. High solids saccharification can be defined as the processing of a thick slurry (absence of free liquid) in which the separation of liquid and the solid phase is not spontaneous (Hodge, 2005). Processing with high solids content can improve overall processing efficiency if the rate of glucose released from cellulose can be maintained near that of lower solids concentrations.

Viscosity & Power Correlation:

Biomass slurries pose mixing problems at high solids concentrations since they are highly viscous by nature. The presence of free water in biomass slurries depends strongly on both the insoluble solids level and the glucan content of the solids, which influences lignocellulose-water interactions and cellulose swelling. For PCS (pretreated corn stover) solids, the high solids region begins at approximately 12%-15% insoluble solids by weight (Hodge, 2004). The viscosities of biomass slurries increase rapidly above about 10% solids concentration as they are non-Newtonian particulate suspensions and the interparticle distance decreases drastically with increasing solids concentration, therefore leading to more resistance to flow (Pimenova *et al.*, 2003; Dasari, 2007a; Dasari, 2007b). Hence, conventional stirred tanks with typical impeller configurations are not practical for this application due to high power requirements from the high stirring speeds needed to mix the slurry and keep the solids suspended.

Processing of high-solids biomass non-Newtonian slurries is challenging due to their very high viscosities which cause problems with mixing that will result in poor mass transfer and heat transfer. Various reactor configurations have been developed to manage the high-solids slurries: a laboratory ball mill (Mohagheghi *et al.*, 1992), a theoretical continuous tower reactor design (Nguyen, 1998), a paddle-impeller reactor of Tengborg *et al.* (2001), and an attrition bioreactor (ABR) (Jones and Lee, 2004). All of these laboratory-scale reactors require high power for agitation, which makes the process unrealistic on an industrial scale.

According to Equation (3) (Tchobanoglous, 1991), the higher the viscosity of the fluid (resulting from high solids concentration), the higher the power required for processing. Operating the reactor at lower agitation speed will result in lower power consumption. However, low agitation speed may not provide adequate mixing for high solids concentrations resulting in poor heat and mass transfer that directly affects the cellulose conversion reaction rates.

$$P = k\mu N^2 D^3 \quad (3)$$

where, P - power (Watts), k - dimensionless proportionality constant, μ – viscosity (Pa·s), N - impeller speed (rps), D – impeller diameter.

Scraped surface reactors are prevalent and effectively used for processing highly viscous materials and particulate suspensions such as: ice cream, tomato pulp, peanut butter, etc. to provide better heat transfer and to enhance mixing (Wang et al, 1999). Heat transfer in scraped surface reactors has been studied by many authors in the past (Wang et al, 1999; Boxtel, 1983; Landfeld, 2006; Sun et al, 2004; Sangrame et al, 2000;

Miyashita, 1997) for mixing of various materials like tomato pulp, starch solutions, etc., with varying solids content between 10% and 45%. However, power consumption for mixing in scraped surface reactors is less studied. The power consumption in scraped surface reactors, excluding bearing losses, consists of two parts: the power required to maintain rotational flow in the annulus and the power required to rotate the blades (Benezech, 1988). The power required for mixing is a function of the number of blades fixed to the rotor, mass of the blades, speed of rotation, and physical properties such as surface tension, density, and viscosity of the fluid (Abichandani, 1988). The power due to the scraping of the blades against the heat exchange wall accounts for over 75% of the total power consumption; the power increases with the viscosity of the fluid and the rotational speed of the blades (Benezech, 1987). It is a very complex procedure to develop the power correlation for a scraped surface reactor as it varies with the blade geometry (Harrod, 1986).

Fed-batch processes combine the benefits of both batch and continuous processes to improve reaction conditions and, therefore, give the desired results. Researchers have employed a fed-batch approach for various reasons such as: to minimize the effect of inhibitory compounds in the hydrolyzate liquors on the fermentative microorganism (Rudolf *et al.*, 2004; Nilsson *et al.*, 2002; Tehzadeh *et al.*, 2000; Söderström *et al.*, 2004; Wingren *et al.*, 2004), to recycle the enzyme for the saccharification of steam exploded willow (Pristavka *et al.*, 2000), and to overcome rheological limitations in the reactor due to high-solids concentration (Ballesteros *et al.*, 2002; Varga *et al.*, 2004). All of them achieved better results than in batch operations. Rivard (1990) operated a novel type of

reactor in fed-batch mode to anaerobically digest municipal solid waste for methane gas production and achieved final solids concentrations as high as 36%.

Rheology of Biomass Slurries:

Rheological properties are important for the design and modeling of reactors and handling and treating of fluids at industrial scale. Figure 7 shows the rheology of various types of fluids (Enderlin, 2008). Most of the non-Newtonian fluids are identified as pseudoplastic / shear thinning fluids in nature, i.e. the viscosity of fluid decreases with increasing shear rate. A Newtonian fluid's viscosity remains constant at a given temperature and pressure, regardless of the applied shear rate (Bird et. al., 2002).

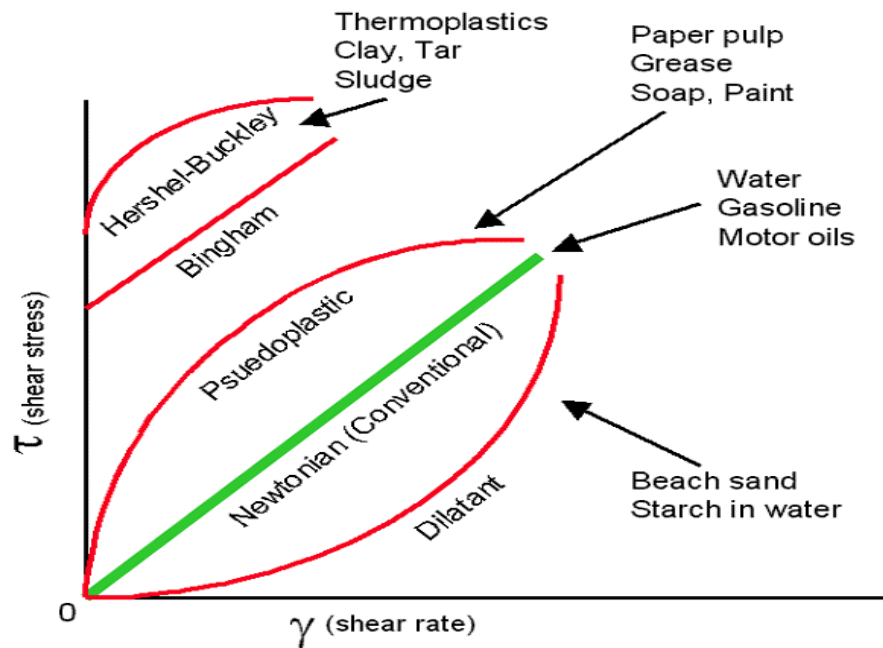


Figure 7. Rheological behavior of various types of fluids.

Various empirical models are available to describe the behavior of non-Newtonian fluids such as: the power-law, Casson, Bingham, and Herschel-Bulkley models. The power-law model remains the simplest and most widely used to describe the rheological properties of non-Newtonian fluids (Bird et al., 2002):

$$\tau = K|\dot{\gamma}|^n \quad (4)$$

The power law works well over a narrow range of shear rates. The apparent viscosity is determined by modifying Equation (4):

$$\eta_a = \frac{\tau}{\dot{\gamma}} = K|\dot{\gamma}|^{n-1} \quad (5)$$

where, η_a - apparent viscosity (Pa·s), τ - shear stress (Pa), $\dot{\gamma}$ - shear rate (s^{-1}), K - flow consistency index ($Pa \cdot s^n$), n – flow behavior index.

The consistency index constant, K , measures consistency of a fluid's viscosity. The higher a fluid's K , the more viscous is the fluid. The flow behavior index number, n , measures the degree of non-Newtonian behavior. Index numbers less than one describe pseudoplastic fluids (Uhl and Gray, 1966). The closer 'n' becomes to 1 the more the fluid approaches Newtonian behavior.

At high-solids concentrations, lignocellulosic biomass slurries exhibit non-Newtonian rheological properties. Pimenova and Hanley (2003) estimated the viscosities of PCS-water slurries (average fiber length = 120 μm) by using a helical ribbon impeller viscometer. The viscosities vary with shear rate in a power law relation, with order of magnitude increases starting at approximately 0.05 Pa·s (Newtonian) at a level of 5% solids (w/w, dry basis) and reaching more than 10^3 Pa·s (highly non-Newtonian) at a level of 30% solids.

Viscosity Measuring Techniques:

The measurement of the exact rheological properties of biomass solids slurries is a real challenge because the solid particles settle fast under gravity in suspensions. Conventional viscometers like cone and plate, concentric cylinders, etc. cannot be used for viscosity measurements of these slurries. An agitation system is required along with the viscosity measuring instrument in order to keep the solids from settling. Some viscosity techniques are presented below for measuring the viscosity of settling suspensions.

A modified capillary tube viscometer, to prevent particle sedimentation during measurement, was developed specifically for fast settling mineral slurries. The viscosity of quartz, chromite, phlogopite and sulphide ore slurries at a pulp density in the range of 0-36% solids by volume is measured using this viscometer. These slurries behave as non-Newtonian liquids. Empirical equations are developed to estimate the rheological parameters of test slurries (Laapas, 1984).

An elongated double gap cup and bob viscometer has been developed to measure the rheological properties of coarse suspensions exhibiting zone-settling properties. The bob is positioned in such a way that it is completely within the constant density zone of the settling slurry during the viscosity measurement. The presence of vertical grooves on the shearing surfaces of the cup and bob reduce wall slip errors to reduce the non-Newtonian shear rate effects (Klein et al., 1995).

An agitator mounted with a torque sensor can serve a dual purpose. The torque generated by the impeller's rotation in the slurry sample can be measured and the apparent viscosities of high viscosity slurries can be estimated at given rotational speeds

(Tran, 1993). Better agitating systems can improve the confidence of the viscosity measurements. Each of these techniques has limitations and is not guaranteed to provide uniform suspensions so there remains a strong need for a rigorous viscosity measuring system and better technique.

Just Suspended Speed (JSS) & Uniform Suspension Speed (USS):

According to Oldshue (1983), the just suspended speed (N_{js}) is defined as the minimum impeller speed at which all solids are suspended off the vessel bottom. The entire surface area for mass transfer is utilized efficiently and effectively once the slurry has reached N_{js} , and at speeds above N_{js} mass transfer increases slowly (Nienow, 1968). But operating the process at N_{js} does not necessarily mean that the system is homogeneous (Lyons, 1967). The N_{js} only means that there are no solid particles left unsuspended at the bottom of the vessel. Molerus and Latzel (1987) stated that the complete suspension of fine-grained particles is achieved at mean circulation velocities of the fluid exceeding the settling velocities of the particles by orders of magnitude. So, for a uniform suspension it takes higher speeds than that required for the just suspended speed, N_{js} . Also, the stirrer speed required for the suspension of the particles should be able to produce the upward wall jet flow that is greater than gravity minus buoyancy. Although various empirical models are available for the estimation of N_{js} in stirred tanks, the model presented in Equation (6) developed by Zwietering (1958) is widely used for baffled tanks as it is simple and reliable. The study was on mixing of sand (0.5-20% by weight) in water with four types of impellers: paddle stirrer, six blade turbine, vane disc, and propeller.

$$N_{js} = \psi \left(\frac{T}{D} \right)^t \frac{g^{0.45} (\rho_p - \rho)^{0.45} \mu^{0.1} D_p^{0.2} (100R)^{0.13}}{D^{0.85} \rho^{0.55}} \quad (6)$$

where, N_{js} - just suspended speed (rpm), T - vessel diameter (m), D – impeller diameter (m), g - acceleration due to gravity (9.8 m/s^2), D_p - particle diameter (m), t – exponent, R - weight ratio of solid to liquid, ρ_p - particle density (kg/m^3), ρ - liquid density (kg/m^3), ψ – constant, μ - viscosity ($\text{Pa}\cdot\text{s}$).

The parameter R is the weight ratio of solid to liquid. The parameters ψ and t depend on the type of impeller and relative blade height which can be determined from the graphs in the Zwietering (1958) article. Pavlushenko et al. (1957) developed another correlation, Equation (7), to determine the just suspended speed using sand and iron ore with various liquids at a 1 to 4 weight ratio for mixing in an unbaffled vessel with a marine impeller.

$$N_{js} = 0.105 \frac{g^{0.6} \rho_p^{0.8} D_p^{0.4} T^{1.9}}{\mu^{0.2} \rho^{0.6} D^{2.5}} \quad (7)$$

where, N_{js} - just suspended speed (rpm), g - acceleration due to gravity (9.8 m/s^2), D_p - particle diameter (m), D – impeller diameter (m), ρ_p - particle density (kg/m^3), ρ - liquid density (kg/m^3), μ - viscosity ($\text{Pa}\cdot\text{s}$).

In the design of any effective mixer for suspending a particulate slurry, the impeller speed and construction, impeller clearance, and the vessel geometry are important features. The uniformity of solids suspension depends on the properties of the solid-liquid system considered, such as particle size, shape, and density, solids concentration, and density and viscosity of the liquid phase (Thring, 1990). Armenante (1998) investigated the effect of the ratio, off bottom clearance to tank diameter, with

various impeller types on N_{js} for the systems with off bottom impeller clearances as low as 1/20. He derived an empirically modified Zwietering equation to incorporate the effect of low off bottom clearance and achieved good agreement between the experimental and calculated N_{js} values.

CUTTING EDGE TECHNOLOGIES

Several technical and natural problems are encountered in the process of bioethanol production, and extensive research has been conducted to overcome these barriers. The areas of investigation include: genetic modification of feedstock, genetic modification of cellulase enzymes and fermentation microorganisms, development of techno-economic models such as high-solids processing, simultaneous saccharification and fermentation, immobilization of microorganisms, and cell-free ethanol production.

It is found that adding BSA (Bovine Serum Albumin) to a reaction slurry would significantly reduce the loss of enzyme to lignin through irreversible binding. In particular, treatment of pretreated corn stover solids with 1% BSA prior to enzymatic hydrolysis increased 72 h glucose yields from about 82% to about 92% at a cellulase loading of 15 FPU/g cellulose or achieved about the same yield at a loading of 7.5 FPU/g cellulose (Yang, 2006).

Recent developments of genetically engineered bacteria that ferment both five carbon and six carbon sugars derived from biomass to ethanol at high yields have been the key to reducing costs (Wyman, 1999) and for the economical production of ethanol (Dien et. al., 2000). The pentose-fermenting *Escherichia coli* (Ingram et al., 1987) and

Klebsiella oxytoca (Burchhardt, 1992) have been generated by introducing ethanologenic genes from *Zymomonas mobilis*.

Cell-free ethanol production, using only the enzymes involved in the conversion of glucose to ethanol, may offer a practical and beneficial alternative. Mathematical modeling by Allain (2007) of such a system has suggested that a cell-free process should be capable of producing ethanol much more efficiently than the microbial based process.

The immobilization of fermentation microorganism has shown higher efficiencies than the usual operations. By adding immobilized microbial cells, the removal of microorganisms from downstream product can be omitted and the loss of intracellular enzyme activity can be kept to a minimum level (Najafpour, 1990).

In a fermenter, if ethanol concentration is higher than 8 %, fermentation ceases. Therefore, ethanol needs to be separated from the fermentation broth. Activated carbon cloth has been shown to have an extremely high capacity for ethanol in liquid phase adsorption from ethanol-water solutions (Rudy, 2005).

Simultaneous saccharification and fermentation (SSF) processes first described by Takagi et al. (1977), combine enzymatic hydrolysis of cellulose with simultaneous fermentation of the sugars obtained to ethanol. In the SSF process, the stages are virtually the same as in separate hydrolysis and fermentation systems, except that both are performed in the same reactor. Thus, the presence of yeast together with the cellulolytic enzyme complex reduces the accumulation of sugars within the reactor—thereby increasing glucose yield, saccharification rate of cellulose, and therefore higher ethanol concentrations with respect to separate saccharification and fermentation (Wyman, 1988). Another advantage of this approach is that a single fermenter is used for the entire

process, thereby curbing the investment costs. In addition, the presence of ethanol in the culture medium causes the mixture to be less vulnerable to invasion by undesired microorganisms (Wyman, 1994).

COMPUTATIONAL FLUID DYNAMICS (CFD)

Computational fluid dynamics (CFD) is a branch of fluid mechanics that solves numerically the set of governing mathematical equations to predict fluid flow, heat and mass transfer, chemical reactions, and related phenomena. Computers are used to perform the millions of calculations required to simulate the interaction of fluids and gases with the complex surfaces used in engineering and, therefore, reduces the total effort required in the experiment design and data acquisition.

The various modeling applications of CFD include: flow and heat transfer in industrial processes (boilers, heat exchangers, combustion equipment, pumps, blowers, piping, etc.), aerodynamics of ground vehicles, aircraft, missiles, film coating, thermoforming in material processing applications, flow and heat transfer in propulsion and power generation systems, ventilation, heating, and cooling flows in buildings, chemical vapor deposition (CVD) for integrated circuit manufacturing, heat transfer for electronics packaging applications etc..

CFD offers many advantages in problem solving such as: relatively low cost, short simulation times, ability to simulate real conditions, ability to simulate ideal conditions, possibility to examine a large number of locations in the region of interest, and yields a comprehensive set of flow parameters for examination.

The basis of any CFD problem is the set of Navier-Stokes equations, which define

any single-phase fluid flow. The most fundamental consideration in CFD is how a continuous fluid is treated in a discretized fashion on a computer. One method is to discretize the spatial domain into small cells to form a volume mesh or grid, and then apply a suitable algorithm to solve the equations of motion (Navier-Stokes equations). Supported mesh types include 2D triangular/quadrilateral, 3D tetrahedral/hexahedral/pyramid/wedge/polyhedral, and mixed (hybrid) meshes. The methodology in solving a CFD problem is shown in Figure 8.

The basic equations of conservation of mass, momentum, and energy are presented in the following (Fluent Inc., 2006):

$$\text{Conservation of mass: } \frac{\partial \rho}{\partial t} + \frac{\partial}{\partial x_i}(\rho u_i) = S_m \quad (8)$$

where, ρ - liquid density (kg/m^3), u_i - velocity of component 'i', t - time (s), and x - direction vector.

This equation is the general form of the mass conservation equation and is valid for incompressible as well as compressible flows. S_m is the source term.

$$\text{Conservation of momentum: } \frac{\partial}{\partial t}(\rho \vec{v}) + \nabla \cdot (\rho \vec{v} \vec{v}) = -\nabla p + \nabla \cdot (\overline{\overline{\tau}}) + \rho \vec{g} + \vec{F} \quad (9)$$

where p - static pressure, $\overline{\overline{\tau}}$ is the stress tensor, and $\rho \vec{g}$ and \vec{F} are the gravitational force and external body force, respectively.

The stress tensor $\overline{\overline{\tau}}$ is given by,

$$\overline{\overline{\tau}} = \mu[(\nabla \vec{v} + \nabla \vec{v}^T) - \frac{2}{3} \nabla \cdot \vec{v} I] \quad (10)$$

where, μ - molecular viscosity, I - unit tensor, and the second term on the right hand side is the effect of volume dilation.

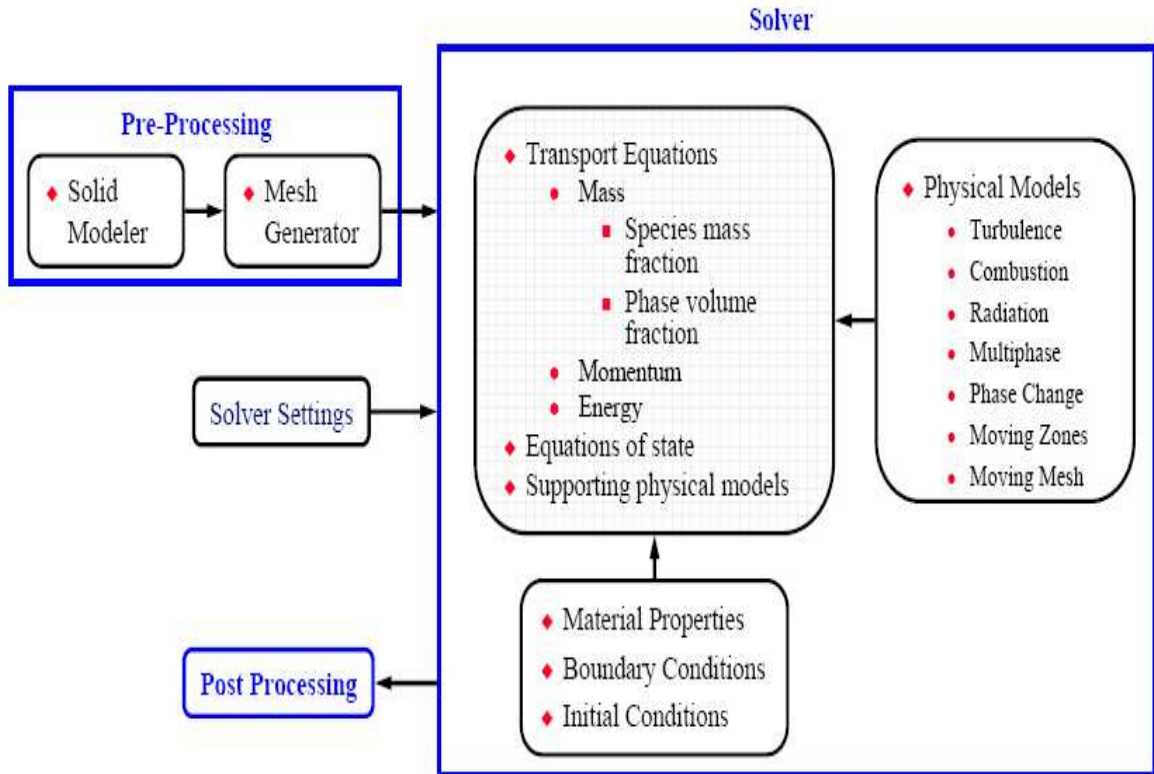


Figure 8. Schematic of the algorithm for problem solving in CFD.

FLUENT:

FLUENT is a state-of-the-art computer program for modeling the transport phenomena in complex geometries. FLUENT provides complete mesh flexibility, and has the ability to solve flow problems with complex geometries with relative ease. FLUENT is basically written in the C computer language. FLUENT uses client/server architecture, and this allows it to run as separate simultaneous processes on client desktop workstations and powerful compute servers. FLUENT can accurately predict laminar and

turbulent flows, various modes of heat transfer, chemical reactions, multiphase flows, and other phenomena with complete mesh flexibility.

GAMBIT is Fluent's geometry and mesh generation software. GAMBIT's single interface for geometry creation and meshing brings together most of Fluent's preprocessing technologies in one environment. As a state-of-the-art preprocessor for engineering analysis, GAMBIT has several geometry and meshing tools in a powerful, flexible, tightly-integrated, and easy-to use interface. A comprehensive set of highly automated and size function driven meshing tools ensures that the best mesh can be generated, whether structured, multiblock, unstructured, or hybrid. GAMBIT also has an excellent boundary layer mesher for growing optimum grid cells off wall surfaces in geometries for fluid flow simulation purposes. Its graphical user interface (GUI) makes the basic steps of building and meshing a model simple and intuitive and it is versatile enough to accommodate a wide range of modeling applications. GAMBIT can be used to build a 2-D mesh using a "bottom-up" approach. The "bottom-up" approach is to first create some vertices, connect the vertices to create edges, and connect the edges to create volumes. The mesh created is intended for use in FLUENT, so it must be a single block, unstructured mesh. This type of mesh is sometimes called a mapped mesh. The algorithm of a GAMBIT process is shown in Figure 9.

The stepwise procedure of Fluent involves:

- Mesh import from GAMBIT
- Selecting problem solver and physical models
- Set material properties
- Defining boundary conditions

- Initializing calculations
- Post processing i.e. analysis of results

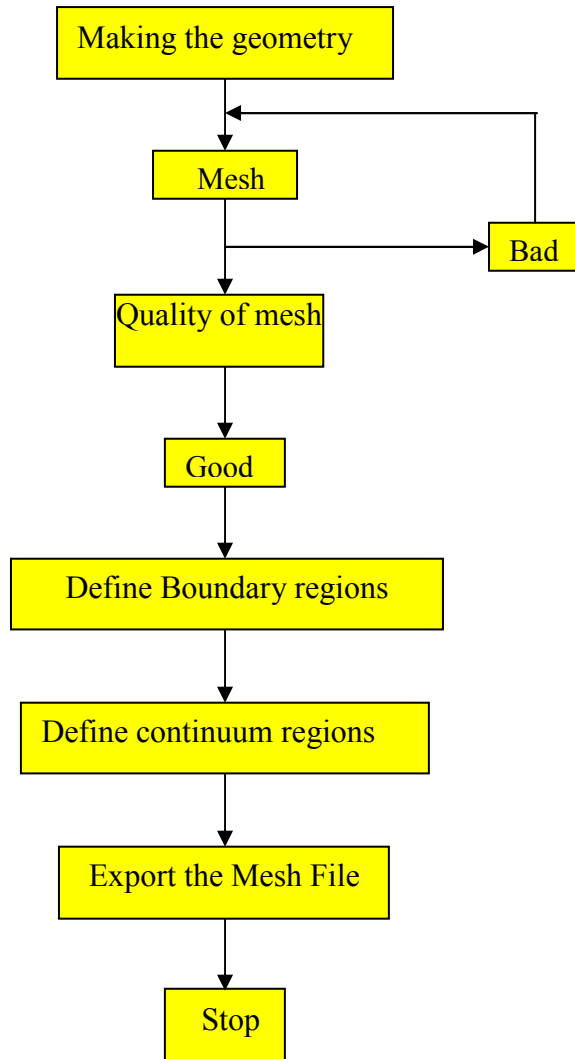


Figure 9. Algorithm of a GAMBIT process.

Multiphase Model:

A phase can be defined as a material that has a particular dynamic response to the flow and the potential field in which it is submerged. One of the phases is considered

continuous (primary) and the others (secondary) are considered to be dispersed within the continuous phase.

For instance, different-sized solid particles of the same material can be treated as different phases because each collection of same-sized particles will have a similar dynamical response to the flow field. The other various examples for multiphase flow regimes are bubble flow (absorbers, aeration, air lift pumps, evaporators, and scrubbers), droplet flow (absorbers, atomizers, combustors, cryogenic pumping, dryers, evaporation, gas cooling, and scrubbers), slug flow (large bubble motion in pipes or tanks), stratified or free-surface flow (sloshing in offshore separator devices and boiling and condensation in nuclear reactors), particle-laden flow (cyclone separators, air classifiers, dust collectors, and dust-laden environmental flows, pneumatic transport (transport of cement, grains, and metal powders), fluidized bed (fluidized bed reactors and circulating fluidized beds), slurry flow (slurry transport and mineral processing) etc.

Fluid flows are governed by conservation laws for the transport of mass, momentum, and energy. Amongst the various models in FLUENT for solving multiphase flow, i.e., Eulerian model, Volume of fluid model, and Mixture model, the Eulerian model remains the primary choice for its suitability for the case of a suspension of biomass particles.

Eulerian Model:

The Eulerian model is the most complex of the multiphase models in FLUENT. It solves a set of momentum and continuity equations for each phase. Coupling is achieved through the pressure and interphase exchange coefficients. The manner in which this coupling is handled depends upon the type of phases involved. For granular flows, the

properties are obtained from application of kinetic theory. Momentum exchange between the phases is also dependent upon the type of mixture being modeled. Applications of the Eulerian multiphase model include bubble columns, risers, particle suspension, and fluidized beds.

The Eulerian multiphase model in FLUENT allows for the modeling of multiple separate, yet interacting phases. The phases can be liquids, gases, or solids in nearly any combination. With the Eulerian multiphase model, the number of secondary phases is limited only by memory requirements and convergence behavior. The Eulerian multiphase model is a result of averaging of the Navier-Stokes equations over the volume including arbitrary particles and the continuous phase. The result is a set of conservation equations for each phase. Since both phases coexist simultaneously, conservation equations for each phase contain single-phase terms (pressure gradient, thermal conduction, etc.) and interfacial terms. Interfacial terms express interfacial momentum (drag), heat, and mass exchange. The Eulerian model can be applied to flow regimes like bubbly flow, droplet flow, slurry flow, fluidized beds, particle-laden flow, dilute to dense volume loading, low to high particulate loading, a turbulence phase, and all ranges of stokes numbers.

The modified governing equations for the Eulerian model are given in Equations (11) and (12). **Continuity equation:**

$$\frac{\partial(\alpha_q \rho_q)}{\partial t} + \nabla \cdot (\alpha_q \rho_q \mathbf{u}_q) = \sum_{p=1}^n \dot{m}_{pq} \quad (11)$$

where, α_q - volume fraction of the q^{th} phase and \dot{m}_q – mass of q^{th} phase.

Equation of momentum for qth phase: (Equation 12)

$$\frac{\partial(\alpha_q \rho_q u_q)}{\partial t} + \nabla \cdot (\alpha_q \rho_q u_q u_q) = -\alpha_q \nabla p + \alpha_q \rho_q g + \nabla \cdot \tau_q + \sum_{p=1}^n (R_{pq} + \dot{m}_{pq} u_q) + \alpha_q \rho_q (F_q + F_{\text{lift}q} + F_{\text{vm}q})$$

(12)

where, $F_{\text{lift},q}$ is the virtual mass force.

Interphase forces exchange coefficients are given by

$$R_{pq} = K_{pq}(u_p - u_q) \quad (13)$$

where K_{pq} is the exchange coefficient

Volume Fractions:

The description of multiphase flow as interpenetrating continua incorporates the concept of phasic volume fractions, denoted here by α_q . Volume fractions represent the space occupied by each phase and are defined as the ratio of the volume of secondary phase or phases in a domain to volume of the domain. The laws of conservation of mass and momentum are satisfied by each phase individually. The volume of phase q, V_q , is defined by,

$$V_q = \int_V \alpha_q dV \quad (14)$$

where

$$\sum_{q=1}^n \alpha_q = 1 \quad (15)$$

The effective density of phase q is

$$\rho_q = \alpha_q \rho_q \quad (16)$$

where ρ_q is the physical density of phase q.

Post Processing:

Post-processing is the process that examines and analyzes the flow field solutions, including contours, vectors, streamlines, iso-surfaces, and animations. This is the final step in CFD analysis, and it involves the organization and interpretation of the predicted flow data and the production of CFD images and animations. Post processing involves tasks such as: calculation of derived variables (vorticity, shear stress), calculation of integral variables (forces, lift/drag coefficients), and calculation of turbulent quantities (Reynolds stresses, energy spectra).

For Eulerian multiphase calculations, graphical plots or alphanumeric reports can be generated for diameter of the particle, volume fraction, mass or molar fraction of species, enthalpy relative humidity, etc. For Eulerian calculations, it is possible to display velocity vectors for the individual phases using the Vectors panel, compute fluxes through boundaries for an individual phase, compute forces or moments on wall boundaries for an individual phase, and a report can be obtained of mass flow rate for each phase (and the mixture) through each flow boundary using the report/mass-flow text command.

CFD Modeling of a Solid Suspension in a Mixing Tank:

A large amount of literature is available on CFD modeling of solids suspensions in a stirred tank suggesting that there has been significant research in this particular area. This is because mixing and mechanical agitation are very common unit operations in process industries. In many industrial units, especially those involving crystallization, it is

very important to have information on particle distribution within the agitated liquid. Several investigations into solids distribution in a stirred tank have been carried out by various authors for different vessels with different impeller types (Bohnet and Niesmak, 1980; Barresi and Baldi, 1987; Rieger and Dilt, 1988; Shamlou and Koutsakos, 1989; McKee et al., 1995, Helene, 2001). It is, however, difficult to obtain the profile of solid suspension density distribution in the whole tank and a computational tool predicting the suspension density distribution together with the flow measurements or visualization would be of utmost importance for research of suspension behavior in stirred tanks (Sha et al., 2001).

Helene (2001) used the Eulerian model to estimate the solids distribution profile in a two baffle stirred tank of $\sim 5 \text{ m}^3$ with solids concentrations higher than 20% (v/v) and found significant agreement between experimental and numerical results. Ochieng (2006) also simulated a Nickel solids distribution profile (1-10% v/v) in a stirred tank with a propeller type impeller using the Eulerian model with only one quarter of the tank geometry in order to reduce the computational time but with the same quality of result.

Modeling of the viscosity measuring technique with a vane impeller (the present case) for biomass particulate suspensions in viscometer is similar to the CFD modeling of solids suspensions in a stirred tank except that the side wall clearance in the viscometer cup is very small.

CHAPTER III

EXPERIMENTAL PLAN

Effect of Initial Particle Size on Saccharification Rates and Rheology of Sawdust

Slurries:

Untreated sawdust is used as a cellulosic substrate to work towards objectives 1, 2 & 3. Sawdust is sieved in a set of US standard sieves for 30 minutes to obtain the following initial particle size (x) ranges: $33 \mu\text{m} < x \leq 75 \mu\text{m}$, $75 \mu\text{m} < x \leq 104 \mu\text{m}$, $104 \mu\text{m} < x \leq 150 \mu\text{m}$, $150 \mu\text{m} < x \leq 180 \mu\text{m}$, $295 \mu\text{m} < x \leq 425 \mu\text{m}$, $590 \mu\text{m} < x \leq 850 \mu\text{m}$. The following sieves are used: 20, 30, 40, 80, 100, 140, and 200 US mesh.

The goal of these tests is to perform the saccharification reaction on sawdust with various particle size ranges to determine if mechanical size reduction can replace the chemical pretreatment step since chemical pretreatment results in inhibitors toxic to the fermentation and requires extra water usage. The sawdust particles have already undergone a mechanical pretreatment in which the size comminution occurs due to cutting in mills. No extra energy is spent on this size reduction process as the material is a waste product of lumber industries in Kentucky. It is mentioned in the Literature Review that mechanical pretreatment reduces the crystallinity of substrate and thus leads to increased accessibility by enzymes. Also, since more surface area is available with smaller particles, this factor may also contribute to achieving higher saccharification rates.

The detailed experimental plan is shown in Table 6 for saccharification tests with sawdust. The size ranges $590 \mu\text{m} < x \leq 850 \mu\text{m}$ and $33 \mu\text{m} < x \leq 75 \mu\text{m}$ are the high and the low ends of particle sizes of the sawdust batch supplied. Two other particle size ranges ($150 \mu\text{m} < x \leq 180 \mu\text{m}$ and $295 \mu\text{m} < x \leq 425 \mu\text{m}$) are selected between the high and the low end in order to investigate a wide range of particle sizes. The effect of initial particle size on saccharification rate is investigated with this set of four different particle size ranges.

The experimental plan for the investigation of rheology of sawdust slurries is shown in Table 7. Viscosities cannot be measured for the largest size ranges described above because the particles are too big to create a homogeneous solution. Also, there is a higher tendency for settling due to gravity, as compared to slurries with smaller particles. Hence, four different particle size ranges from the lower end are selected for the investigation of rheology of sawdust slurries. Saccharification tests are performed on sawdust with these size ranges with different initial solids concentrations in order to study the viscosity changes over time during reaction.

Effect of Solids Loading on Saccharification Rate and Power Consumption in a Bench-Scale Reactor:

Corn stover, pretreated with dilute sulfuric acid, is used as the substrate to work towards objectives 1, 3, 4 & 5. The aims of the study with corn stover are: to investigate the effect of initial solids loading on saccharification rate, to understand the changes in slurry viscosity over time during saccharification, and to study the power consumption patterns in a bench-scale reactor during enzymatic saccharification. The saccharification

reaction of biomass slurries eventually needs to be scaled up from laboratory scale in shaker flasks to bench scale and then to industrial scale without loss of performance. The bench-scale reactor used in the present study for the investigation of the saccharification of pretreated corn stover (PCS) slurries is designed for scale-up from a laboratory scale shake flask. Saccharification experiments are designed for corn stover slurries with two kinds of substrate feeding, batch and semi-batch. The detailed experimental design is shown in Table 8 and Table 9 for batch and semi-batch tests, respectively. The tests are performed in both a bench-scale reactor (discussed in the Materials and Methods) and in shake flasks which are used as a control. The 20% semi-batch test is started with 12% initial insoluble solids, and the solids concentration is increased to 16% and 20% after the first 8 and 16 hours of saccharification by addition of substrate. The 25% and 30% semi-batch tests are started with 10% insoluble solids, and new solids are fed in 5% increments every 8 hours until the final equivalent solids concentration is reached. The torque required for turning the shaft in the reactor, glucose release, and viscosity measurements are measured as the reaction proceeds in the reactor. Similar data are recorded in the shake flasks except for the torque measurements.

Table 6Saccharification Experiments for Tests with Sawdust as Substrate

% Initial solids	Sawdust particle size range			
	10	33 $\mu\text{m} < x \leq 75 \mu\text{m}$	150 $\mu\text{m} < x \leq 180 \mu\text{m}$	295 $\mu\text{m} < x \leq 425 \mu\text{m}$
13	33 $\mu\text{m} < x \leq 75 \mu\text{m}$	150 $\mu\text{m} < x \leq 180 \mu\text{m}$	295 $\mu\text{m} < x \leq 425 \mu\text{m}$	590 $\mu\text{m} < x \leq 850 \mu\text{m}$

Table 7Experiments for Viscosity Measurements During Saccharification Tests with Sawdust as Substrate

% Initial solids	Sawdust particle size range			
	10	33 $\mu\text{m} < x \leq 75 \mu\text{m}$	75 $\mu\text{m} < x \leq 104 \mu\text{m}$	104 $\mu\text{m} < x \leq 150 \mu\text{m}$
13	33 $\mu\text{m} < x \leq 75 \mu\text{m}$	75 $\mu\text{m} < x \leq 104 \mu\text{m}$	104 $\mu\text{m} < x \leq 150 \mu\text{m}$	150 $\mu\text{m} < x \leq 180 \mu\text{m}$

Table 8Design of Experiments for Batch Tests with Corn Stover as Substrate

	% Initial solids			
Reactor	10	15	20	25
Shake flask	10	15	20	25

Table 9Design of Experiments for Semi-batch Tests with Corn Stover as Substrate

	% Final equivalent solids		
Reactor	20	25	30
Shake flask	20	25	30

Technique to Measure Viscosity of Solid Suspensions:

It is necessary for all the solid particles to be uniformly suspended in a liquid-solid slurry to obtain accurate viscosity measurements. Hence, the uniform suspension speed (USS) is determined for PCS slurries with various solids concentrations in the viscometer cup. In order to visually observe the particle behavior which cannot be seen in the actual viscometer cup, testing is performed in a separate assembly using a glass cup

and prototyped vane impeller with the same cup and vane dimensions as in the Anton Paar MCR viscometer.

Premixing of the slurry is required to allow time for the viscosity to reach steady-state. When a shear is applied to the slurry, particles align with the flow direction until the viscosity reaches a steady state. Premixing also ensures the particles are adequately suspended. For these reasons, the slurry must be premixed before measuring the actual viscosity. Since the shear and duration of the premixing affects the viscosity measurement, the effect of premixing parameters is investigated. The premixing test is performed on PCS slurries with various initial solids concentration at various premixing shear rates. The detailed experimental plan is shown in Table 10.

Table 10

Various PCS Solids Concentrations and Shear Rates of the Premixing Tests

Premixing Shear /	160	400	800	1200	1600
% Solids (wt)					
5	X	X	X	X	X
7.5	X	X	X	X	X
10	X	X	X	X	X
15	X	X	X	X	X
20	X	X	X	X	X

CFD Simulations of Flow in the Viscometer Cup:

CFD simulations using FLUENT can help visualize the flow field and particle distribution in solids suspensions. Determining the USS experimentally can be difficult due to the large number of particles in suspension. Thus, FLUENT simulations will be performed on the MCR viscometer cup and vane impeller system in order to help verify the experimentally determined USS. The plan is to run simulations for a 5% PCS slurry at various speeds surrounding the experimentally determined USS. The FLUENT model, when validated with experimental data, can be used for further improvement of the viscosity measurement technique.

The problem involves the mixing of a solids slurry by a vane impeller in the viscometer cup; the arrangement is similar to a mixing tank. The solids slurry is well mixed by a stirrer in the cup and, thus, the solids are assumed to be uniformly suspended at the beginning of the simulation. The aim of this study is to investigate the impeller rotational speed required to suspend all the solids uniformly in the liquid by examining the simulation of the solid particle distribution throughout the viscometer cup. This rotational speed is the USS needed to premix the slurry prior to viscosity measurements.

CHAPTER IV
EFFECT OF SUBSTRATE PARTICLE SIZE ON SACCHARIFICATION
RATES AND RHEOLOGY OF SAWDUST SLURRIES

MATERIALS AND METHODS

Cellulose Substrate and Enzyme:

The cellulose substrate used in these experiments is red oak sawdust obtained from Garrard wood products of Lancaster, Kentucky. The carbohydrate components of the sawdust contain 39.7 % cellulose, 18.8 % hemi-cellulose and 25% lignin. Ash and protein account for the remaining portion. As mentioned in the Experimental Plan, the sawdust is sieved in a set of US standard sieves for 30 minutes to obtain the following initial particle size (x) ranges: $33 \mu\text{m} < x \leq 75 \mu\text{m}$, $75 \mu\text{m} < x \leq 104 \mu\text{m}$, $104 \mu\text{m} < x \leq 150 \mu\text{m}$, $150 \mu\text{m} < x \leq 180 \mu\text{m}$, $295 \mu\text{m} < x \leq 425 \mu\text{m}$, $590 \mu\text{m} < x \leq 850 \mu\text{m}$. The following sieves are used: 20, 30, 40, 80, 100, 140, and 200 mesh. The sawdust is hydrolyzed without any pretreatment by Multifect GC Cellulase enzyme from Genencor International, Inc (Lot # 301-04328-224), with a concentration of 15FPU / g of cellulose,.

Processing of sawdust is performed in a 1 M citrate buffer which is prepared by adjusting the pH to 4.8 with NaOH as given in the NREL standard procedure LAP 006, and is diluted to 5% of the total mass to yield an effective molality of 0.05 mol/kg.

Saccharification Procedure:

The initial particle size ranges of sawdust used for the saccharification studies are: $33 \mu\text{m} < x \leq 75 \mu\text{m}$, $150 \mu\text{m} < x \leq 180 \mu\text{m}$, $295 \mu\text{m} < x \leq 425 \mu\text{m}$, $590 \mu\text{m} < x \leq 850 \mu\text{m}$. All the materials: sawdust, buffer, de-ionized water, and shake flasks, are sterilized in an autoclave at $121 \text{ }^\circ\text{C}$ before use for 20 minutes. The amount of water lost during autoclaving is replaced with autoclaved deionized water before starting the test. Enzymatic saccharification is performed at $55 \text{ }^\circ\text{C}$ in an Innova 4230 incubator shaker (New Brunswick Scientific Co., Inc., U.S.A) at 250 rpm for 72 hours. The operating temperature and pH for the Multifect GC Cellulase enzyme are based on the optimum conditions as specified by the manufacturer. All experiments with sawdust as substrate are performed in 250 mL shake flasks with a working mass of 100 grams for both 10% and 13% (wt/wt) initial solids concentrations for tests performed in batch mode. The addition of enzyme to the shake flask contents and sample collection at various time intervals are performed under a Labconco purifier class II safety cabinet (Labconco Corp., Kansas City, MO) to maintain aseptic conditions in the reaction mixture.

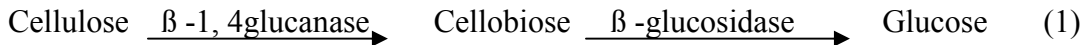
Sampling and Sugar Measurement:

Sawdust slurry samples are collected every 2 hours for the first 12 hours and every 24 hours afterwards for glucose concentration determination. 1 mL Fisher Scientific sterile pipettes are used to collect slurry samples by suctioning of the thick slurry with the pipettor (Drummond Scientific Co., Broomall, PA). Sample sizes of 1-1.5 mL are collected in 1.5 mL centrifuge vials and are frozen immediately at -16^0 C to stop the reaction and stored for later analysis.

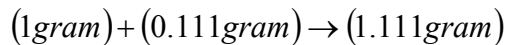
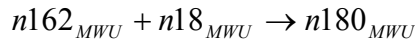
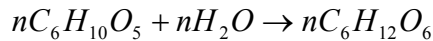
The slurry samples are defrosted and centrifuged in a Beckman GPR centrifuge (Beckman Instruments, Inc., CA) at 4000 rpm for 15 minutes to separate the solids from the liquid. The supernatant is diluted with deionized water using micropipettes in order to bring the glucose concentration level into the YSI working range (0-25g/L). Glucose concentration is measured with a YSI-2700 bio-chemistry analyzer (Yellow Springs, OH).

Calculation of Glucose yield:

The percentage of glucose release is calculated based on the initial amount of cellulose present in the substrate and the stoichiometry of the reaction, which are presented in the Literature Review section. They are given in the following;



The stoichiometry of the above equation can be written for glucose in the form of elemental composition as shown below;



where, n – number of molecules and MWU – molecular weight unit.

The molecular weight is written below its corresponding compound. A water molecule is added to each cellulose molecule to give a glucose molecule, and the mass is conserved

as shown above. It can be seen from the stoichiometric equation that 1.111 grams of glucose is released for every gram of cellulose consumed.

For S % of the initial solids concentration, the glucose yield is calculated as follows;

$$S = \% \text{ Initial solids concentration}$$

$$S_0 = \text{Total initial solids} = 1000 * S \text{ (g/L)}$$

$$C = \text{Amount of cellulose} = X * S_0 \text{ (g/L)}$$

$$X = \text{Fraction of cellulose in substrate}$$

$$G_t = \text{Amount of glucose released at time 't' (g/L)}$$

$$Y_t = \% \text{ Glucose yield at time 't'}$$

$$Y_t = \frac{G_t}{(1.111 * C)} * 100 \quad (15)$$

Equation (15) can be rewritten as;

$$Y_t = \frac{G_t}{(1.111 * X * S_0)} * 100 \quad (16)$$

The term $(1.111 * C)$ represents the amount of 100% glucose release. This is called the theoretical yield, whereas Y_t is the experimental yield.

Viscosity Measurements:

The viscosity of each slurry is measured with an Anton Parr Modular Compact Rheometer (MCR) (Ashland, VA) that is connected to a computer for online data recording. The viscometer consists of a six-bladed vane impeller in a 40 mL cup and works based on the principle of rotating concentric cylinders. The vane dimensions are 1.6 cm long by 0.9 cm wide by 1 mm thick. The viscometer employs a peltier temperature control system for making measurements at the reaction temperature.

Sample size used in the cup is 30 mL, which is enough volume to cover the impeller blades. The MCR is shown in Figure 10.



Figure 10. Anton Parr Modular Compact Rheometer.

The viscosities of the sawdust particle slurries with the following initial particle size ranges are measured: $33 \mu\text{m} < x \leq 75 \mu\text{m}$, $75 \mu\text{m} < x \leq 104 \mu\text{m}$, $104 \mu\text{m} < x \leq 150 \mu\text{m}$, $150 \mu\text{m} < x \leq 180 \mu\text{m}$. The viscosity of each slurry is measured for all four size ranges over an applied shear rate range of 1 s^{-1} to 100 s^{-1} and at different time intervals of the enzymatic saccharification (0, 24, 48, and 72 hr). It is well known that as the viscosity of the slurry increases, the power to agitate also increases significantly ($P = K\mu N^2 D^3$) (Tchobanoglous, 1991). So, to reduce the power consumption while retaining a high solids loading, it is necessary to run the reactors at low rpm. For instance, the High Solids Bioreactor (HSBR) was operated at 7 rpm with 32% of initial insoluble solids by Hodge *et al.* (Hodge, 2005). Therefore, all rheological measurements of the sawdust slurries are

measured at a low steady-state shear rate of 10.8 s^{-1} , which is in the approximate shear rate range of a slow mixing vessel.

Measurements are made after 10 minutes of stirring in the viscometer cup at 100 s^{-1} , which is an estimate of the amount of time needed to overcome time dependent changes in viscosity (this estimate was made prior to the data collected later on PCS slurries). The viscosity of each slurry is measured twice over a range of shear rates ($1-1000 \text{ s}^{-1}$) immediately after the stirring and the average viscosity of the two sweeps is presented. In continuous measurements, the viscosity of the slurries is measured for the first 12 hours of the enzymatic saccharification. For these 12 hours viscosity tests, the enzymatic saccharification reaction is performed directly in the viscometer cup at reaction temperature so the viscosity can be continuously measured. Viscosity data is collected at 10 min intervals. The cup of the viscometer is covered with parafilm to avoid evaporation. The buffer and enzyme concentrations are the same as those in the enzymatic saccharification tests.

RESULTS & DISCUSSION

As discussed in the Introduction section, the upstream processing takes up 30-35% of the capital cost of the biomass-to-ethanol conversion process. Hence, the aim of the first part of this study was to start with an untreated biomass substrate in an effort to eliminate the pretreatment step completely by initiating the reaction with lower substrate particle sizes. The advantages of eliminating the pretreatment step are discussed in the Experimental Plan. Size reduction itself can be an expensive, high energy consumption process. Sawdust waste indigenous to the Kentucky lumber industry is used in these

studies since the sawdust already contains particles with a very low size range and no further size reduction is required. If this technique proves feasible, the conversion of wood residues, which are currently a burden to regional sawmills and other businesses, to ethanol offers a savings when compared to the energy spent on crop production and harvesting.

The specific objective of this research with untreated sawdust is to investigate the effect of substrate particle size on the enzymatic saccharification rate and on slurry rheology. The rheological behavior of sawdust slurries with various particle sizes as the reaction proceeds are also investigated.

The Effect of Substrate Particle Size on Saccharification Rate:

The extent of glucose release from cellulose during the course of an enzymatic saccharification reaction for four particle size ranges ($33 \mu\text{m} < x \leq 75 \mu\text{m}$, $150 \mu\text{m} < x \leq 180 \mu\text{m}$, $295 \mu\text{m} < x \leq 425 \mu\text{m}$, $590 \mu\text{m} < x \leq 850 \mu\text{m}$) is determined and the results are presented in Figure 11 and Figure 12.

The reaction rate trend during enzymatic saccharification for all particle size ranges is similar to many past results (Wald, 1984; Gusakov, 1985 and David, 1996), i.e., two phase kinetics. The rate of glucose release is very fast during the initial hours of the reaction. It appears to be zero order kinetics based on a linear relationship between glucose and time (not including the 0 hour glucose concentration), then the rate decreases as the reaction order increases to higher order kinetics sometime after 8 hours. Supporting the fact that the rate of reaction is faster during the initial hours, 60-74% of the maximum achievable glucose in 72 hours was obtained within the first 8 hours of the

saccharification. The amount of glucose released during the initial 8 hours of the reaction is shown in Table 11 for sawdust slurries with 10% and 13% initial solids concentrations as a percentage of the maximum glucose attainable in 72 hours.

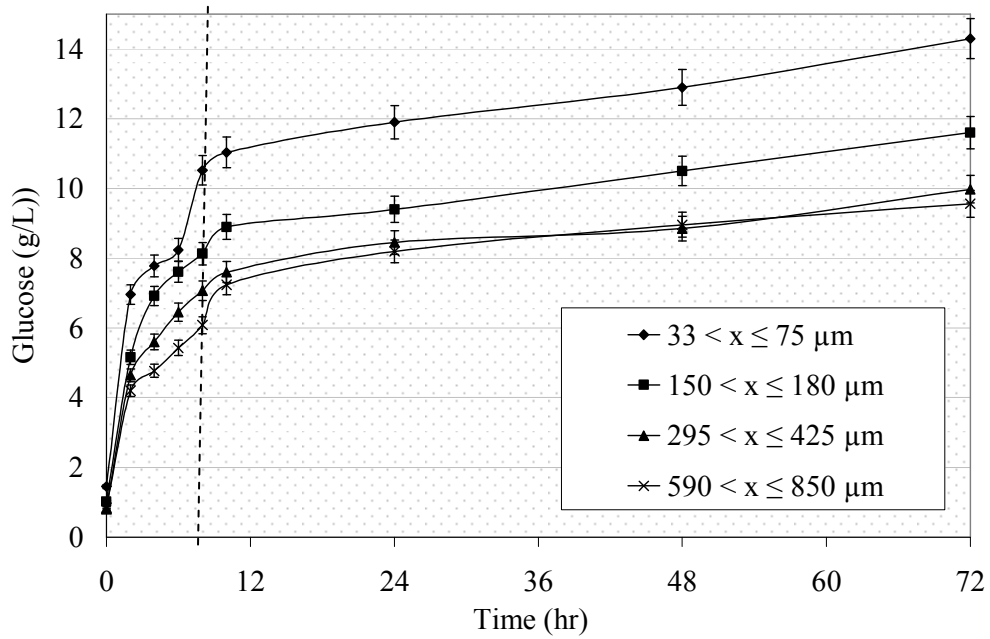


Figure 11. The effect of initial particle size on glucose production with 10 % initial solids concentration.

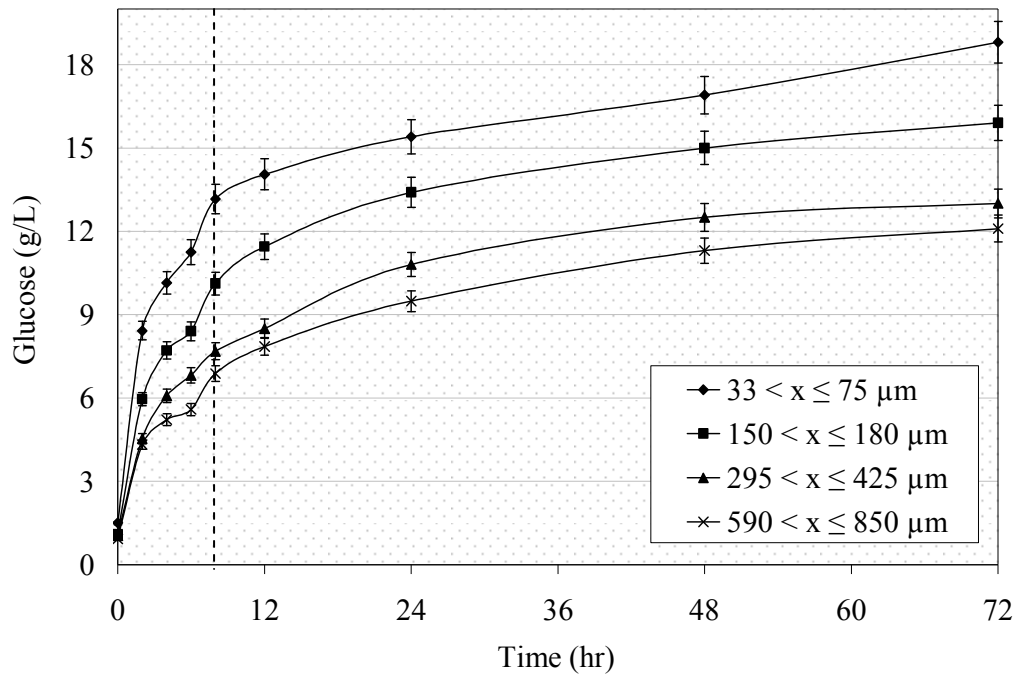


Figure 12. The effect of initial particle size on glucose production with 13 % initial solids concentration.

Table 11

Glucose Obtained During the First Eight Hours of Saccharification as a Percentage of the Maximum Glucose Attainable In 72 Hours

% solids / Particle size range	10%	13%
590 μm < x ≤ 850 μm	63.6	56.9
295 μm < x ≤ 425 μm	70.8	59.1
150 μm < x ≤ 180 μm	70.1	63.7
33 μm < x ≤ 75 μm	73.6	70.0

The percentage of maximum glucose released during the first 8 hours increases with decreasing particle size and with decreasing initial solids content. The reasons for

higher glucose yields at lower solids concentrations and with lower size particles are discussed in the following paragraphs. The postulated reasons for the decrease in the rate of enzymatic saccharification reaction over time are:

- The increase in the fraction of crystalline cellulose in biomass during the course of the saccharification reaction (Norkrans, 1950; Halliwell, 1965; Fan, 1980; Bertran, 1985; Saddler, 1986; and Kyriacou, 1987) since the crystalline form of cellulose is harder for enzymes to digest.
- The decrease in the specific surface area, internal and external, of substrate over time because of the dissolution of solids into the liquid phase (Puri, 1984; Henrissat, 1985; Grethlein, 1985; Weimer, 1985 and Saddler, 1986)
- Inhibition of the enzymes by glucose and cellobiose (Mandels, 1963; Mandels, 1963; Ladisch, 1980; Ladisch, 1981; Fan, 1983; Marsden, 1986 and Kiran 2004).
- The adsorptive loss of enzyme to lignin due to irreversible binding (Gregg, 1996 and Palonen, 2004) or failure to release from the substrate after catalytically processing cellulose chain (Eriksson, 2002).
- The deactivation of enzyme through thermal, mechanical and chemical actions (Gregg, 1996).

It is observed that for smaller particle sizes the rate of release of glucose is higher. An amount of 50% and 55% more glucose is produced for the size range $33 \mu\text{m} < x \leq 75 \mu\text{m}$ than for the size range $590 \mu\text{m} < x \leq 850 \mu\text{m}$ for an equivalent initial solids

concentration, of 10% and 13% respectively, in 72 hrs. Smaller particles have larger surface area per unit volume and, therefore, more cellulose may be accessible for the enzyme to reach and at a faster rate. Another possibility is that smaller particles may have been exposed to more mechanical grinding at the surface resulting in a reduction of crystallinity and an increase in amorphous nature at the surface (Millet *et al.*, 1976 and Fan *et al.*, 1982). Peters *et al.* (Peters, 1991) found no significant difference in the extent of sugar produced and the rate of glucose release for the cellulosic substrate Avicel PH 102 as particle size range varies between 38 and 75 μm . Since Avicel is crystalline structured cellulose and the authors found no significant difference in the rate between different particle sizes, this may indicate that the latter of the two possible explanations is the more likely reasoning for the increased rate.

The Effect of Substrate Particle Size on Rheology of Sawdust Slurries:

Initial Viscosity Measurements Prior to Reaction:

The effect of the initial particle size of the substrate on the slurry viscosity is studied for the size ranges $33 \mu\text{m} < x \leq 75 \mu\text{m}$, $75 \mu\text{m} < x \leq 104 \mu\text{m}$, $104 \mu\text{m} < x \leq 150 \mu\text{m}$, $150 \mu\text{m} < x \leq 180 \mu\text{m}$ for equivalent initial solids concentrations. The sawdust particulate suspensions are observed to be pseudoplastic in nature, for which the viscosity decreases with increasing shear rate, as shown in Figure 13 for various particle size ranges. The viscosity data in Figure 13 also reveal that slurries with larger size particles have higher viscosities. For instance, for the sawdust slurry with 13% initial solids concentration, as the particle size range decreases from $150 \mu\text{m} < x \leq 180 \mu\text{m}$ to $33 \mu\text{m} < x \leq 75 \mu\text{m}$, a significant drop in viscosity occurs from 16500 cP to 206 cP at 10 s^{-1} shear

rate. The reason for this significant difference in viscosity with varying particle size is attributed to the nature of the particle-particle interactions, which is discussed later in this section.

As discussed in the Literature Review, the rheological behavior of biomass slurries can be modeled by using the Oswald power law (Equation 4 & 5). The power law fit for the viscosity data for the particle size range $33 \mu\text{m} < x \leq 75 \mu\text{m}$ is shown in Figure 13. The regression coefficient, R^2 and the two power law parameters, consistency index- K ($\text{Pa}\cdot\text{s}^n$) and flow behavior index- n , are presented in Table 12 for all the data curves. The value of the consistency index, K , varies directly with the slurry viscosity, so slurries with larger size particles have higher K values. The flow index numbers (n) for pseudoplastic (shear thinning) materials have values less than 1 (Uhl and Gray, 1966), and the data shown here for sawdust slurries indicate that they are shear thinning fluids.

Table 12

Power Law Model Parameters for Sawdust Slurries With 13% Initial Solids at '0' Hour for Various Particle Size Ranges

	$33 \mu\text{m} < x \leq 75 \mu\text{m}$	$75 \mu\text{m} < x \leq 104 \mu\text{m}$	$104 \mu\text{m} < x \leq 150 \mu\text{m}$	$150 \mu\text{m} < x \leq 180 \mu\text{m}$
R^2	0.9668	0.9903	0.9935	0.9911
$K (\text{Pa}\cdot\text{s}^n \times 10^3)$	0.8266	157.5	181.814	227.305
n	0.4681	-0.1973	-0.2071	-0.1509

Table 13

Power Law Model Parameters for Sawdust Slurries With 10% Initial Solids at '0' Hour for Various Particle Size Ranges

	$33 \mu\text{m} < x \leq 75 \mu\text{m}$	$75 \mu\text{m} < x \leq 104 \mu\text{m}$	$104 \mu\text{m} < x \leq 150 \mu\text{m}$	$150 \mu\text{m} < x \leq 180 \mu\text{m}$
R^2	0.8952	0.9863	0.9874	0.9696
$K (\text{Pa}\cdot\text{s}^n \times 10^5)$	0.2936	5.874	12.369	70.29
n	0.4553	0.1238	-0.0278	-0.2538

The power law model parameters for 10% initial solids concentration with various particles size ranges at time '0' hour, are presented in Table 13.

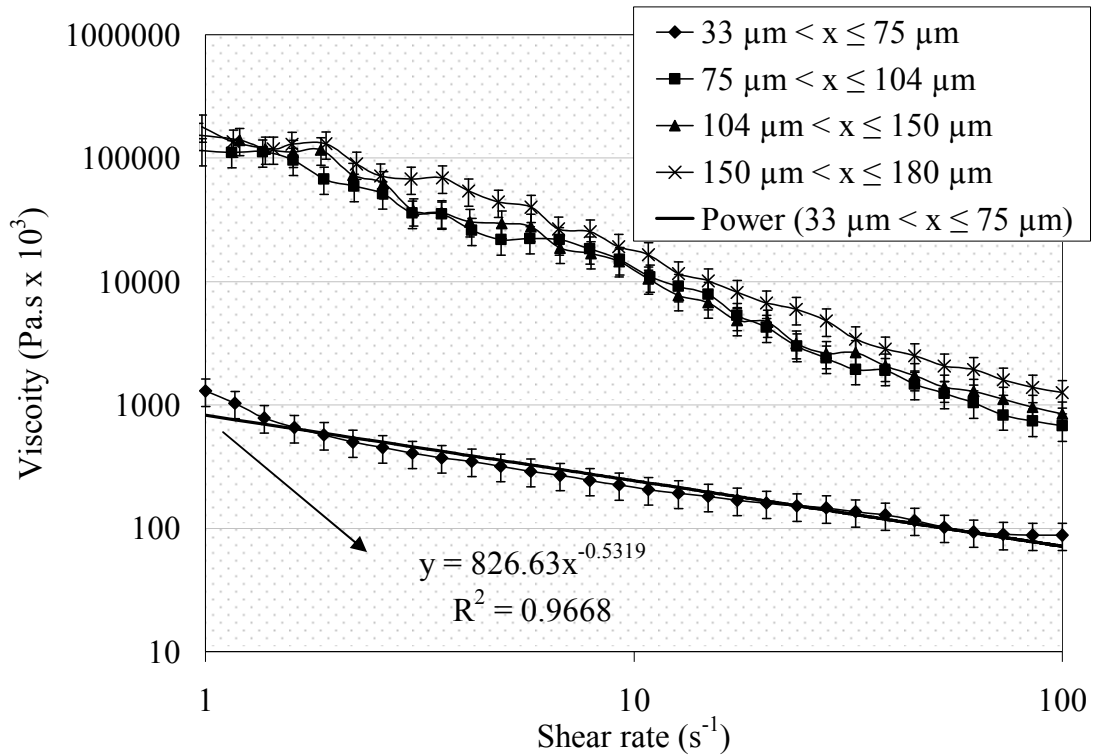


Figure 13. Viscosity vs. shear rate ($t = 0$ hr, 13% initial solids concentration) and the power law fit.

A fiber, by definition, is a particle which has a length more than 3 times its diameter or width. Cellulose fibers of sawdust are observed with a SEM (scanning electron microscope) to have branched surface fibers attached to the main fiber. The SEM images of the particle size ranges $33 \mu\text{m} < x \leq 75 \mu\text{m}$ and $590 \mu\text{m} < x \leq 850 \mu\text{m}$ are shown in Figure 14. It is noticed that larger size particles ($590 \mu\text{m} < x \leq 850 \mu\text{m}$) have larger side branch fibers and smaller size particles ($33 \mu\text{m} < x \leq 75 \mu\text{m}$) have few or no side branch fibers. It is to be noted that the images shown in Figure 14 are at different magnification for the purpose of a better visual illustration. It is also observed that the

particle surface is very rough. Thus, it is reasoned that larger particles have more friction between them than smaller particles leading to higher viscosity for an equivalent mass of solids.

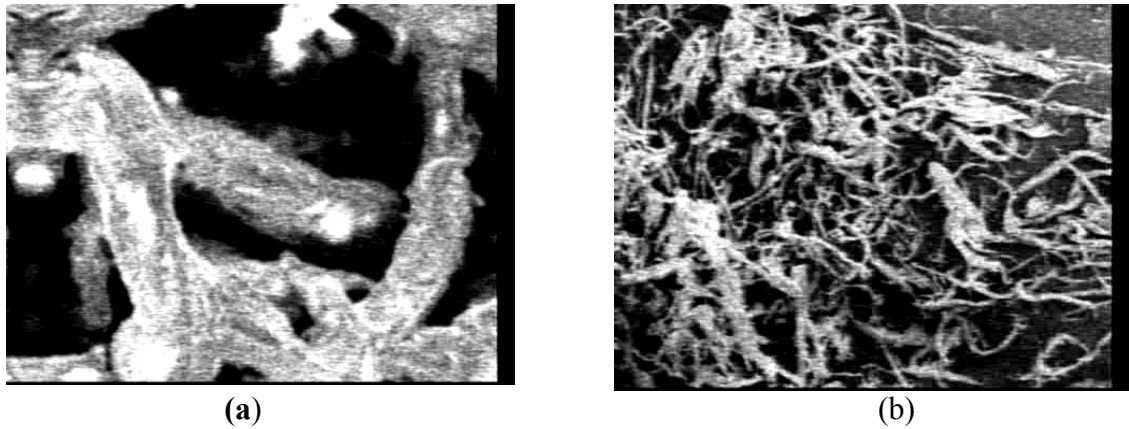


Figure 14. SEM images of sawdust particles.

(a) $33 \mu\text{m} < x \leq 75 \mu\text{m}$, 3500x magnification **(b)** $590 \mu\text{m} < x \leq 850 \mu\text{m}$, 35x magnification

It is also speculated that, when in solution, the sawdust particles entangle with each other because of the highly branched surface fibers which leads to increased resistance to flow. Since the larger particles are observed to have more and longer surface fibers, this causes larger resistance to flow resulting in higher viscosities, which explains the increase in the viscosity proportional to the particle size in Figure 13. The entanglement between the fibers increases with the solids concentration which leads to a complex mesh like structure. This imparts a highly non-Newtonian nature to the slurry and causes a drastic increase in viscosity. Luc et al. (2006) have identified that the viscosity of wood fiber pulp, which is used in paper manufacturing, is an indirect

measure of the fiber length. They found that the slurries with a longer average fiber length have a higher degree of polymerization and higher viscosity.

The trend of increasing viscosity for increasing size of biomass particles contradicts the trend seen in coal-water slurries. Unlike in sawdust particle slurries, the viscosity of coal-water slurries is seen to be inversely proportional to the coal particle size (Logos, 1996; Majumder, 2006 and Turian, 2002). The proposed reason is that the coal particles are spherical in shape and do not have entangled fibers on their surface. The primary reason for resistance to flow in coal-water slurries is the friction between the particles which is proportional to the external surface area of the particles, and so the friction is higher for smaller size particles which have a higher surface area to volume ratio.

Since power consumption is proportional to viscosity, and smaller size particles result in lower viscosity, operating with smaller initial particle sizes is a way to reduce the slurry viscosity during processing and, therefore, lower operating costs. Also, smaller size particles can achieve higher rates of glucose release and extents since they consist of more surface area than larger size particles for an equivalent amount of mass. Starting with lower viscosity also leads to better heat and mass transfer characteristics in the reaction media and, therefore, faster reaction rates.

Figure 15 demonstrates the increase in viscosity of the slurry due to the increase in solids concentration for the particle size range $33 \mu\text{m} < x \leq 75 \mu\text{m}$. The 19% sawdust solids concentration for the particle size range $33 \mu\text{m} < x \leq 75 \mu\text{m}$ is extremely viscous; the vane impeller of the MCR viscometer starts to form a channel without actually mixing the slurry between the edge of the vane and the wall of the viscometer cup. The

collection of viscosity data is not performed for solids concentrations higher than 19% as the data would not be reliable for this reason. The power law model parameters for the data in Figure 14 are presented in Appendix A.

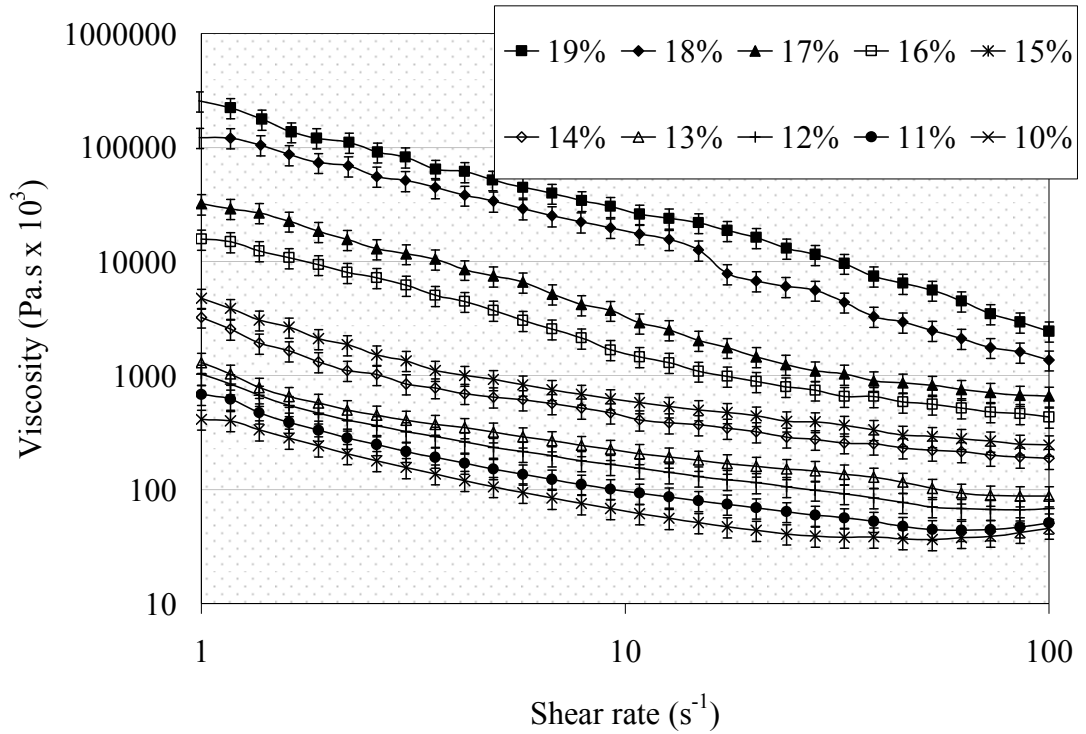


Figure 15. Viscosity vs. shear rate for various initial solids concentrations (time = 0 hr, size range = $33 \mu\text{m} < x \leq 75 \mu\text{m}$).

As is common with many non-Newtonian fluids, the rheological behavior of the sawdust slurries becomes less associated with shear above and below certain applied shear rates. In the cases studied here, these shear rates are near 85 s^{-1} and 1 s^{-1} , but the exact shear rate appears to depend on the initial solids concentration (Figure 15). This phenomena occurs above 85 s^{-1} and below 1 s^{-1} for solids concentrations of 18% and higher in the case of sawdust slurries. This is why the viscosity does not appear to change with shear rate for the 18% and 19% cases in Figure 15. The same effect also appears to

be independent of the time of the saccharification reaction (Figure 16), with a steadying of the viscosity above a shear near 40 s^{-1} . The viscosity actually appears to increase slightly with increasing shear above this point, but the apparent effect is likely due to better stirring in the viscometer cup at the higher rotation rate of the impeller which may better suspend the solids.

The shear thinning nature of the material is explained by Ebeling *et al.* (1999), who reported that the cellulose microcrystal orientation is dependent on the shear rate. At a shear rate above a certain value, the microcrystals align horizontally along the shear direction as do the cellulose fibers in a similar way. At a certain degree of fiber alignment, the resistance to flow becomes approximately constant, and hence, viscosity stops changing. As a side note, the orientation phenomenon is completely reversible (Eriksson, 2002).

Discrete Viscosity Measurements During the Saccharification Reaction:

The viscosity data throughout saccharification tests on sawdust slurries for various particle size ranges ($33 \mu\text{m} < x \leq 75 \mu\text{m}$, $75 \mu\text{m} < x \leq 104 \mu\text{m}$, $104 \mu\text{m} < x \leq 150 \mu\text{m}$ and $150 \mu\text{m} < x \leq 180 \mu\text{m}$) with 10% and 13% initial solids concentrations are collected over a 72 hour period. The viscosity data for the size range $33 \mu\text{m} < x \leq 75 \mu\text{m}$ with 13% initial solids concentration is shown in Figure 16 over a range of shear rates from $1 - 100 \text{ s}^{-1}$; the power law model parameters are presented in Table 14. Plots and power law model parameters for other particle size ranges with 10% and 13% initial sawdust solids concentration are presented in Appendix A.

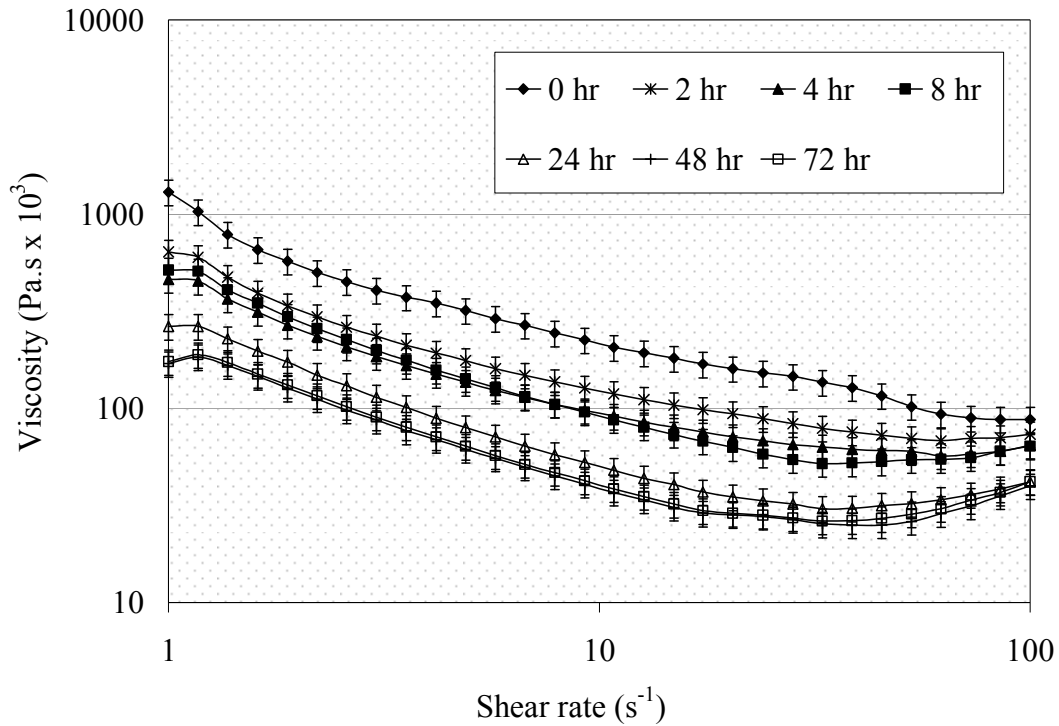


Figure 16. Viscosity vs. shear rate at different times during enzymatic saccharification (Size range: $33 \mu\text{m} < x \leq 75 \mu\text{m}$, 13% initial solids concentration).

Supporting the fact that 70% of the overall glucose release in 72 hours is obtained in the first 8 hours of the saccharification reaction, a significant drop in slurry viscosity is observed within the first 8 hours of the saccharification reaction. For instance, the viscosity drops from 206 cP to 87.4 cP at a shear rate of 10 s^{-1} within the first 8 hours of the reaction, which is about 70% of the total drop after 72 hours. The drop in viscosity is due to a combination of the decrease in solids concentration and the fragmentation of the cellulose particles (Peters, 1991). As the saccharification reaction proceeds, the particles break down into smaller particles and eventually the undissolved cellulose particles are converted into dissolved glucose. A similar trend, decrease in viscosity over saccharification reaction time, for other particle size ranges ($75 \mu\text{m} < x \leq 104 \mu\text{m}$, 104

$\mu\text{m} < x \leq 150 \mu\text{m}$ and $150 \mu\text{m} < x \leq 180 \mu\text{m}$) with 13% and 10% initial solids is observed. The viscosity vs. reaction time plots for these data and the power law model parameters are presented in Appendix A.

Continuous Viscosity Measurements During the Saccharification Reaction:

The studies on rheology of sawdust slurries during the enzymatic saccharification revealed that the drop in viscosity is most dramatic during the initial hours of the reaction due to higher reaction rates at the beginning. From the data shown in Appendix A, for the 10% initial solids slurry with the three larger size ranges ($75 \mu\text{m} < x \leq 104 \mu\text{m}$, $104 \mu\text{m} < x \leq 150 \mu\text{m}$, $150 \mu\text{m} < x \leq 180 \mu\text{m}$), 96% of the initial viscosity is reduced within the first 24 hours of the saccharification reaction whereas only 76% of the initial viscosity is reduced for the smaller size particles ($33 \mu\text{m} < x \leq 75 \mu\text{m}$). Thus, in order to better track the viscosity change during the initial stage of the enzymatic saccharification reaction, viscosity is measured at 10 minute intervals during the first 12 hours of the reaction.

For the purpose of obtaining continuous viscosity data, a single shear rate must be chosen. Viscosity measurements of the sawdust slurries are measured at a low steady-state shear rate of 10 s^{-1} , which is in the approximate shear rate range of a very slow mixing vessel such as the HSBR or the SSBR to be tested here. Slurries with a particle size range of $150 \mu\text{m} < x \leq 180 \mu\text{m}$ with an initial solids concentration of 13% and slurries with a particle size range of $33 \mu\text{m} < x \leq 75 \mu\text{m}$ with an initial solids concentration of 10% are investigated at an applied shear rate of 10 s^{-1} .

Table 14

Power Law Model Parameters for Sawdust Slurries With 13% Initial Solids ($33 \mu\text{m} < x \leq 75 \mu\text{m}$) Concentration at Various Times of

Enzymatic Saccharification

	0 hour	2 hours	4 hours	8 hours	24 hours	48 hours	72 hours
R²	0.9668	0.9267	0.908	0.8963	0.8269	0.8207	0.8118
K (Pa·sⁿ x 10³)	0.8266	0.4347	0.3275	0.3663	0.1963	0.1379	0.1416
n	0.4681	0.527	0.5744	0.4918	0.5208	0.5697	0.5754

These two sets have the highest and the lowest viscosities in the range studied so a wide spectrum of viscosities can be covered to investigate the continuous viscosity changes. The viscosity data during the enzymatic saccharification are shown in Figure 17 and Figure 18.

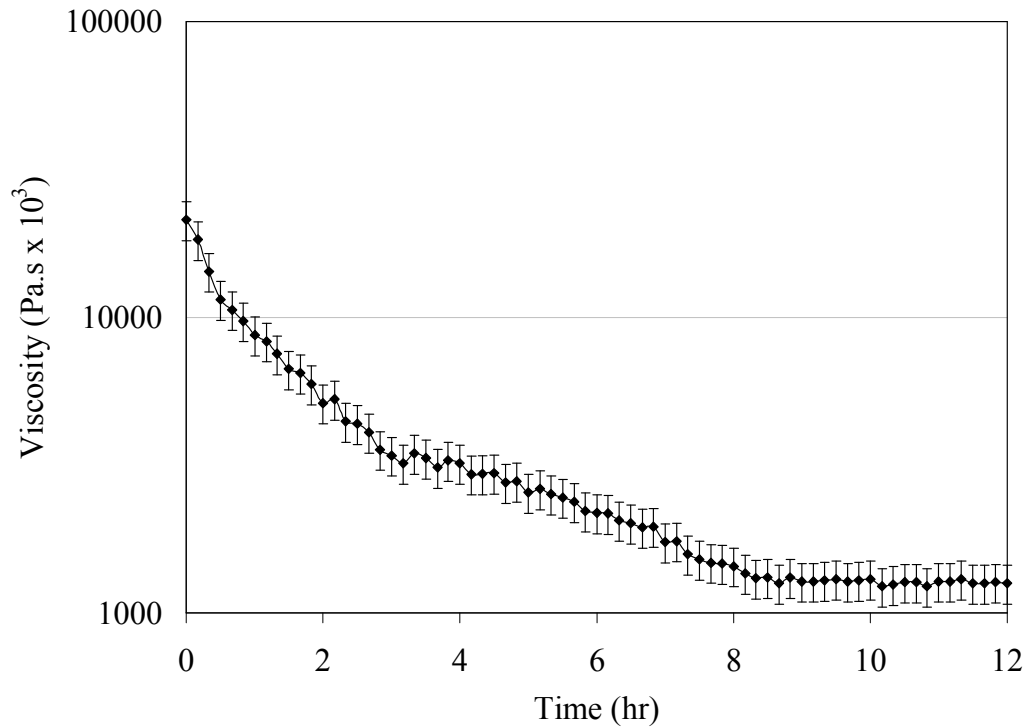


Figure 17. Continuous viscosity vs. time measurement (13% initial solids concentration, $150 \mu\text{m} < x \leq 180 \mu\text{m}$, 10 s^{-1}).

From these figures it can be seen that the biggest drop in viscosity occurs in the first 8.5 hours of the saccharification reaction, indicating the fastest reaction kinetics are actually occurring in this first 8.5 hour period. This observation supports the higher glucose yields during the initial stage of enzymatic saccharification discussed in the beginning of this chapter. The viscosity drop is more obvious for the slurry with the particle size range of $150 \mu\text{m} < x \leq 180 \mu\text{m}$ than for the slurry with the particle size range

of $33 \mu\text{m} < x \leq 75 \mu\text{m}$. For the size range $150 \mu\text{m} < x \leq 180 \mu\text{m}$, 94% of the initial viscosity is reduced within the first 8.5 hours of the saccharification reaction whereas only 47% of the initial viscosity is reduced for the smaller size particles, $33 \mu\text{m} < x \leq 75 \mu\text{m}$.

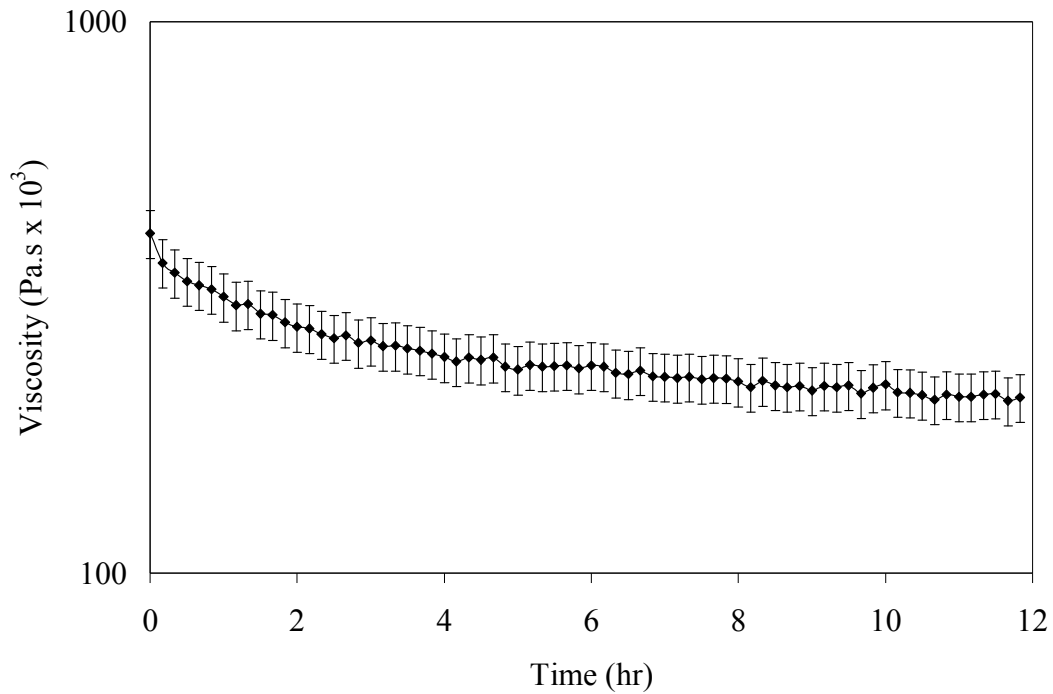
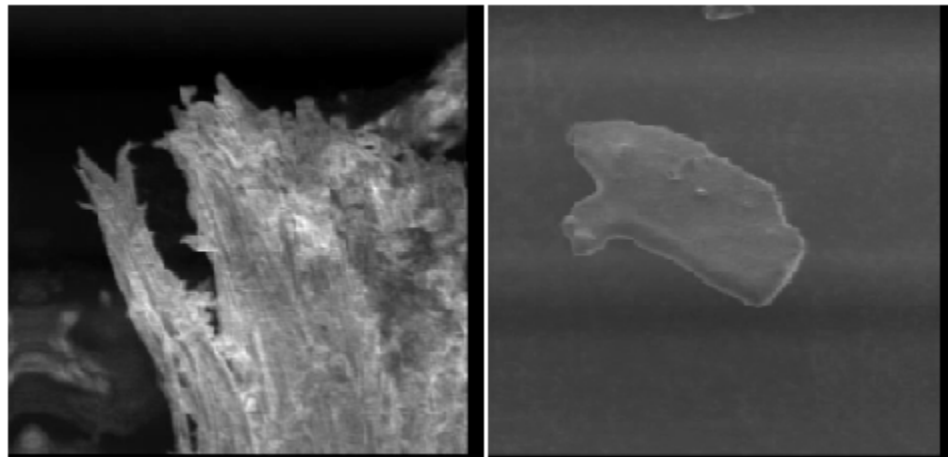


Figure 18. Continuous viscosity vs. time measurement (10% initial solids concentration, $33 \mu\text{m} < x \leq 75 \mu\text{m}$, 10 s^{-1}).

The SEM images of the particle size range $150 \mu\text{m} < x \leq 180 \mu\text{m}$ at 0 hour and at 8 hours of the saccharification reaction are shown in Figure 19. It can be noticed that most or all of the branched surface fibers disappeared after 8 hours. The surface fibers are supposedly amorphous in nature which is more rapidly digested by the enzyme. The enzyme also has more access to substrate area on these amorphous surface fibers. Therefore, glucose is released at faster rate during this initial stage of saccharification

because of the digestion of the amorphous surface fibers. The sawdust particles are seen to have a smoother surface after 8 hours because of the digestion of the surface fibers. This allows the particles to slide by each other with less resistance to flow, and thus, leads to the rapid decrease in viscosity.



(a)

(b)

Figure 19. SEM images (1000x magnification) of sawdust particles with the size range $150 \mu\text{m} < x \leq 180 \mu\text{m}$ **(a)** '0' hour **(b)** '8' hour

Peters *et al.* (1991) reported that the rate of cellulose fragmentation which results in smaller fragments is higher for larger size particles. Results here show that the smaller size particles display a slower rate of viscosity drop. So, it is expected that the higher the rate of cellulose fragmentation, the faster the drop in viscosity of the slurry. This explains the faster viscosity drop in the first 8 hours for larger size particles.

CHAPTER V

SACCHARIFICATION USING THE SCRAPED SURFACE BIO-REACTOR

MATERIALS AND METHODS

Cellulose Substrate and Enzyme:

Dilute acid pretreated corn stover, batch # P041116CS and batch # P065104CS, supplied by the National Renewable Energy Laboratory is used as the cellulose substrate in these experiments. The corn stover solids are comprised of 60% cellulose, 5% hemicellulose, and 32% lignin. Ash and protein account for the remaining portion. Prior to testing, the corn stover solids are washed with distilled water equal to 10 times the weight of the solids and are dried by vacuum filtering. The washing and filtering process is repeated three times. Spezyme CP cellulase enzyme from Genencore International Inc (Rochester, NY) from Lot # 301-05021-011 is used with a concentration of 15FPU / g of cellulose.

Processing of corn stover is performed in a 1 M citrate buffer which is prepared by adjusting the pH to 4.8 with NaOH as given in the NREL standard procedure LAP 006, and is diluted to 5% of the total mass to yield an effective molality of 0.05 mol/kg.

Saccharification Procedure:

The experiments, both batch and semi-batch, with corn stover as substrate are performed in an 8L Scraped Surface Bio-Reactor (SSBR) with a working mass of 6 kg. The reactor description and its components are described in the following sections. The enzymatic saccharification reaction is performed in shake flasks with identical conditions as those in the SSBR for all tests in the Innova 4230 incubator shaker at 250 rpm and with a working mass of 100 grams at a temperature of 50 °C. The empty SSBR and the empty shake flasks are autoclaved at 120⁰ C for 20 minutes before use. Sterile conditions in the reaction mixture are maintained with Cycloheximide and Tetracycline in 70% ethanol as given in the NREL standard procedure LAP 009. The operating temperature (50 °C) and the pH (5) for Spezyme CP Cellulase enzyme are based on the optimum conditions as specified by the manufacturer.

Sampling and Sugar Measurement:

Corn stover slurry samples are collected from three positions in the SSBR: the two sampling ports and the feeding port. To collect corn stover samples, tips of 1 mL Fisher Scientific sterile pipettes are broken off in order to handle suctioning of the thick slurry with the pipettor (Drummond Scientific Co., Broomall, PA). The storage and measurement methods of the glucose samples are similar to those with sawdust slurry samples. Glucose concentration is measured with a YSI-2700 bio-chemistry analyzer (Yellow Springs, OH). Sugar values reported for corn stover samples from the SSBR are an average of the samples taken from the three sampling locations. All enzymatic

saccharification experiments are performed in duplicate and the average results are presented.

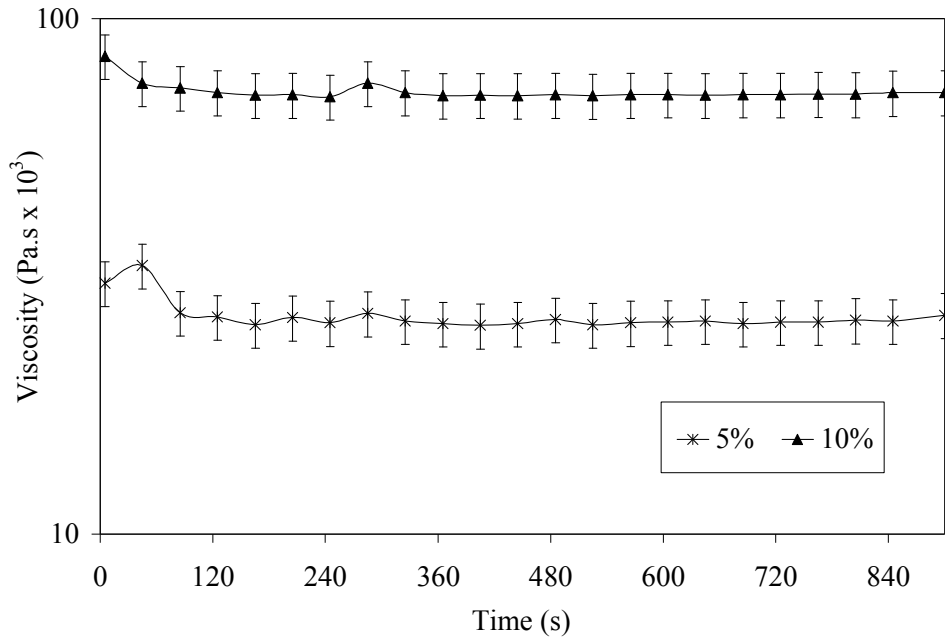
Viscosity Measurements:

The slurry viscosity of each sample is measured with an Anton Parr Modular Compact Rheometer (Ashland, VA), which is described in Chapter IV. The viscosity of the corn stover slurry is measured at the same time intervals as the glucose measurements. The reaction is initiated in several shake flasks of identical content, and one flask is used at each time interval for the viscosity measurement. The contents of the shake flask are disposed of after the viscosity measurement. Samples collected from the SSBR are returned to the reactor after viscosity measurements in order to maintain a constant volume so as not to affect the torque measurements.

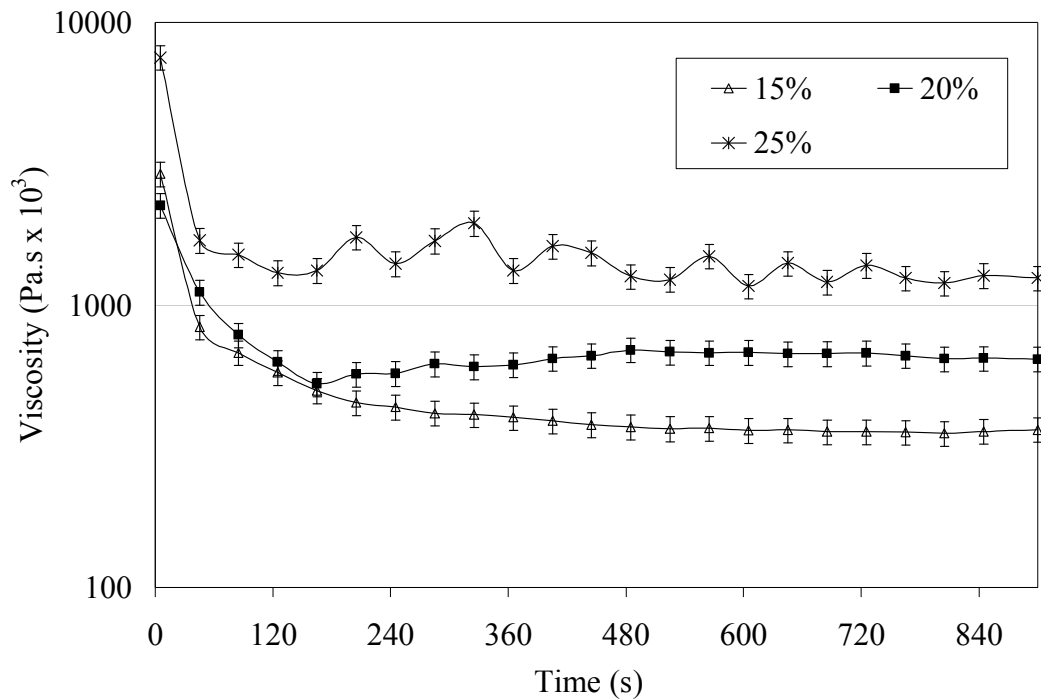
The viscosity is measured over the shear rate range of $0.1\text{-}100\text{ s}^{-1}$ for PCS slurries. Each viscosity value is an average of two sweeps between the reported shear rates range. Similar to sawdust slurry viscosity measurements, premixing is also necessary for PCS slurries in order to achieve steady state viscosity of the slurry and a uniform solids suspension. The minimum speed required to suspend all the biomass solid particles in the viscometer cup is estimated from the Pavlushenko *et al.* (1957) correlation (Equation 7) based on the geometry of the viscometer cup, vane impeller, and the material properties. The rotational speed of the impeller estimated from Equation (7) is about 370 rpm, which corresponds to a shear rate of 180 s^{-1} in the viscometer. The Rheoplus, the MCR supporting software to record viscosity data online, converts impeller speed to the corresponding shear rate and vice versa. The Pavlushenko *et. al.* correlation was actually

developed for large mixing tanks with larger impeller clearances. However, the viscometer cup and vane impeller system has a very small clearance and requires a lower speed than the estimated value. Hence, all the viscosity measurements are performed with premixing at a shear rate value of 160 s^{-1} .

The premixing of PCS slurries with various initial solids concentrations is performed in the viscometer cup for 15 minutes at 160 s^{-1} , in order to determine the time required to establish the steady state viscosity. The transient viscosities for the 5% and 10% PCS slurries exhibit much less of a change from the zero hour viscosities, plus the magnitudes are one to two orders less than the 15%, 20%, and 25% viscosities, so the premixing test data are shown separately in Figures 20 & 21. It is noticed that the viscosity reaches a steady state value for 5% and 10% solids after about 3 minutes and for 15, 20, & 25% after about 6 minutes. However, all the slurries are premixed for 6 minutes prior to the viscosity measurements in order to maintain consistency.



Figures 20. Premixing test for 5% and 10% PCS slurries at 160 s^{-1} .



Figures 21. Premixing test for 15, 20 & 25% PCS slurries at 160 s^{-1} .

Reactor and Torque Sensor Assembly:

The custom built SSBR (shown in Figure 22) is 58.5 cm long with a diameter of 13.9 cm. It has three scraping blades that are spaced 120° apart and are staggered along the length of the shaft in three segments. The blades are attached to a central shaft which is 2.55 cm in diameter and 64.5 cm long. Each blade is 18.5 cm long and 3.2 cm wide with a thickness of 0.8 cm. The reactor has two sampling ports with a diameter of 1.7 cm located 9 cm from each end, and a rectangular feeding port at the center with dimensions of 7.62 cm by 5.08 cm that can also be used for sampling. The cylinder is made of Pyrex glass, and the shaft and blades are made of stainless steel. A 5 mm wide styrene rubber strip is attached along the length of each blade which scrapes the interior of the cylinder

surface. The ends of the reactor are covered with aluminum lids containing ball bearings on which the rotating shaft rests.

The shaft is driven by an electrical DC motor with a range of 0-10 rpm. The DC motor drive and the reactor shaft are coupled with a rotating slip ring torque sensor from Sensor Developing Inc. (Orion, MI). The torque sensor has a hand held Peak Tracking Instrument that displays the torque exerted on the reactor shaft. The entire assembly is seen in Figure 23. The reactor is operated at 2 rpm for all tests in order to minimize power consumption while still maintaining good mixing.

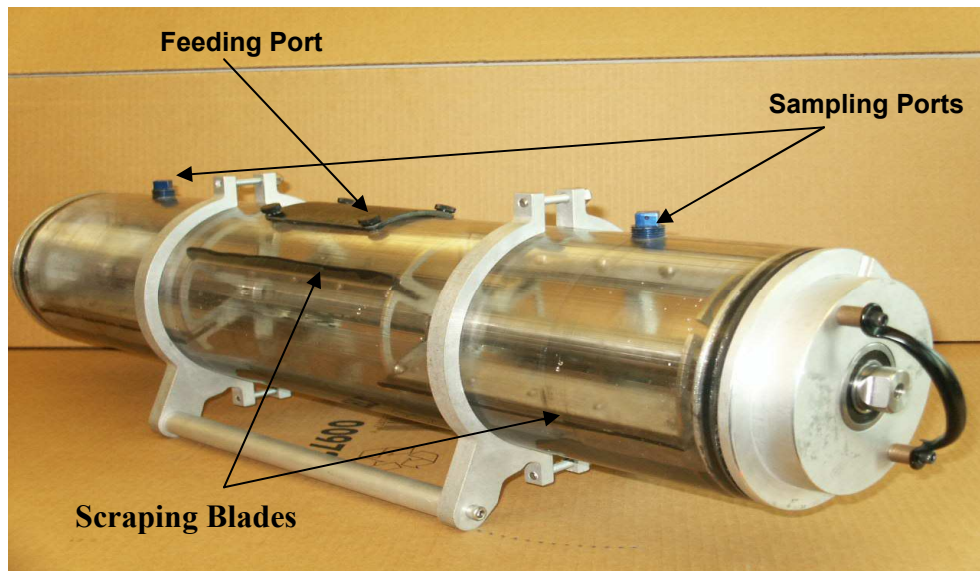


Figure 22. Scraped Surface Bio-Reactor.

The reactor and torque sensor assembly resides in a custom incubator. The incubator consists of a wood frame covered with 15 mm Styrofoam sheets, thermostat, heater, and plexiglass window. The temperature in the incubator and, thereby, reaction

medium in the reactor is maintained at a constant 50 °C. The air-heated incubator allows for a well controlled environment for testing purposes. At larger scale, an insulated heating jacket around the reactor can be used to maintain the operating temperature.

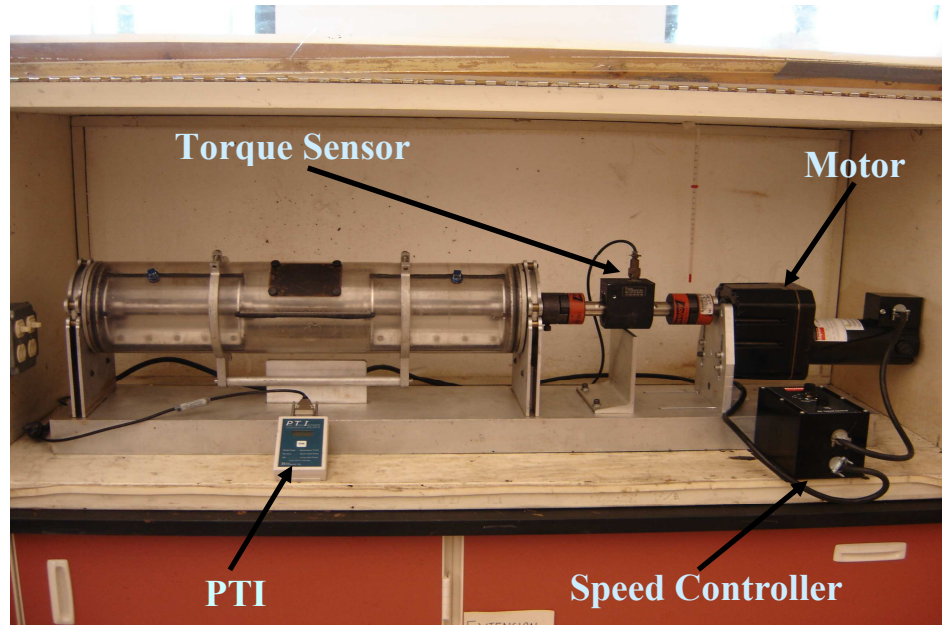


Figure 23. Reactor and torque assembly inside the insulation box.

RESULTS AND DISCUSSION

Saccharification of PCS Slurries in the SSBR:

The investigation using sawdust as a substrate revealed that processing with untreated sawdust results in a glucose release amount of no more than 40-45% of the theoretical maximum during enzymatic saccharification. Hence, it is recommended to perform studies with pretreated biomass material; corn stover is chosen as the pretreated substrate for the present study.

Although it was noticed from untreated sawdust experiments that lower particle size substrate resulted in higher amounts of glucose release, the pretreated corn stover substrate is not separated into different particle size ranges because of the difficulty in sieving wet material. Nevertheless, the particles typically undergo a spontaneous size reduction during chemical pretreatment. Particle size measurements on PCS solids indicate that the average particle size is 30 μ m following chemical pretreatment. This size is on the order of the lowest particle size range for the studies with untreated sawdust. The aim of the studies with PCS is to investigate the effectiveness of the bench scale reactor (SSBR) as a potential large-scale design that is capable of efficiently processing high solids slurries with reasonable low power requirements. Results are compared to laboratory scale tests in shaker flasks. Enzymatic saccharification with a range of low to high solids concentrations is tested, and the rheological behavior of the PCS slurries and the power consumption patterns are investigated.

Effect of Initial Solids Loading on Enzymatic Saccharification

Enzymatic saccharification experiments are performed on PCS solids with various initial solids concentrations. Experiments are performed in two modes of processing, batch and semi-batch. Results obtained in the SSBR are compared to laboratory scale shake flasks.

Saccharification with Batch Loading:

The batch saccharification tests are conducted with 10, 15, 20 and 25% PCS solids concentrations. Glucose release as a percentage of the theoretical maximum versus time is seen in Figure 24a for tests in the SSBR. The reaction rate trend during enzymatic saccharification in the SSBR is similar to that observed in saccharification reaction with sawdust slurries. The rate of glucose release is rapid during the initial hours of the reaction, and then the rate decreases as the reaction order increases to higher order kinetics somewhere between 8 and 12 hours as the final glucose release percentage asymptotes to some value less than 100%. The postulated reasons for the decrease in the rate of enzymatic saccharification reaction over time are: increase in the fraction of crystallinity, decrease in surface area, product inhibition on enzymes, and enzyme deactivation. The same reasons are outlined in the Results & Discussion of Chapter IV. Sarkar (2001) reported that the saccharification rate in a continuous reactor with three flow rates (0.12, 0.36 and 0.84 L/min) declined by 78-82% after the first two hours of reaction for raw cotton fibers with cellulase enzyme. Ooshima (1990) showed for pretreated wood with various initial solids concentrations (5, 10 and 15%) that the available surface area would be only 20% by the time 50% of the theoretical glucose

release was achieved and indicated that this trend was independent of solids concentration.

The rate and the final extent of glucose release decreases as the initial solids concentration increases. A similar plot for batch saccharification in shake flasks with various initial solids concentrations is presented in Appendix B. This drop in rate is likely due to poor diffusion of enzymes between substrate particles due to the lack of free water at higher solids concentrations. The drop in rate may also be partially attributed to inhibited mass and heat transfer in viscous slurries

Similar to saccharification of sawdust slurries, glucose yields between 30-55% of the maximum amount that can be achieved in 72 hours, depending on the initial solids concentration, are obtained during the first 8 hours. At 72 hours, the amount of glucose released has reached about 90% of the amount released in 168 hours. It takes an additional 96 hours for the final 10% to be released. The amounts of glucose release during the initial 8 hours of the reaction are presented in Table 15 as a percentage of the actual amount that is released in 72 hours in both the SSBR and shake flask (shake flask data is shown in Figure 24b and Appendix B and discussed in more detail later). As the solids concentration increases in the shake flask, the glucose release during the first 8 hours decreases. This is because the amount of free water decreases with increasing solids concentration which leads to inefficient mixing of the slurry. The percentage of glucose released during the first 8 hours is approximately equal for all solids concentrations except for the 10% solids slurry in the SSBR. Less glucose is released during the first 8 hours in the SSBR as compared to the shake flask except for the 25% solids slurry. However, more glucose release is noticed in the SSBR than in the shake

flask after 24 hours until the end of the test, for all solids concentrations. Rotational speeds higher than 2 rpm may help achieve greater glucose release during the initial hours.

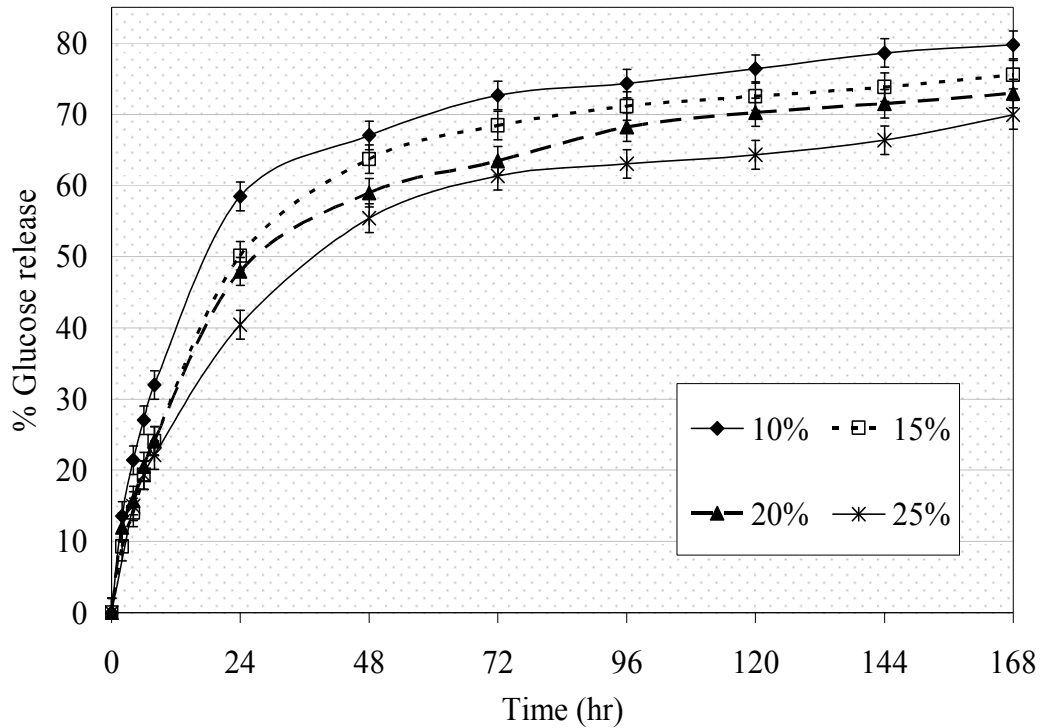


Figure 24a. Glucose release during batch enzymatic saccharification in the SSBR with various initial PCS solids concentrations.

In Figure 24b, amounts of glucose release are compared between a shake flask and the SSBR for batch testing with 25% initial PCS solids concentration. About 10% more glucose is produced in the SSBR than in shake flask over 168 hours of the saccharification reaction. Similarly, higher amounts of glucose release are achieved for saccharification experiments in the SSBR than in a shake flask with 10, 15 and 20% initial PCS solids concentrations; the data are presented in Appendix-B.

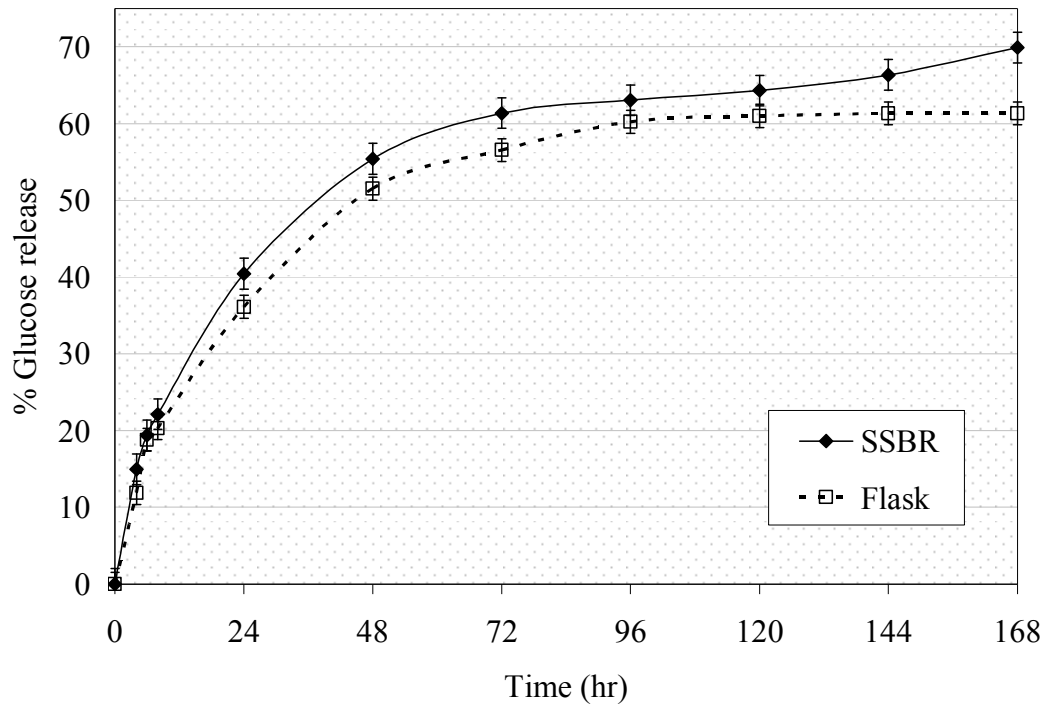


Figure 24b. Comparison of percent glucose release between the SSBR and the shake flask during enzymatic saccharification with 25% initial PCS solids concentrations.

Table 15

Glucose release during the First 8 Hours of Saccharification as a Percentage of the Actual Amount That is Released in 72 Hours

% Initial PCS solids	10	15	20	25
SSBR	44.0%	35.0%	37.6%	36.1%
Shake Flask	54.7%	46.7%	44.5%	36.2%

This highlights the advantage that the SSBR processing environment can provide, especially at higher solids concentrations. Higher amounts of glucose release in the SSBR is attributed to improved mixing and heat transfer due to the horizontal rotation and scraping of the reactor blades. With each rotation in the SSBR, material is scooped up by

the blades and then dropped back into the bulk slurry as the blades approach the top of the reactor. Random angular and radial intermixing of the material occurs in the SSBR that does not occur in shake flasks (and does not occur well in conventional stirred tank reactors with viscous slurries). Heat transfer is also improved due to the scraping action of the blades which prevent build-up of material on the heat transfer surface. A more uniform temperature distribution also exists throughout the slurry due to the mixing provided by the scraping blades.

Buchs *et al.* (2000b) reported that for high liquid viscosity conditions, a phenomenon called ‘out-of-phase’ occurs, which is characterized by the fact that the liquid does not follow the movement of the shaker and this phenomenon is used for later reference. It is postulated that a similar phenomenon might have occurred in the shake flask during saccharification with higher solids concentrations. In support of this postulate, visual observations of the 25% slurry in the shake flask revealed that the material is not moving with the path of the shaker, but rather exhibits no movement. Hence, no mixing occurs in shake flasks at solids concentrations higher than 20%.

Hodge (2006a) achieved higher amounts of glucose release in a bench scale reactor, the Bioflo 3000 (New Brunswick, New Jersey, U.S.A.), than in a shake flask with 10% initial PCS solids. However, lower amounts of glucose release were observed in the Bioflo than in shake flasks at and above 15% initial PCS solids concentration. They postulated that improved bulk mixing and inefficient control of temperature are the reasons for these two observations, respectively. The Bioflo 3000 with custom impellers such as a marine impeller or a Rushton turbine is designed for mixing of low viscous fluids only. In a simple mixing experiment with the Bioflo 3000, a clear unmixed or

stable outer ring of solids was observed at higher solids concentrations indicating that the Bioflo is not efficient for mixing of highly viscous slurries.

Hodge (2006b) was able to achieve 70% glucose release in a HSBR (high solids bioreactor) with 25% initial PCS solids concentration within 168 hours using an enzyme concentration of 20mg/mL (which corresponds to approximately 18 FPU, calculated based on FAO, 1997). However, 70% glucose release is achieved in 168 hours by using a lower enzyme amount, 15 FPU, in the SSBR tested here. This is an important result because reduction in enzyme usage can reduce the operating cost which is one of the major barriers for the commercialization of ethanol production from lignocellulosics.

Jorgensen (2007) used a liquefaction reactor to investigate the enzymatic saccharification of wheat straw. The reactor works similar to the SSBR, i.e., it rotates horizontally at very low speeds (3.3 to 11.5 rpm) at which the material mixing occurs based on the gravity of free falling material. The liquefaction reactor was able to achieve 50% glucose release within the first 96 hours with 25% dry matter. However, about 65% glucose release is achieved in the SSBR in 9 hours of saccharification with 25% initial insoluble PCS solids. The SSBR is operated at only 2 rpm, which is a lower speed than that of the liquefaction reactor. This is also an important result since the power consumption for mixing increases proportionally to the square of the rotational speed (N^2) in the laminar region and to the cube of the rotational speed (N^3) in the turbulent region (Tchobanoglous, 1991). At industrial scale it is vital to operate a reactor at as low a speed as possible so as to reduce operating costs of the plant.

The higher percentages of glucose release obtained in the SSBR as compared to the HSBR and liquefaction reactor are attributed to the better temperature control by

operating the reactor in an incubator and the improved heat transfer characteristics in the reaction medium by the scraping action of the blades. Unlike in the SSBR, the temperature in the HSBR and liquefaction reactor is only partly controlled by the use of heating water jackets. Deactivation of the enzyme occurs in conventional reactors due to very high shear rates as they need to be operated at higher rotational speeds in order to handle the high viscous slurries. However, the SSBR completely eliminates this factor as it is operated at 2 rpm which gives rise to very low shear rate values.

Rheology of PCS Slurries:

The rheological behavior of PCS slurries is extensively investigated in this research. The viscosity for slurries with various initial solids concentrations is measured using a Modular Compact Rheometer (MCR) with a cup and vane geometry as described in the Material and Methods of Chapter IV. The viscosity data at '0' hour for slurries with 10%, 15%, 20%, and 25% initial PCS solids concentrations are shown in Figure 25.

The rheological behavior of PCS slurries is observed to be shear thinning and can be fit to the power law model for non-Newtonian fluids. The viscosity curve for a 25% solids slurry at '0' hour is fit to the power law and shown in Figure 25. The power law model parameters for the 25% slurry viscosity and for the remaining curves (10%, 15%, and 20% viscosity data) are presented in Table 16. Similar to the sawdust slurries, the viscosity of PCS solids slurries increases with increasing solids concentration. Since the corn stover particles are fibrous, it can be postulated that an increase in viscosity is caused by the increase in the particle-particle interactions. As the solids concentration increases, the average distance between the particles in the slurry decreases, leading to a

drastic increase in the tangling of fibers, which results in more friction and resistance to flow and, therefore, leads to higher viscosity.

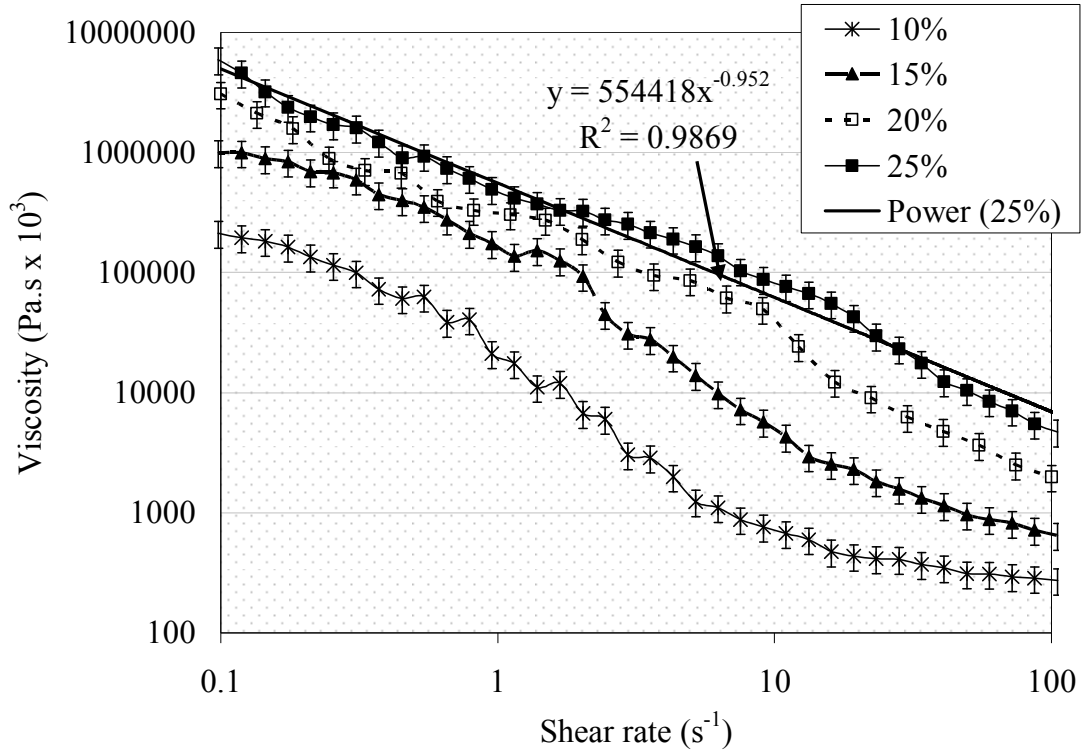


Figure 25. Viscosity vs. shear rate for PCS slurries with various initial solids concentrations at '0' hour.

Table 16

Power Law Parameters for Viscosity Data of PCS Slurries with Various Initial Solids Concentrations at '0' Hour

% Solids	10	15	20	25
R²	0.9612	0.9816	0.9848	0.9869
K (Pa·sⁿ x 10³)	18189	118850	292293	554418
n	-0.1289	-0.225	-0.0506	0.048

Rheology of PCS Slurries During Batch Saccharification:

Since the solids are being digested and the glucose becomes dissolved in liquid during enzymatic saccharification, the amount of insoluble solids decreases over time which leads to a reduction in slurry viscosity. The viscosity changes are tracked throughout the reaction for all batch saccharification tests in the SSBR and shake flasks. The viscosity change throughout the saccharification in the SSBR for 10% initial PCS solids concentration is presented in Figure 26 over a shear rate range of 0.1-100 s⁻¹.

Similar to the result with sawdust slurries, the viscosity drops considerably during the first 8 hours of the reaction. About 90% of the total viscosity reduction is achieved during the initial 8 hours of the reaction in the SSBR, however, only about 32% of glucose is released during the initial 8 hours. Although 32% is a high amount of glucose release for the first 8 hours of saccharification, based on the 90% drop in viscosity, a higher amount of glucose release should be expected. It is speculated that the viscosity change of a particulate slurry could be minimal below a certain substrate particle size, and this size range is achieved within the first 8 hours of the reaction. This is why the viscosity reduction is smaller after the first 8 hours although more glucose is released by further digestion of solids and size reduction in particle size. The point during the reaction when further viscosity changes are minimal is defined as the 'state of minimal change' for future reference.

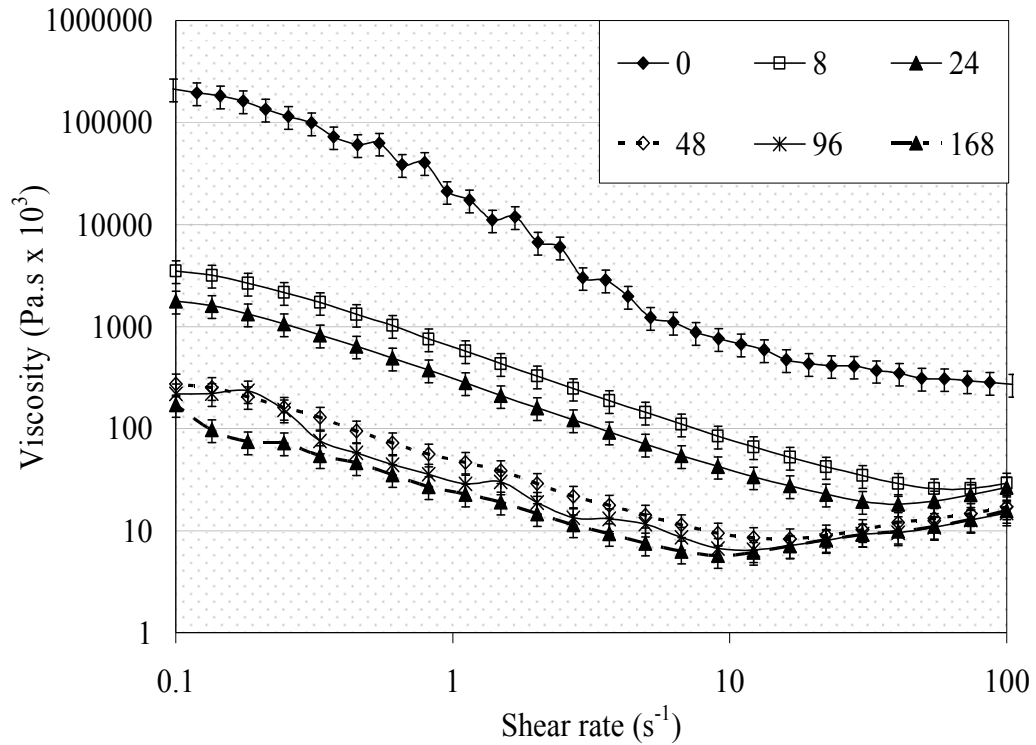


Figure 26. Viscosity changes throughout the saccharification reaction in the SSBR for 10% initial PCS solids concentration.

The viscosity changes during the saccharification reaction are tracked in shake flasks also, and the viscosity data for 10% initial solids is presented in Figure 27.

Since the PCS slurries are shear thinning, viscosity decreases with increasing shear rate. Similar to the effect seen in sawdust slurries, an increase in viscosity after a certain shear rate is also observed in PCS solids slurries. Figure 26 shows that for the 8 and 24 hour data curves, the increase in viscosity occurs at about 40s^{-1} , whereas for the last three data curves (48, 96, and 168 hours) the viscosity starts to increase at approximately 10 s^{-1} . This supports the speculation that this phenomenon (steadying or

increase of viscosity for non-Newtonian fluids above a certain shear rate) occurs at lower shear rates for low viscous slurries and at higher shear rates for high viscosity slurries.

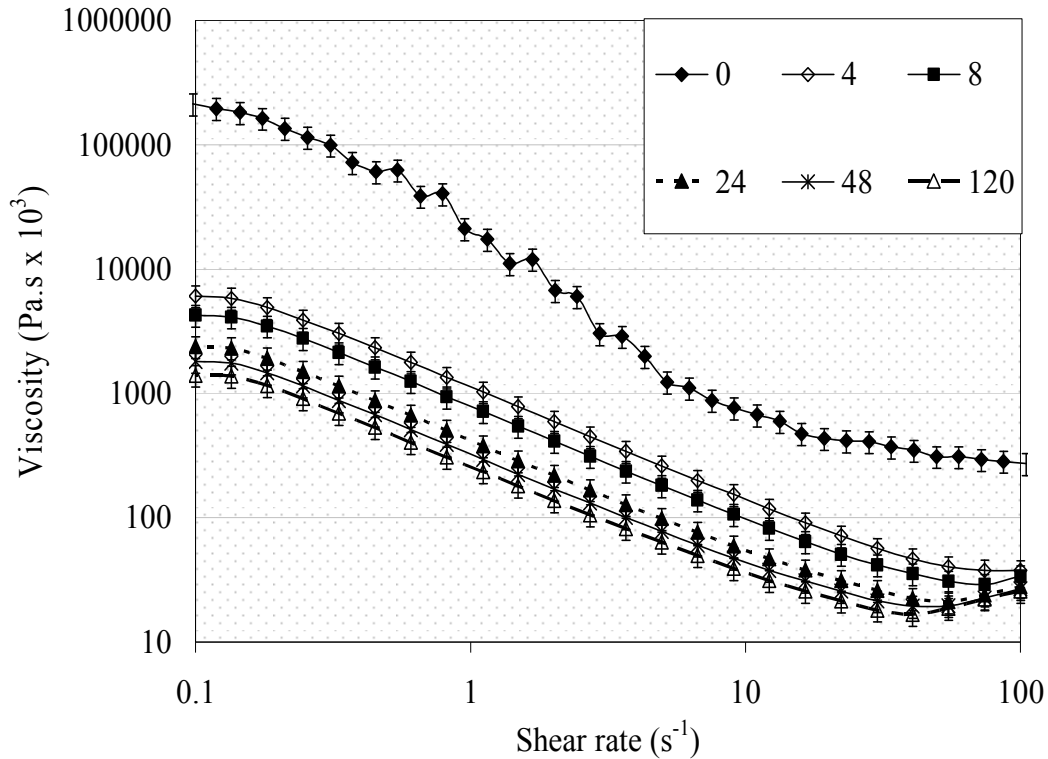


Figure 27. Viscosity changes throughout the saccharification reaction in the shake flask for 10% initial PCS solids concentration.

The viscosity data for the 10% PCS slurry during the saccharification reaction are fit to the power law model and the parameters are presented in Tables 17 and 18 for the SSBR and the shake flask, respectively. Since showing non-Newtonian viscosity at a single shear rate is not technically reasonable, the consistency index, K ($\text{Pa}\cdot\text{s}^n$), is plotted versus time in order to represent the viscosity drop in another way that may be better for visual depiction. The consistency index is plotted against reaction time for the SSBR and the shake flask in Figure 28. It can be noticed that the ‘K’ value becomes approximately

constant after about 48 hours for both the shake flask and the SSBR indicating that the slurry viscosity has reached its ‘state of minimal change’. The lower ‘K’ values (~ lower slurry viscosity) for the SSBR indicates that the solids are digested at a faster rate releasing more glucose, which supports the faster saccharification rate trends in the SSBR. The ‘K’ values (~slurry viscosity) appear to be increasing after about 144 hours which may be because of the increased glucose concentration leading to thickening of the slurry.

Table 17

Power Law Parameters for Viscosity Data During Enzymatic Saccharification of 10%

PCS Solids in the SSBR

Time	0	8	24	48	96	120	168
R²	0.9612	0.9867	0.9611	0.8226	0.7632	0.5298	6839
K (Pa·sⁿ x 10³)	18189	610.22	306.79	56.473	42.496	20.512	28.914
n	0.1289	0.1987	0.2593	0.4949	0.5107	0.6834	0.6163

Table 18

Power Law Parameters for Viscosity Data During Enzymatic Saccharification of 10%

PCS Solids in the Shake Flask

Time	0	4	8	24	48	120	168
R²	0.9612	0.9932	0.9885	0.9758	0.9671	0.9573	0.9836
K (Pa·sⁿ x 10³)	18189	1081.2	760.31	420.18	326.79	262.87	752.65
n	-0.1289	0.1722	0.1885	0.2312	0.2597	0.2849	0.2059

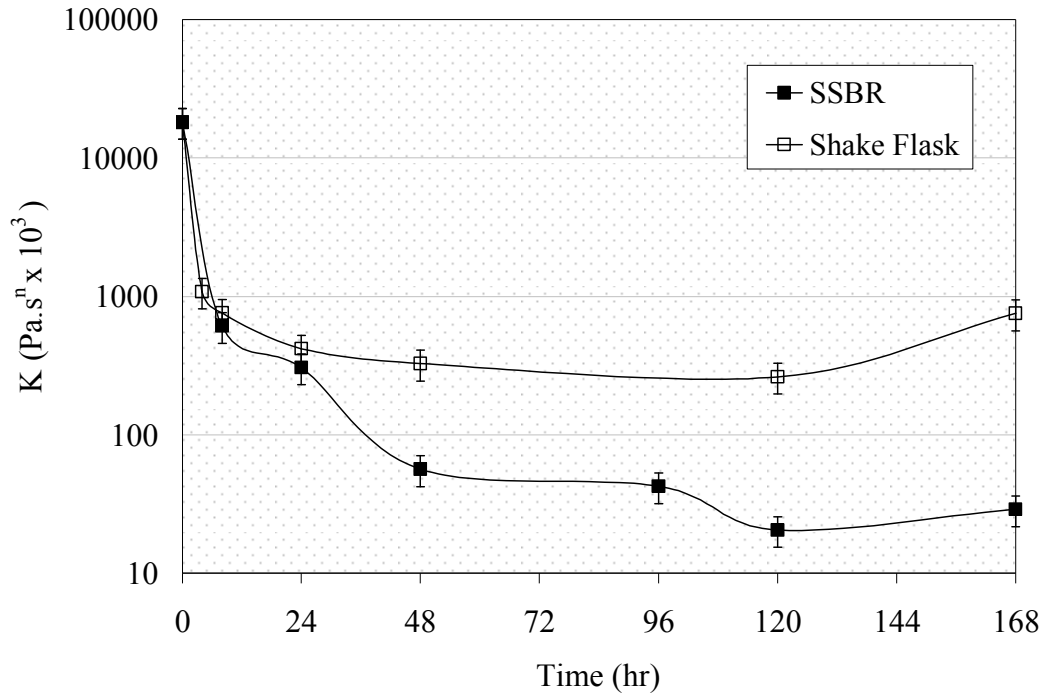


Figure 28. Consistency index throughout the saccharification reaction for 10% initial PCS solids concentration in the SSBR and the shake flask.

The viscosity changes during enzymatic saccharification of PCS solids slurry with 25% initial solids concentration are presented in Figures 29a and 29b for the SSBR and shake flask, respectively. 10% and 25% are the minimum and the maximum initial solids loadings tested for the saccharification reaction, respectively. So, the tests results for these solids concentrations are presented in the main text here and the results for the remaining solids concentrations (15% and 20%) are presented in Appendix B. It is noticed that for both the shake flask and SSBR, about 88% of the initial viscosity value is reduced during the first 8 hours of the reaction. However, only about 20-22% glucose release is obtained during the first 8 hours. Visual observations are not in agreement with the 90% viscosity drop because the slurry looks like a thick paste until 24 hours. After

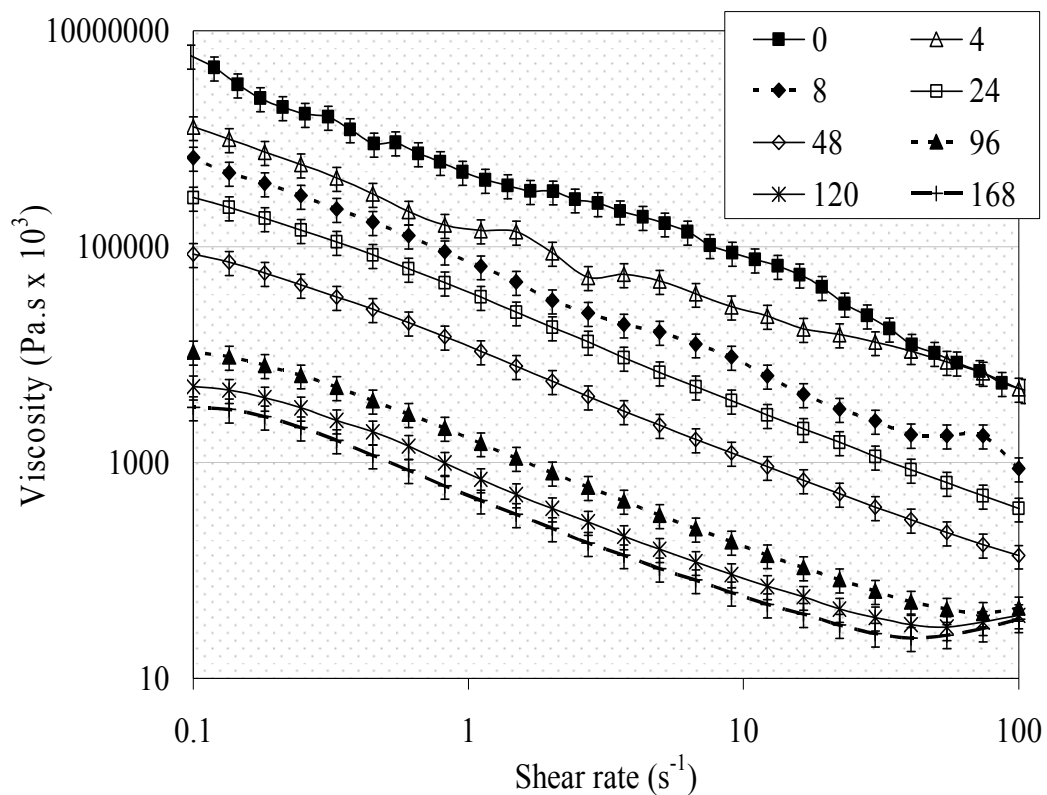


Figure 29a. Viscosity changes throughout the saccharification reaction in the SSBR for 25% initial PCS solids concentration.

Table 19a

Power Law Parameters for Viscosity Data During Enzymatic Saccharification of 25% PCS Solids in the SSBR

Time	0	4	8	24	48	96	168
R^2	0.9869	0.992	0.9962	0.9991	0.9989	0.9916	0.9626
$K (Pa \cdot s^n \times 10^3)$	554418	171156	72816	34787	11023	1586.5	514.98
n	0.048	0.2153	0.0416	0.0067	0.0283	0.0997	0.1952

that time it starts to liquefy, which leads to further reduction in viscosity. This might be because of the inaccuracies involved in measuring the viscosity for highly viscous paste-like materials using the vane impeller due to channel formation. During this phenomenon, the impeller forms a sort of virtual cylinder with a diameter equal to the diameter of the impeller. The “cylinder” rotates with material packed between the blades without imparting any momentum to the material between the edge of the cylinder and the wall. So, a channel is created where the material between the blades rotates with the blades while material in the annular space is stationary. The power law model parameters for 25% PCS batch saccharification test are presented in Table 19a and 19b for the SSBR and shake flask, respectively. The consistency index (K) plot is shown for the SSBR and shake flask in Figure 30.

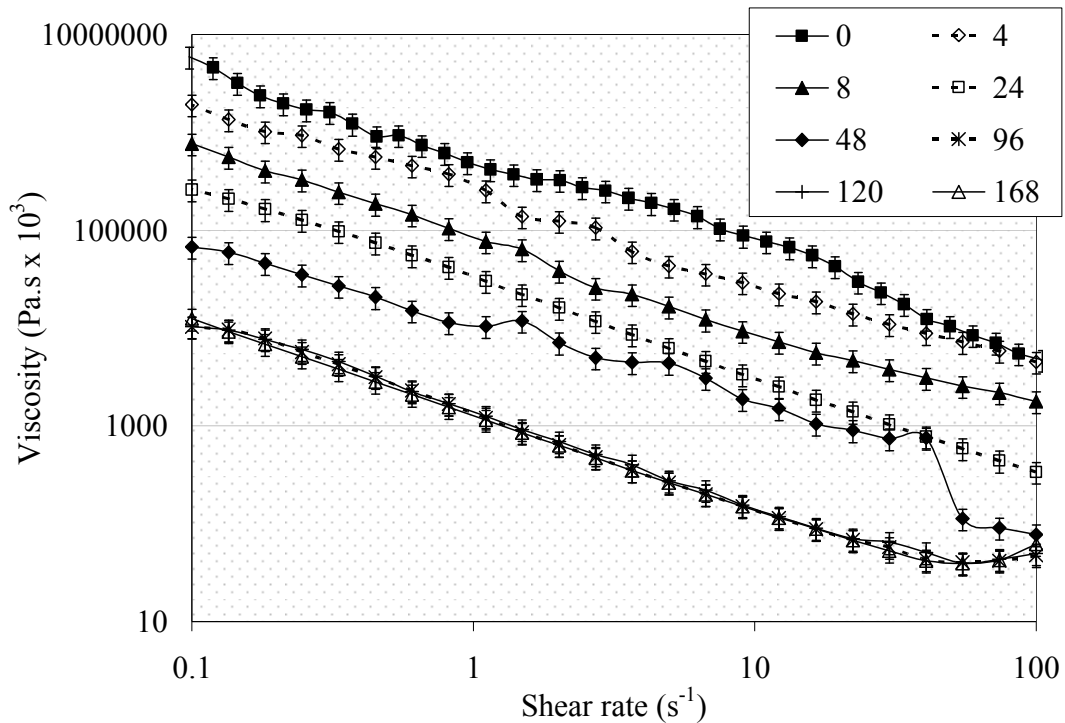


Figure 29b. Viscosity changes over reaction time in the shake flask for 25% initial PCS solids concentration.

Table 19b

Power Law Parameters for Viscosity Data During Enzymatic Saccharification of 25% PCS Solids In the Shake Flask

Time	0	4	8	24	48	96	120
R^2	0.9869	0.9945	0.9937	0.9992	0.9548	0.9846	0.9857
$K (\text{Pa}\cdot\text{s}^n \times 10^3)$	554418	240227	83496	31109	11304	1359.4	1409.2
n	0.048	0.0982	0.0915	0.0083	0.0824	0.1019	0.1098

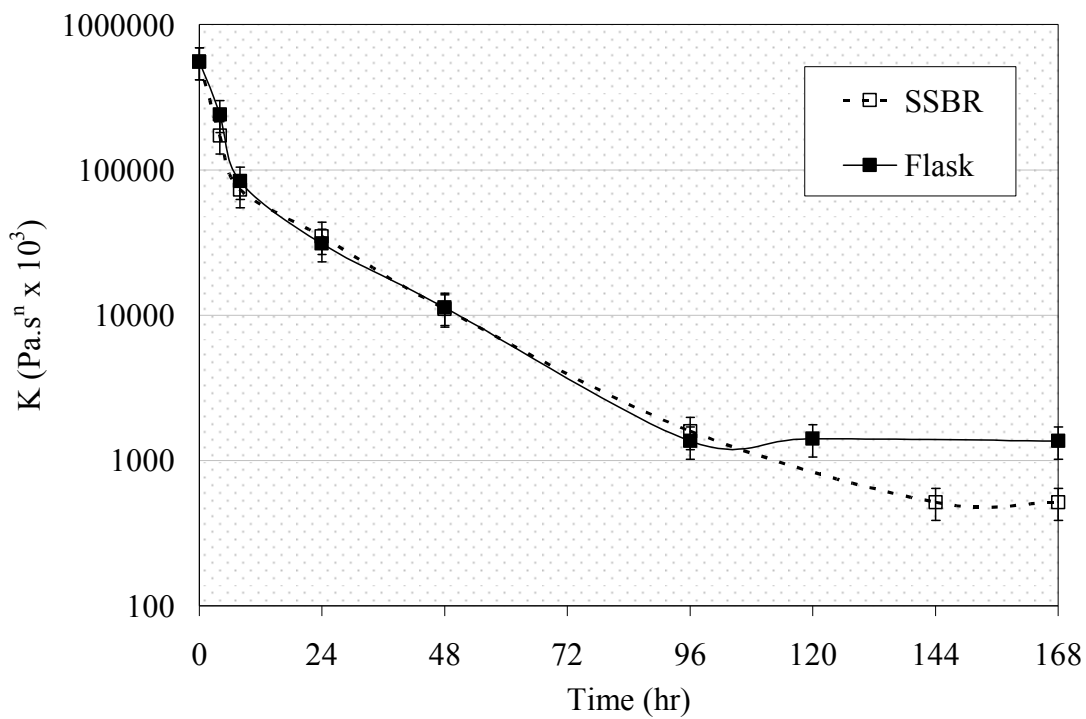


Figure 30. Consistency index vs. reaction time for 25% initial PCS solids concentration for the SSBR and the shake flask.

The steadying or increase of viscosity can be seen in Figures 29a and 29b for 96, 120, and 168 hour curves at about 50 s^{-1} shear rate; this effect is not seen in viscosity data for “0” hour times. As explained in the Results & Discussion of Effect of Particle Size on Saccharification Rate and Rheology, the steadying of or increase in viscosity occurs above and below a certain range of shear rates depending on the solids concentration. For slurries with higher viscosity, this shear rate range is above 100 s^{-1} and below 0.1 s^{-1} .

The ‘K’ value in Figure 30 decreases with time indicating the decrease in viscosity during the saccharification reaction. Generally, ‘n’ increases as the slurry viscosity decreases, although, a few inconsistencies are noticed in the trend of ‘n’ values in Tables 19a and 19b. This is an indication that the slurry is moving closer to Newtonian behavior. The nearer the value of ‘n’ is to 1, the more closely the slurry behaves as a Newtonian fluid. Another indication that the slurry becomes closer to Newtonian behavior is that the steadying of viscosity starts to occur at lower shear rates for lower viscosity slurries.

The ‘K’ versus time curves for the shake flask and SSBR are very close to each other contrary to the expected pattern based on the visual appearance of the slurries. It is likely that the vane of the MCR viscometer at higher solids concentrations forms a channel, similar to the phenomenon in the Bioflo 3000, without actually shearing the slurry material from the tip of the impeller to the cup wall. Thus, there is a high probability that accurate torque readings are not recorded by the vane impeller leading to incorrect viscosity measurements. Measuring the viscosity of highly viscous slurries with settling particulate solids is very challenging. Nevertheless, higher amounts of glucose release are achieved in the SSBR than in the shake flask, which is an indication of more

solids being digested, leading to lower viscosity after 96 hours than in shake flask as seen in Figure 30.

The 'K' value change over time for the SSBR appears to still be decreasing after 168 hours while it has become constant for the shake flask as seen in Figure 30. This phenomenon is in agreement with the increasing glucose release curve for the SSBR while it has reached an asymptotic value for the shake flask as seen in Figure 24b. The viscosity changes during enzymatic saccharification and the power law model parameters for 15% and 20% initial PCS solids concentrations for the SSBR and shake flask are presented in Appendix B.

The 'K' values are compared for saccharification of PCS slurries in the SSBR with various initial solids concentrations and are presented in Figure 31. The value of 'K' (~ viscosity) becomes constant after a certain time during saccharification. The time needed for the value of 'K' to become approximately constant increases with the solids concentration. The times for 10%, 15%, 20% and 25% solids slurries during saccharification are 48, 48, 120 and 144 hours ,respectively.

This implies that the time when viscosity values become approximately constant increases with initial solids concentration. At higher solids concentrations, the rate of solids degradation and fragmentation by enzyme is slower because of the lack of free water, and hence, the rate of glucose release becomes essentially diffusion-limited. The final 'K' value (viscosity) after 168 hours is higher for slurries with higher initial solids concentration.

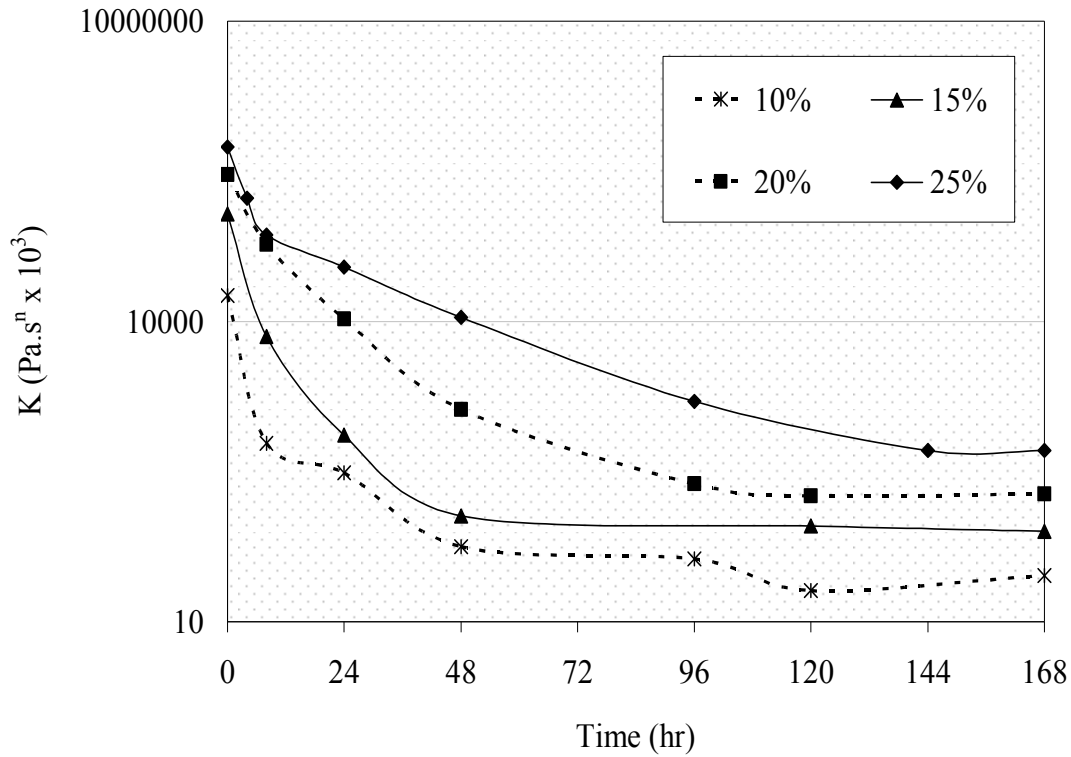


Figure 31. Comparison of Consistency index values (K) for saccharification of PCS slurries in the SSBR for various initial solids concentrations.

Power Consumption in the SSBR:

The torque to turn the shaft for mixing the PCS slurry in the SSBR is measured throughout the enzymatic saccharification. The power consumption and the specific power consumption are estimated based on the following correlations:

$$P = 2\pi NM \tag{17}$$

$$P_v = \frac{P}{V} \tag{18}$$

As mentioned in the Materials and Methods, all the tests are performed at 2 rpm in order to have minimal power consumption while still maintaining good mixing of the slurry. The power consumption is estimated for mixing PCS slurries with various initial

solids concentrations for a processing volume of 6 liters at various rotation rates. The data are presented in Figure 32. The SSBR is operated in the laminar region for all the tests. The power consumption increases with solids concentration, and the amount of increase appears greater between successively increasing solids concentrations due to the drastic increase in slurry viscosity. At 2 rpm, the power consumption increase is minimal for initial solids concentrations of 10% to 20%; from 20% to 25%, a 100% increase is observed in the power demand. The difference in power consumption for various solids concentrations increases with shaft speed; the amount of increase becomes higher for higher solids concentrations. At lower rotational speeds, the no load (empty SSBR) power consumption accounts for a large fraction of the total power consumption for mixing the PCS slurries. At 2 rpm, the no load power consumption is about 57%, 47%, 31% and 16% of the total power consumption that is required for mixing the PCS slurries with 10%, 15%, 20% and 25% insoluble solids concentrations, respectively. The fraction of no load power consumption becomes smaller with increasing solids concentration because more power is spent in lifting the viscous (very high density) slurry against the gravitational force than for scraping the surface of the reactor.

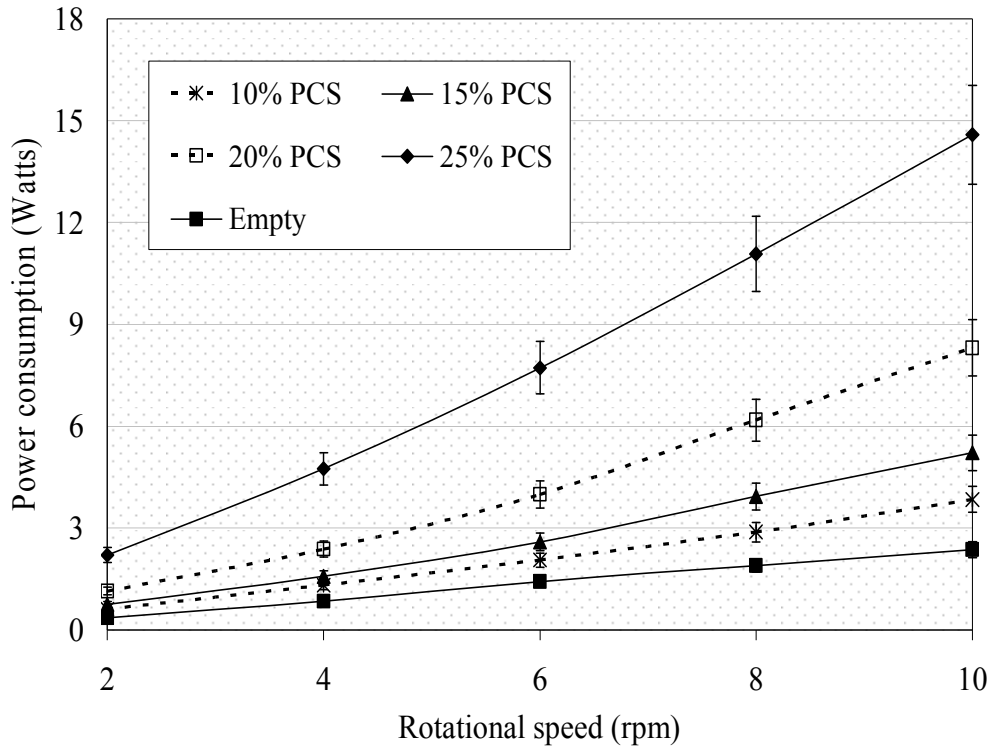


Figure 32. Comparison of power consumption for mixing PCS slurries with various initial solids concentrations in the SSBR at various speeds at ‘0’ hour time of saccharification.

A few models are available in the literature to estimate the power consumption in scraped surface reactors. However, each model is unique for the reactor based on which it is developed. Maingonnat and Corrieu (1986) proposed a generalized correlation between the power number (P_0) and the rotational Reynolds number (N_{Re}) in the laminar region, and the correlation is presented in Equation (19):

$$P_0 = KN_{Re}^a \quad (19)$$

where,

$$a = -1.2 \quad 20 < Re < 20,000$$

and the rotational Reynolds number is given in Equation (20):

$$N_{Re} = \frac{D^2 N \rho}{\mu} \quad (20)$$

where, D – impeller diameter (m), N – impeller speed (rps), ρ - liquid density (kg/m^3), and μ – liquid viscosity (Pa·s).

Equation (3) from the Literature Review is modified here to incorporate the Power number and the length of the SSBR, and it can be rewritten as:

$$P_0 = \frac{P}{\mu N^2 D^2 L} \quad (21)$$

where, P – power consumption (W) and L – reactor length (m).

Combining Equations (19), (20), and (21) to obtain the dependence of power consumption in a scraped surface reactor on various individual physical properties of the system gives:

$$P = KN^{0.8} \mu^{2.2} D^{-0.4} \rho^{-1.2} L \quad (22)$$

Although Equation (22) displays the strong correlation between the power consumption and the viscosity of the slurry, it is not possible to compare the present data on the SSBR to this model for estimating the power consumption. Since the PCS slurries are non-Newtonian, viscosity depends on shear rate and thus the model is not unique for non-Newtonian slurries in regards to the viscosity. Ignoring the viscosity term in Equation (22), the exponents for ‘N’ and ‘D’ are in good agreement with the results obtained by non-linear regression of data in Polymath program for 10% PCS slurry from Figure 32. However, no unique values can be obtained for PCS slurries with other concentrations by regression. Much more data is needed for all the parameters in order to develop a robust model, which is not the main objective of the present study.

Power Consumption in the SSBR during Batch Saccharification:

The power consumption data over time for the enzymatic saccharification tests with 10, 15, 20 and 25% initial PCS solids are shown in Figure 33. Power data is one of the most important factors that can aid in process and reactor design at industrial scale. The power data in Figure 33 indicates that processing at an initial solids concentration of 25% is not recommended because of the very high power requirement. The 100% increase in power requirement from the 20% solids slurry to the 25% solids slurry corresponds to the more than 100% increase in viscosity from the 20% slurry to the 25% slurry. Nevertheless, it is very important to note that the specific power consumption at 2 rpm for 25% PCS initial solids (the highest initial solids concentration tested) is 0.56 kW/m^3 , which is approximately half of the lower limit of the typical power requirement range at industrial level, $1\text{-}5 \text{ kW/m}^3$ (Arjunwadkar, 1997). Even at this low rpm, the SSBR was able to achieve 70% of the theoretical maximum glucose release in 168 hours.

As mentioned in the Experimental Plan, the SSBR is intended as a scale-up of the saccharification from a laboratory-scale shake flask to bench-scale. The results in the SSBR can be used as a basis for scale-up of the saccharification reaction to larger scale, such as pilot-scale or industrial production scale. Power per unit volume is the most commonly used scale-up criterion for mixing as it is easily understandable, practical, and it correlates well with mass-transfer characteristics of the mixing system (Wilkens, 2003).

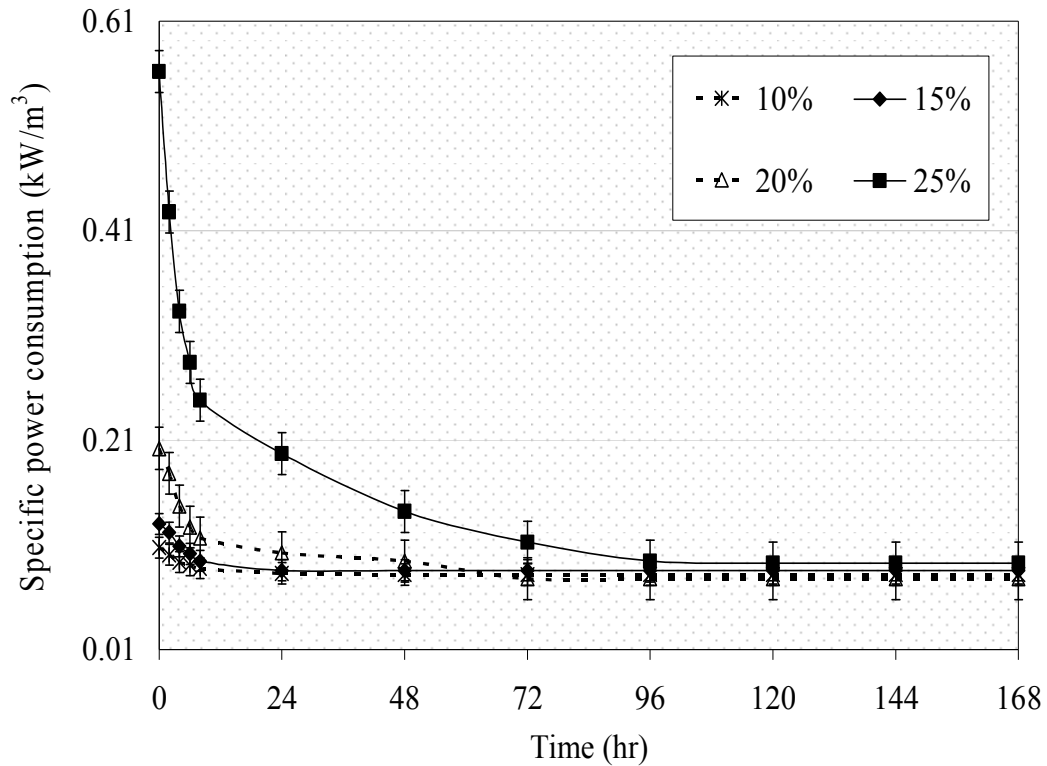


Figure 33. Specific power consumption in the SSBR during batch enzymatic saccharification of PCS slurries with various initial solids concentrations.

The trends in power consumption during the reaction are similar to the trends in viscosity changes, i.e., a large drop in power consumption occurs during the first few hours before reaching a steady state value, for all the solids concentrations tested. This is the expected trend because the power consumption is directly proportional to the slurry viscosity. The length of time to reach the minimum power consumption at steady state varies with initial solids concentration, ranging from about 4 hours for 10% initial solids to greater than 48 hours for 20% initial solids. 65-80% of the total drop in power consumption occurs during the first 8 hours of the reaction, depending on the initial solids concentration, corresponding to the large drop in viscosity during that time.

Interestingly, the amount of specific power consumption drop during the first 8 hours increases with an increase in the initial solids concentration. This might be because that the slurry with lower solids concentration reaches the ‘state of minimal change’ much earlier than the slurry with higher solids concentration.

Ghadge *et al.* (2005) discovered that 0.1-0.7 FPU/mL of mechanical deactivation of enzyme occurs when the specific power input range is between 1.6–12.56 kW/m³. Based on this finding, very little or no deactivation of the enzyme due to shear should occur in the SSBR as the estimated power consumption in the present work is less than 1.6 kW/m³. One way to reduce the power consumption further is to employ hinged blades instead of the fixed blades used in the present case; hinged blades are lighter in weight, too. Rozanov (1969) found that the power consumption in a 0.33 diameter scraped surface mixer with hinged scrapers for mixing a highly viscous slurry of poly-methylsiloxanes, with a viscosity as high as 352,000 Pa·s x 10³, is as low as 30 watts at 30 rpm, which highlights the importance of hinged blades.

Efficiency of the SSBR During Batch Saccharification:

The efficiency of the enzymatic saccharification reaction has been discussed only in terms of rate and extent of glucose release throughout previous literature. However, energy input into the system is a key economic factor at industrial scale. The efficiency of the enzymatic saccharification reaction is defined here as:

$$\text{Efficiency} = \text{Sugar Released} / \text{Energy Input} \quad (23)$$

Specific power required in the reactor for mixing PCS slurries depends (at a constant rpm) on the viscosity of the suspensions as shown by Equation (22). Thus, knowing the

power consumption trends in the SSBR can aid in developing better engineering techniques to reduce the energy input and in improving the processing strategy, which will result in lower operating costs. Thus, with this definition of efficiency, the effectiveness of the SSBR is characterized not only in terms of its ability to produce glucose, but it also considers the energy required to produce it.

Efficiency data of the SSBR for all the batch saccharification tests are shown in Figure 34 as a function of reaction time. The specific power consumption is numerically integrated using the Trapezoidal rule in order to obtain the cumulative energy input at each interval of time during the enzymatic saccharification reaction.

The efficiency of the batch saccharification seen in Figure 34 starts at the highest value and decreases over reaction time, to approach a constant value after 72 hours. The trend is similar for all the solids concentrations. Although higher amounts of glucose are produced with higher solids concentrations, the efficiency is less as compared to lower solids concentrations. This is because of the very high viscosity of the high solids slurry and, therefore, the high energy demand in the SSBR for mixing the slurry. The 25% peak efficiency value is about 70% less than that of the 10% peak efficiency.

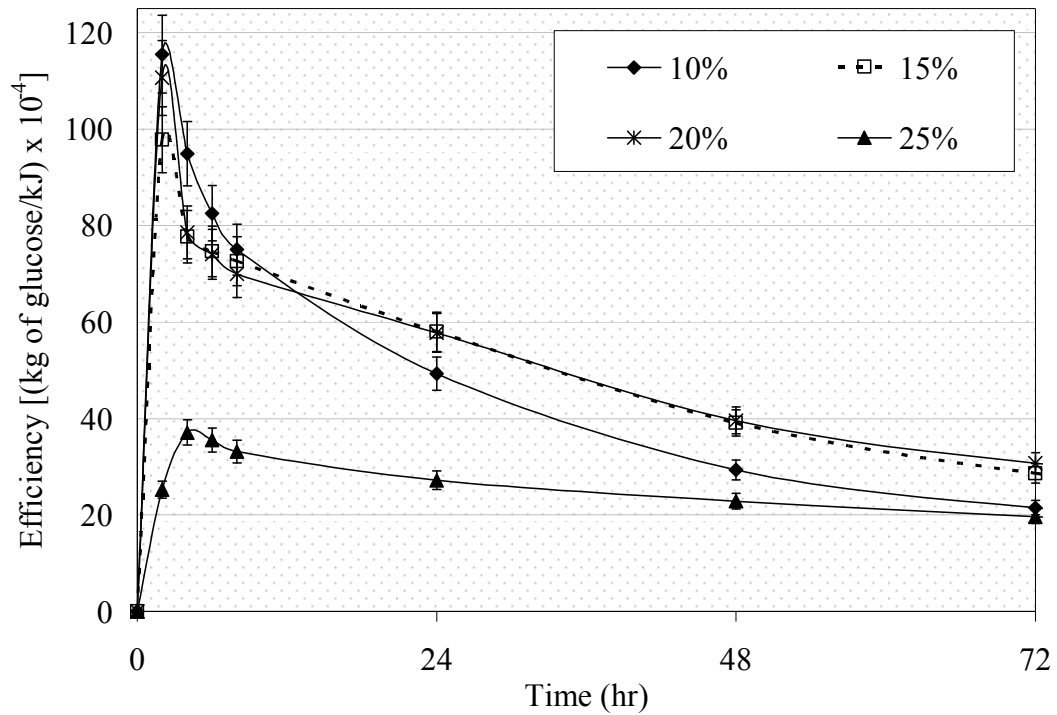


Figure 34. Comparison of efficiency for saccharification of PCS slurries with various initial solids concentrations throughout the first 72 hours.

The efficiency of the SSBR for saccharification decreases drastically because of the cumulative energy and also decreasing percent sugar release with time. The final values of efficiency for all solids concentrations after 72 hours are closer to each other because of the accumulated energy over time, which indicates that it is not recommended to maintain batch reactions for long periods. Since the SSBR has its highest efficiency at the initial hours, one recommendation is to use the SSBR to run the reaction initially, and then the contents can be transferred to a conventional mixing system. Or, fresh substrate can be added periodically after this point.

Although the 20% PCS slurry is very viscous, it was more efficient as compared to the 10% solids slurry in terms of glucose released per energy input. Therefore, the

recommended level of initial solids loading is 20% in batch operation as its efficiency is better than the 25% solids slurry and almost equal to the 10% solids slurry.

Saccharification in Semi-Batch Mode:

To reduce power requirements for high solids slurries, a semi-batch technique is employed where the process is initiated with low solids concentration, and then substrate material is added intermittently until a final equivalent higher solids concentration is reached. To illustrate this strategy, a batch is initiated with 12% PCS solids concentration, then 4% solids are added after the first 8 hours and another 4% solids are added after the next 8 hours, which results in a final 20% equivalent solids concentration. Enzyme is added proportionally with the solids during the each substrate feeding. The eight hour time increment for feeding is based on the approximate minimum time for the slurry to be able to absorb additional solids following digestion of the initial solids by the enzyme. This also corresponds to the peak efficiency previously shown. The viscosity data and the power consumption data from batch saccharification tests (Figures 31 and 33 respectively) show that the fastest rate of drop in slurry viscosity and power consumption occurs during the first 8 hours. The semi-batch test is initiated with 12% solids concentration since this is approximately the upper range where the slurry has enough free liquid for good flow and mixing.

Figure 35 shows a comparison of percent glucose release between the batch and the semi-batch saccharification tests with 20% equivalent solids in the SSBR. About 20% more glucose is released (glucose release % increases from 72% to 88%) in the semi-batch test as compared to the amount in the batch test. During semi-batch operation, a

lower slurry viscosity with better mixing and heat transfer characteristics is maintained through out the test. The semi-batch test contains less than 20% un-dissolved solids at any time while achieving a 20% final equivalent solids concentration. This result supports results obtained by others that achieved higher reaction rates and higher amounts of glucose release using a semi-batch method (Chen, 2007; Guido, 1988; and Wei, 2005).

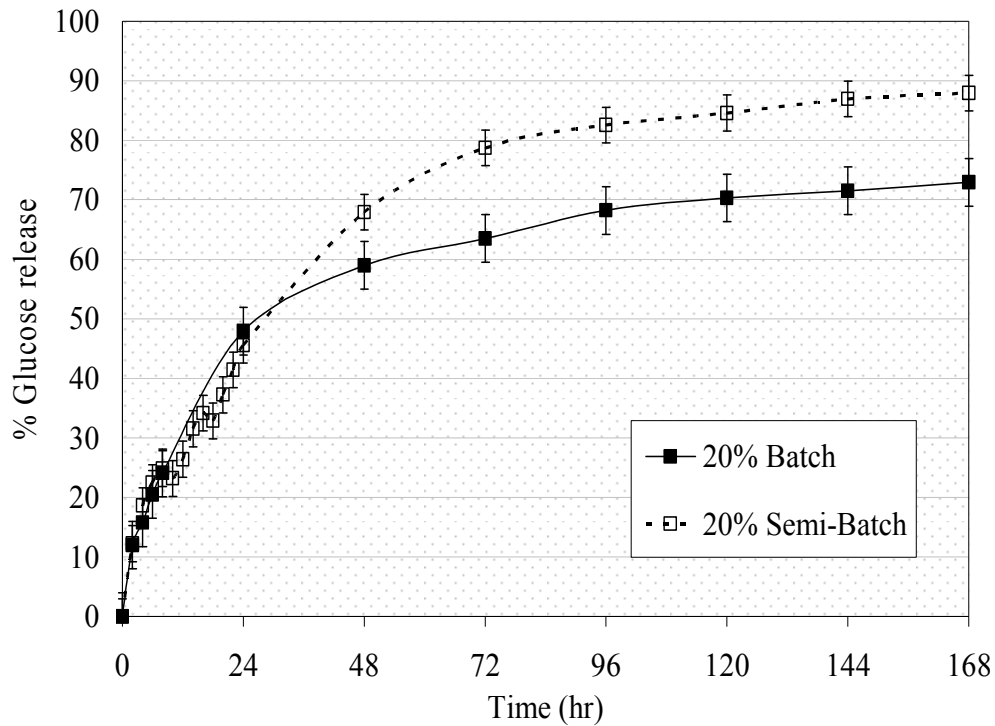


Figure 35. Comparison of percent glucose release in the SSBR at 2 rpm between batch and semi-batch enzymatic saccharification with 20% equivalent PCS solids concentration.

Rheology of PCS Slurries and Power Consumption in the SSBR during Semi-Batch

Saccharification:

Specific power consumption and consistency index (indication of slurry viscosity) data during the batch and semi-batch saccharification tests with 20% PCS solids concentrations are presented in Figure 36 and Figure 37, respectively. Power consumption for the semi-batch test starts at a lower value than that of the batch test and remains low throughout the course of the reaction because of the lower viscosity maintained during the test. The two spikes in power consumption for the semi-batch curve occur at 8 and 16 hours, when additional substrate is fed to the reactor. Viscosity and, therefore, power consumption reach a steady state value after about 120 hours. At this point, additional glucose release from un-dissolved solids is very slow (Figure 35), so the viscosity is minimally impacted. The final values of the slurry viscosity and the specific power consumption are approximately the same for both the batch and semi-batch tests. This might be because both slurries have attained a particle size range below which the slurry viscosity and the power consumption are approximately the same. However, it is to be realized that the particle size of the substrate in the batch test could be higher than that of in semi-batch as the rate of solids digestion is lower in batch test.

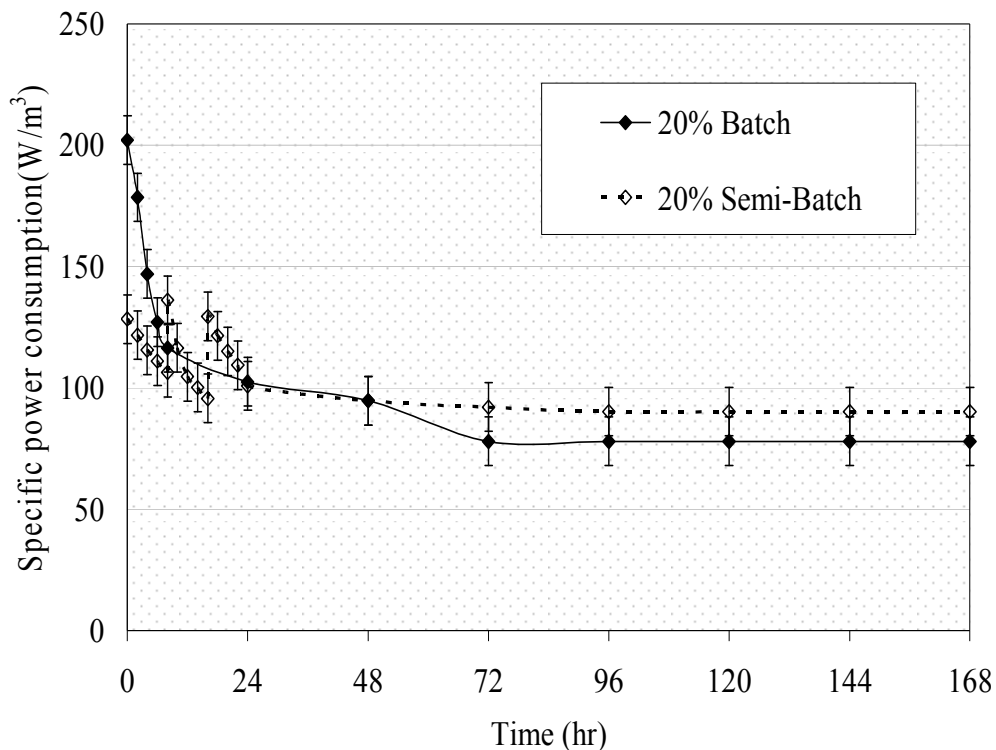


Figure 36. Comparison of power consumption in the SSBR at 2 rpm between batch and semi-batch operation during enzymatic saccharification with 20% equivalent PCS solids concentration.

The amounts of glucose release are compared between the shake flask and the SSBR for the 20% semi-batch saccharification test in Figure 38. About 8.5% higher glucose release is obtained in the SSBR as compared to the shake flask. Although the shake flask had a higher rate of glucose release during the initial hours (this might be due to better mixing in the shake flask which rotates at 250 rpm than in the SSBR at lower solids concentrations), the SSBR becomes more efficient at later hours with the increase in solids concentration.

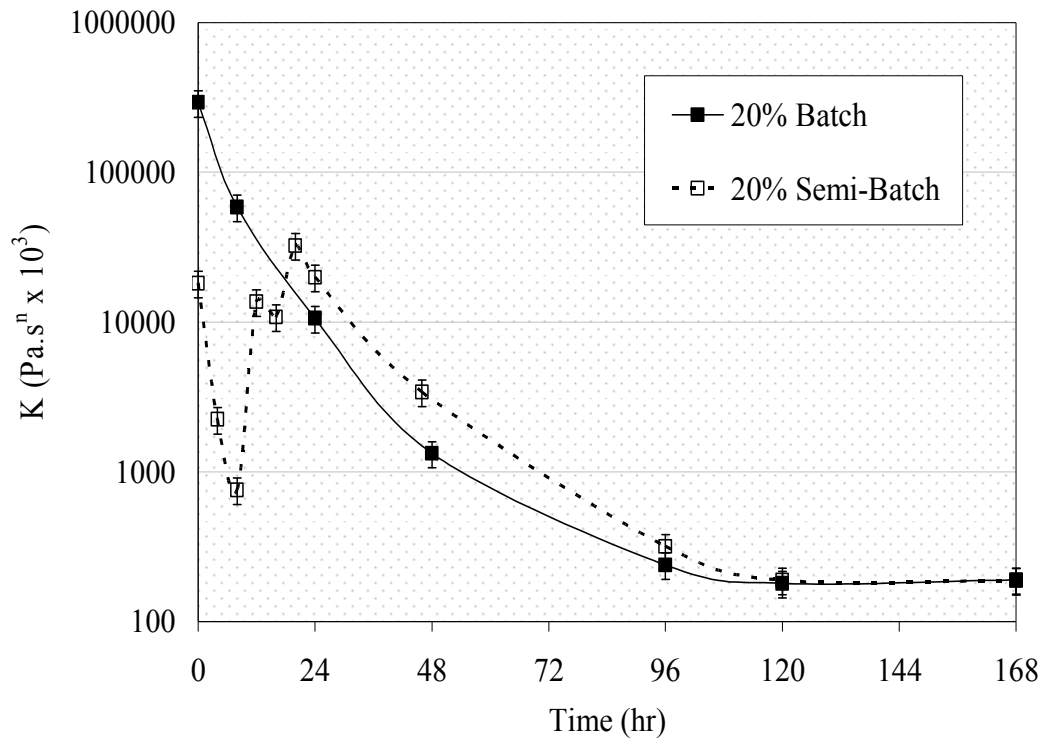


Figure 37. ‘K’ values in the SSBR at 2 rpm during batch and semi-batch enzymatic saccharification with 20% equivalent PCS solids concentration.

The actual viscosity curves over the range of shear rates ($0.1-100 \text{ s}^{-1}$) at various time intervals and the ‘K’ values during saccharification are presented in Figures 39a and 39b and Tables 20a and 20b for the SSBR and the shake flask, respectively for the 20% semi-batch test. Viscosity becomes approximately constant after about 120 hours in both the SSBR and the shake flask, which can be seen from the overlapping of the 120 hours and later viscosity data curves in Figure 39a and Figure 39b. Similar to the previous cases, the steadying of or increase in viscosity can be seen at later times (> 96 hours) of the reaction for low viscosity slurries.

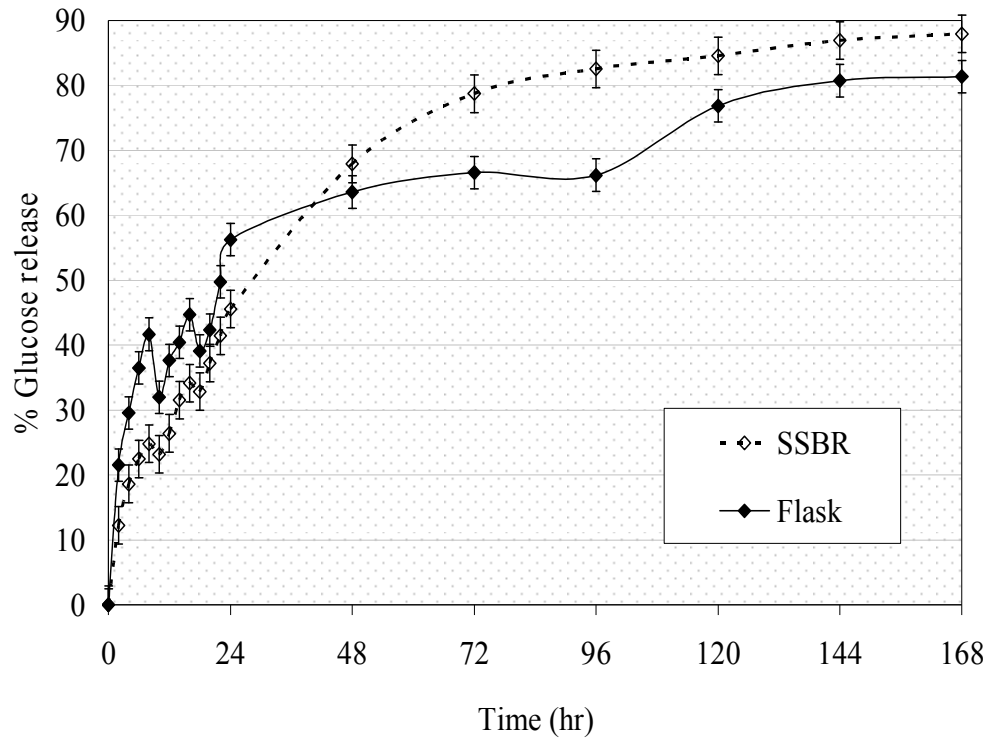


Figure 38. Comparison of percent glucose release in the SSBR and the shake flask at 2 rpm during semi-batch enzymatic saccharification with 20% equivalent PCS solids concentration.

Two other semi-batch tests are performed starting with 10% PCS solids in order to investigate the effect of lower initial viscosity on the rate of saccharification and the power consumption. The two final equivalent solids concentrations are 25% and 30%. The substrate is fed to the SSBR after every 8 hours at an increment of 5% solids concentration until the final equivalent solids concentration is achieved. The equivalent final solids concentration for 25% and 30% semi-batch tests is reached in 24 and 32 hours, respectively. Shake flask tests, as controls, are conducted simultaneously.

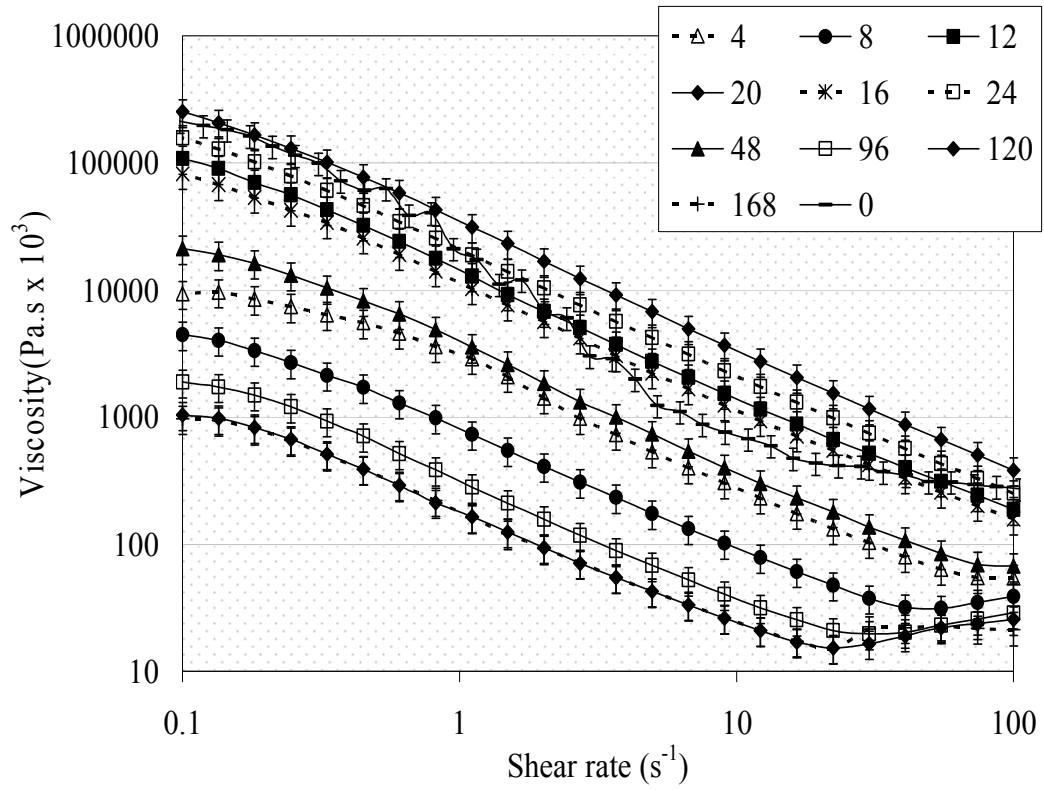


Figure 39a. Viscosity changes during semi-batch enzymatic saccharification in the SSBR for 20% equivalent PCS solids concentration.

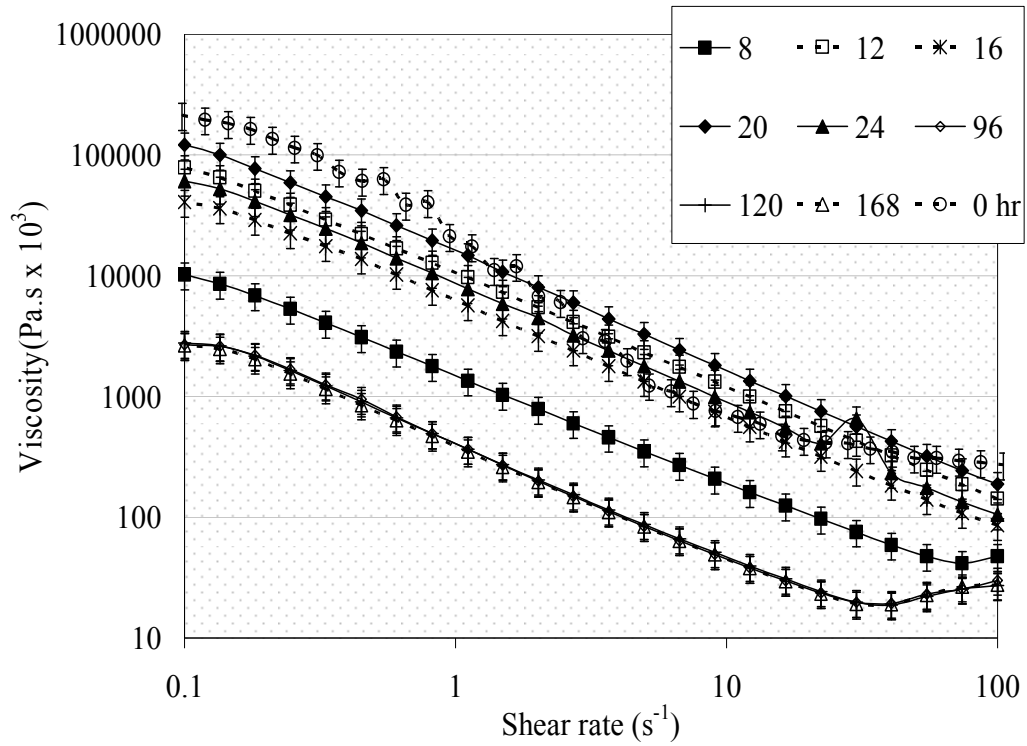


Figure 39b. Viscosity changes during semi-batch enzymatic saccharification in the shake flask for 20% equivalent PCS solids concentration.

Table 20a

Power Law Parameters for Viscosity Data During Semi-Batch Saccharification of 20% Equivalent PCS Solids in the SSBR

Time	0	2	8	12	16	20	24	46	96	120	168
R^2	0.9612	0.9868	0.9816	0.9988	0.9987	0.9991	0.9994	0.9954	0.9464	0.9144	0.9226
$K \text{ (Pa}\cdot\text{s}^n \times 10^3)$	18189	2234.8	757.49	13661	10828	32464	19948	3413.6	317.56	189.22	188.03
n	-0.128	0.1387	0.1892	0.0437	0.0572	0.0296	0.0416	1.9181	-7463	0.3331	0.3398

Table 20b

Power Law Parameters for Viscosity Data During Semi-Batch Enzymatic Saccharification of 20% Equivalent PCS Solids in

the Shake Flask

Time	0	8	12	16	20	24	96	120	168
R^2	0.9612	0.9956	0.9998	0.999	0.9996	0.9942	0.9564	0.9626	0.9589
$K \text{ (Pa}\cdot\text{s}^n \times 10^3)$	18189	1483.3	10318	5944.5	15262	8303	415.62	416.77	398.83
n	0.1289	0.15	0.0706	0.0698	0.0394	0.0628	0.1972	0.1959	0.2062

The amounts of glucose release over time for the saccharification of 25% and 30% final equivalent PCS solids concentrations in the SSBR and shake flask are shown in Figure 40.

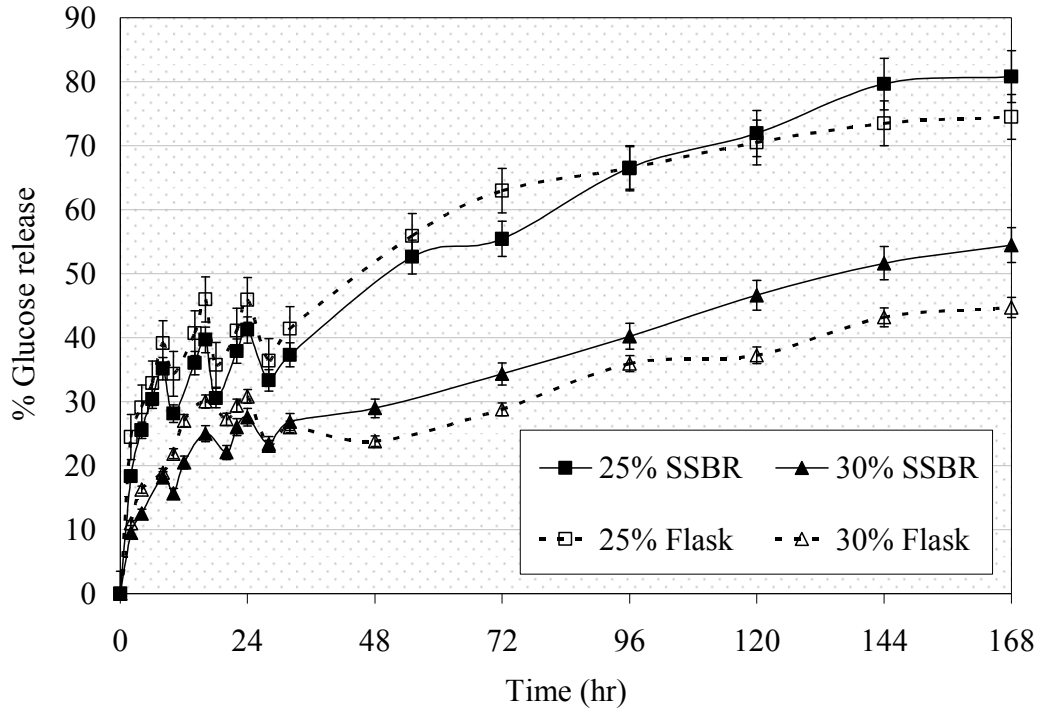


Figure 40. Comparison of percent glucose release between the SSBR and the shake flask during semi-batch saccharification with 25% and 30% final equivalent PCS solids concentrations.

As seen in Figure 40, the SSBR was able to achieve higher amounts of glucose release than in the shake flask in both the semi-batch tests with 25% and 30% final equivalent PCS solids concentrations. Similar to the 20% semi-batch test, the flask showed higher reaction rates at initial hours and lower rates at later hours than in the SSBR. This is due to the better mixing in shake flasks for low viscosity fluids and poor mixing characteristics for highly viscous slurries.

About 10% and 6% higher amounts of glucose release are obtained over 168 hours in the SSBR than in the shake flask for 25% and 30% semi-batch tests, respectively. Spikes are seen in the percent glucose release at 8, 16 and 24 hours for the 25% semi-batch test and at 8, 16, 24 and 32 hours for the 30% semi-batch test. The spikes result from the addition of fresh substrate which follows drops in concentration due to the dilution caused by the feeding of substrate. The spikes represent faster glucose release rates similar to that observed at the start of batch tests.

The slurry was still highly viscous for both 25% and 30% tests after the final feeding was completed. However, the slurry started liquefying in the SSBR after about 96 hours, whereas the slurry did not liquefy even after 168 hours in the shake flask and remained like a paste throughout the course of saccharification. This is attributed to the lack of good mixing due to the out-of-phase phenomenon.

The amounts of glucose release obtained during the first 24, 32 and 40 hours of reaction for 20, 25 and 30% semi-batch tests respectively, in the semi-batch saccharification tests are presented in Table 21 for both the SSBR and the shake flask as percentage of the maximum achievable glucose in 168 hours. These specific times are selected to report the glucose release in order to consider the 8 hours time period after the final equivalent solids concentration is achieved by several successive feedings. The batch saccharification test results are presented after the first 8 hours of the reaction and so, the semi-batch results are also presented after 8 hours of the completion of the final feeding, for comparison in a better way and also to allow the fastest reaction rates to occur during the first 8 hours period after the feeding. . The amounts of glucose release are about 14% and 11% higher than those obtained in batch saccharification (Table 15) in

the SSBR for 20% and 25% equivalent PCS solids, which is an indication of higher reaction rates obtained as a result of semi-batch feeding. The higher amounts of glucose release can also be attributed to the maintaining of lower viscosity and thus better mixing during semi-batch operation.

Table 21

Glucose Release in Semi-Batch Saccharification after 8 Hours of Final Feeding As Percentage of the Maximum Achievable Glucose in 168 Hours

% Final Equivalent PCS Solids	20	25	30
SSBR	51.75	47	50
Shake Flask	58	55.5	53.7

The consistency index (indication of slurry viscosity) and the specific power consumption data during the semi-batch tests with 25% and 30% final equivalent PCS solids concentrations are presented in Figure 41a, Figure 41b, and Figure 42, respectively.

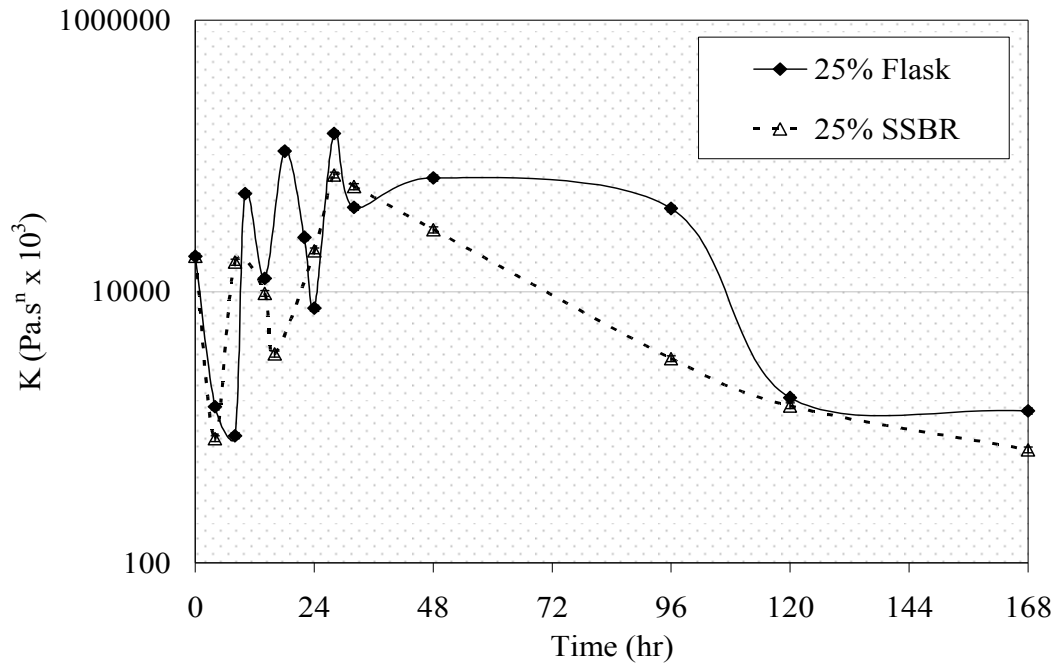


Figure 41a. ‘K’ values during semi-batch saccharification in the SSBR and the shake flask with 25% final equivalent PCS solids concentrations.

Since the viscosity increases with increasing solids, the spikes occur when fresh substrate is fed during saccharification. It can be seen that there is not a big change in viscosity for the 30% semi-batch test after the final feeding in both the SSBR and the shake flask. It should be pointed out that viscosity measurements at solids concentrations higher than 20% might not be completely reliable as the slurry has no free liquid, which limits the accuracy of the measurement due to channeling as previously discussed. The actual viscosity plots over the range of shear rates ($0.1-100\text{s}^{-1}$) for 25% and 30% semi-batch tests at various time intervals of the saccharification reaction and the power law parameters for the SSBR and the shake flask are presented in Appendix B.

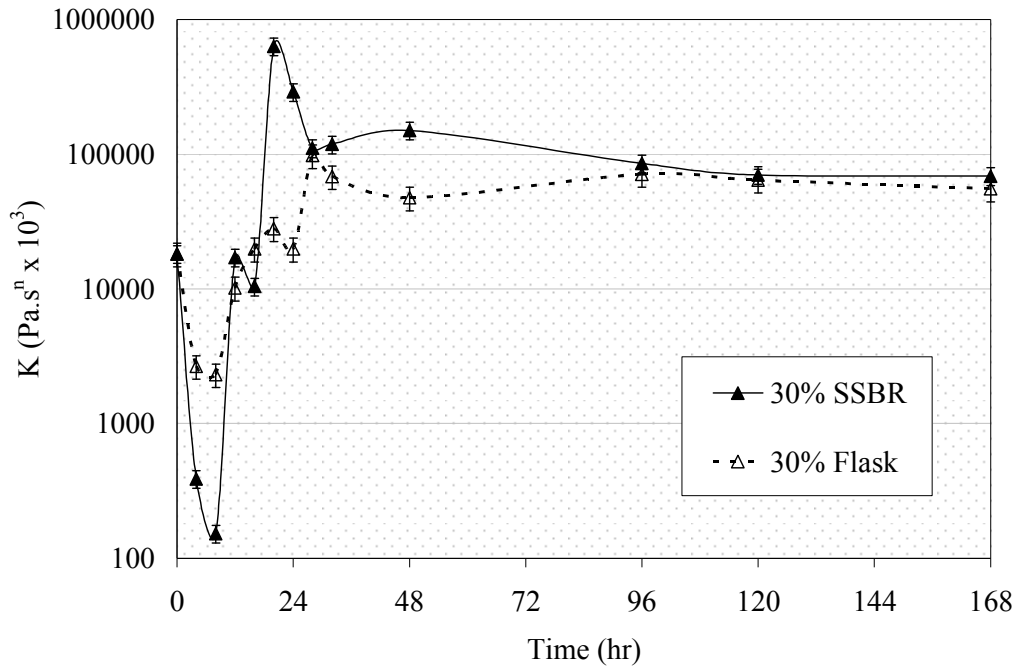


Figure 41b. ‘K’ values during semi-batch saccharification in the SSBR and the shake flask with 30% final equivalent PCS solids concentrations.

The specific power consumption throughout the reaction time is shown in Figure 42 for 25% and 30% semi-batch saccharification tests. The power consumption data for the 25% batch saccharification test is also shown in Figure 42 in order to compare with the 25% semi-batch test. It can be seen from Figure 42 that the power consumption was very low when the 25% semi-batch test was initiated as compared to the power in the batch test and was maintained at a lower value throughout the reaction. For 30% semi-batch, the power consumption starts at a lower value, but it increases to a very high value after the final feeding is completed at 32 hours. This is because of the high amount of solids loading (almost 70% of total solids) in the final feeding. This particular feeding

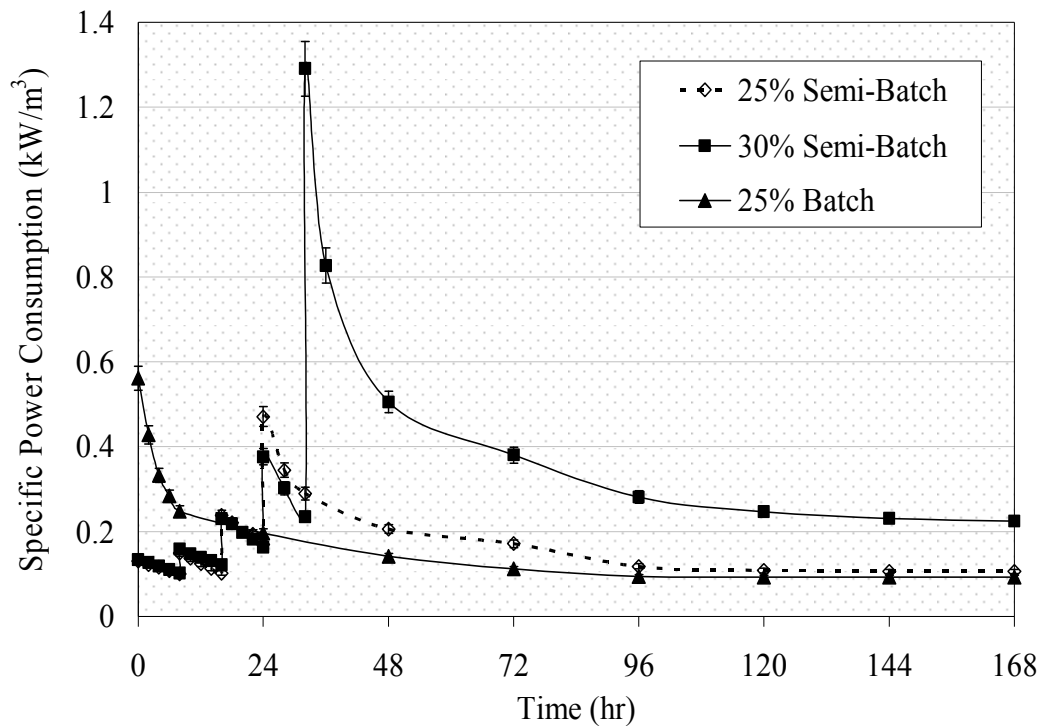


Figure 42. Specific power consumption during saccharification for 25% and 30% semi-batch and 25% batch tests with PCS solids.

strategy is followed in order to achieve the exact percentages of 10, 15, 20, 25 and 30% after each feeding. All the liquid is added at the beginning of the test and the solids and the enzyme (proportional to amount of solids) are added at various time intervals. So, specific amounts of solids are added to the reaction system in order to achieve the exact solids percentages at those time intervals and the same final volume as in the batch tests. This feeding pattern resulted in more solids being loaded during the final feeding. Although the power consumption decreases over time in the 30% semi-batch saccharification test, this feeding pattern is not recommended because of the very large increase in power consumption after the final feeding. However, the peak value of the

specific power consumption vs. time curve, 1.2 kW/m^3 , is still at the lower range of power consumption at industrial scale ($1\text{-}5 \text{ kW/m}^3$).

Efficiency of the SSBR During Semi-Batch Saccharification:

The efficiency plots are shown in Figure 43 for 20%, 25%, and 30% semi-batch saccharification tests in order to see the effectiveness of the SSBR both in terms of sugar release and power consumption.

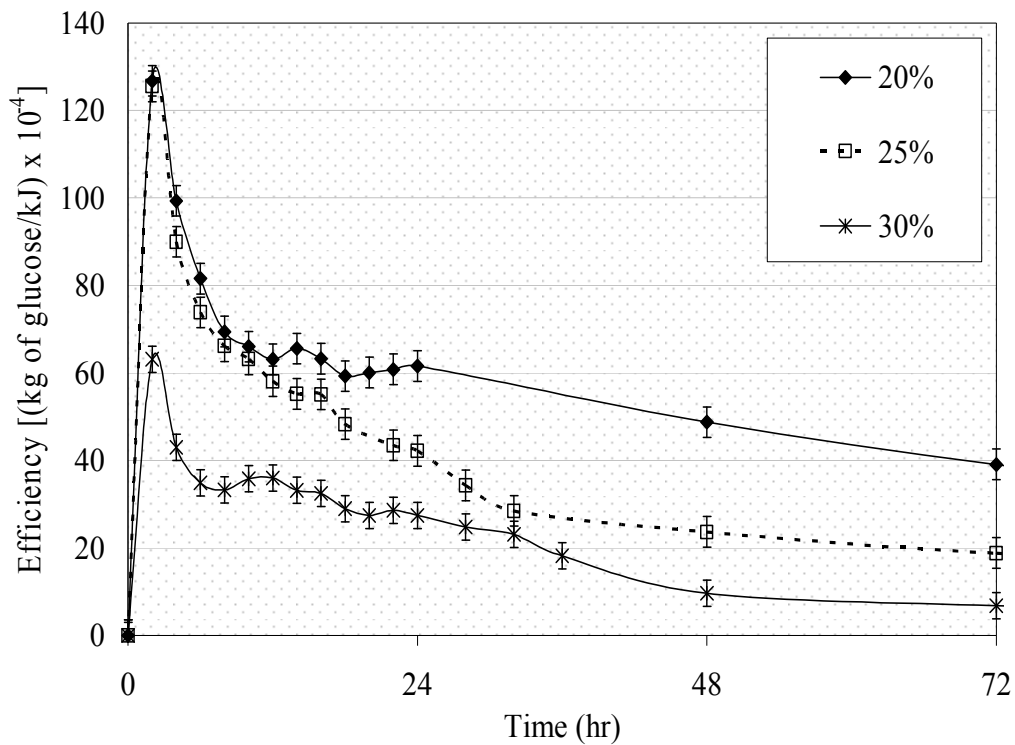


Figure 43. Efficiencies during semi-batch saccharification in the SSBR with 20, 25 & 30% equivalent PCS solids concentrations.

The efficiency is higher at initial stages of the reaction, decreases at later hours, and then starts to become approximately constant after about 72 hours. The amount of sugar release and the change in viscosity and power consumption are minimal after 72

hours, thus the efficiency curve starts to become flat after 72 hours. The 20% semi-batch efficiency is 27% higher than the 20% batch efficiency, based on the integrated values at 72 hours. Approximately the same efficiency is observed for both the batch and semi-batch saccharification tests with 25% equivalent solids concentration. This is against the expected result that the semi-batch saccharification efficiency should be higher than the efficiency during batch operation. It might be because, although a higher amount of glucose is produced, the semi-batch cumulative energy is higher than that of the batch value due to the high solids loading in the final feeding for 25% equivalent solids test. The 30% semi-batch efficiency value is only 17.5% of the 20% semi-batch efficiency after 72 hours. Therefore, based on the final efficiency values at 72 hours, the recommended final equivalent solids loading in the SSBR is 20% for semi-batch tests with the feeding policy used.

Other Semi-Batch Saccharification Tests:

During semi-batch saccharification tests, the slurry with reaction contents becomes highly viscous with the feeding policy used in the previous experiments. The shake flask was incapable of achieving good mixing due to the out-of-phase phenomenon at higher solids concentrations. Hence, another semi-batch test is performed in the shake flask, with similar conditions as in the previous semi-batch saccharification tests, with 25% final equivalent PCS solids concentration. This time the reaction contents in the shake flask are mixed with a stirrer (hand-mixing) in this semi-batch test after every feeding in order to better disperse the enzyme in the slurry. The amounts of glucose

release are compared for both of the semi-batch tests with 25% equivalent solids, with and without hand mixing after the feeding, in Figure 44.

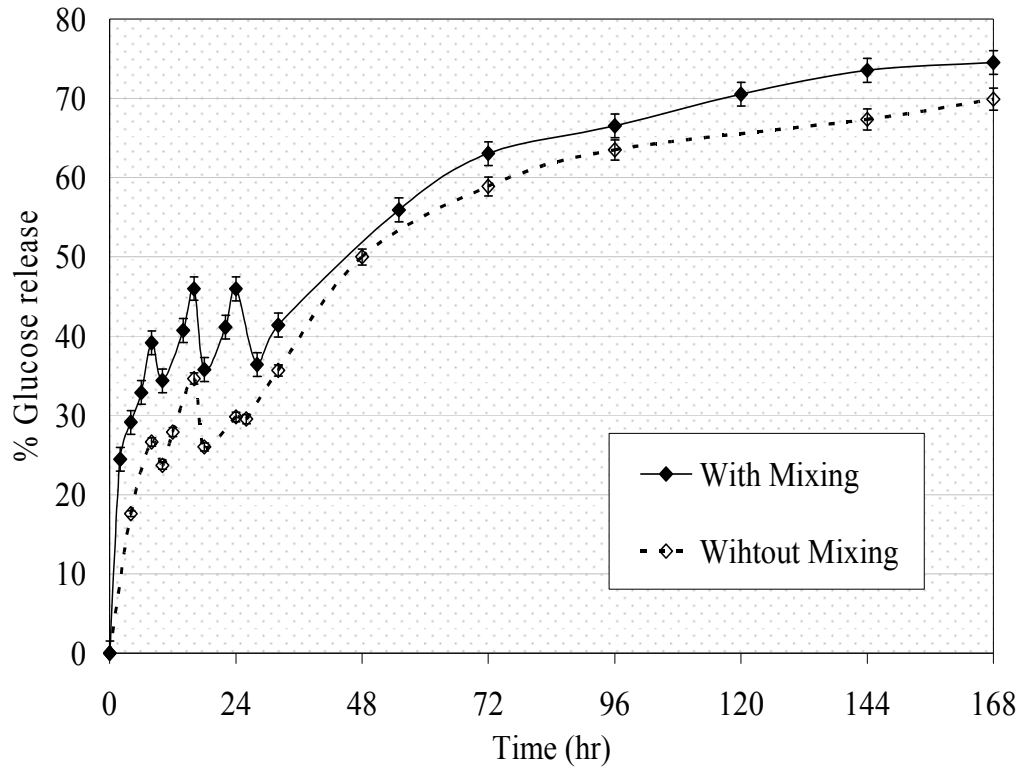


Figure 44. Comparison of percent glucose release in the shake flask between semi-batch saccharification tests (with and without hand-mixing) with 25% final equivalent PCS solids concentrations.

It can be seen from Figure 44 that increased reaction rate and extent of glucose release are obtained for the test with hand-mixing as compared to the test without the hand-mixing. About a 5% increase is obtained in the final extent of glucose release for the test with hand-mixing. This experiment clearly explains the inefficiency of the shake flask at higher solids concentrations. The viscosity plot and the power law parameters are presented in Appendix B.

Since the final solids loading decreased the overall efficiency in the semi-batch saccharification test with 30% equivalent solids in the SSBR, another test is performed in the SSBR with a new feeding policy for 30% equivalent PCS solids. The test is initiated with 20% initial PCS solids since it was concluded in the batch saccharification tests that 20% initial solids is the recommended loading. In this semi-batch test, the feeding is done after the slurry becomes more liquefied in the reactor, and the measured difference between the two consecutive viscosity readings (4 hours apart) is small. The remaining solids are divided into three equal parts after starting the test with 20% initial solids concentration. The feeding times in the semi-batch test with the second type of feeding are: 28, 60 and 84 hours, and the corresponding equivalent solids concentrations are: 26, 29 & 30%. The amounts of glucose release for this semi-batch saccharification test with the second type of feeding for 30% equivalent solids are compared to those in the semi-batch test with the first type of feeding, and the data are shown in Figure 45.

It can be seen from Figure 45 that the second type of feeding achieved about a 15% higher glucose extent after 168 hours than the first type of feeding. This is because the feeding in the second policy is performed after the reaction media has reached the 'state of minimal change', which allows the maximum capacity for solids absorption into the system. Similar to the other saccharification tests, about 15% higher glucose extent is observed in the SSBR than in shake flask for the second type of feeding. The rates of glucose release appear to be similar for both the SSBR and the shake flask during the initial hours of the saccharification reaction. However, as the solids concentration increases with the substrate feeding, the reaction slurry in the shake flask becomes like a thick paste with little motion in the flask because of the out-of-phase phenomenon.

Unlike in the flask, the blades in the SSBR mix the thick paste continuously and aid in liquefaction of the reaction contents after about 12 hours of the final feeding. This is the reason for the observed increasing separation between the percent glucose release curves (seen in Figure 45) for the SSBR and the flask after 72 hours.

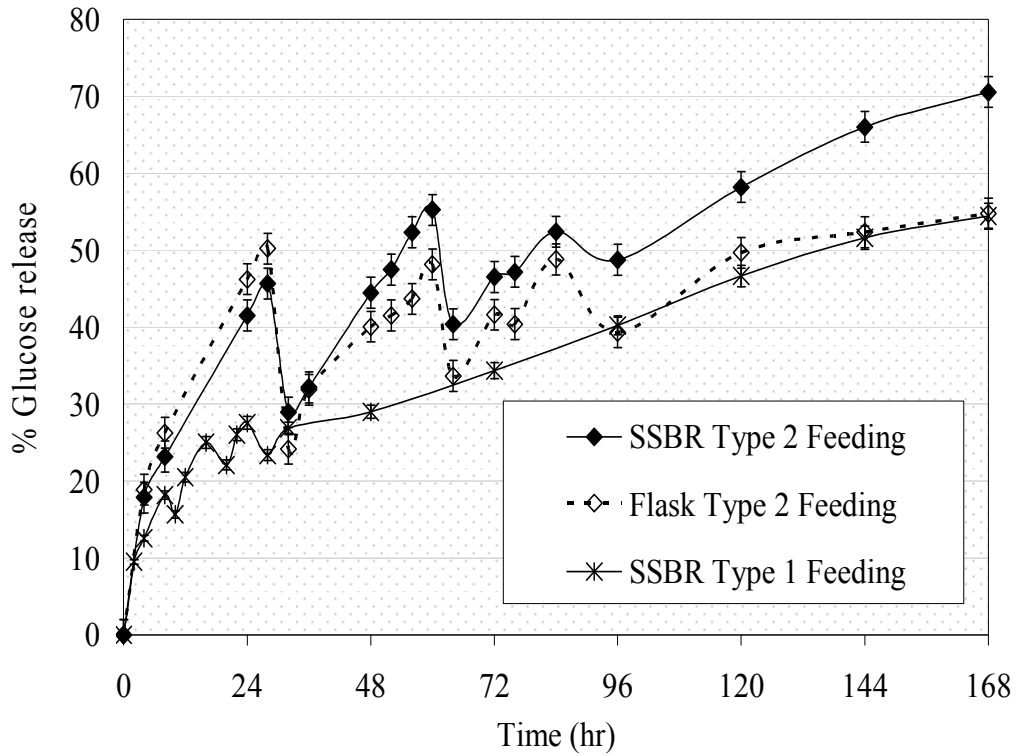


Figure 45. Comparison of percent glucose release between semi-batch saccharification tests with 30% final equivalent PCS solids concentrations for two types of feeding policies.

The consistency index (indication of viscosity behavior) and the specific power consumption data for the semi-batch test with the second type of feeding with 30% equivalent solids are presented in Figures 46 and 47. The viscosity plots and the power law parameters for the SSBR and the shake flask are presented in Appendix B. Similar to

the case of previous semi-batch tests, the peaks can be seen in Figure 46 when substrate is fed into the system. The final feeding is completed in the test at 84 hours which may be the reason why the slurry viscosity has not yet reached the steady state value as the time was not sufficient to reach the ‘state of minimal’ change.

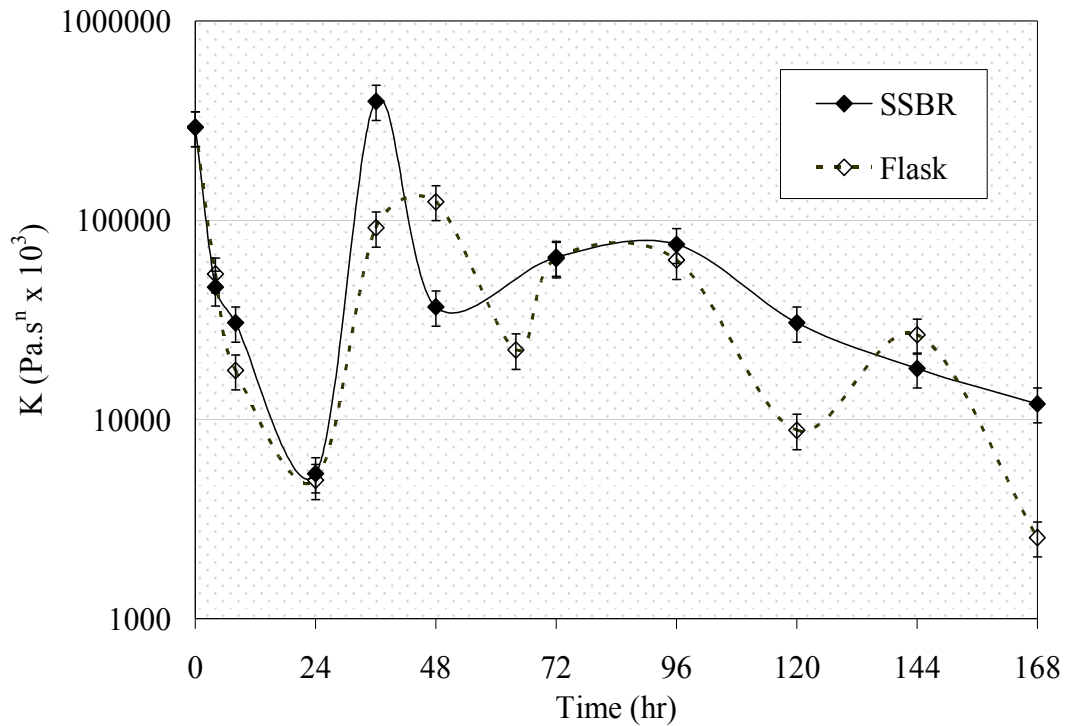


Figure 46. Comparison of changes in ‘K’ values during the semi-batch saccharification with 30% PCS equivalent solids with the second type of feeding policy.

A very large difference can be seen in Figure 47 between the power consumption of the first and second type of feedings. The power consumption in the test with the second type of feeding started and remained at a much lower value than in the first type of feeding. The power consumption maintains an average near 200 W/m³ throughout the reaction time. This is in accordance with the viscosity trend as the consistency index also oscillates about an average value of 92,000 Pa·sⁿ × 10³. Maintaining the slurry viscosity

at a lower value allowed for better mixing and, thus, resulted in higher amounts of glucose release than in the semi-batch test with the first type of feeding.

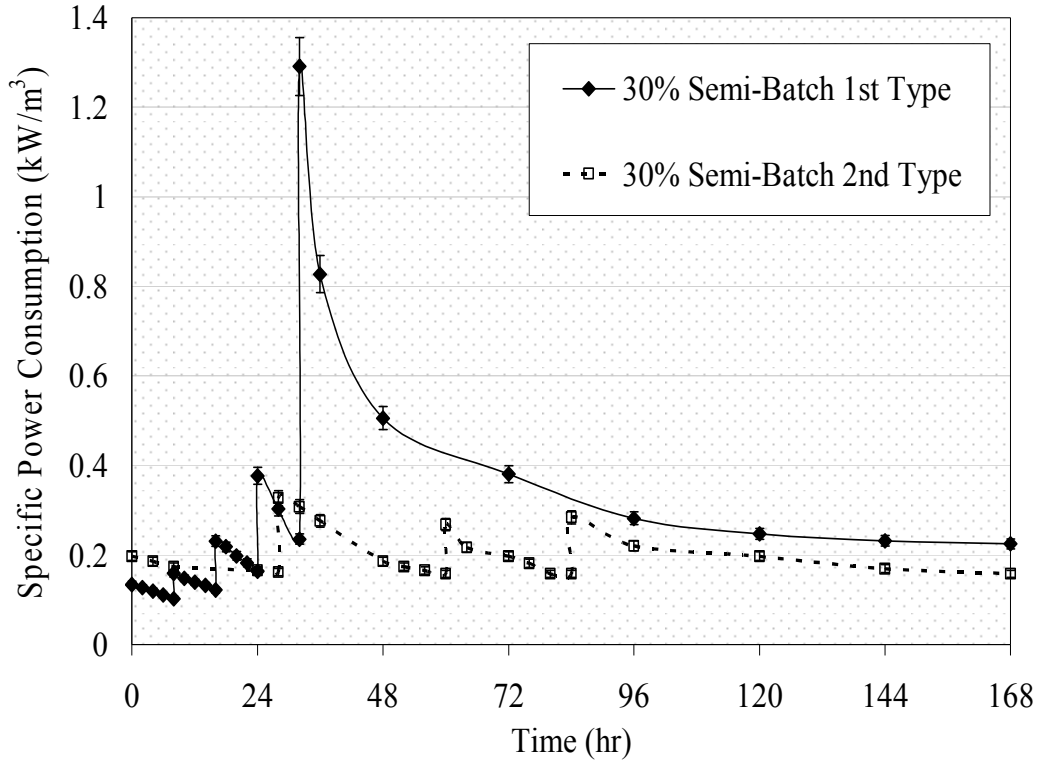


Figure 47. Comparison of specific power consumption between the first and second type of feeding during semi-batch saccharification with 30% equivalent solids.

The efficiency is compared between the first and second type of feedings in Figure 48. The efficiency of the test with the second type of feeding remains lower throughout the reaction time. The efficiency starts to become approximately constant after 72 hours. The efficiency of the test with the second type feeding is about 60% higher than the test with the first type of feeding at 96 hours. Thus, it can be concluded that the SSBR is capable of efficiently handling higher equivalent solids concentrations, as high as 30%, provided a proper feeding policy is developed and followed. With a

robust feeding policy, the SSBR may be operated efficiently at solids concentration higher than 30%.

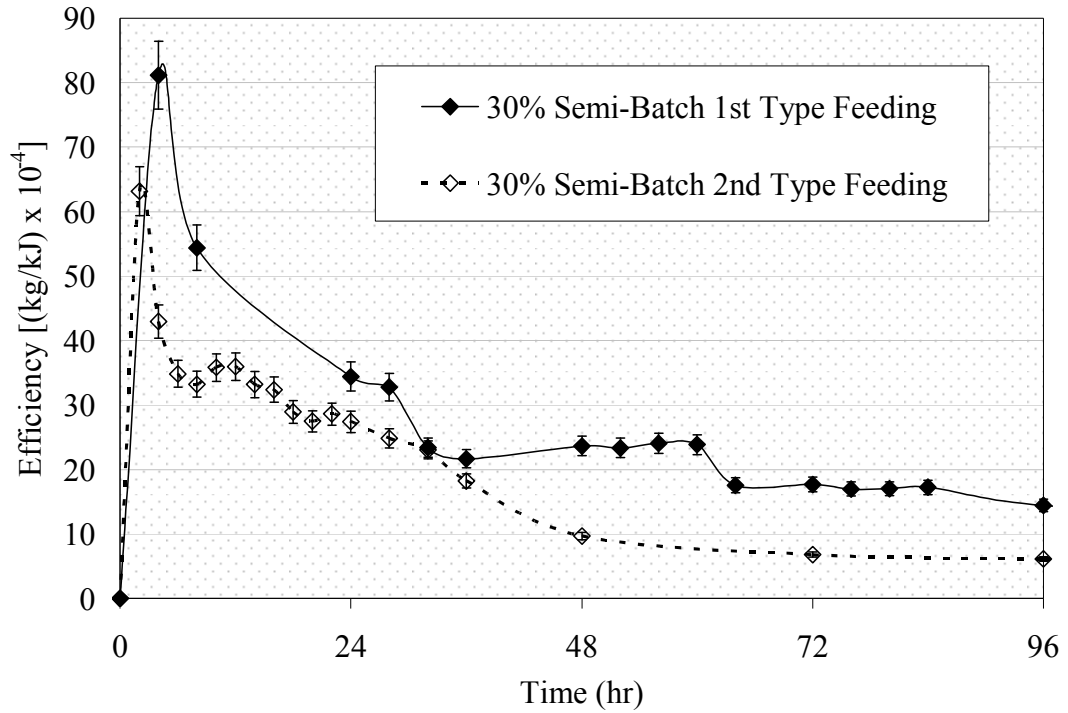


Figure 48. Comparison of efficiency during saccharification in the SSBR between the first and second type of feedings with 30% equivalent PCS solids concentrations.

As a summary, the efficiency values are presented for all the tests in Table 22 at 96 hours.

Table 22

Efficiency of Saccharification Tests with Various Concentrations of PCS Solids in the SSBR

% of PCS Solids	Batch				Semi-Batch			
	10	15	20	25	20	25	30-1 st Type	30-2 nd Type
Efficiency [(Kg/KJ)x10 ⁻⁴]	16.7	22.6	26.4	17	31.5	17	6.1	14.4

Table 22 shows that the 20% semi-batch test has the highest efficiency, with a value of 31.5 (kg/kJ) x 10⁻⁴ of all the tests studied in this investigations. Thus, it is recommended that the reactor operate with a 20% semi-batch feeding policy. It should also be emphasized that the SSBR is most efficient during the initial hours of saccharification for all the tests, independent of solids concentration. Since the SSBR is most efficient during the initial hours, one possible recommendation is to run the enzymatic saccharification reaction in the SSBR for a few hours until the solids degrade and the viscosity drops to a certain point, and then transfer all or some of the reaction slurry to a conventional stirred tank for further processing.

Since the performance of the SSBR is better than the shake flask, the design works well for an intermediate stage scale-up of the saccharification reaction from laboratory scale to pilot plant scale. The specific power consumption in the SSBR for saccharification of PCS slurries with various solids concentrations has proven to be less than the typical power requirement in conventional reactors, which is 1-5 kW/m³. The average specific power consumption in the SSBR for semi-batch saccharification of 20%

equivalent PCS solids (which resulted in the highest efficiency) is about 0.107 kW/m^3 . Hence, the SSBR performs very well as compared to conventional reactors operating with less viscous fluids as it demands very low power and, therefore, results in lower operating costs.

CHAPTER VI

TECHNIQUE TO MEASURE VISCOSITY OF SOLID SUSPENSIONS

MATERIALS AND METHODS

Determination of Just Suspended Speed and Uniform Suspension Speed:

An experimental setup is established, shown in Figure 49, in order to visually determine the Just Suspended Speed (JSS) and the Uniform Suspension Speed (USS) for PCS slurries in a cup and vane system in the Anton Paar MCR. The setup consists of a glass cup and a vane impeller with the exact dimensions as the cup and impeller of the actual viscometer. The glass cup is obtained from the Louisville Custom Glass Blowing Company (Louisville, KY) and the impeller is fabricated at the University of Louisville's Rapid Prototype Center. The vane impeller is glued to a shaft that fits into a Labmaster Lightnin Mixer (Lightnin SPX Corp, Wytheville, VA). The mixer has a motor which can drive the shaft in the range of 0-1800 rpm. The glass cup and a flash light are held in place with clamps. A mirror is placed at an angle which makes it easier to view the bottom of the cup where the light illuminates the slurry.

Slurries with various PCS solids concentrations (5%, 7.5%, and 10%) are loaded in the glass cup. The behavior of the slurry is observed both directly and in the mirror. The rotation rate is increased in increments of 10 rpm. JSS is judged to be at the rpm where no solid particles settle at the bottom of the cup for more than 2 seconds (Zwietering,

1958). USS is judged to be at the rpm where all the particles are completely suspended and moving along with the bulk flow of the liquid.

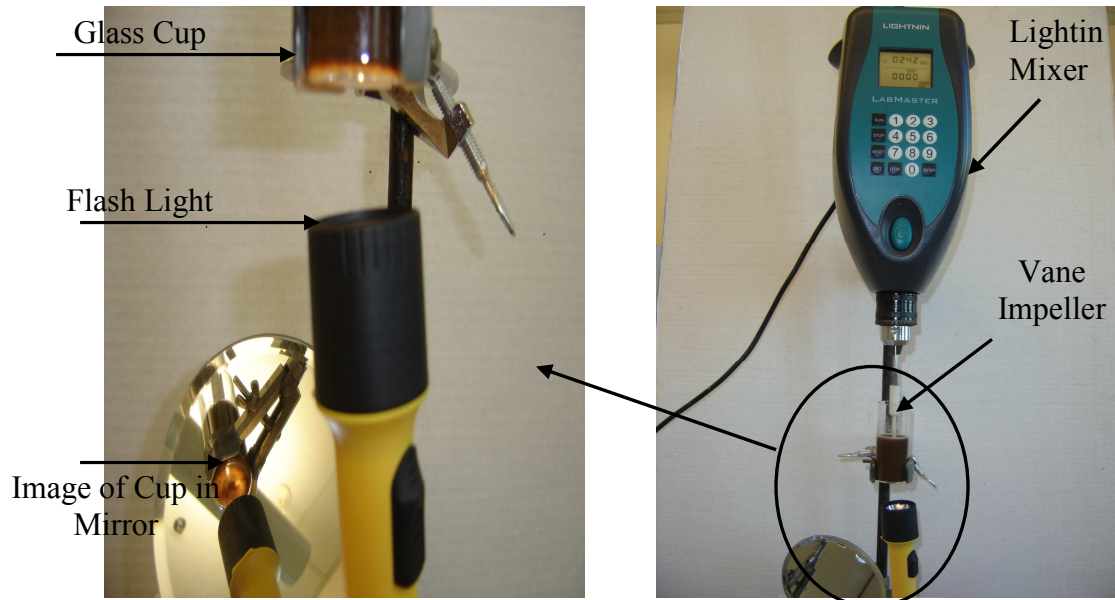


Figure 49. Experimental set up for experimental determination of JSS and USS.

RESULTS & DISCUSSION

Determination of JSS and USS for PCS Slurries:

Measuring the viscosity of particulate suspensions is difficult because the solid particles tend to settle at the bottom of the viscometer cup due to gravity. Typical mixing type viscometers have an impeller to mix the slurry and a cup to hold the sample. Since most particulate suspensions are typically non-Newtonian, viscosity is measured over a range of shear rate values for complete characterization. For accuracy, it is necessary to achieve a homogenous suspension with all the solid particles well suspended in the liquid.

A premixing technique developed here offers an improved method for measuring viscosity of solid suspensions. Premixing was performed at 160 s^{-1} shear rate for all of the previous viscosity measurements for PCS slurries, which corresponds to an estimated JSS based on the Zwietering (1958) and Pavlushenko et al. (1957) correlations (Equation 6 and 7) that were originally developed for baffled and unbaffled mixing tanks, respectively. Also, the biomass fibers require a certain amount of time in order to reach a steady state alignment with the direction of flow, so viscosity measurements without premixing may lead to inaccurate results. Thus, premixing is performed for two reasons: to achieve uniform suspension and to establish steady state viscosity.

There was no experimental support to verify if the theoretical premixing speed (JSS) resulted in a uniform solids suspension for the previous viscosity measurements on PCS slurries. So, experiments are performed using the experimental setup shown in Figure 49 in order to experimentally determine the actual speed required to achieve a uniform suspension for PCS slurries with various solids concentrations. The data are

presented in Table 23. The data shows that premixing at 160 s^{-1} shear rate was able to achieve uniform suspension only for slurries with solids concentrations of at or below 5%. The typical reporting shear rate interval in the literature for non-Newtonian viscosity varies between 0.01 and 1000 s^{-1} . Thus, solids suspensions may not be homogeneous at the lower end of the shear rate range.

Table 23

Just Suspended Speed (JSS) and Uniform Suspension Speed (USS) For PCS Slurries with Various Solids Concentrations and Corresponding Shear Rate in the Viscometer

% PCS Solid	Speed (rpm)		Shear rate (s^{-1})
5	JSS	270	145
	USS	305	150
7.5	JSS	800	393
	USS	930	457
10	JSS	-	-
	USS	-	-

The JSS and USS for 10% PCS slurry are higher than 1800 rpm, which is the maximum speed limit on the Labmaster Lightnin Mixer. Premixing to achieve the USS is required only for slurries with solids concentration under about 12%, because above a 12% solids concentration the slurry becomes like a paste with very little free water, so solids settling is hindered. Since most of the water gets absorbed by the solids, an instantaneous separation of solid and liquid phases does not occur for slurries with solids concentrations above about 12%. Further, the inter-particle distance is reduced drastically at solids concentrations higher than 12% which leads to a high degree of

entanglement between fibers, thus slowing the settling of particles at the bottom of the viscometer cup. Premixing is still required to achieve a steady state viscosity.

Since the settling of solid particles leads to inaccuracies mainly when measuring the viscosity of lower solids concentrations, it is necessary to study the solids distribution in the viscometer cup at solids concentrations below 10%. CFD (computations fluid dynamics) is used to help determine the solids distribution at various cross sections of the viscometer cup, which is explained in detail in Chapter VII.

Effect of Premixing on Viscosity Measurements:

Based on the experiments using the setup in Figure 49, 160 s^{-1} shear rate was not enough to achieve a uniform suspension for solids concentrations above 5%. Also, the viscosity data can be inaccurate at the low end of the reporting shear range for viscosity of PCS slurries with solids concentrations lower than 10%. So, an investigation is carried out in order to understand the effect of premixing shear rate on the accuracy of viscosity measurements for PCS slurries. Viscosity is measured for PCS slurries with various solids concentrations by premixing at various shear rates for a pre-defined amount of time according to the Table 23. The goal of the investigation is to determine if a slurry can remain uniformly suspended during viscosity measurements over the range of shear rates (0.1s^{-1} - 1000s^{-1}) when premixed at shear rates greater than that required to achieve a uniform suspension (a postulate).

Determination of Time to Reach Steady State Viscosity for PCS Slurries:

It is realized that solids are not uniformly suspended during viscosity measurements at the low end of the shear rate range which leads to a large variance in viscosity values. So, PCS slurries with various initial solids concentrations are subjected to premixing at various shear rates in order to determine the time to reach steady state viscosity with the Anton Paar MCR. Once this is determined, each slurry (with various solids concentrations) is premixed for that particular time prior to the viscosity measurement. This is in order to prove the postulate stated in the above section. Experiments at each shear rate are repeated three times and average data are presented.

The biomass fibers align in the direction of the flow (at steady state viscosity) after a shear rate is applied for a certain amount of time. So, a new sample of slurry is prepared for each test in order to eliminate the previous shear effects. The premixing viscosity data for the 5% PCS slurry is shown in Figure 50. Viscosity reaches a steady state value within one minute for premixing at 160, 400, and 800 s^{-1} shear rates. Since PCS slurries are non-Newtonian, viscosity decreases with increasing shear rate. However, higher viscosities are observed at shear rates of 400 and 800 s^{-1} than that at 160 s^{-1} . This might be because the solid particles are better suspended at shear rates of 400 and 800 s^{-1} than at 160 s^{-1} since the impeller speeds corresponding to 400 and 800 s^{-1} shear rates are well above the USS. When more solids are well suspended, more particles come in contact with the impeller which leads to an increase in the torque which results in higher viscosity.

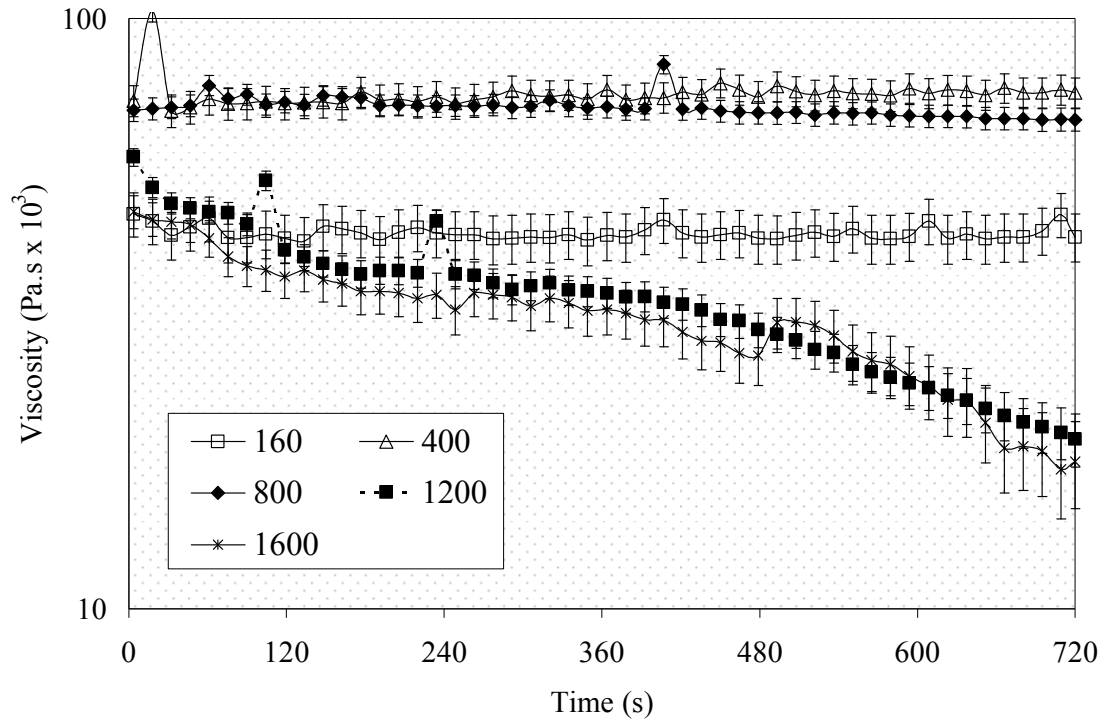


Figure 50. Premixing test with a 5% PCS slurry.

Viscosity changes are small over time for premixing at 400 and 800 s^{-1} shear rates, which indicates that the slurry quickly reaches its steady state viscosity value because of the higher shear force. Thus, it can be concluded that biomass fibers take less time to align in the flow direction at shear rates higher than the USS.

The slurry splashed out of the viscometer cup at the highest impeller speeds of 1200 and 1600 s^{-1} . Therefore, the premixing data for 1200 and 1600 s^{-1} shear rates are probably unreliable for the 5% slurry. The lower viscosity observed at 1200 and 1600 s^{-1} shear rates may be because the impeller shaft forms a vortex and entrains atmospheric air into the slurry at very high impeller speeds leading to a lower viscosity.

The premixing data for the 7.5% PCS slurry is shown in Figure 51. The viscosity change over time is very small for all premixing shear rates.

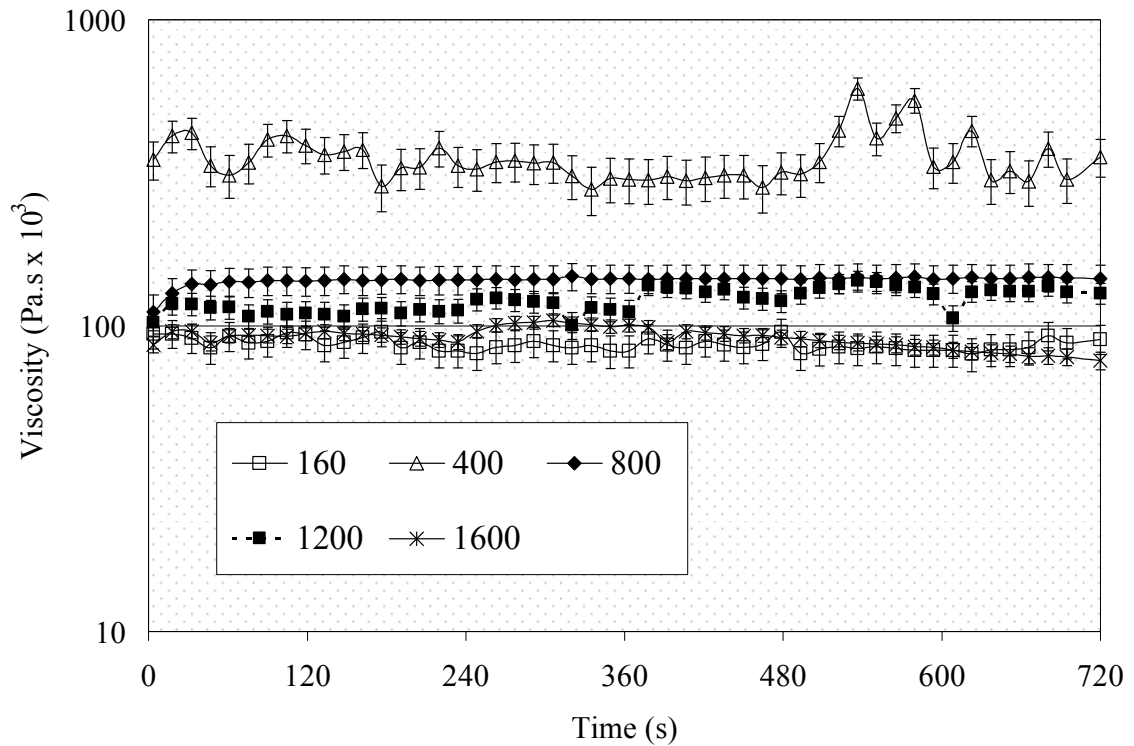


Figure 51. Premixing test with a 7.5% PCS slurry.

The time to reach the steady state viscosity for the 7.5% PCS slurry is less than one minute at 160, 400, 800, 1200, and 1600 s^{-1} shear rates. The slurry again splashed out of the viscometer cup at 1200 and 1600 s^{-1} shear rates for the 7.5% solids concentration, and vortex formation was also observed which resulted in unreliably low viscosity measurements.

The premixing viscosity data for 10%, 15%, and 20% slurries are shown in Figures 52, 53 and 54, respectively. The premixing test results at 160 s^{-1} shear rate for slurries with these solids concentrations are presented in the Materials and Methods of Chapter V. So, premixing tests are performed only at the remaining shear rates; 400, 800, 1200, and 1600 s^{-1} .

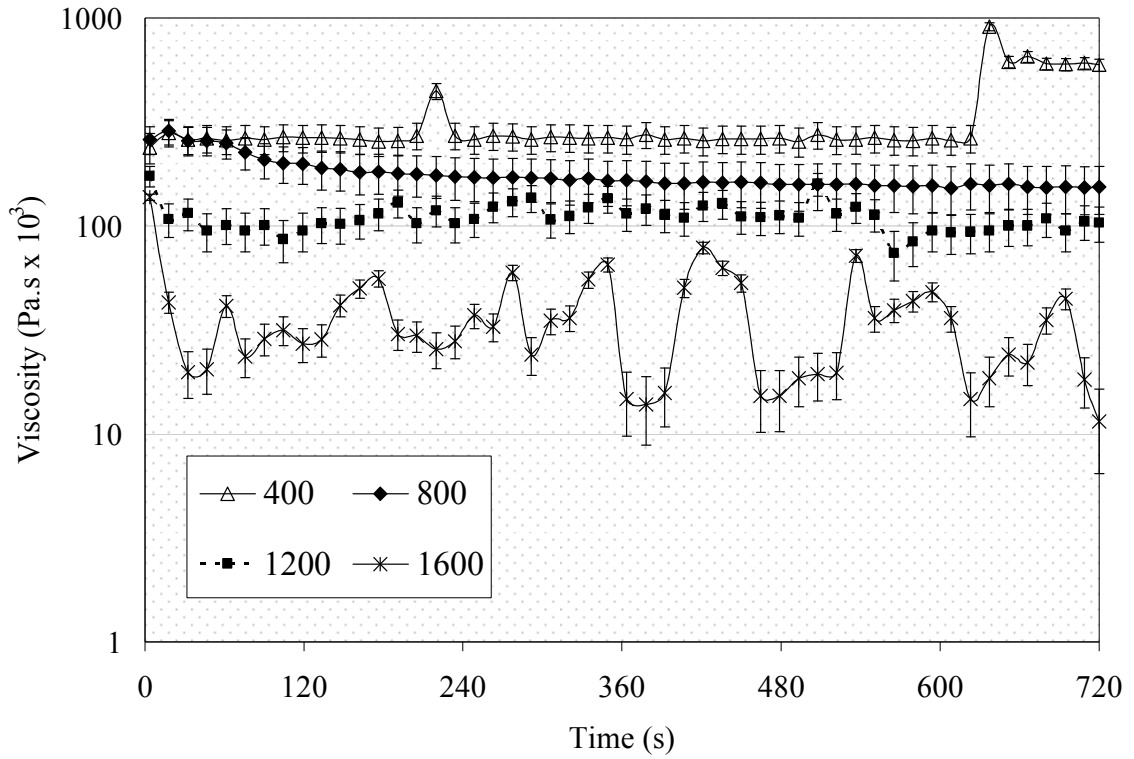


Figure 52. Premixing test with a 10% PCS slurry.

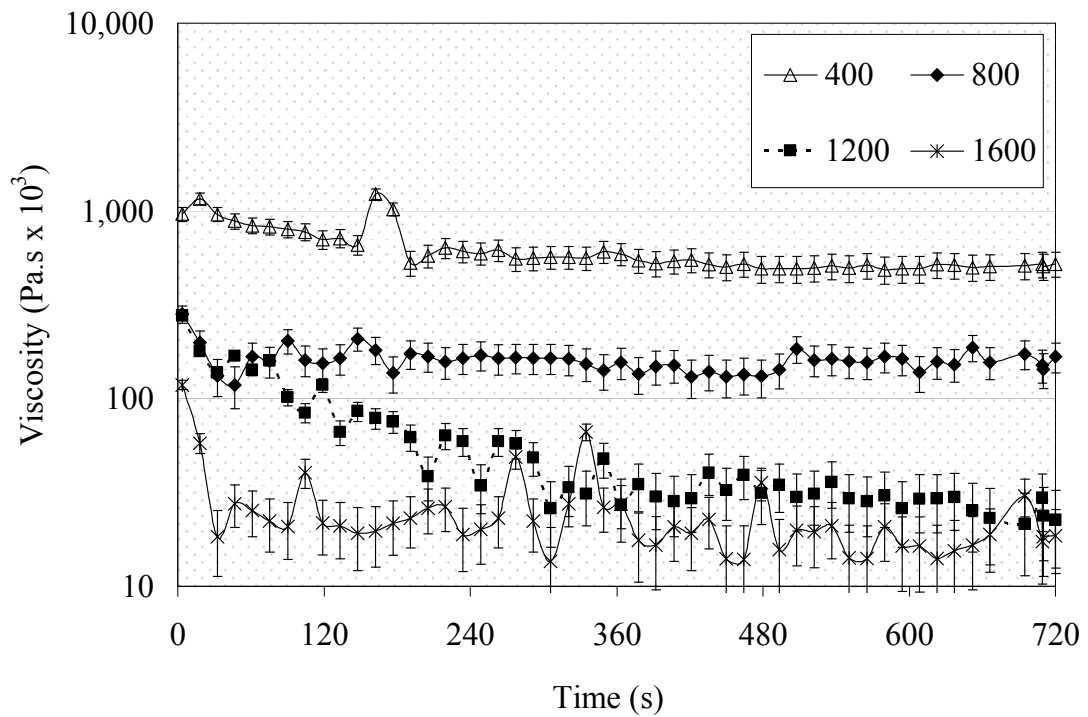


Figure 53. Premixing test with a 15% PCS slurry.

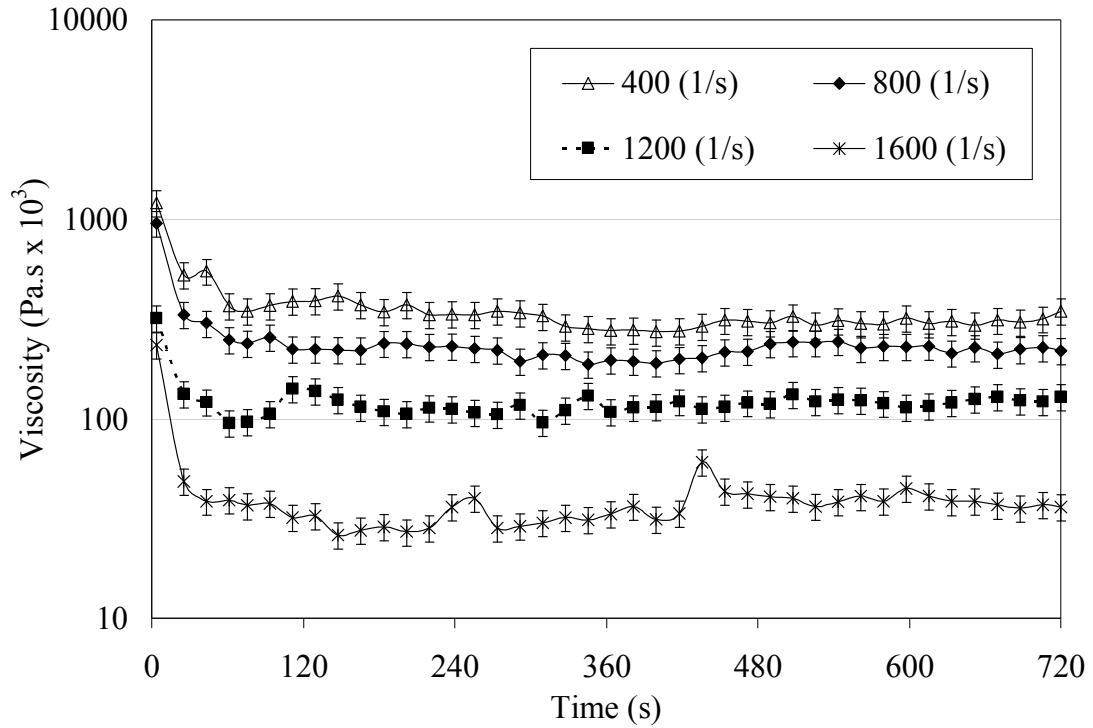


Figure 54. Premixing test with a 20% PCS slurry.

Lower viscosities are observed for PCS slurries with increasing shear rate for the 10, 15, and 20% solids slurries, a typical trend for non-Newtonian liquids. At higher shear rates slurry splattering is observed for lower solids concentrations than 10% and thus the 400 s⁻¹ shear rate is taken as a basis for premixing in order to have reliable data. The time needed for the viscosity to reach steady state for the 5, 7.5, 10, 15, and 20% solids slurries with premixing at 400 s⁻¹ shear rate is presented in Table 24.

Table 24

Time to Reach Steady State Viscosity for PCS Slurries with Various Solids Concentrations at Various Premixing Shear Rates

Shear rate (s ⁻¹) / % of PCS solids	5	7.5	10	15	20
400	60 s	60 s	60 s	360s	360s

Viscosity Measurements for PCS Slurries with Premixing at Various Shear Rates:

The time to reach steady state viscosity for PCS slurries with various solids concentrations by premixing at various shear rates is determined in the previous section. Each slurry is now premixed for that particular amount of time at each shear rate and then viscosity is measured over a range of shear rates using the MCR. Slurries are premixed at each shear rate for the predetermined time (refer Table 24 for 400 s⁻¹ shear rate) in order to achieve steady state viscosity. Viscosity is measured over a range of shear rates from 0.1-1000 s⁻¹. Each viscosity measurement is repeated three times and average results are presented. The software for the MCR is programmed to sweep the shear range twice in each measurement, first from 0.1-1000 s⁻¹ and then from 1000-0.1 s⁻¹.

The viscosity data for 5% PCS solids slurry, with premixing at various shear rates, are presented in Figure 55. The figure shows that the viscosity of the slurry increases with premixing shear rate. This result supports the postulate that premixing at shear rates higher than the corresponding USS helps the solids stay suspended longer.

It is known that the viscosity data for low solids concentrations (<10%) might not be accurate at the low end of the measured shear rate range (< 50 s⁻¹) due to the settling particles. However, each sweep of shear rates (1000-0.1 s⁻¹ or 0.1-1000 s⁻¹) takes only 70 seconds to collect about 30 data points. Thus in the present study, viscosity data should be reliable to a certain extent because the premixing technique helps the biomass particles stay suspended longer.

Viscosities of the 5% solids slurry are approximately equal above a shear rate of 150 s⁻¹ (seen in Figure 55) for all premixing shear rates. This data supports the result obtained in the premixing tests that the rpm corresponding to the 150 s⁻¹ shear rate is

about the USS for a 5% PCS solids slurry (Table 23). Viscosity of the 5% slurry is approximately the same for premixing shear rates of 800, 1200, and 1600 s^{-1} over the entire measured shear rate range, which confirms the postulate that premixing at higher shear rates helps in suspending the solid particles longer and helps to make the viscosity data reliable even at the low end of the shear rate range.

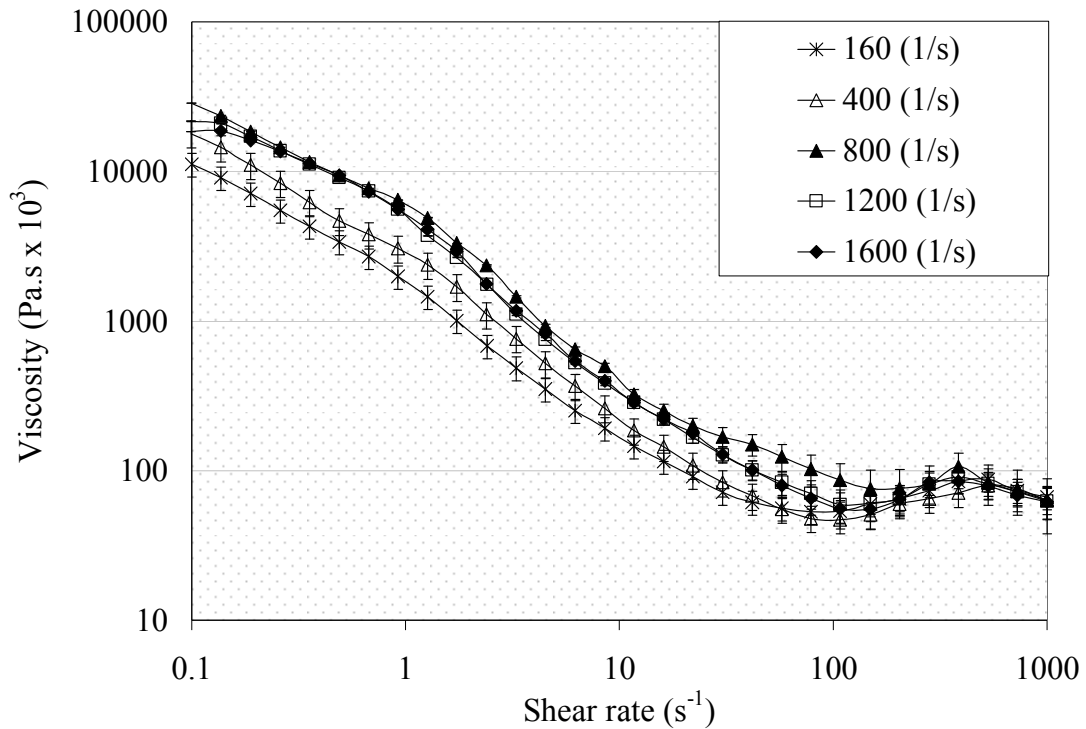


Figure 55. Viscosity data for a 5% PCS solids slurry with premixing at various shear rates.

The viscosity data for the 7.5% PCS solids slurry, with premixing at various shear rates, are presented in Figure 56. Similar to the viscosity data for the 5% solids slurry, the viscosity of the 7.5% solids slurry increases with the premixing shear over the measured shear rate range. Figure 56 also shows that the viscosity data is approximately the same over the entire measured shear rate range for 800, 1200, and 1600 s^{-1} premixing shear rates. The viscosity also appears to be about the same regardless of premixing

shear above about 450 s^{-1} , which is approximately the shear rate that corresponds to the USS for 7.5% solids slurry.

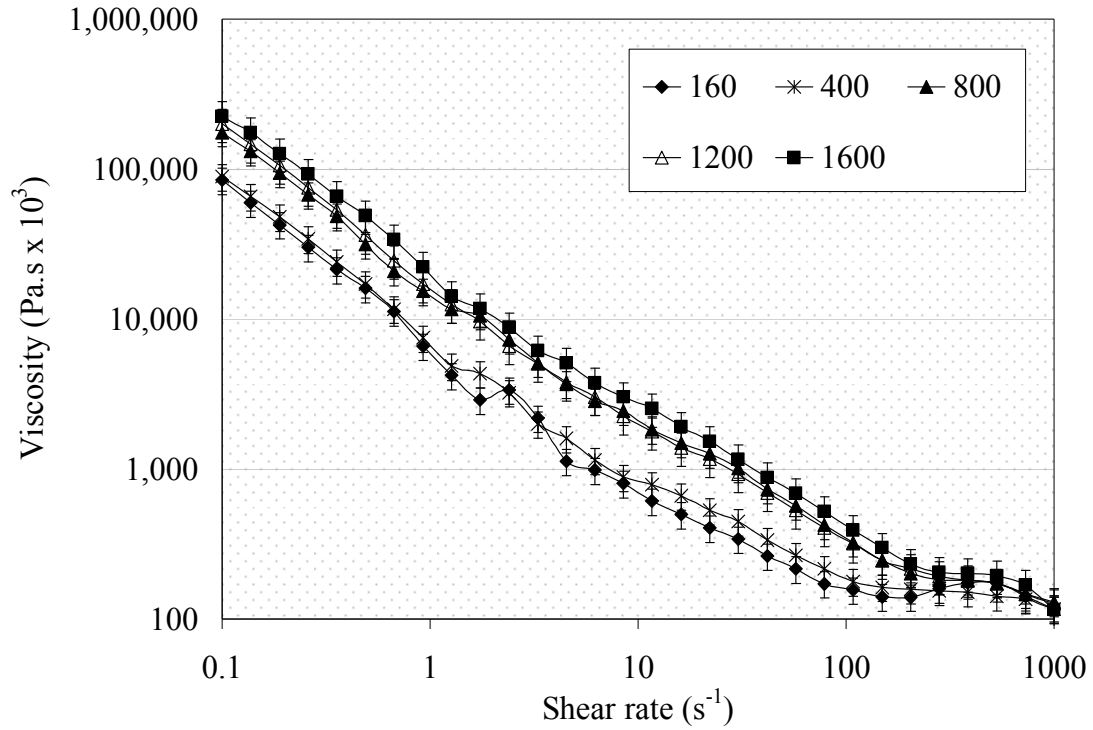


Figure 56. Viscosity of a 7.5% PCS solids slurry with premixing at various shear rates.

The viscosity data for the 10% PCS solids slurry, with premixing at various shear rates, are presented in Figure 57. The 10% slurry contains less free water as compared to the 5% and 7.5% slurries. Thus, it is easier to keep the solids suspended in the 10% slurry as compared to 5% and 7.5% solids slurries, even with mixing at a low shear rate. This might be the reason the viscosity data curves over the measured shear rate range appear very close together. The data curves appear farther apart at the low end of the shear rate range ($< 5 \text{ s}^{-1}$) and the curves become closer above a shear rate of about 10 s^{-1} .

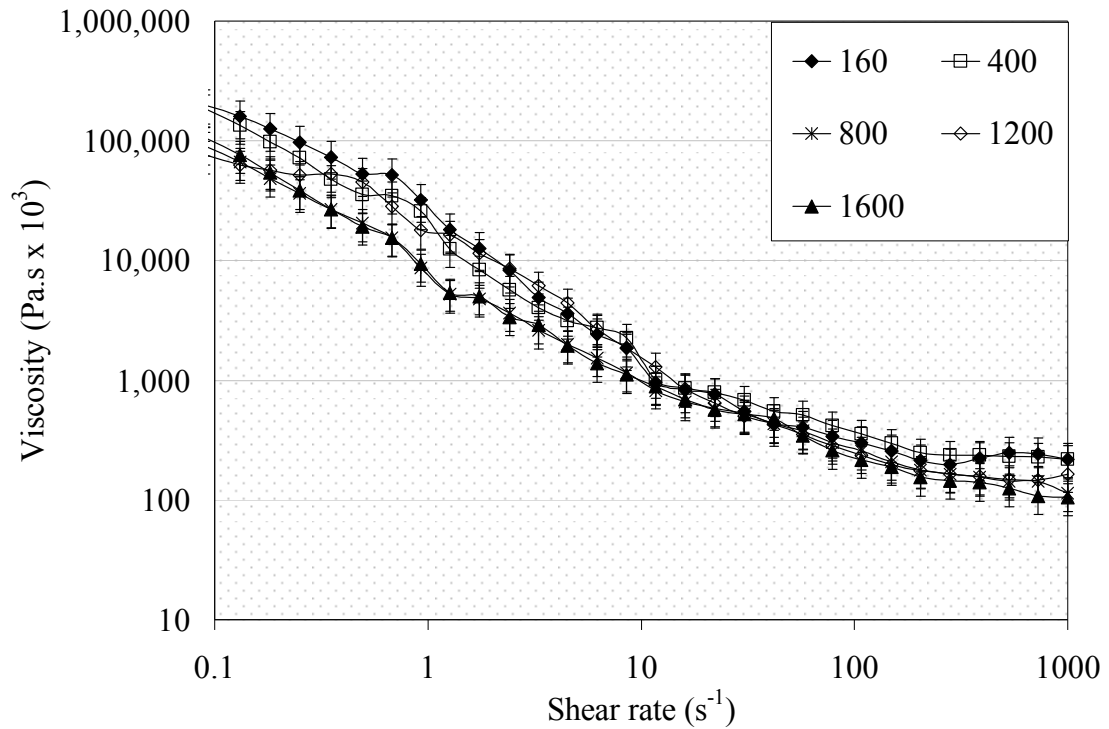


Figure 57. Viscosity of a 10% PCS solids slurry with premixing at various shear rates.

The viscosity data for the 15% and 20% PCS solids slurries, with premixing at various shear rates, are presented in Figure 58 and Figure 59. Since the PCS slurries with solids concentrations above 12% are paste-like materials, particle settling does not occur even at very low shear rates. Figure 58 and Figure 59 show that the viscosity data curves overlap, indicating that the measured viscosity is the same regardless of the premixing shear rate. Thus, it can be concluded that the viscosity data is reliable with this technique for slurries above 12% solids concentrations. For slurries with less than 12% PCS solids concentrations, a minimum premixing shear rate of about 800 s^{-1} (± 200) is recommended in order to obtain accurate viscosity data at the low end (under the USS of the corresponding solids concentration) of the measured shear rate range.

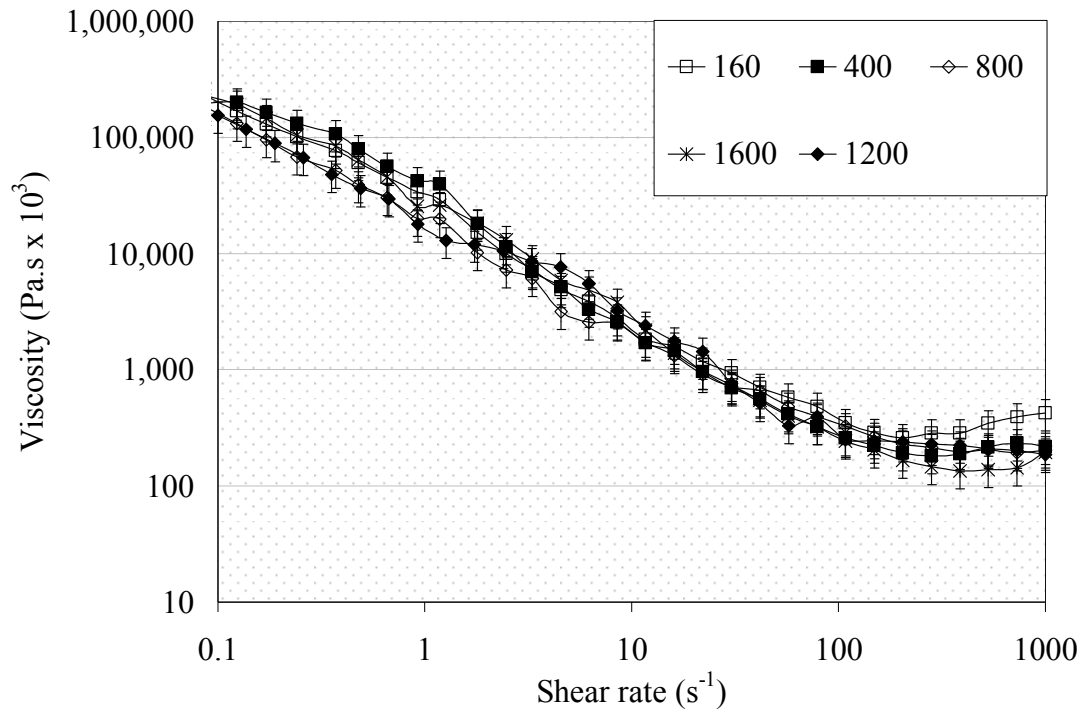


Figure 58. Viscosity of a 15% PCS solids slurry with premixing at various shear rates.

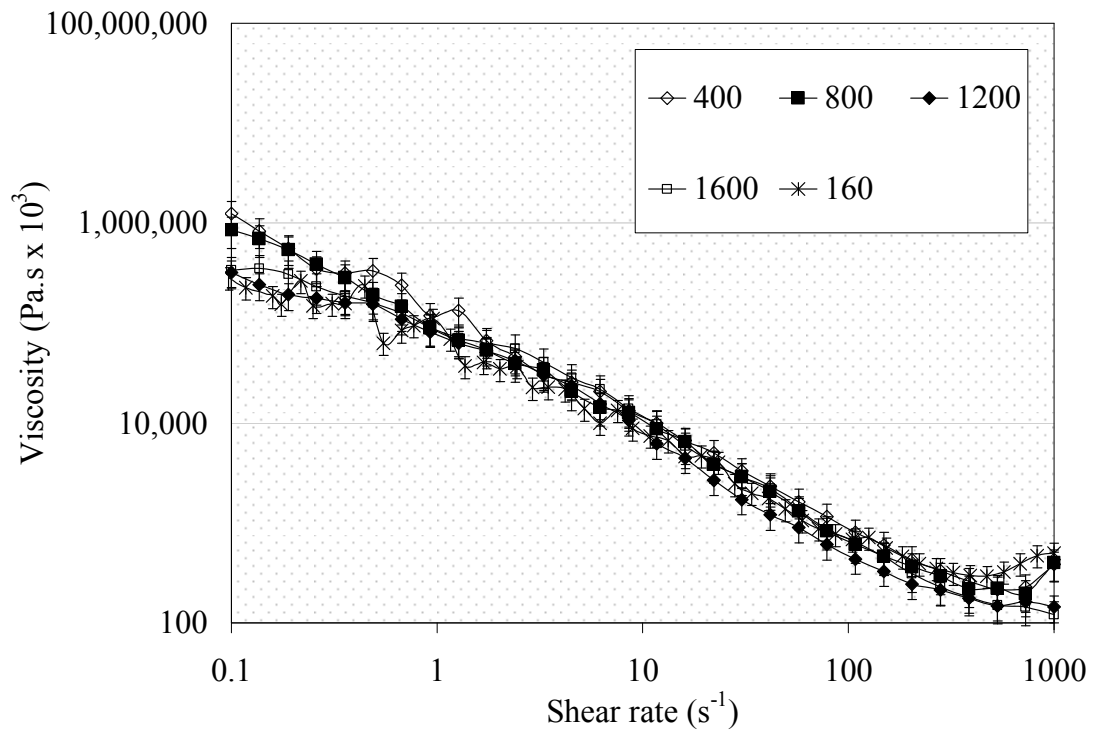


Figure 59. Viscosity of a 20% PCS solids slurry with premixing at various shear rates.

CHAPTER VII

CFD SIMULATIONS OF SOLIDS SUSPENSIONS IN A VISCOMETER CUP

CFD Simulation Problem Set-Up

3D Geometry Creation

The 3D geometry of the viscometer cup and the vane impeller is created with their exact dimensions using the commercial preprocessor, GAMBIT 2.4.6, from ANSYS. The two entities, the vane impeller and the cup, are connected together using the volume-split tool to make a single entity, as per the requirement of performing simulations in FLUENT. In order to reduce the computational time, only one-sixth of the complete geometry needs to be modeled since rotational periodic boundary conditions can be used. Therefore, only one vane blade and a 60° pie shape of the circular viscometer cup is drawn and meshed. The GAMBIT geometry drawing is shown in two different views in Figure 60a and 60b.

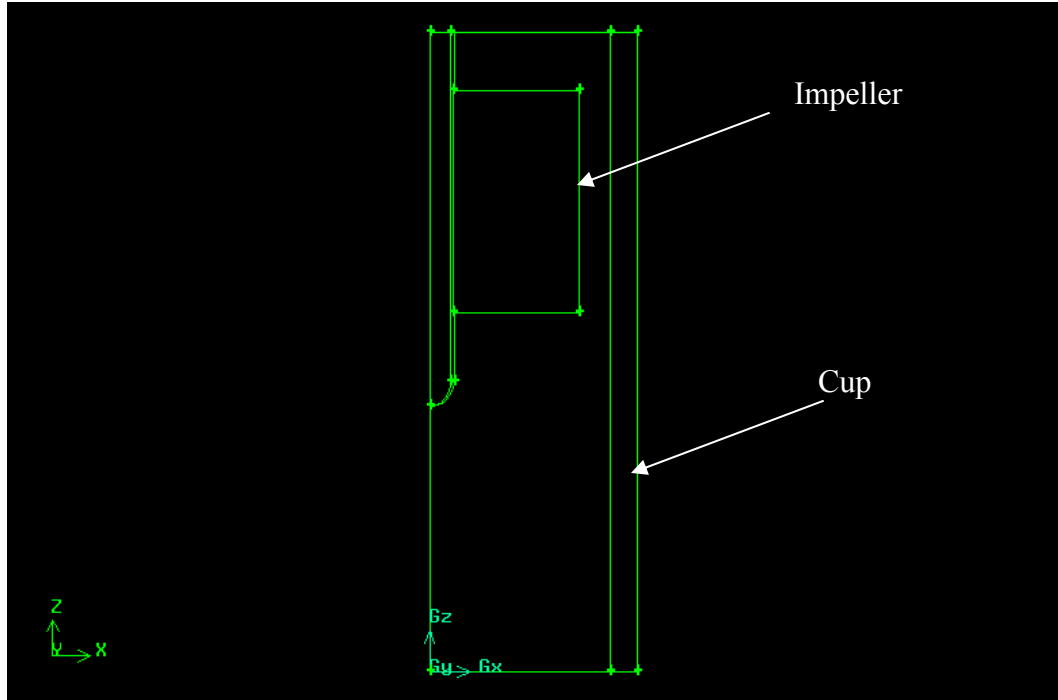


Figure 60a. GAMBIT drawing of the MCR cup and vane impeller (View 1).

The two side faces of the pie shape are hard-linked by the use of the link-face tool and are specified as periodic type as required in order to apply the rotational periodic boundary condition in FLUENT. This condition can be applied to faces through which the pressure fields entering and leaving are the same.

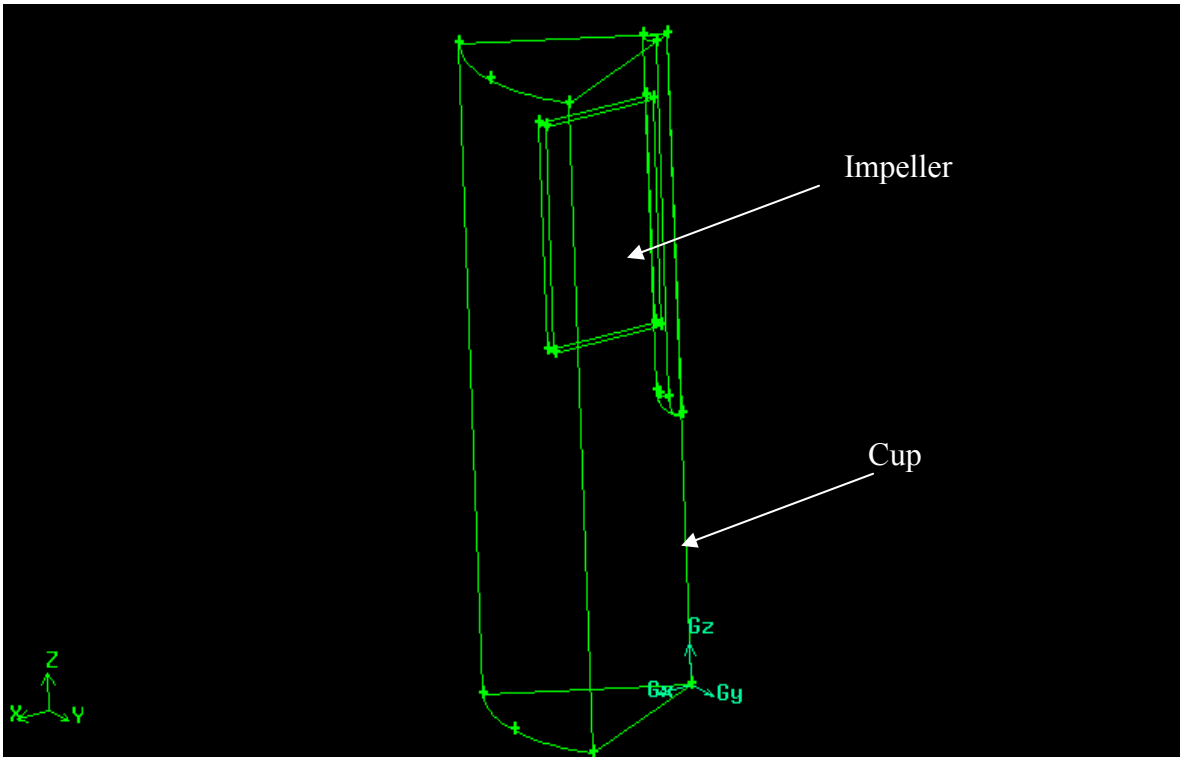


Figure 60b. GAMBIT drawing of the MCR cup and vane impeller (View 2).

Mesh Generation:

The faces of the geometry are meshed with quadrilateral face mesh elements using the Quad:Pave meshing scheme in the mesh-face tool to create unstructured quadrilateral mesh elements as shown in Figure 61. Then the volume of the cup is meshed using the mesh-volume tool with T-Grid, which specifies that the mesh is composed primarily of tetrahedral mesh elements but may include hexahedral, pyramidal, and wedge elements where appropriate. A sample of the tetrahedral mesh is shown in Figure 62, however only a few of those elements created in the meshing operation are shown. The quality of the mesh is examined and the skewness, which is an indication and a measure of mesh element quality, is confirmed to be less than 0.97.

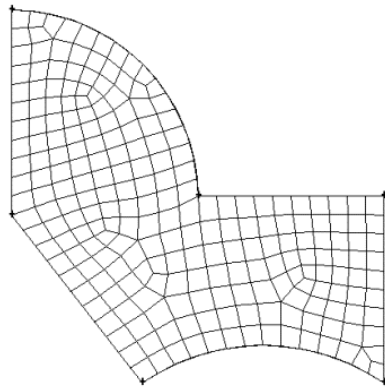


Figure 61. Quad:Pave face meshing scheme-example mesh (Fluent Inc., 2006).

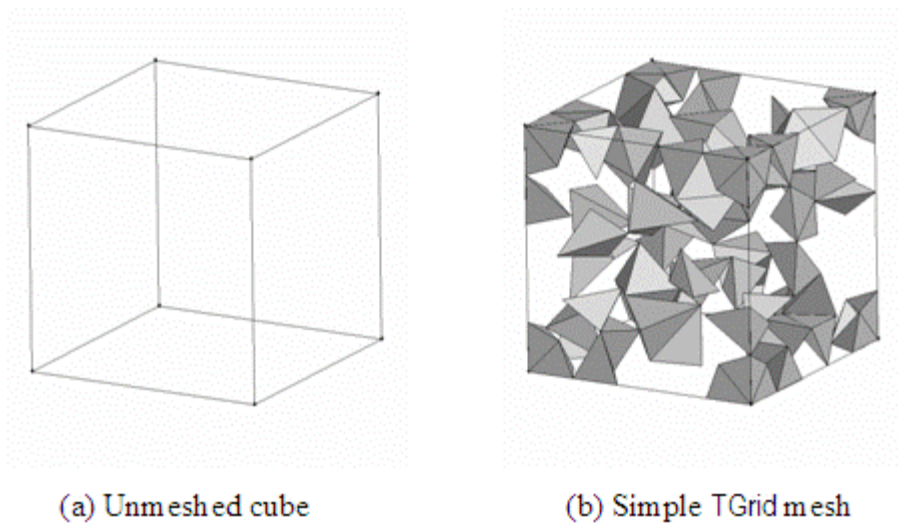


Figure 62. Sample T-Grid meshing scheme (Fluent Inc., 2006).

The actual meshed geometry is shown in Figure 63. There are 279,842 computational cells in the mesh.

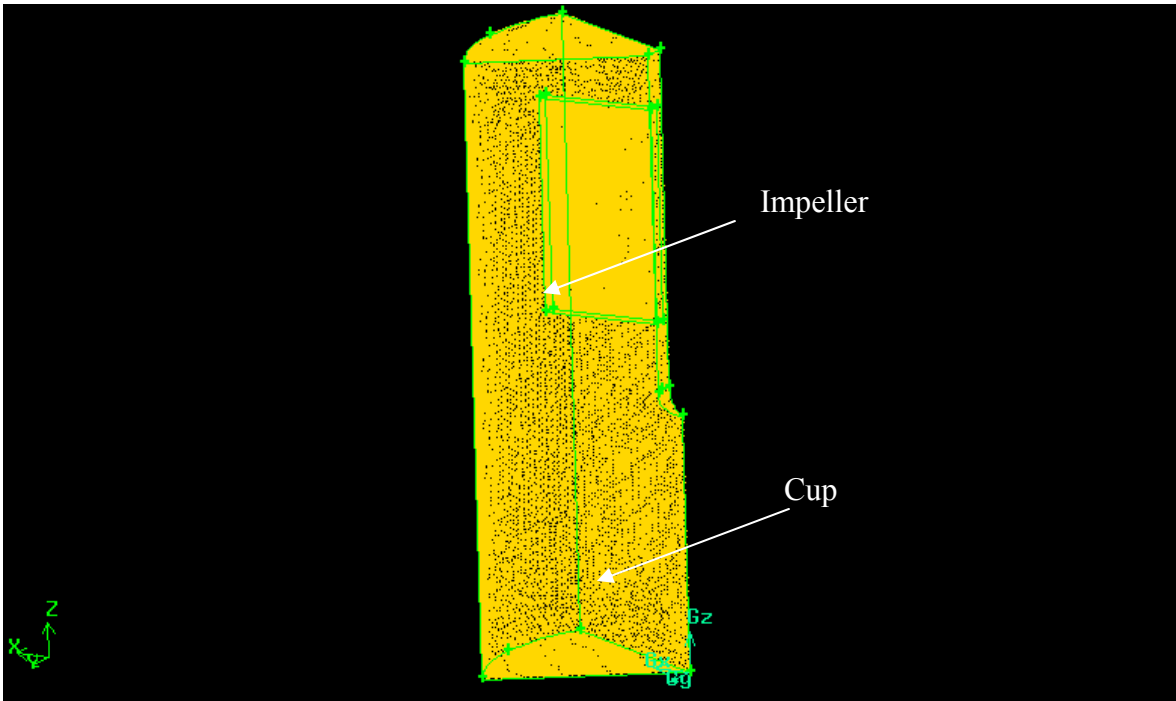


Figure 63. Meshed geometry of a pie shaped wedge of the viscometer cup and vane impeller.

The solver type is changed to FLUENT5/6 in order to specify the boundary and continuum types in GAMBIT and to communicate with FLUENT. All the impeller faces and the viscometer cup faces are specified as surface wall-type except the two side faces of the pie shape. These two faces are specified as periodic boundary type in order to apply the rotational boundary condition. The volume of the cup, excluding the impeller volume, is specified as a fluid continuum. The 3D meshed geometry is exported to create a .msh file that can be recognized by FLUENT.

Eulerian Multiphase Model:

Setup and Solution:

The FLUENT panel consists of various tabs such as: File, Grid, Define, Solve, Adapt, Surface, Display, Plot, Report and Parallel, which are used to define model parameters. The model setup for viscometer simulations is explained in detail for each of the tabs. Sample panels from various drop-down menu options are shown adjacent to the main FLUENT panel.

- 1) The .msh (case) file is read in FLUENT 6.2.26 and the grid (mesh) is checked for any negative volumes.

File → Read → Case

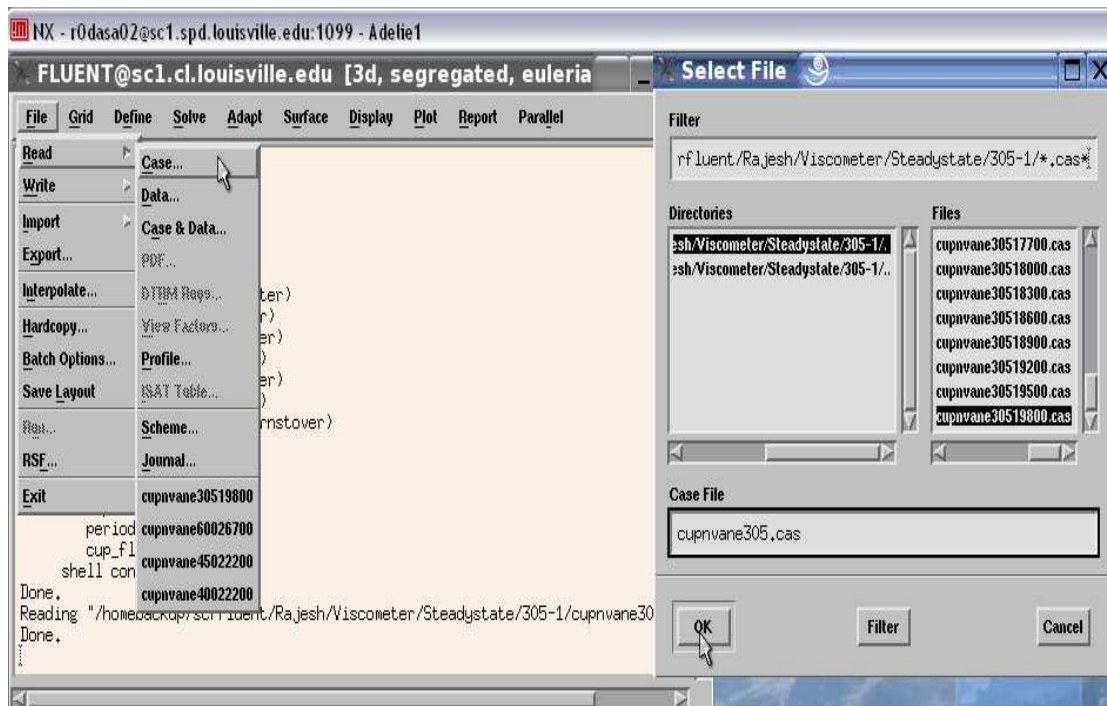


Figure 64. Read→Case panel.

Grid → Check



Figure 65. Grid → Check panel.

If negative volumes exist, the mesh has to be refined or redrawn in GAMBIT.

2) Use the Display tab to view the full tank (360°).

Display → Views

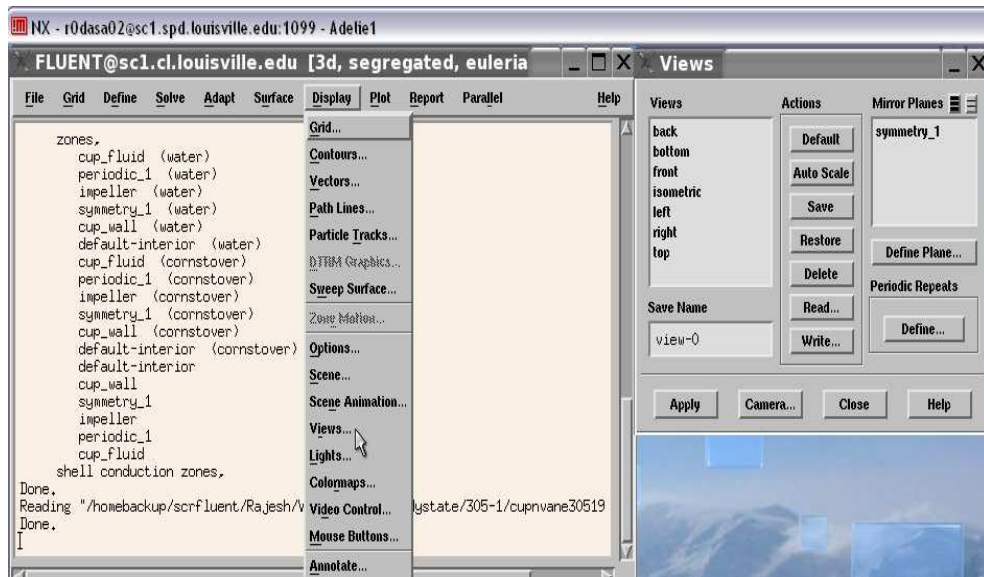


Figure 66. Display → Views panel.

The Define tab is clicked to define the rotational periodicity of the drawing as 360° .

- 3) Define – Retain the steady state option with the other default options in the model panel.

Define → Models → Solver

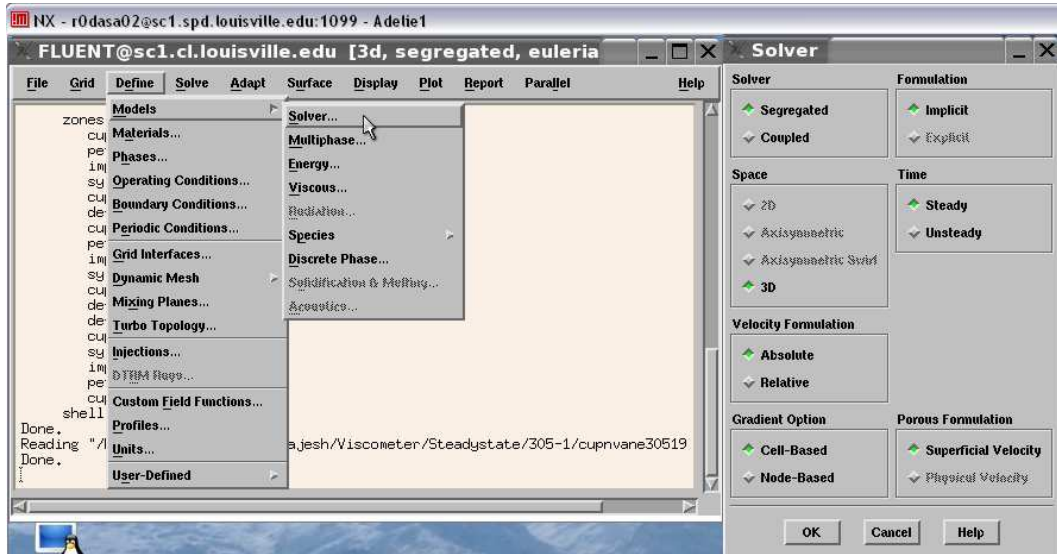


Figure 67. Solver panel.

- 4) The Eulerian multiphase model is enabled with 2 phases.

Define → Models → Multiphase

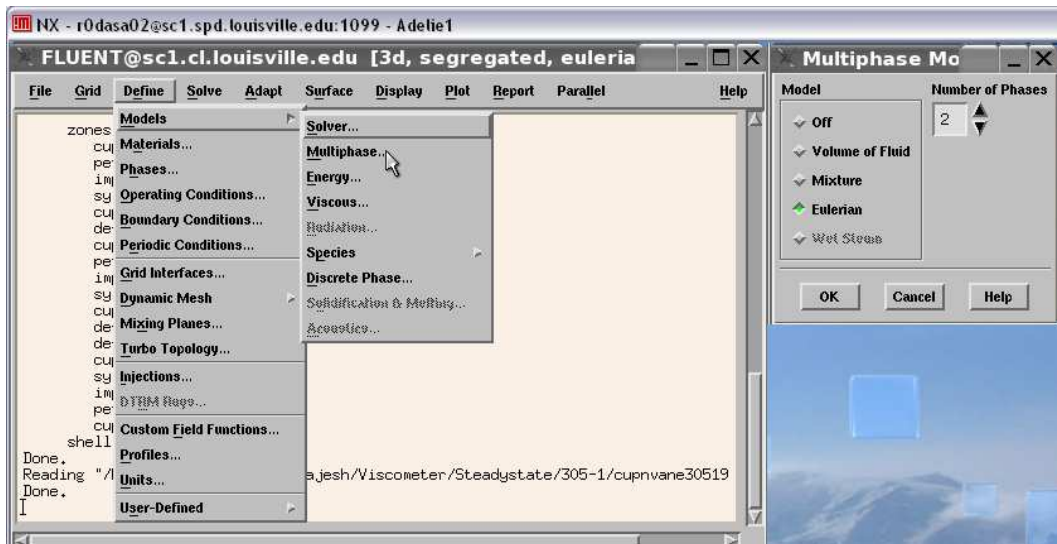


Figure 68. Multiphase model panel.

- 5) The default option, laminar flow, is retained.

Define → Models → Viscous



Figure 69. Viscous model panel.

The Reynolds's (N_{Re}) number for each case is calculated based on the density, viscosity, and rotational speed, and all cases are found to be laminar ($N_{Re} < 50$).

$$N_{Re} = \frac{\rho ND^2}{\mu} \quad (17)$$

6) Set the gravitational acceleration.

Define → Operating Conditions



Figure 70. Operating conditions panel.

The gravitational value is defined as -9.8 m/s^2 in the z-direction.

- 7) FLUENT has a very large materials database; liquid water from the database is copied for the first phase. A new fluid material is created for corn stover and the density is specified.

Define → Materials

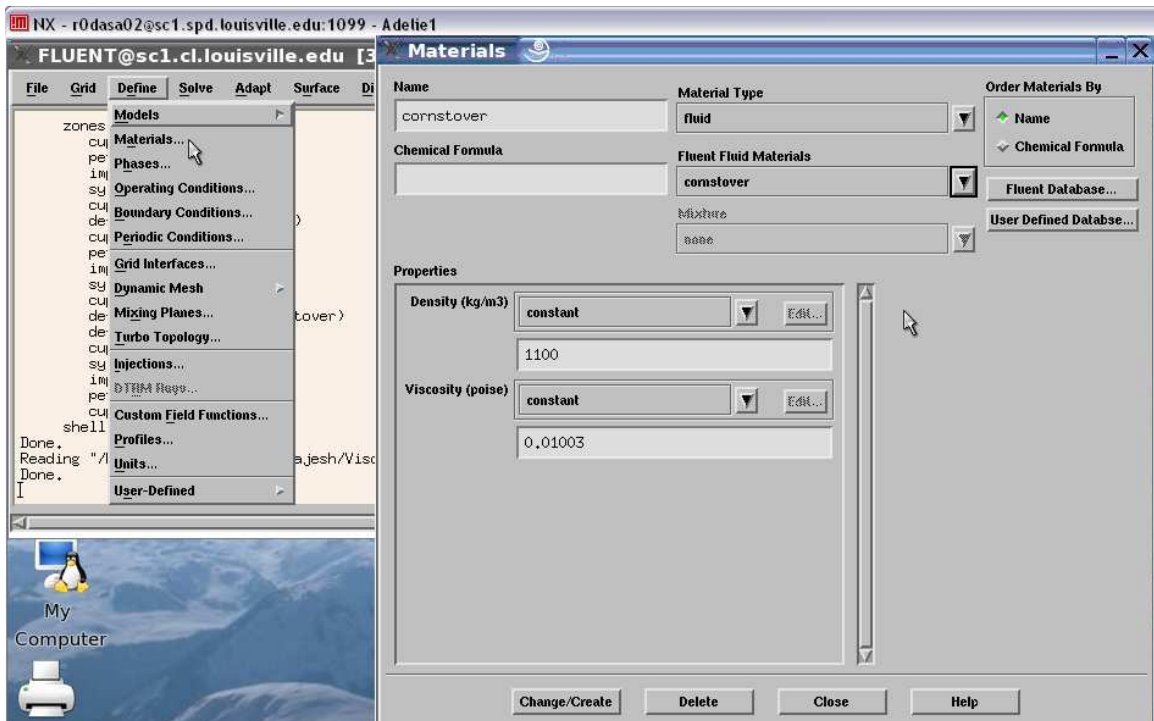


Figure 71. Materials panel.

Simulations are performed for the slurry with 5% solids concentrations (by weight). The wet density of PCS (pretreated corn stover) solids is not reported anywhere in the literature, presumably because of the same difficulty encountered during this work in measuring the density of the wet PCS solids in solution. So, the density is estimated using FLUENT simulations and the procedure is explained below in the Results and Discussion.

- 8) The two phases are specified as water and PCS solids.

Define → Phases

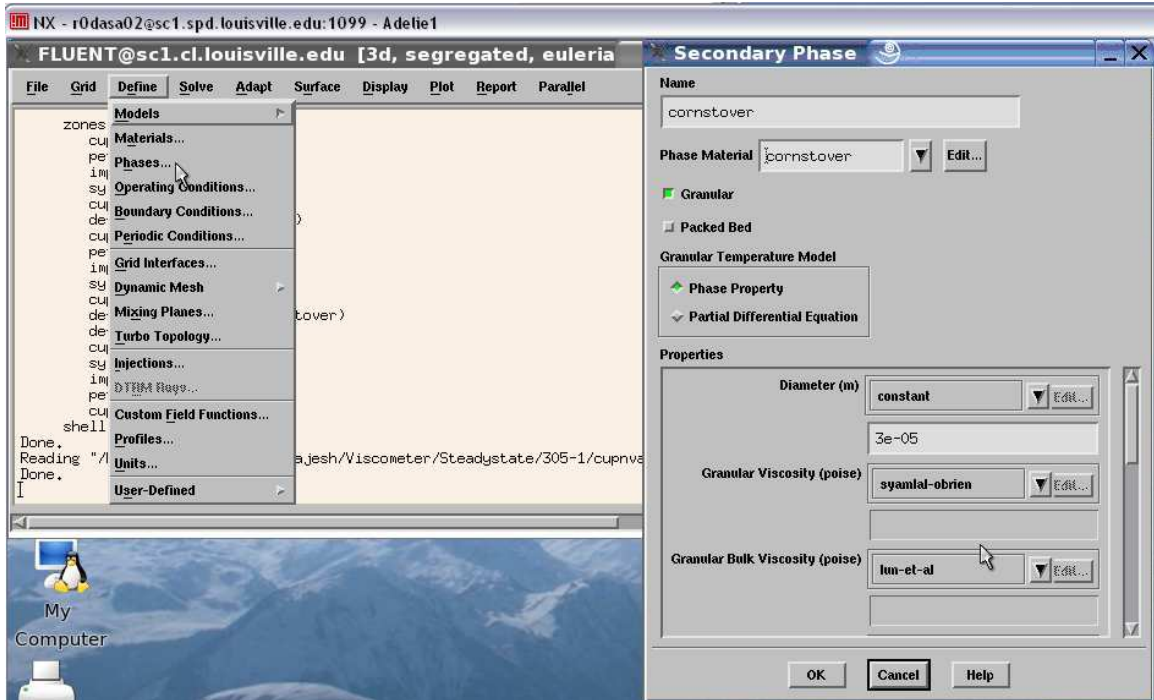


Figure 72. Phases panel.

Water is set as the primary phase, PCS solids are set as the secondary phase, and the Granular model is enabled for PCS solids. Syamlal-Obrien from the Granular Viscosity drop-down list and Lun-et-al from the Granular Bulk Viscosity drop-down list are specified. These models are recommended when using the Eulerian multiphase model (Fluent Inc., 2006). The average particle size for PCS solids is measured with a Master Sizer particle size analyzer (Malvern Instruments Inc., United Kingdom) and is found to be $30\mu\text{m}$. The packing limit for corn stover slurries is specified in the material panel as 0.6, with an assumption that the slurries are mono-dispersed. The gidaspow drag-coefficient is chosen for phase interaction from the Interaction panel.

- 8) The boundary conditions are specified.

Define → Boundary Conditions

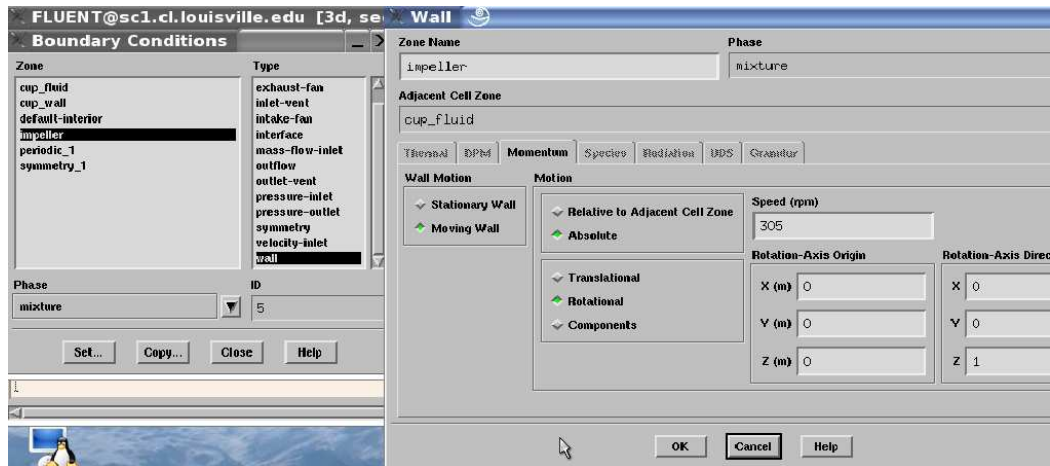


Figure 73. Boundary Conditions panel.

The boundary conditions (BC) are set for each surface and the fluid zone separately in the BC panel. The viscometer cup walls, except the periodic surfaces, are set to be stationary, while the impeller is set to have a specific rotational speed for each simulation. The liquid zone is set with the default values, which is stationary with respect to the adjacent zone which gives it the same speed as the impeller. The periodic surfaces are set to have a periodic boundary condition.

- 9) The solution parameters are set.

Solve → Controls → Solution

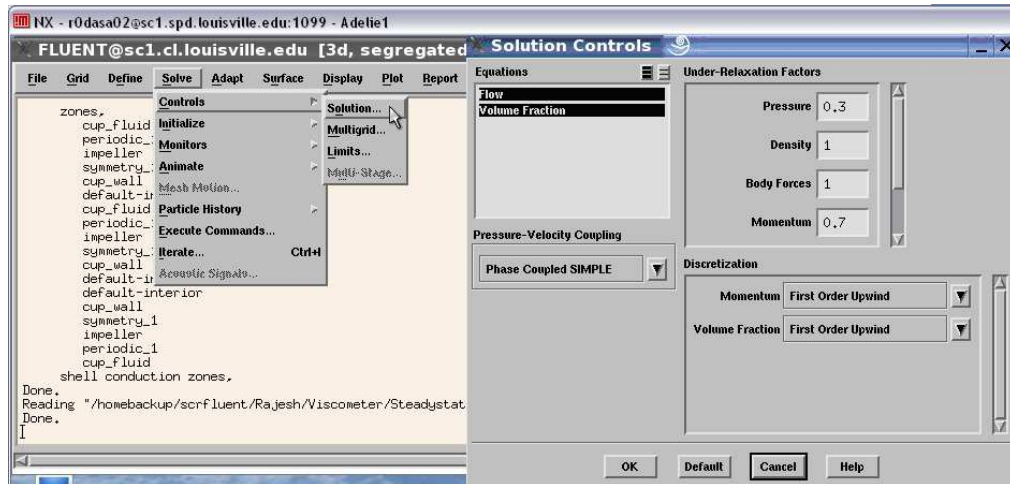


Figure 74. Solution Controls panel.

The flow and volume fraction equations are enabled and the default values are retained for Pressure-Velocity coupling, Discretization, and Under-Relaxation factors.

- 10) The plotting of residuals during calculation is enabled and a value of $1e-3$ is specified for each solution parameter and $1e-5$ is specified for the continuity equation residuals.

Solve → Monitors → Residuals

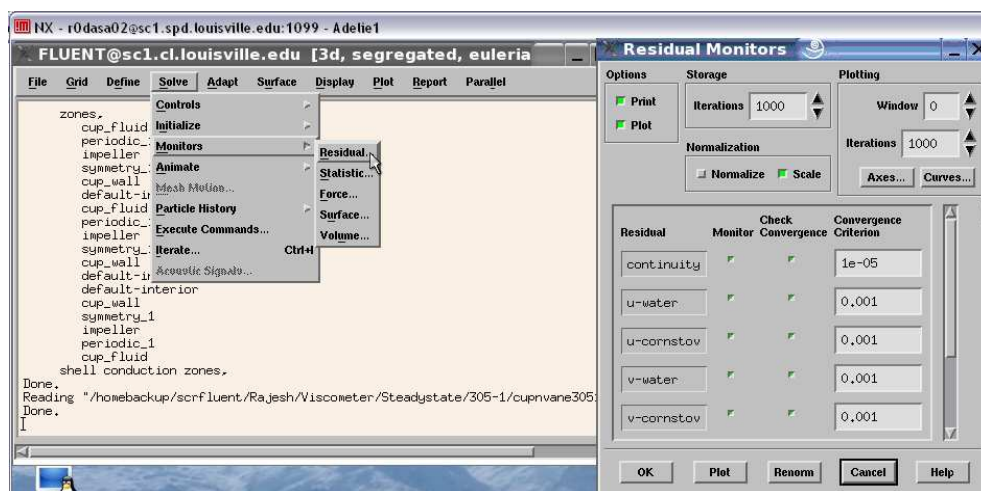


Figure 75. Residuals panel

11) Five surface monitors are created at different levels of height (0.5, 5, 10, 20, and 30 mm) from the bottom of the viscometer cup for analysis of solids distribution in the cup during post-processing.

Solve → Monitors → Surface

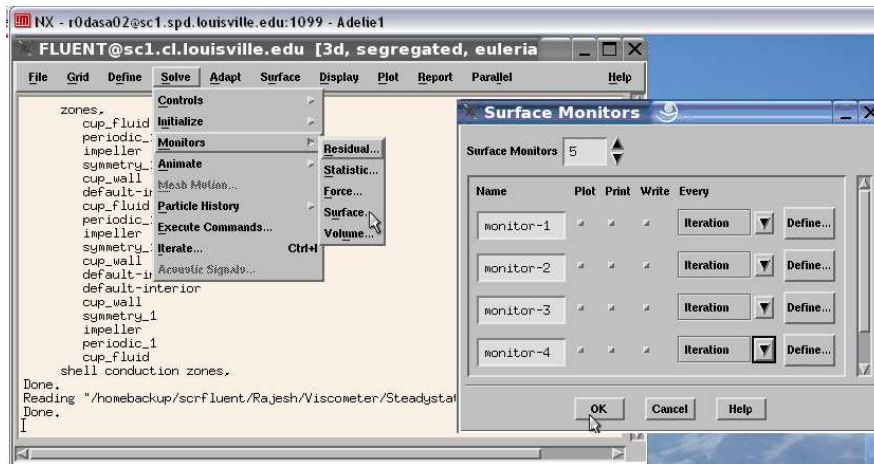


Figure 76. Surface Monitors panel.

12) The solution is initialized with the default values.

Solve → Initialize → Initialize

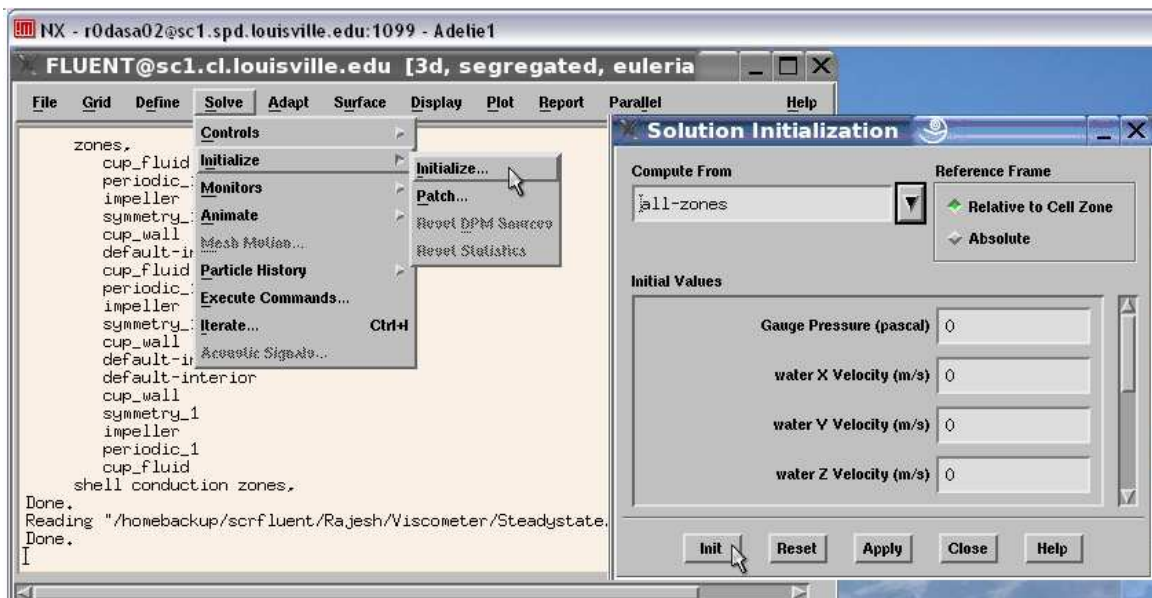


Figure 77. Solution Initialization panel.

- 13) The solids are patched into the liquid flow field assuming a uniform suspension at the start of the solution. This is to simulate the condition created by hand mixing of samples prior to viscosity measurements.

Solve → Initialize → Patch

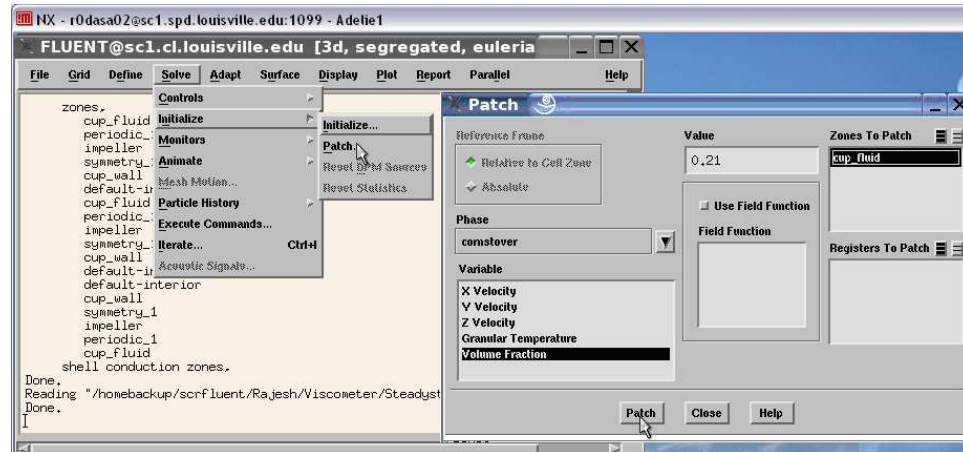


Figure 78. Patch-Volume Fraction panel.

Volume fraction is determined for 5% PCS solids by centrifuging the slurry in 20 mL centrifuge tubes at 4000 rpm until no change is observed in the height of the solids bed (5 hours). The ratio of height of the settled solids to the total height is considered as the volume fraction of the solids and the value is 0.21. The PCS solids are patched into the slurry (the total fluid zone volume) with the volume fractions specified as determined for each simulation.

- 14) The number of iterations is set in the Iteration panel.

Solve → Iterate



Figure 79. Iteration panel.

15) The case and data files are saved.

Write → Case & Data

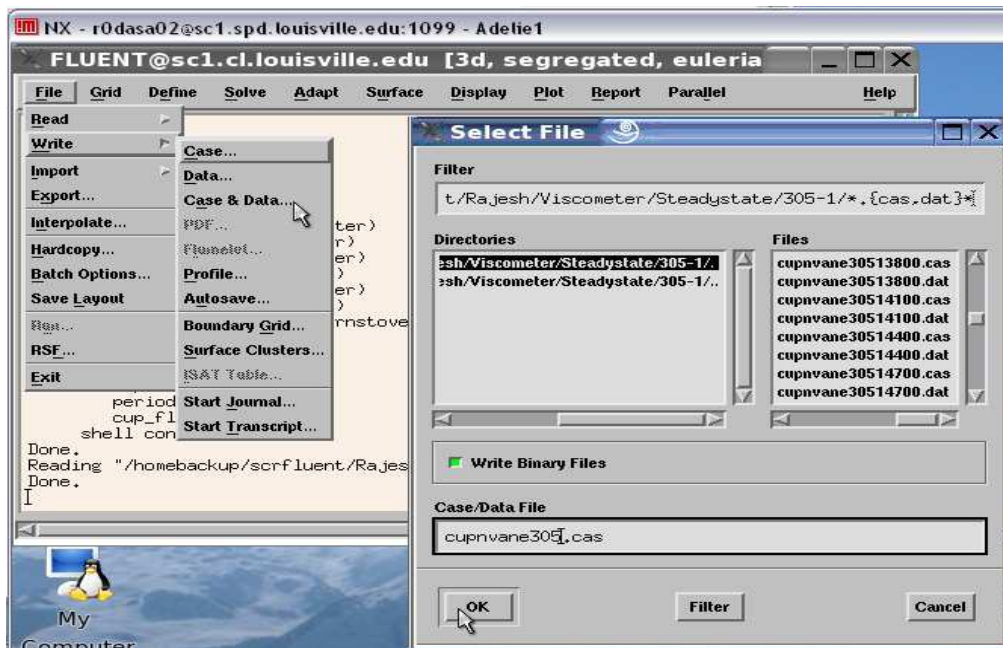


Figure 80. Write → Case & Data panel.

16) The solution iteration routine is started

Solve → Iterate → Iterate

Residuals for solution parameters are manually monitored for the first 50 iterations to determine if the residuals are approaching the specified values, or if the residual values are asymptoting upward early. If the residual values are asymptoting early or approaching an infinite value, the iteration is stopped. The Discretization and Under-Relaxation factors are varied in order to obtain a solution that can converge in a reasonable time.

A script is run in order to submit each case in batch mode on the Speed School Adelle network. The script files are given in Appendix C.

Although the JSS and the USS are determined from experimental observations, CFD is used to determine only the USS. This is because experimental determination of JSS is easier than USS because it is easier to judge particles settling at the bottom than it is to visually determine a uniform suspension of solids. USS is more subjective and CFD can help discern this by measuring and examining the solids distribution at various cross sections (horizontal and vertical) of the viscometer cup.

RESULTS AND DISCUSSION

Determination of Wet Density of PCS Solids:

The wet density of PCS solids is not cited in the literature and it is typically difficult to determine the density of the wet solids. PCS solids have a tendency to absorb liquid because of the porous structure. So, difficulty lies in determining the weight of the wet solids when present in liquid at their maximum capacity for liquid absorption. Attempts to experimentally determine the wet density of PCS solids resulted in densities less than water, but since the solids do not float, this must be incorrect. Hence, the first

objective of this section is to use FLUENT simulations to determine the wet density of PCS solids. The second objective of this section is to determine the USS for a 5% PCS solids slurry by performing FLUENT simulations on the cup and vane system of the Anton Paar MCR with the newly determined wet density of PCS solids.

A series of FLUENT simulations are run with various densities (1100, 1200, 1300, and 1400 kg/m³) at an impeller speed of 305, which corresponds to the experimentally determined USS for the 5% PCS solids slurry. These densities were chosen because they are higher than that of water, and the PCS solids are known to sink in an aqueous solution. The contours of volume fractions of PCS solids in the slurry at various horizontal cross-sections (0.5, 5, 10, 20, and 30 mm from the bottom of the viscometer cup) and at a vertical cross-section along the vertical axis of the viscometer cup are shown for each simulation. The density of wet solids is determined to be the value of the case for which the solids appear to be uniformly suspended (since the simulation is run at the USS).

The contours of volume fraction for the simulation at 305 rpm with 1100 kg/m³ density are shown in Figure 81 and Figure 82. Based on the color scale on the left side of the figures, it appears that the volume fraction of PCS solids is uniform in the entire cup with a value of about 0.2, which is approximately equal to the patched volume fraction, 0.21.

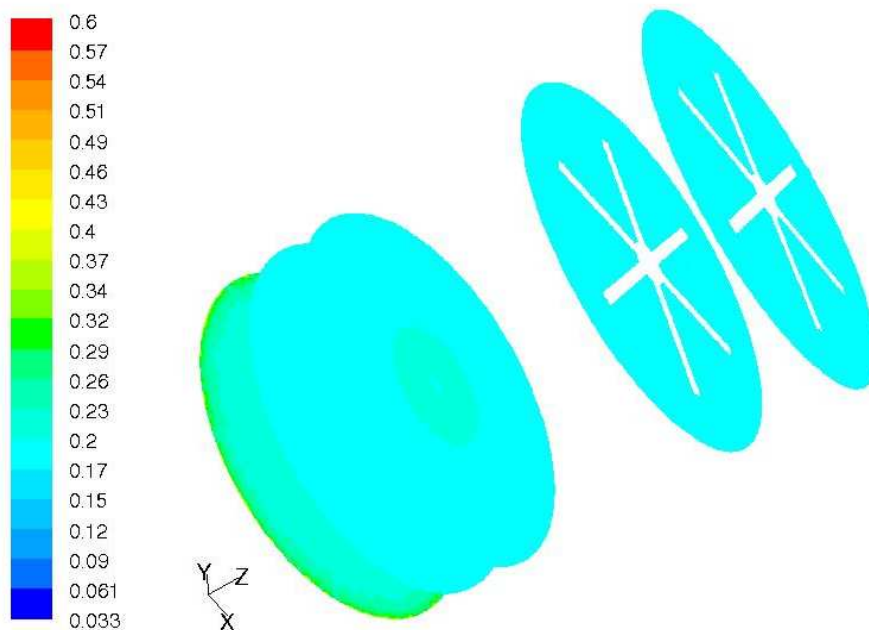


Figure 81. Contours of volume fraction of PCS solids in the slurry at various horizontal cross-sections of the viscometer cup at 305 rpm with 1100 kg/m^3 density.

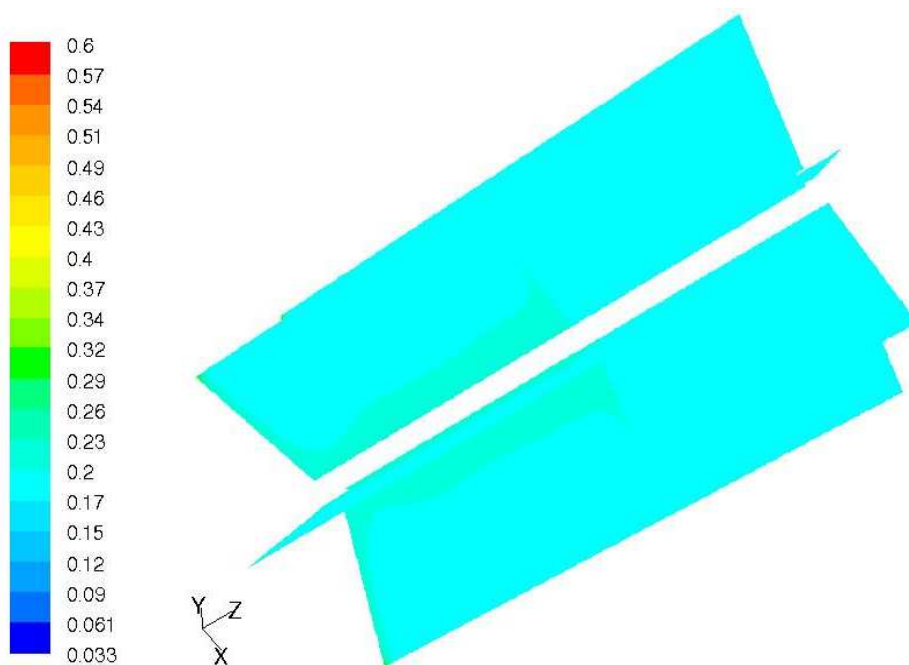


Figure 82. Contours of volume fraction of PCS solids in the slurry along the vertical axis of the viscometer cup at 305 rpm with 1100 kg/m^3 density.

The contours of volume fraction for the simulation at 305 rpm with 1200 kg/m³ density are shown in Figure 83 and Figure 84. It can be seen from the figures that the volume fraction of the solids at the bottom of the cup is as high as 0.45, which is higher than at any other level of the viscometer cup. The higher volume fraction of PCS solids near the bottom indicates that the particles are settling at the bottom, so the 1200 kg/m³ is probably higher than the actual density of wet PCS solids.

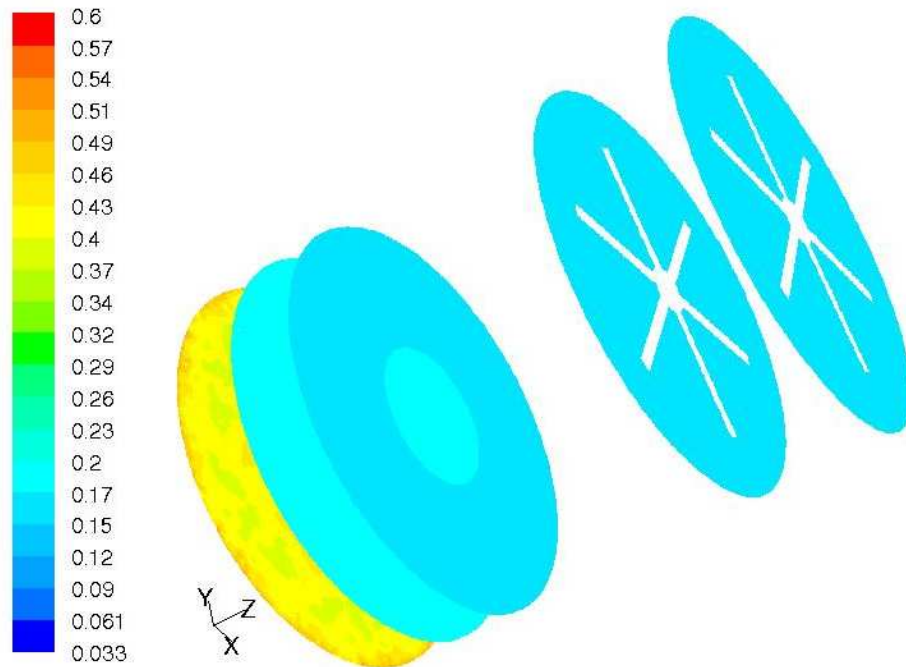


Figure 83. Contours of volume fraction of PCS solids in the slurry at various horizontal cross-sections of the viscometer cup at 305 rpm with 1200 kg/m³ density.

The contours of volume fraction for the simulation at 305 rpm with 1300 kg/m³ density are shown in Figure 85 and Figure 86. The volume fraction of the solids at the bottom of the cup is as high as 0.6, which is again higher with more

solids residing near the bottom than in the case of the 1200 kg/m³ density. Therefore, 1300 kg/m³ also is likely higher than the density of wet PCS solids.

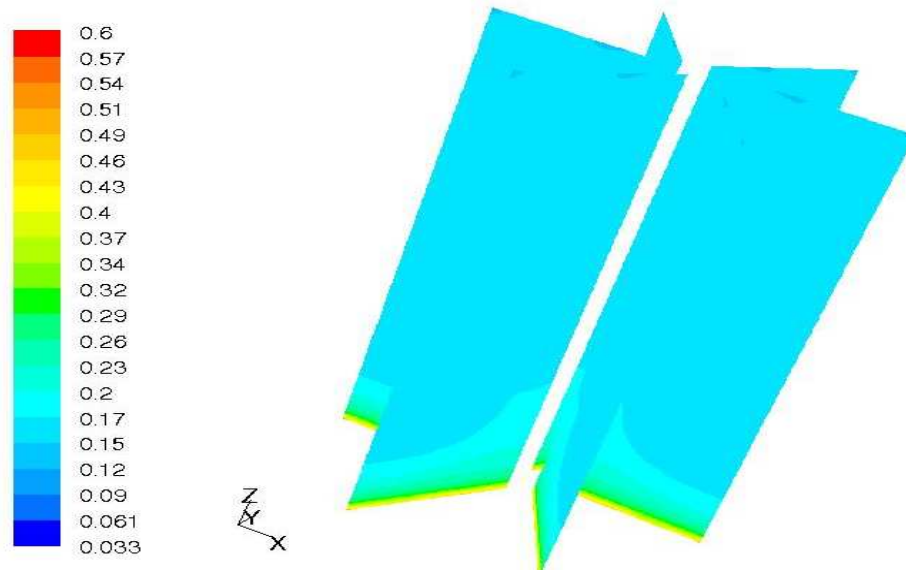


Figure 84. Contours of volume fraction of PCS solids in slurry along the vertical axis of the viscometer cup at 305 rpm with 1200 kg/m³ density.

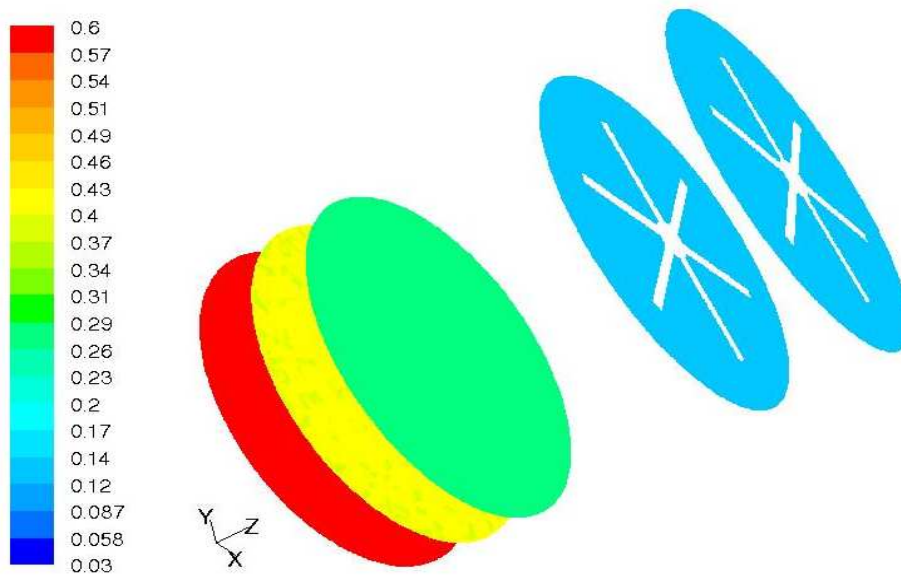


Figure 85. Contours of volume fraction of PCS solids in slurry at various horizontal cross-sections of the viscometer cup at 305 rpm with 1300 kg/m³ density.

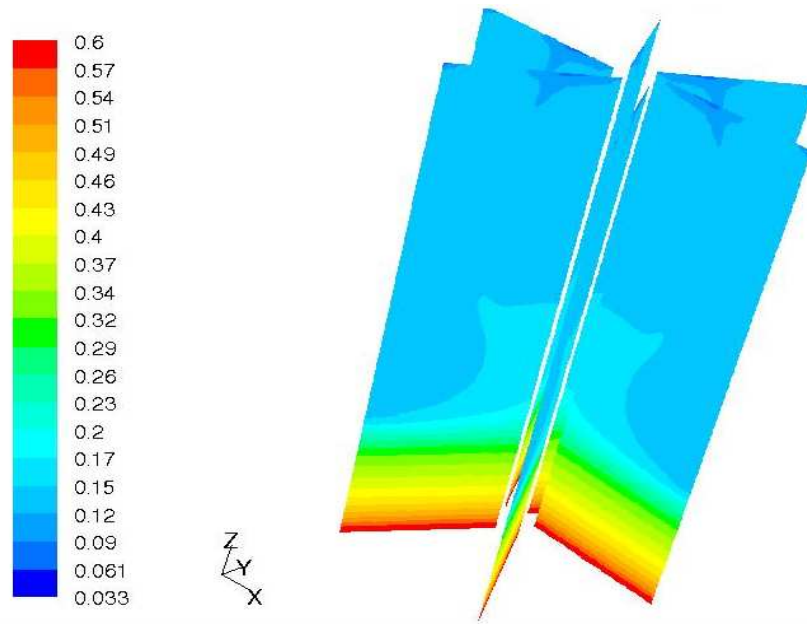


Figure 86. Contours of volume fractions of PCS solids in slurry along the vertical axis of the viscometer cup at 305 rpm with 1300 kg/m^3 density.

The contours of volume fraction for the simulation at 305 rpm with 1400 kg/m^3 density are shown in Figure 87 and Figure 88.

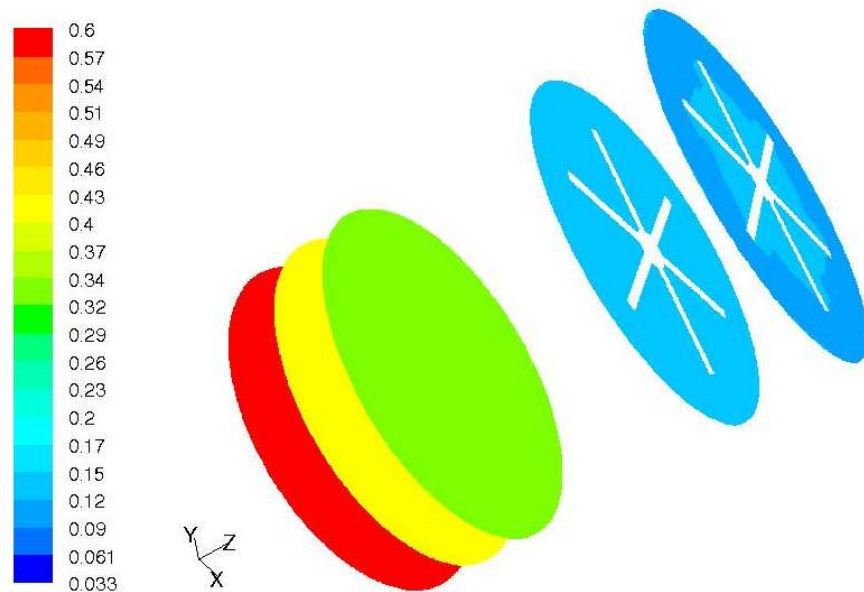


Figure 87. Contours of volume fraction of PCS solids in slurry at various horizontal cross-sections of the viscometer cup at 305 rpm with 1400 kg/m^3 density.

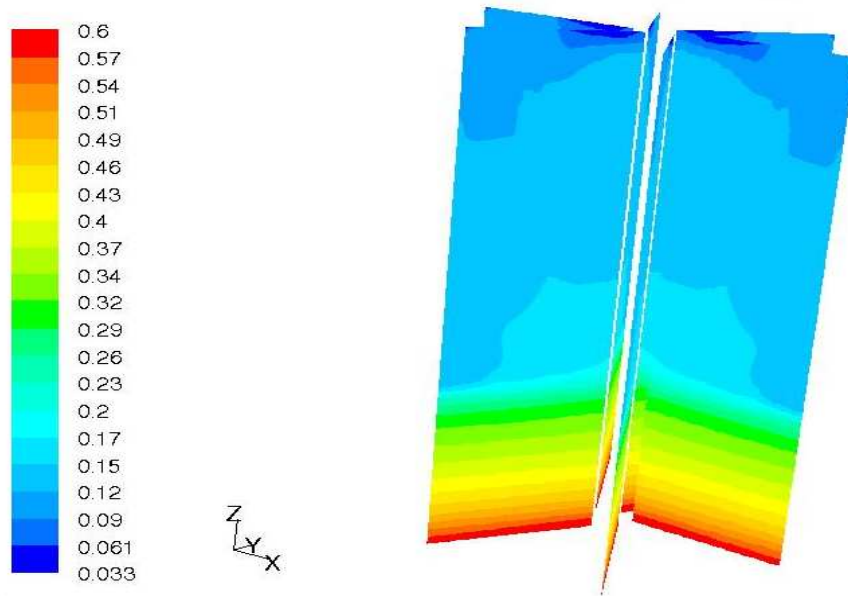


Figure 88. Contours of volume fraction of PCS solids in slurry along the vertical axis of the viscometer cup at 305 rpm with 1400 kg/m^3 density.

The volume fraction of the solids at the bottom of the cup is as high as 0.6, which is higher than at any other level of the viscometer cup. The fraction of settling solids is further increased as compared to the case with a 1300 kg/m^3 density. The contours with the most uniform volume fraction over the entire viscometer cup region are obtained for the slurry with the 1100 kg/m^3 density. Therefore, the wet density of PCS solids is concluded to be 1100 kg/m^3 and this value is used for all future simulations.

Another series of FLUENT simulations is performed at various speeds above and below 305 rpm in order to either confirm or fine tune the USS for the 5% PCS slurry. The contours of volume fraction for the simulation at 230 rpm are shown in Figure 89 and Figure 90.

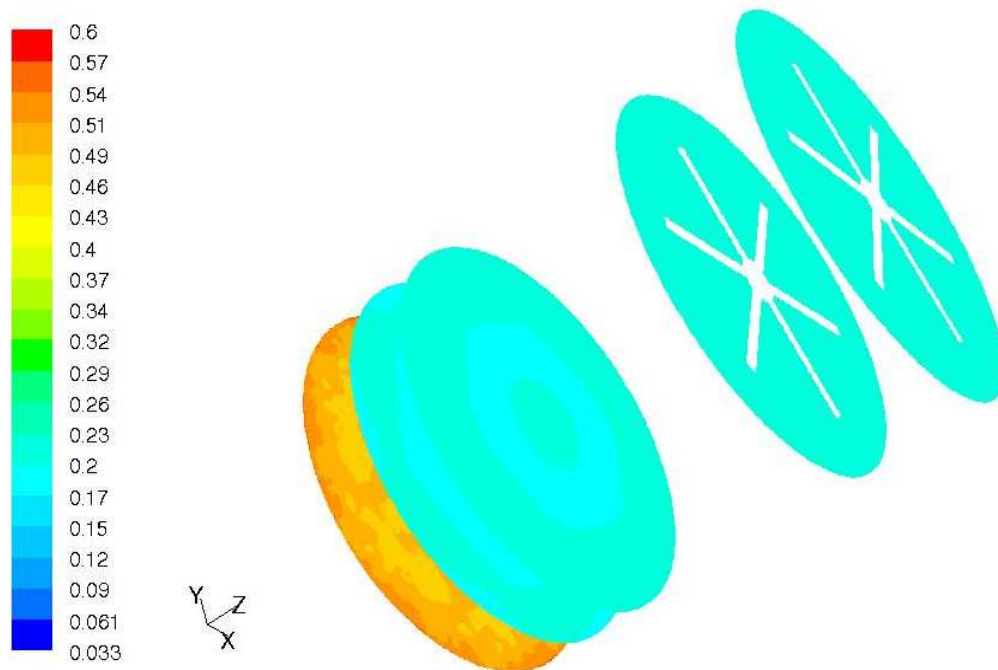


Figure 89. Contours of volume fraction of PCS solids in the slurry at various horizontal cross-sections of the viscometer cup at 230 rpm.

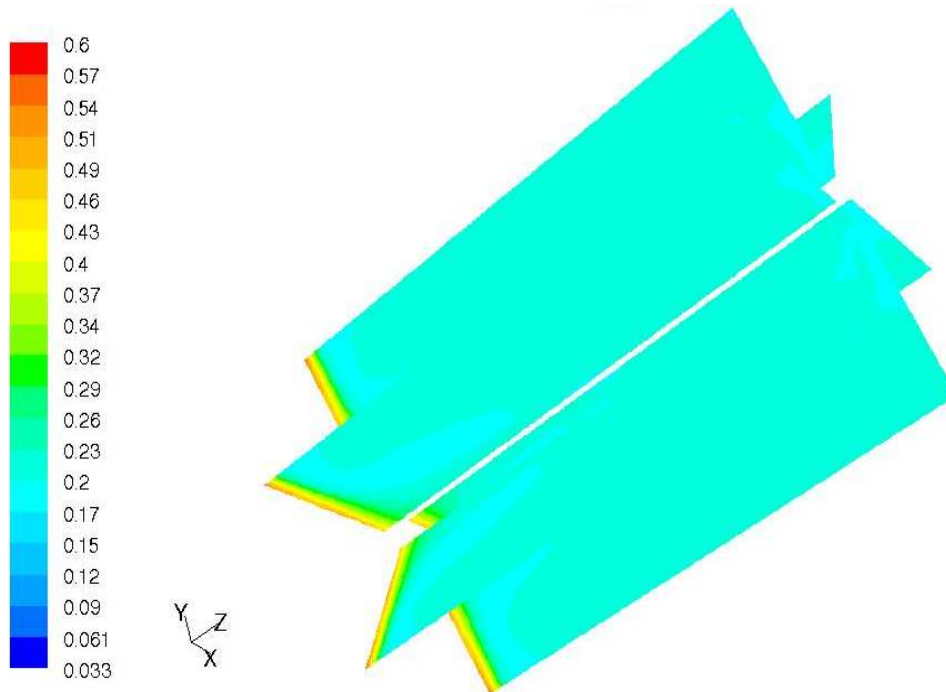


Figure 90. Contours of volume fraction of PCS solids in the slurry along the vertical axis of the viscometer cup at 230 rpm.

The volume fraction of PCS solids at the bottom is as high as 0.5, which is higher than at any other part in the viscometer cup, which indicates that 230 rpm is not a sufficient impeller speed to lift all the solid particles off the bottom.

The contours of volume fraction for the simulation at 270 rpm are shown in Figure 91 and Figure 92.

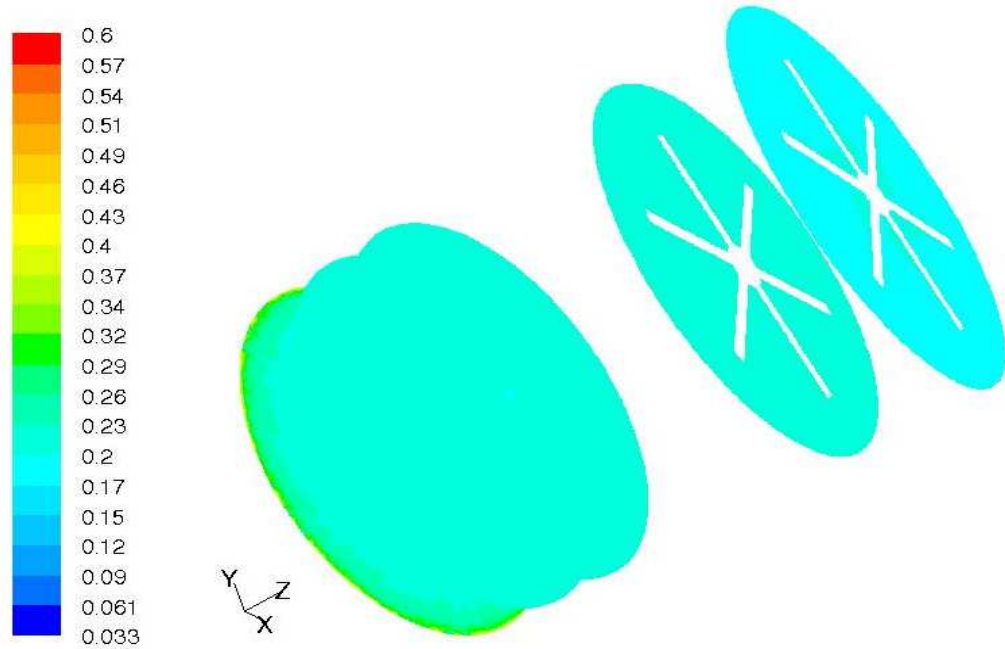


Figure 91. Contours of volume fraction of the PCS solids in slurry at various horizontal cross-sections of the viscometer cup at 270 rpm.

The volume fraction of PCS solids over the bottom $3/4^{\text{th}}$ part of the cup averages to about 0.24, and the rest of the slurry has a solids volume fraction of about 0.2. This can be considered a very close match to the JSS speed that was found experimentally for the 5% PCS solids slurry.

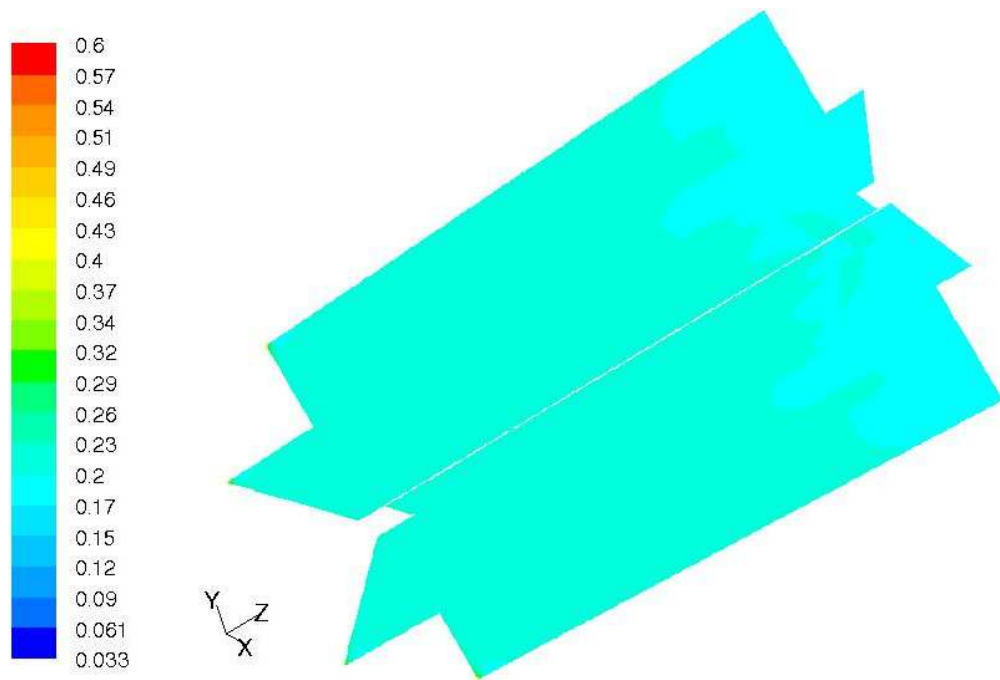


Figure 92. Contours of volume fraction of PCS solids in the slurry along the vertical axis of the viscometer cup at 270 rpm.

The JSS as determined by the Zwietering equation [Equation (6)] and the Pavlushenko equation [Equation (7)], which were originally developed for baffled and unbaffled mixing tanks with large impeller clearance, are about 285 and 370. In the present case, the impeller clearance between the walls of the viscometer cup and the vanes is very small. The smaller clearance requires less rotational speed to suspend the solids than Equations (6) and (7) estimate. This could be the reason that the JSS from both the experimental and computational results are lower than the estimated values.

The simulation with 1100 kg/m^3 density at 305 rpm shows a homogeneous suspension for the 5% PCS solids slurry (Figure 81 and Figure 82). It was also determined experimentally (Table 23) that 305 rpm is the USS for the 5% PCS solids slurry. Therefore, it can be concluded that 305 rpm is the USS for the 5% PCS solids slurry.

The contours of volume fraction for simulations at various speeds above 305 rpm: 340, 400, 450, and 600 rpm are shown in Figure 93, Figure 94, Figure 95, and Figure 96, respectively.

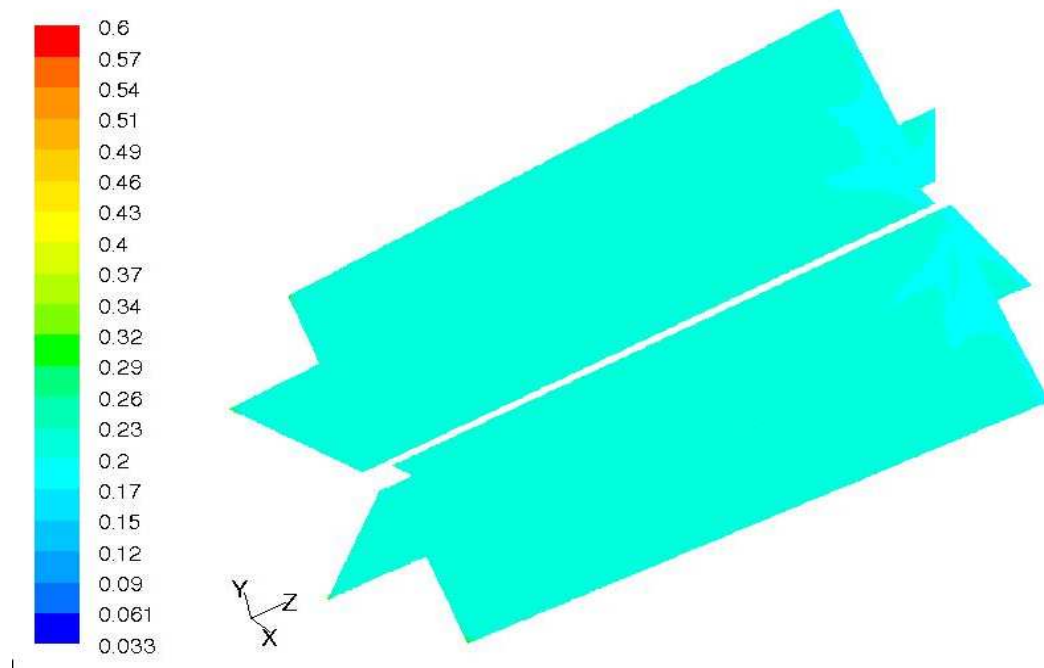


Figure 93. Contours of volume fraction of PCS solids in the slurry along the vertical axis of the viscometer cup at 340 rpm.

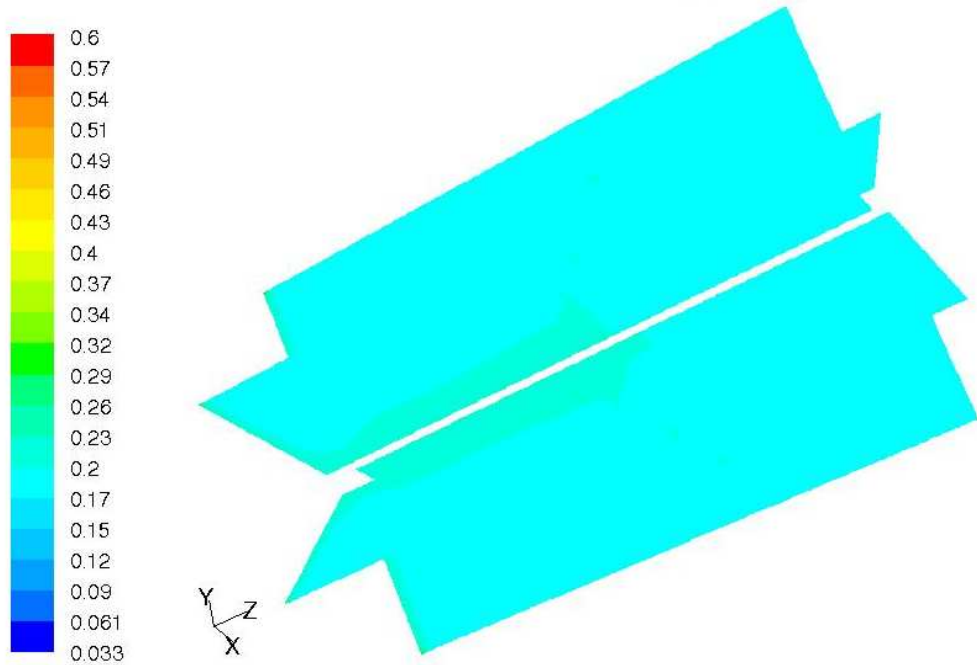


Figure 94. Contours of volume fraction of PCS solids in the slurry along the vertical height of the viscometer cup at 400 rpm.

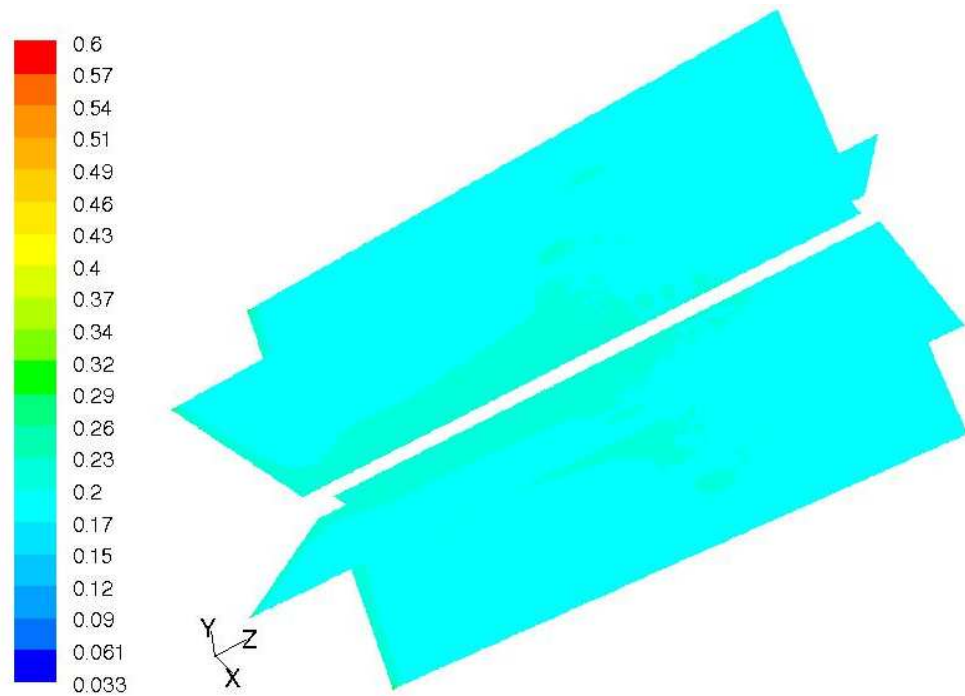


Figure 95. Contours of volume fraction of PCS solids in the slurry along the vertical of the viscometer cup at 450 rpm.

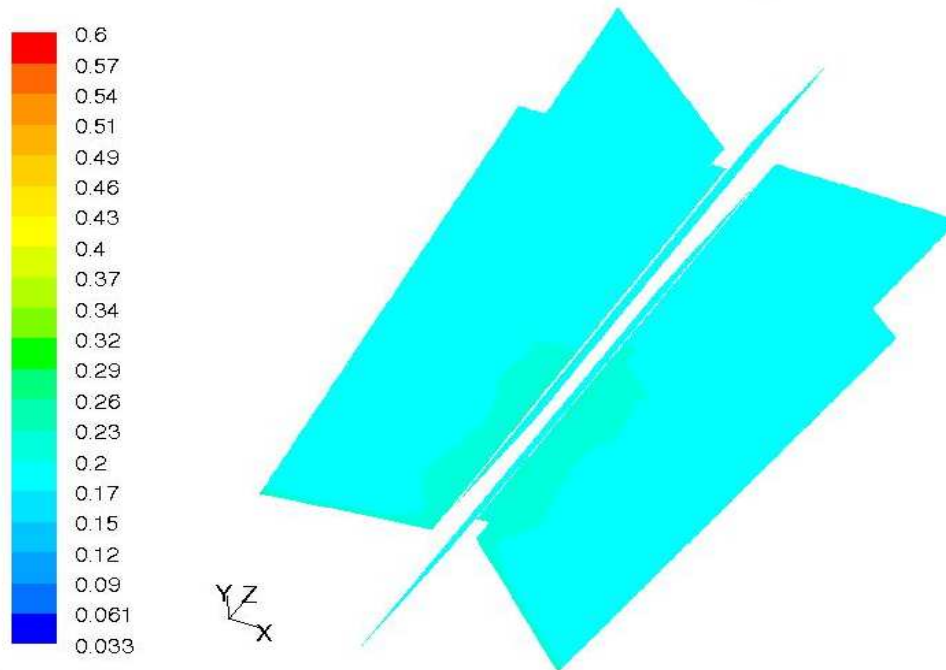


Figure 96. Contours of volume fraction of PCS solids in the slurry along the vertical axis of the viscometer cup at 600 rpm.

It can be seen from Figure 93, Figure 94, Figure 95, and Figure 96 that a uniform solids distribution is achieved at all regions of the viscometer cup with an average volume fraction of about 0.2 and, thus, homogeneous suspension is achieved at all speeds above the USS. So, it can be concluded that the two-phase model developed for the viscometer simulation is valid as it is in very good agreement with the experimental results. The model can be used for further investigation of solids distribution in the viscometer cup at solids concentrations higher than 5%. The model can also be used for developing other impeller designs that may help to accurately measure the viscosity of suspensions at very low solids concentrations, which is a challenge due to particle settling.

CHAPTER VIII

CONSLUSIONS AND RECOMMENDATIONS

Conclusions and recommendations are presented by topic as discussed in the dissertation.

Effect of Substrate Particle Size on Saccharification Rates and Rheology of Sawdust

Slurries

Conclusions:

- The saccharification reaction rate appears to be zero order kinetics based on a linear relationship between glucose and time (not including the 0 hour glucose concentration), then it decreases as the reaction order increases to higher order kinetics sometime after 8 hours.
- Substrate with smaller particle sizes resulted in faster rate and extent of glucose release. Fifty to fifty-five percent more glucose is released for the size range $33 \mu\text{m} < x \leq 75 \mu\text{m}$ than for the size range $590 \mu\text{m} < x \leq 850 \mu\text{m}$ with an equivalent initial solids concentration, 10% and 13%, respectively, in 72 hrs.
- Slurry viscosity decreases with decreasing substrate particle size. As the particle size range of the sawdust slurry with 13% initial solids concentration decreases from $150 \mu\text{m} < x \leq 180 \mu\text{m}$ to $33 \mu\text{m} < x \leq 75 \mu\text{m}$, a significant drop in viscosity occurs from $16,500 \text{ Pa}\cdot\text{s} \times 10^3$ to $206 \text{ Pa}\cdot\text{s} \times 10^3$ at 10 s^{-1} shear rate.

- The fastest drop in viscosity occurs in the first 8.5 hours of the saccharification reaction, confirming that the fastest reaction rate is also occurring during that period.
- Viscosity drops faster for larger particle size ranges due to faster fragmentation during the first 8.5 hours. For the size range $150 \mu\text{m} < x \leq 180 \mu\text{m}$, 94% of the initial viscosity is reduced within the first 8.5 hours of the saccharification reaction, whereas only 47% of the initial viscosity is reduced for the smaller size particles, $33 \mu\text{m} < x \leq 75 \mu\text{m}$.

Recommendations:

- Start the saccharification reaction with smaller size particles ($\sim 30 \mu\text{m}$) to take advantage of: 1) low viscosity, which leads to low power consumption and 2) high surface area, which leads to a faster rate and higher extent of glucose release.
- Adopt a semi-batch feeding method for processing and add new substrate material after 8.5 hours, when the slurry viscosity drops to a lower value.

Saccharification Using the Scraped Surface Bio-Reactor

Conclusions:

- For batch testing with 25% (highest in the range considered) initial PCS solids concentration, about 10% more glucose is released in the SSBR than in the shake flask after 168 hours of the saccharification reaction.
- The rate and the final extent of glucose release decreases as the initial solids concentration increases. In batch saccharification testing with the SSBR, about a

10% lower glucose extent is observed for the PCS slurry with 25% initial solids than for 10% initial solids slurry over 168 hours.

- For semi-batch testing with a 30% (highest in the range considered) final equivalent PCS solids concentration, about 16% more glucose is released in the SSBR than in the shake flask after 168 hours of the saccharification reaction.
- The slurry viscosity and, therefore, the power consumption, become approximately constant after about 96 hours of the saccharification test, independent of the initial solids concentration.
- The efficiency of the SSBR for saccharification decreases drastically with time because of a combination of the cumulative energy used and decreasing sugar yield over time.
- Although the 20% PCS slurry is more viscous, it was about 10% more efficient as compared to the 10% solids slurry in terms of glucose released per energy input.
- The 20% semi-batch saccharification test efficiency is 27% higher than the 20% batch saccharification test efficiency at 72 hours in the SSBR.
- The SSBR is better than conventional reactors since the specific power consumption is less than the lower end of the typical power consumption at industrial scale (1-5 kW/m³) for all PCS solids concentrations tested.

Recommendations:

- Operate the SSBR at speeds higher than 2 rpm to test for improvements in the rate and extent of the saccharification reaction.
- Modify the design of the blades similar to a double helix and run the two blade assembly (inner and outer) in opposite directions in order to further improve the

bulk mixing for slurries with solids concentrations higher than 15%, while still maintaining the scraping with outer blade.

- A jacketed heat exchanger should be tested on the SSBR since the controlled incubated environment will not be possible at larger-scale.

Technique to Measure Viscosity of Solid Suspensions

Conclusions:

- The uniform suspension speed (USS) in the viscometer cup for PCS slurries with solids concentrations 5% and 7.5% are determined to be 305 ± 5 and 930 ± 5 rpm, respectively.
- Premixing before measuring the slurry viscosity is required only for slurries with solids concentrations less than 12%.
- For PCS slurries with 5% and 7.5% solids concentration, premixing at a shear rate higher than 400 s^{-1} is necessary to keep the solid particles suspended longer and, hence, give more reliable viscosity measurements over the shear rate range of 0.1-1000 s^{-1} .
- Viscosities of PCS slurries with 10%, 15%, and 20% solids concentrations measured over the shear rate range (0.1-1000 s^{-1}) are not a function of the premixing shear rate.

Recommendations:

- For slurries with less than 12% PCS solids concentrations, a minimum premixing shear rate of about 400 s^{-1} (± 200) for a minimum of 4 minutes is recommended in

order to obtain accurate viscosity data at the low end (below the USS of the corresponding solids concentration) of the measured shear rate range.

- The clearance should be lowered between the bottom of the cup and the impeller in order to prevent particles settling at low shear rates.
- Use a curved cup bottom to hold the slurry sample for viscosity measurements in order to eliminate stagnant zones at the low end of the shear rate sweep.

CFD Simulations of Solids Suspensions in a Viscometer Cup:

- A CFD model to determine USS in a viscometer cup has been experimentally validated.
- The wet density of PCS solids is determined to be 1100 kg/m^3 based on the computationally determined volume fraction distribution of solids in a 5% slurry at the USS, $305 \pm 5 \text{ rpm}$.
- The USS of the PCS slurry with 5% solids concentration is determined both experimentally and computationally to be $305 \pm 5 \text{ rpm}$.

Recommendations:

- The model can be used for further investigation of solids distribution in the viscometer cup at solids concentrations higher than 5%.
- The model can also be used for developing other impeller designs that may help to accurately measure the viscosity of suspensions at very low solids concentrations, which is a challenge due to particle settling.

REFERENCES

- Abichandani, H., & Sarma, S. C. (1988). Heat transfer and power requirements in horizontal thin film scraped surfaced heat exchangers. *Chem. Eng. Sci.* 43 (4), 871-881.
- Acevedo, F., & Aroca, G. (1986). Studies on the agitation and power characteristics of mineral slurries. Fundamental and applies biohydrometallurgy. *Proceedings of the Sixth Biohydrometallurgy*. Vancouver. B.C. Canada, 255-261
- Adams, R. S. (1998). Corn stover as feed for cattle. Dairy and Animal Science. Document number 28902108. Penn State University. University Park. PA.
- Allain, E. J. (2007). Cell-free ethanol production: the future of fuel ethanol?. *Journal of Chemical Technology & Biotechnology.* 82 (2), 117 – 120.
- Altway, A., Setyawan, H., Margono, & Winardi, S. (2001). Effect of particle size on simulation of three-dimensional solid dispersion in stirred tank. *Trans ICheE.* 79 (PartA), 1011-1016.
- Araki, J., Wada, M., Kuga, S., & Okano, T. (1998). Flow properties of microcrystalline cellulose suspension prepared by acid treatment of native cellulose. *Colloids and Surfaces, A: Physicochemical and Engineering Aspects.* 142, 75-82.
- Aravinth, S., Rao, G. P., & Murugesan, T. (1996). Critical impeller speed for solid suspension in turbine agitated contactors. *Bioprocess Engineering* 14, 97-99.

- Arjunwadkar, S. J., Saravanan, K., Pandi, A. B., & Kukarni, P. R. (1997). Optimizing the impeller combination for maximum hold-up with minimum power consumption. *Biochemical Engineering Journal*. 1, 25-30.
- Armenante, P. M., Huang, Y. T., & Li, T. (1992). Determination of the minimum agitation speed to attain the just dispersed state in solid-liquid and liquid-liquid reactors provided with multiple impellers. *Chemical Engineering Science* 47, 2865-2870.
- Armenante, P. M., & Li, T. (1993). Minimum agitation speed for off-bottom suspension of solids in agitated vessels provided with multiple flat-blade impellers. A.I.Ch.E. Symposium. Ser. 89, 105-111.
- Armenante, P. M., & Nagamine, U. E. (1998). Effect of low off-bottom impeller clearance on the minimum agitation speed for complete suspension of solids in stirred tanks. *Chemical Engineering Science* 53 (9), 1757-1775.
- Ayers, G. E., & Buchele, W.F. (1982). Harvesting and storing corn plant forage. ASAE paper no. 71-665: American Society of Agricultural Engineers. St. Joseph. MI.
- Baldi, G., Conti, R., & Alaria, E. (1978). Complete suspension of particles in mechanically agitated vessels. *Chemical Engineering Science* 33, 21-25.
- Ballesteros, I., Oliva, J. M., Negro, M. J., Manzanares, P., & Ballesteros, M. (2002). Ethanol production from olive oil extraction residue pretreated with hot water. *Applied Biochemistry and Biotechnology* 98-100, 717-731.
- Barrue, H., Bertrand, J., Crystol, B., & Xuereb, C. (2001). Eulerian simulation of dense solid liquid suspension in multi-stage stirred vessel. *Chemical Engineering*

Journal of Japan. 34 (5), 585-594.

- Benezech, T., & Maingonnat, J. F. (1988). Modeling the power consumption in scraped-surface heat exchangers treating Newtonian and non-Newtonian liquids. *Journal of Food Engineering.* 7 (4), 289-311.
- Berressi, A., & Baldi, G. (1987). Solid dispersion in an agitated vessel. *Chem. Engg. Sci.* 142, 2949-2956.
- Bertran, M. S., & Dale, B. E. (1985). Enzymatic hydrolysis and recrystallization behavior of initially amorphous cellulose. *Biotechnology Bioengineering* 27, 177-81.
- Bird, R. B., Warren, W. S., & Lightfoot, E. N. (2002). *Transport phenomena*, 2nd edition, New York, John Wiley & Sons, Inc.
- Bohnet, M., & Niesmak, G. (1980). Distribution of solids in stirred suspensions, *Ger. Chem. Eng.* 3, 57-65.
- Benezech, T., & Maingonnat, J. F. (1987). Study of power consumption in scraped surface heat exchangers utilizing Newtonian and non-Newtonian fluids. *Revue Generale de Thermique.* 26 (308-309), 440-444.
- Buchs, J., Maier, U., Milbradt, C., & Zoels, B. (2000a). Power consumption in shaking flasks on rotary machines: I. Power consumption measurements in unbaffled flasks at low viscosity. *Biotechnol. Bioeng.* 68 (6), 589-593.
- Buchs, J., Maier, U., Maier, U., & Zoels, B. (2000b). Power consumption in shaking flasks on rotary machines: II. Nondimensional description of specific power consumption and flow regimes in unbaffled flasks at elevated liquid viscosity. *Biotechnol. Bioeng.* 68 (6), 594-601.

- Burchhardt, G., & Ingram, L. O. (1992). Conversion of xylan to ethanol by ethanologenic strains of *Escherichia coli* and *Klebsiella oxytoca*. *Appl. Environ. Microbiol.* 58, 1128–1133.
- CEC. (1999). Timetable for the phase-out of MTBE from California's gasoline supply. Docket No. 99-GEO-1: Fuel Resources Office. Energy Information and Analysis Division, California Energy Commission: Sacramento, CA.
- Chapman, C. M., Nienow, A. W., Cooke, M., & Middleton, J. C. (1983). Particle-gas-liquid mixing in stirred vessels, Part 1: particle-liquid mixing. *Trans. Inst. Chem. Eng.* 61, 71-81.
- Chudacek, M. W. (1985). Solids suspension behavior in profiled bottom and flat bottom mixing tanks. *Chemical Engineering Science* 409, 385-392.
- Chudacek, M. W. (1986). Relationships between solids suspension criteria, mechanism of suspension, tank geometry, and scale-up parameters in stirred tanks. *Ind. Engng Chem. Fundam* 25, 391-401.
- Converse, A. O., & Optekar, J. D. (1993). A synergistic kinetics model for enzymatic cellulose hydrolysis compared to degree-of-synergism experimental results. *Biotechnology and Bioengineering* 42 (1), 145-148.
- Cox, D. R. G., Gerrard, A. J., & Wix, L. (1993). Power consumption and backmixing in horizontal scarped surface heat exchangers. *Trans IChemE.* 71, Part C. 187-193.
- Dasari, R. K., & Berson, R. E. (2007). The effect of particle size on hydrolysis reaction rates and rheological properties in cellulosic slurries. *Appl. Biochem. & Biotech.* 136-140, 289-299.
- Dasari, R. K., Dunaway, K., Ye, Z., & Berson, R. E. (2007). Power consumption in a

scraped surface bio-reactor for batch and fed-batch enzymatic hydrolysis of pretreated corn stover slurries. *The 29th Symposium on Biotechnology for Fuels and Chemicals*. Denver. CO. U.S.A.

Delucchi, M. A. (1991). Emissions of greenhouse gases from the use of transportation

fuels and electricity. 1, Argonne National Laboratory. Argonne. IL.

Demirbas, A. (2000a). Recent advances in biomass conversion technologies. *Energy Edu.*

Sci. Technol. 6, 19-41.

Demirbas, A. (2006). Biogas potential of manure and straw mixtures. *Energy Sources*

Part A. 28, 71–78.

Dien, B. S., Nichols, N. N., O'Bryan, P. J., & Bothast, R. J. (2000). Development of new

ethanologenic *Escherichia coli* strains for fermentation of lignocellulosic biomass.

Appl Biochem Biotechnol. 84–86, 181–186.

Dohi, N., Takahashi, T., Minekawa, K., & Kawase, Y. (2004). Power consumption and

solid suspension performance of large-scale impellers in gas-liquid-solid three-

phase stirred tank reactors. *Chemical Engineering Journal.* 97, 103-114.

Domier, K.W. (1995). Opportunities for diversification of crop fibres: new uses.

Proceedings of the Special Crops Conference-Opportunities and Profits. July 25–

26. Edmonton. Alberta.

Duncan, R. C., & Youngquist, W. (1999). Encircling the peak of world oil production.

Natural Resources Research. 8 (3), 219-232.

Ebeling, T., Paillet, M., Borsali, R., Diat, O., Dufresne, A., Cavaille, J. Y., & Chanzy, H.

- (1999). Shear-induced orientation phenomena in suspensions of cellulose microcrystals, Revealed by small angle X-ray scattering. *American Chemical Society* 15 (19), 6123-6126.
- Enderlin, C. W. (2008). Sensors & Electronics. Macro Property Measurements. *Pacific Northwest National Laboratory*. URL: <http://www.technet.pnl.gov/sensors/macro/projects/es4FIType.stm>
- EIA, Energy Information Administration. (2003). Annual Energy Outlook with Projections to 2025. Washington. DC. USA - Report No. DOE/EIA-0383.
- Fan, L. T., Lee, Y. H & Beardmore. D. H. (1980). Mechanism of the enzymatic hydrolysis of cellulose: Effects of major structural features of cellulose on enzymatic hydrolysis. *Biotechnology Bioengineering* 22, 177-9.
- Fan, L. T., Lee, Y., & Gharpuray, M. M. (1982). The nature of lignocellulosics and their pretreatments for enzymatic hydrolysis. *Advances in Biochemical Engineering* 23, 157-187.
- Fan, L. T., & Lee, Y. H. (1983). Kinetic studies of enzymatic hydrolysis of insoluble cellulose: Derivation of a mechanistic kinetic model. *Biotechnology Bioengineering* 25, Pp. 2707-33.
- FAO Agricultural Services Bulletins. (1997). Renewable biological systems for alternative sustainable energy production, Series title 128, W7241/E, Table 3.2.
- Fernandez, R. S. & Klopfenstein, T. J. (1989). Yield and quality components of corn crop residues and utilization of these residues by grazing cattle. *Journal of Animal Science*. 67 (2), 597–605.

- Fluent Inc. (2006). FLUENT 6 User's Guide, Lebanon, NH.
- Foley, K. M., & Hooven, D. I. B. (1981). Properties and industrial uses of corncobs.
- Pomeranz, Y., and Munck, L. (Eds). Cereals, A Renewable Resource: Theory and Practice. American Association of Cereal Chemists: St. Paul. Minnesota, 523–543.
- Ingram, L.O. et al. (1987). Genetic engineering of ethanol production in *Escherichia coli*. *Appl. Environ. Microbiol.* 53, 2420–2425.
- Jørgensen, H., Pedersen, J. V., Larsen, J., & Felby, C. (2007). Liquefaction of lignocellulose concentrations. *Biotechnology and Bioengineering* 96 (5), 862-870.
- Ghadge, R. S., Patwardhan, A. W., Sawant, S. B., & Joshi, J. B. (2005). Effect of flow pattern on cellulase deactivation in stirred tank bioreactors. *Chemical Engineering Science.* 60, 1067 – 1083.
- Ghose, T. K., & Das, K. (1971). A simplified kinetic approach to cellulose-cellulase system. *Advances in Biochemical Engineering* 1, 55-76.
- Glassner, D., Hettenhaus, J., & Schechinger, T. (1998). Corn stover collection project—a pilot for establishing infrastructure for agricultural residue and other crop collection for biomass processing to ethanol. *Proc. Bioenergy. Conference.* 4–8 October. Madison. WI, 1100–1110.
- Gregg, D. J., & Saddler, J. N. (1996). Factors affecting cellulose hydrolysis and the potential of enzyme recycle to enhance the efficiency of an integrated wood to ethanol process. *Biotechnology and Bioengineering* 51 (4), 375 – 383.
- Greer, D. (2005). Creating cellulosic ethanol. Spinning straw into fuel. *Biocycle.*, 46, 61-65.

- Grethlein, H. E. (1985). The effect of pore size distribution on the rate of enzymatic hydrolysis of cellulosic substrates. *Bio Technol.* 3, 155-60.
- Gusakov, A. V., Sinitsyn, A. P., Manenkova, J. A., & Protas, O. V. (1992). Enzymatic conversion of industrial and agricultural lignocellulosic wastes: main features of the process. *Appl. Biochem. Biotech.* 34-35, 625-637.
- Hägerdal, B. H., Galbe, M., Grauslund, M. F., Lidén, G., & Zacchi, G. (2006). Bio-ethanol – the fuel of tomorrow from the residues of today. *Trends in Biotechnology.* 24 (12), 549-556
- Halliwell, G. (1965). Hydrolysis of fibrous cotton and reprecipitated cellulose by cellulolytic enzymes from soil micro-organisms. *Biochem. J.* 95, 270-81.
- Harrod, M. (1986). Scraped surface heat exchangers – A literature survey of flow patterns, mixing effects, residence time distribution, heat transfer and power requirements. *J Food Process Eng.* 9, 1-62.
- Helen, H. J., & Babcock, A. B. (2007). Do Biofuels mean inexpensive food is a thing of the past?. *Iowa Ag Review Online*, Summer 13(3).
- Helene, B., Bertrand, J., Cristor, B., & Xuereb, C. (2001). Eulerian simulation of dense solid-liquid suspension in multi-stage stirred vessel. *Journal of Chemical Engineering of Japan.* 34 (5), 585-594.
- Henrissat, B., Driguez, H., Viet, C. & Schulein, M. (1985). Synergism of cellulases from *Trichoderma reesii* in the degradation of cellulose. *Bio Technol.* 3, 722-6.
- Hitzhusen, F. J., & Abdallah, M. (1980). Economics of electrical energy from crop residue combustion with high sulfur coal. *American Journal of Agricultural Economics.* 62 (3), 416–425.

- Hodge, D. B., Karim, M. N., Mohagheghi, A., Schell, D. J., Baker, J. O., & McMillan, J. D. (2005). Scale-up of high solids enzymatic cellulose saccharification from shake flasks to stirred tank reactors. *The Twenty-Sixth Biotechnology Symposium for Fuels and Chemicals. May 1-4. Denver. CO.*
- Hodge, D. B. (2006a). Characterization of rates and rate-associated parameters in high-solids enzymatic saccharification of pretreated corn stover. Doctoral Dissertation, Colorado State University: Fort Collins, CO.
- Hodge, D. B., Karim, M. N., Farmer, J., Schell, D. J., McMillan, J. D. (2006b). High-solids enzymatic saccharification of lignocellulosic biomass. *28th Biotechnology Symposium for Fuels and Chemicals. Denver, CO. U.S.A.*
- Hollaender, A., Rabson, R., Rodgers, P., San Pietro, A., Valentine R., & Wolfe. R. (Eds.). Plenum Publishing. New York, 55-83.
- Holtzapple, M. T., Caram, H. S., & Humphrey, A. E. (1984). A comparison of two empirical models for the enzymatic hydrolysis of pretreated poplar wood. *Biotech. and Bioengg.* 26 (8), 936-941.
- Holtzapple, M., Cognata, M., Shu, Y., & Hendrickson, C. (1990). Inhibition of *Trichoderma reesei* cellulase by sugars and solvents. *Biotechnology and Bioengineering.* 36 (3), 275 – 287.
- Houchin, T. L., & Hanley, T. R. (2004). Determination of the rheology of distillers' grains slurries using a helical impeller viscometer. *Appl. Biochem. & Biotech.* 113/116, 723-732.
- Jones, E. O., & Lee, J. M. (2004). Kinetic analysis of bioconversion of cellulose in attrition bioreactor. *Biotechnology and Bioengineering.* 31 (1), 35 - 40.

- Kadam, K. L., & McMillan, J. D. (2003). Availability of corn stover as a sustainable feedstock for bioethanol production. *Bioresource Technology*. 88 (1), 17-25.
- Kaya, F., Heitmann, Jr. J. A., & Joyce, T.W. (1994). Cellulase binding to cellulose fibers in high shear fields. *J. Biotech*. 36, 1-10.
- Klein, B., Laskowski, J. S., & Partridge, S. J. (1995). *Journal of Rheology*. 39 (5), 827-840.
- Kyriacou, A., MacKenzie, C. R., & Neufeld, R. J. (1987). Detection and characterization of the specific and non-specific endoglucanases of *Trichoderma reesie*: Evidence demonstrating endoglucanase activity by cellobio-hydrolase II. *Enzyme Microb. Technol*. 9, 25-32.
- Laapas, H. R. (1984). Rheology of fast settling mineral slurries. 15th International Mineral Processing Congress: Cannes. France. 3, 28-40.
- Landfeld, A., Kyhos, K., Strohalm, J., Sestak, J., Houska, M. (2006). Heat transfer with heating and cooling granular materials in a scraped-surface homogenizer. *Journal of Food Engineering*. 77, 708–712.
- Ladisch, M. R., Gong, C. S., & Tsao, G. T. (1980). Cellobiose hydrolysis by endoglucanase (glucan glucanohydrolase) from *Trichoderma reesie*: Kinetics and mechanism. *Biotech. Bioeng*. 22, 1107-26.
- Ladisch, M. R., Hong, J., Voloch, M., & Tsao, G. T. (1981). Cellulase Kinetics. *Trends in the Biology of Fermentation for Fuels and Chemicals*.
- Lang, S. S. (2005). Cornell ecologist's study finds that producing ethanol and biodiesel from corn and other crops is not worth the energy. *Cornell News Services*.
- Larsson, S. et al. (2000). Influence of lignocellulose-derived aromatic compounds on

- oxygen-limited growth and ethanolic fermentation by *Saccharomyces cerevisiae*.
Appl. Biochem. Biotechnol. 84–86, 617–632.
- Lee, J. (1997). Biological conversion of lignocellulosic biomass to ethanol. *Journal of Biotechnology.* 56 (1), 1-24.
- Logos, C., & Nguyen, Q. D. (1996). Effect of particle size on the flow properties of a South Australian coal-water slurry. *Power Technology.* 88, 55-58.
- Lynd, L. R., Cushman, J. H., Nichols, R. J., & Wyman, C. E. (1991). Fuel ethanol from cellulosic biomass. *Science.* 251, 1318–1323.
- Lyons, E. J. (1967). Suspension of solids. *Mixing: Theory and Practice.* 2, Uhl, V. W., & Gray, J. B., eds., Academic. New York. Chap. 9, 257.
- Majumder, S. K., Chandna, K., Sankar, D., & Kundu, G. (2006). Studies on flow characteristics of coal–oil–water slurry system. *International Journal of Mineral Processing.* 79 (4), 217-224.
- Mandels, M., & Reese, E. T. (1963). Inhibition of enzymatic hydrolysis of cellulose and related materials. *Advances in Enzymatic Hydrolysis of Cellulose and Related Materials*, Reese, E. T. Pergamon. (Eds.). Press. Oxford, 115-57.
- Mandels, M., & Reese, E. T. (1965). Inhibition of cellulases. *Annual Review of Phytopathology.* Horsfall, J. G., & Baker, K. F. (Eds.). Annual Review, Inc. Palo Alto. 3, 85-102.
- Mariamamma, A., & Muraleedhara, K. G. (1997). Pretreatment studies of cellulose wastes for optimization of cellulose enzyme activity. *Applied Biochemistry and Biotechnology,* 62.

- Marsden, W. L., & Gray, P. P. (1986). Enzymatic hydrolysis of cellulose in lignocellulosic materials. *CRC Critical Reviews in Biotechnology*. 3, 235-76.
- McKee, S. L., Williams, R. A., & Boxman, A. (1995), Development of solid-liquid mixing models using tomographic techniques. *Chem. Engg. J.*, 56, 101-107.
- Merck Index of Chemicals and Drugs, 9th edition.
- Millett, M. A., Baker, A. J., & Scatter, L. D. (1976). Physical and chemical pretreatments for enhancing cellulose saccharification. *Biotechnol. & Bioeng. Symp.* 6, 125-153.
- Miyashita, et al. (1997). Heat transfer correlation in high Prandtl (high Schmidt) number fluid in votator type scraped surface heat exchanger. *Journal of Chemical Engineering of Japan*. 30 (3), 545-549.
- Mohagheghi, A., Tucker, M., Grohmann, K., & Wyman, C. (1992). High solids simultaneous saccharification and fermentation of pretreated wheat straw to ethanol. *Appl Biochem Biotechnol*. 33, 67-81.
- Molerus, O., & Latzel, W. (1987). Suspension of solid particles in agitated vessels. *Particulate Science and Technology*. 5, 235-260.
- Morris, J. G. (1985). Anaerobic metabolism of glucose. *Compr Biotech. The Princip. Appl and Regul of Biotechnol in Ind: Agric and Med*.1, 357-378.
- Mosier, N., Wyman, C. E., Dale, B., Elander, R., Lee, Y.Y., Holtzapple, M., & Ladisch, M. (2005). Features of promising technologies for pretreatment of lignocellulosic biomass. *Bioresource Technology*. 96 (6), 673-686.
- Najafpour, G. D., (1990). Immobilization of microbial cells for the production of organic

- acids. J. Sci. I. R. Iran 1, 172–176.
- Nguyen, Q. A., & Saddler, J. N. (1991). An integrated model for the technical and economic evaluation of an enzymatic biomass conversion, *Bioresource Technology*.
- Nguyen Q. A. (1998). Tower reactors for bioconversion of lignocellulose material. US patent no. 5733758.
- Nguyen, Q. A., Tucker, M., Keller, F., & Eddy, F. (2000). Two-stage dilute acid pretreatment of softwoods. *Appl. Biochem. Biotech.* 84-86, 561-576.
- Nidetzky, B., Steiner, W., Hayn, M., & Claeysens. (1994). Cellulose hydrolysis by the cellulases from *Trichoderma reesei*: a new model for synergistic interaction. *M Biochem. J.* 298, 3705-10.
- Nienow, A. W. (1968). Suspension of solid particles in turbine-agitated, baffled vessels. *Chem. Engng Sci.* 23, 1453-1459.
- Nilsson, A., Taherzadeh, M. J., & Liden, G. (2002). On-line estimation of sugar concentration for control of fed-batch fermentation of lignocellulosic hydrolyzates by *Saccharomyces cerevisiae*. *Bioproc Biosys Eng.* 25,183-191.
- Norkrans, B. (1950). Influence of cellulolytic enzymes from hymenocetes on cellulose preparations of differing crystallinity. *Physiol. Plant.*, 3, 75-81.
- Ochieng, A., & Alison E. L. (2006). Nickel solids concentration distribution in a stirred tank. *Minerals Engineering.* 19, 180-189.
- Oldshue, J. Y. (1983). *Fluid Mixing Technology*. McGraw-Hill Pub. Co. Chapter 3. 52-53.
- Ooshima, H., Burns, D. S., & Converse, A. O. (1989). Changes in the surface area of

pretreated wood during enzymatic hydrolysis.

Pavlushenko, I. S., Kostin, N. M., Matveev, M. S. (1957). Stirrer speeds in stirring of suspensions. *Journal of Appl. Chem. USSR*. 30, 1235-1243.

Peters, L.E., Walker, L.P., Wilson, D.B., & Irwin, D.C. (1991). The impact of initial particle size on the fragmentation of cellulose by the cellulases of *Thermomonospora fusca*. *Bioresource Technology*. 35, 313-319.

Pimenova, N. V., & Hanley, T. R. (2003). Effect of corn stover concentration on rheological characteristics. *Applied Biochemistry and Biotechnology*. 114 (1-3), 347-360.

Pimenova¹, N. V., & Hanley, T. R. (2003). Measurement of rheological properties of corn stover suspensions. *Applied Biochemistry and Biotechnology*. 106 (1-3), 383-392.

Pimentel, D., Pleasant, A., Barron, J., Gaudioso, J., Pollock, N., Chae, E., Kim, Y., Lasiter, A., Schiavoni, C., Jackson, A., Lee, M., & Eaton, A. (2004a). U.S. energy conservation and efficiency: Benefits and costs. *Environment Development and Sustainability*. 6, 279-305.

Pristavka, A. A., Salovarova, V. P., Zacchi, Z., Berezin, I. V., & Rabinovich, M. L. (2000). Enzyme regeneration during hydrolysis of steam-pretreated willow and requirement for cellulose complex composition (Article in Russian). *Prikl Biokhim Mikrobiol*. 36(3), 278-86.

Puri, V. P. (1984). Effect of crystallinity and degree of polymerization of cellulose on enzymic saccharification. *Biotechnol. Bioeng*. 26, 1219-22.

Ramos, L. P., Breuil, C., & Saddler J. N. (1993). The use of enzyme recycling and the

- influence of sugar accumulation on cellulose hydrolysis by *Trichoderma* cellulases. *Enzyme and Microbial Technology*. 15 (1), 19-25.
- Reese, E. T., & Ryu, D. Y. (1980). Shear inactivation of cellulase of *Trichoderma reesei*. *Enzyme and Microbial Technology*. 2, 239–240.
- Reijnders, L. (2006). Conditions for the sustainability of biomass based fuel use. *Energy Policy*. 34, 863–876.
- Richey, C. B., Liljedahl, J. B., & Lechtenberg, V. L. (1982), Corn stover harvest for energy production. *Transactions of the ASAE (American Society of Agricultural Engineers)*. 25 (4), 834–839.
- Rieger, F., & Dilt, P. (1988). Suspension of solid particles: concentration profiles and particle layer on the vessel bottom. *6th European Conference on Mixing*. 251-258.
- Riera, F. A., Alvarez, R., & Coca, J. (1991). Production of furfural by acid hydrolysis of corncobs. *Journal of Chemical Technology and Biotechnology*, 149–155.
- Rivard, J. C., Himmel, E. M., Vinzant, B. T., Adney, S. W., Wyman, E. C., & Grohmann, K. (1990). Anaerobic digestion of processed municipal solid waste using a novel high solids reactor: maximum solids levels and mixing requirements. *Biotechnology Letters* 12 (3), 235-240.
- Rivers, D. B., Emert, G. H. (1988). Factors affecting the enzymatic hydrolysis of bagasse and rice straw. *Biological Wastes*. 26 (2), 85-95.
- Rozanov, L. S., & Lastovtsev, A. M. (1969). Power requirements of mixers with blades for high-viscosity Newtonian liquids. *Translated from Khimicheskoe Neftyanoe Mashinostreonie*. 4, 6-7.

- Rudy, J., Tezel, F. H., Jules, T., Rania, E., & Tolan, J. S. (2005). A.I.Ch.E. Annual Meeting and Fall Showcase, Conference Proceedings, 2442.
- Rudolf, A., Galbe, M., & Liden, G. (2004). Controlled fed-batch fermentations of dilute-acid hydrolysate in pilot development unit scale. *Appl. Biochem. Biotech.* 113-116, 601-617.
- Saddler, J. N. (1986). Factors limiting the efficiency of cellulase enzymes. *Microbiol. Sci.* 3, 84-7.
- Sangrame, G., Bhagavathi, D., Thakare, H., Ali, S., & Das, H. (2000). Performance evaluation of a thin film scraped surface evaporator for concentration of tomato pulp. *Journal of Food Engineering.* 43, 205-211.
- Sarkar, K. A., & Eppers, J. N. (2001). Kinetics of the enzymatic hydrolysis of cellulose. *AATCC Review.* 48-52.
- Schwald, W., Breuil, C., Brownell, H. H., Chan, M., & Saddler, J. N. (1989). Assessment of pretreatment conditions to obtain fast complete hydrolysis on high substrate concentrations. *Appl. Biochem. Biotechnol.* 20/21, 2944.
- Sha, Z., Palosaari, S., Oinas, P., & Ogawa, K. (2001). *Journal of Chemical Engineering of Japan.* 34 (5), 621-626.
- Shamlou, P. A., & Koutsakos, E. (1989). Solid suspension and distribution in liquids under turbulent agitation. *Chem. Eng. Sci.* 44, 529-542.
- Sheehan, J., Aden, A., Paustian, K., Killian, K., Brenner, J., Walsh, & M., Nelson, R. (2004). Energy and environmental aspects of using corn stover for fuel ethanol. *Journal of Industrial Ecology.* 7 (3-4), 117-146.

- Skoog, D. A., West, D. M., & Holler, F. J. (1996). *Analytical Chemistry* 7th Edition. Saunder College Publishing. 681 – 684.
- Söderström, J., Galbe, M., & Zacchi, G. (2004). Effect of washing on yield in one- and two-step steam pretreatment of softwood for production of ethanol. *Biotechnol Prog.* 20(3), 744-9.
- Sun, K. H., Pyle, D. L., Fitt, A. D., Please, C. P., Baines, M. J., & Taylor, N. (2004). Numerical study of 2D heat transfer in a scraped surface heat exchanger. *Computers & Fluids.* 33, 869–880.
- Tarantili, P. A., Koullas, D. P., Christakopoulos, P., Kekos, D., Koukios, E. G., Macris, B. J. (1996). Cross-synergism in enzymatic hydrolysis of lignocellulosics: mathematical correlations according to a hyperbolic model. *Biomass and Bioenergy.* 10 (4), 213-219.
- Takagi, M., Abe, S., Suzuki, S., Emert, G. H., & Yata, N. (1977). A method for production of ethanol directly from cellulose using cellulase and yeast. Ghose, T. K. (Eds.). *Proceedings of Bioconversion Symposium.* Delhi. 551–71.
- Tengborg, C., Galbe, M., & Zacchi, G. (2001). *Biotechnol. Prog.* 17, 110-117.
- Tchobanoglous, G., & Burton, F. L. (1991). *Wastewater engineering treatment, Disposal and reuse.* McGraw Hill, Inc.
- Tengborg, C., Galbe, M., & Zacchi, G. (2001). Influence on enzyme loading and physical parameters on the enzymatic hydrolysis of steam-pretreated softwood. *Biotechnol. Prog.* 17, 110–117.
- Thring, R. W., & Edwards, M. F. (1990). *An experimental investigation into the*

- complete suspension of floating solids in an agitated tank. *Ind. Eng. Chem. Res.* 29, 676-682.
- Tran, Q. K., Trinh, D. T., Horsley R. R., & Reizes, J. A. (1993). Drag coefficients and settling velocities of spheres in yield-pseudoplastic slurries. Proceedings of the ASME Winter Annual Meeting. New Orleans. LA.
- Tsao, G. T., Gong, C. S., & Cao, N. J. (2000). Repeated solid-phase fermentation and extraction for enzyme production. *Appl. Biochem. Biotechnol.* 84-86, 505-24.
- Türe, S., Uzun D., & Ture, I. E. (1997). The potential use of sweet sorghum as a non-polluting source of energy. *Energy.* 22, 17-19.
- Turian, R. M., Attal, J. F., Sung, D. J., & Wedgewood, L. E. (2002). Properties and rheology of coal-water mixtures using different coals. *Fuel.* 81 (16), 2019-2033.
- Uhl, V., & Gray. (1966). *Mixing: Theory and Practice.* 1, Chapter 5. Academic Press. London.
- Varga, E., Klinke, H. B., Réczey, K., Thomsen, A. B. (2004). High solid simultaneous saccharification and fermentation of wet oxidized corn stover to ethanol. *Biotechnol Bioen.* 88 (5), 567-574.
- Wagner, N. C., Ramaswamy, S., & Tschirner, U. (2000). Feasibility of cereal straw for industrial utilization in Minnesota. *American Journal of Alternative Agriculture.* 15 (1), 2-8.
- Walsum, G. P., Allen, S. G., Spencer, M. J., Laser, M. S., Antal, M. J., & Lynd, L. R. (1996). Conversion of lignocellulosics pretreated with liquid hot water to ethanol. *Appl. Biochem. Biotech.* 57, 157-170.
- Walker. L. P., & Wilson, D. B. (1991). Enzymatic hydrolysis of cellulose: An overview.

- Bioresource Technology. 36, 3-14.
- Wang, M. Q. (2002). The greenhouse gases, regulated emissions, and energy use in transportation (GREET) model. Argonne National Laboratory. Argonne, IL.
URL: <http://greet.anl.gov>.
- Wang, W., Walton, J. H., McCarthy, K. L. (1999). Flow profiles of power law fluids in scraped surface heat exchanger geometry using MRI. *Journal of Food Processing Engineering*. 22, 11-27.
- Weimer, P. J., & Weston, W. M. (1985). Relationship between the fine structure of native cellulose and cellulose degradability by the cellulase complexes of *Trichoderma reesei* and *Clostridium thermocellum*. *Biotechnol. Bioeng.* 27, 1540-7.
- Wikens, R. J., Henry, C., & Gates, E. L. (2003). How to scale-up mixing processes in non-Newtonian fluids. *CEP*. 44-52.
- Wingren, A., Söderström, J., Galbe, M., & Zacchi, G. (2004). Process considerations and economic evaluation of two-step steam pretreatment for production of fuel ethanol from softwood. *Biotechnol. Prog.* 20 (5), 1421-1429.
- Wyman, C. E. Biomass ethanol: Technical progress, opportunities, and commercial challenges. *Annual Review of Energy and the Environment*. 24, 189-226.
- Wyman, C. E., & Hinman, N. D. (1988). Ethanol: fundamentals of production from renewable feedstocks and use as a transportation fuel. *Appl. Biochem. Biotechnol.* 24-25, 735-742.
- Wyman, C. E. (1994). Ethanol from lignocellulosic biomass: technology, economics and opportunities. *Bioresour. Technol.* 50, 3-16.

- Yang, B., Wyman, C. E. (2006). BSA treatment to enhance enzymatic hydrolysis of cellulose in lignin containing substrates. *Biotechnology and Bioengineering*. 94 (4), 611 – 617.
- Youngquist, W., & Duncan, R. C. (2003). North American natural gas: data show supply problems. *Natural Resources Research*. 12 (4), 229-240.
- Zwietering, T. N. (1958). Suspending solid particles in liquids by agitators. *Chem. Engng Sci*. 8, 244-253.

APPENDIX - A

VISCOSITY DATA FOR SAWDUST SLURRIES

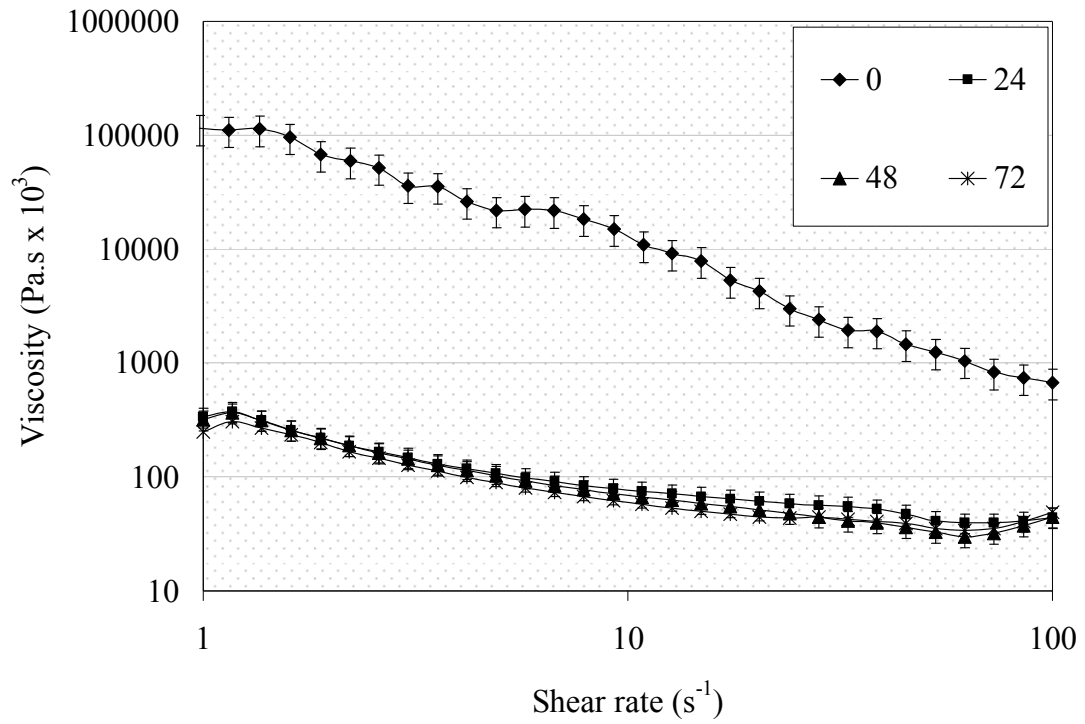


Figure A1. Viscosity vs. shear rate during enzymatic saccharification (Size range: 75 μm $< x \leq 104 \mu\text{m}$, 13% initial solids concentration).

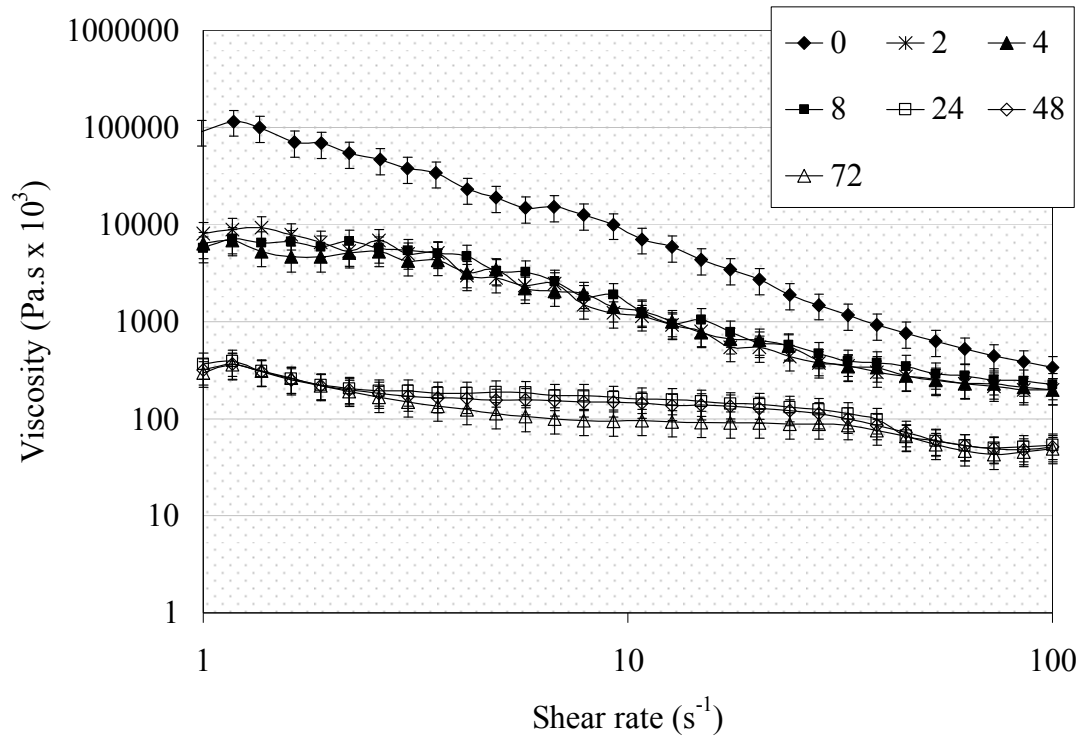


Figure A2. Viscosity vs. shear rate at different times during enzymatic saccharification

(Size range: $104 \mu\text{m} < x \leq 150 \mu\text{m}$, 13% initial solids concentration).

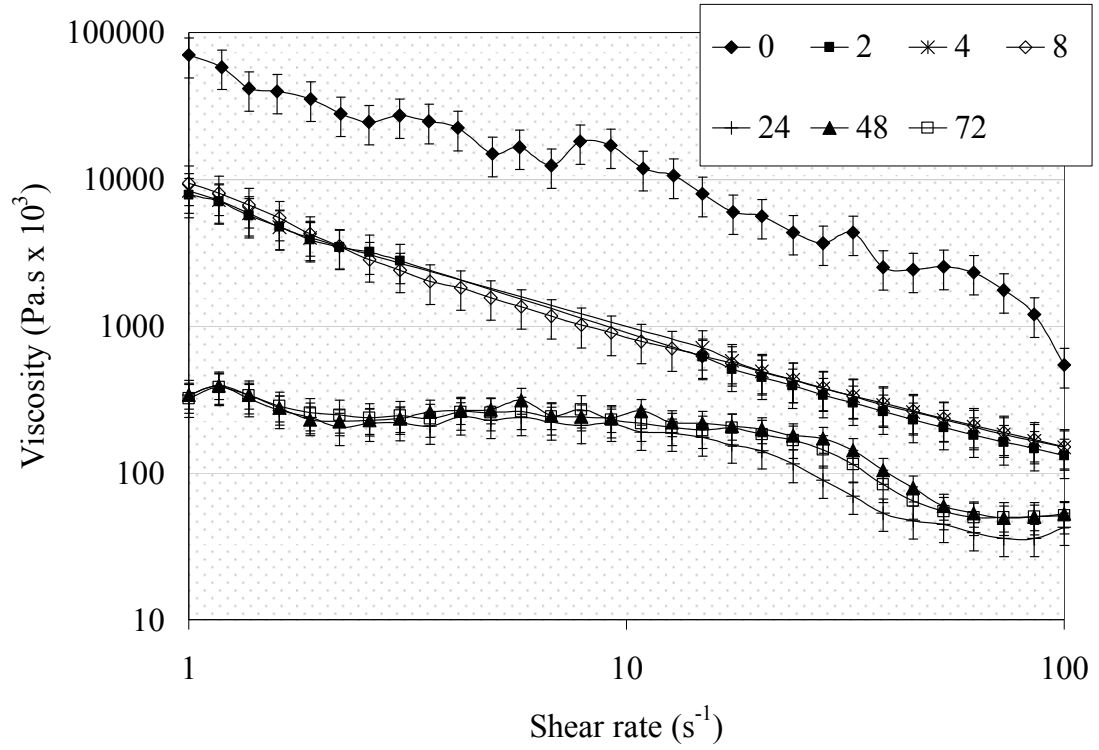


Figure A3. Viscosity vs. shear rate at different times during enzymatic saccharification
 (Size range: $150 \mu\text{m} < x \leq 180 \mu\text{m}$, 13% initial solids concentration).

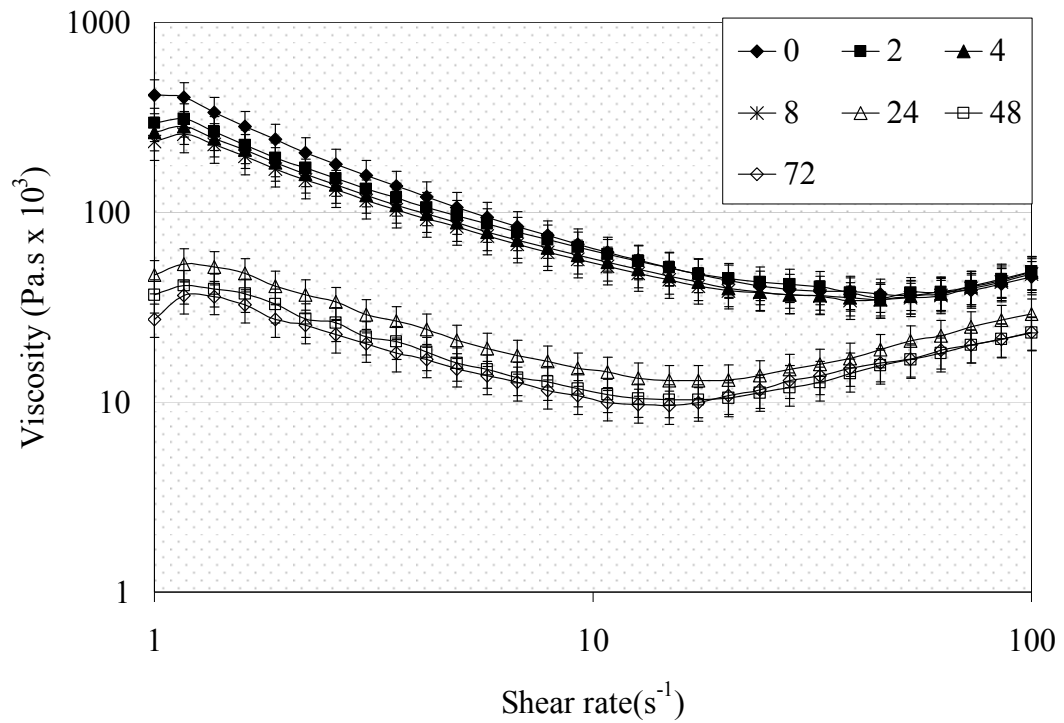


Figure A4. Viscosity vs. shear rate at different times during enzymatic saccharification

(Size range: $33 \mu\text{m} < x \leq 75 \mu\text{m}$, 10% initial solids concentration).

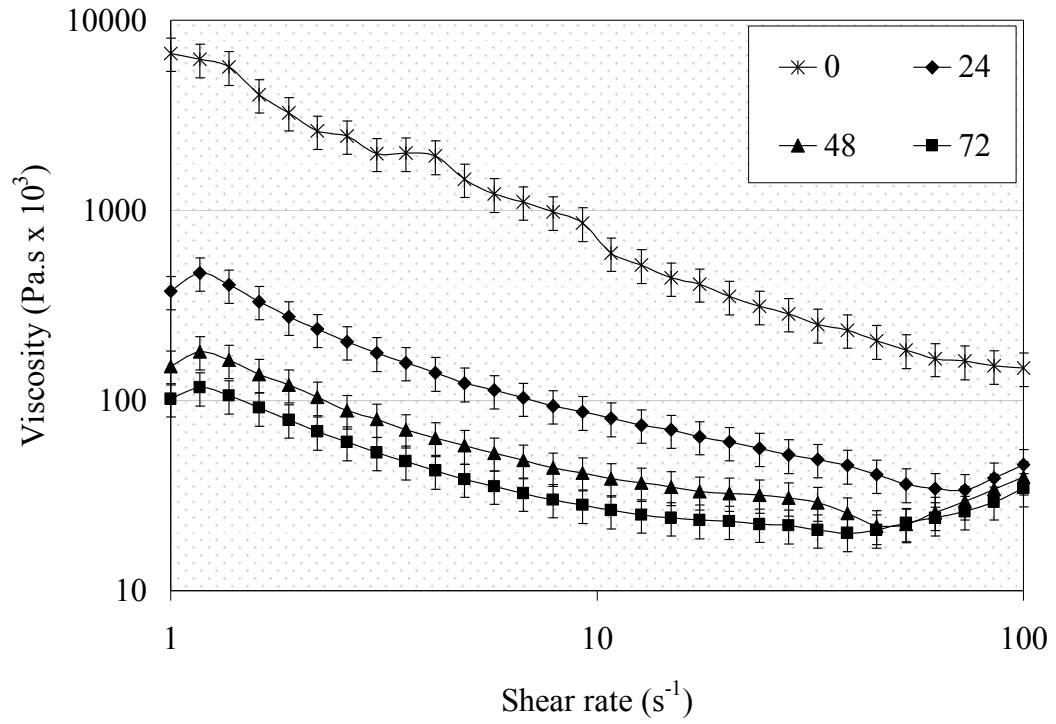


Figure A5. Viscosity vs. shear rate at different times during enzymatic saccharification

(Size range: $75 \mu\text{m} < x \leq 104 \mu\text{m}$, 10% initial solids concentration).

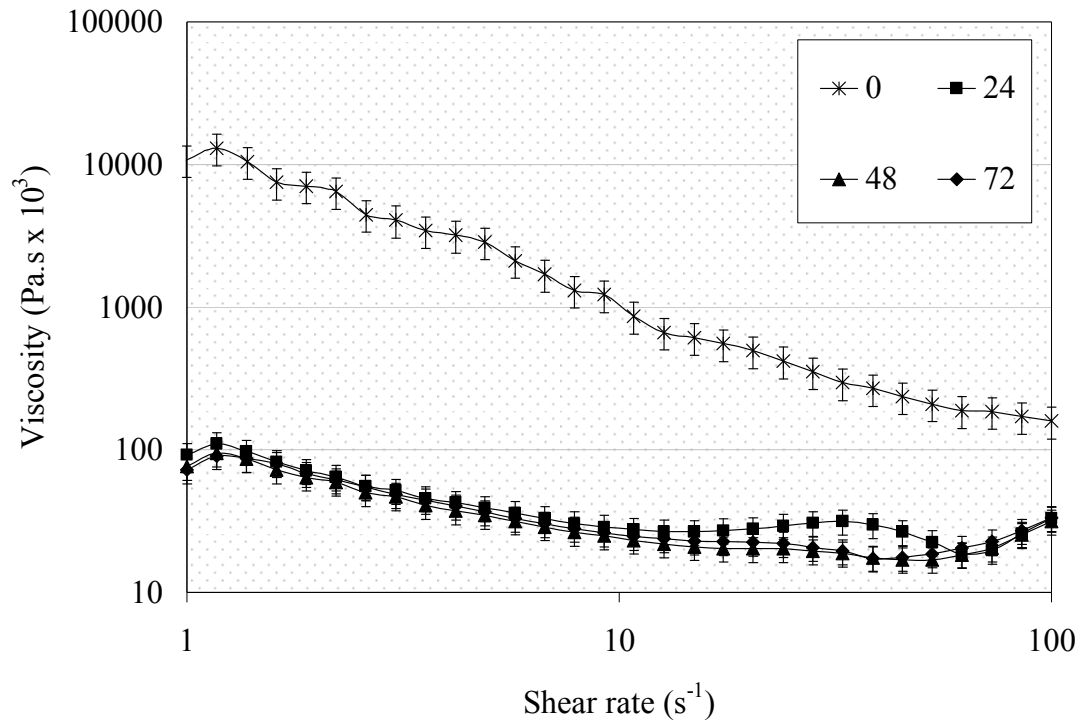


Figure A6. Viscosity vs. shear rate at different times during enzymatic saccharification (Size range: $104 \mu\text{m} < x \leq 150 \mu\text{m}$, 10% initial solids concentration).

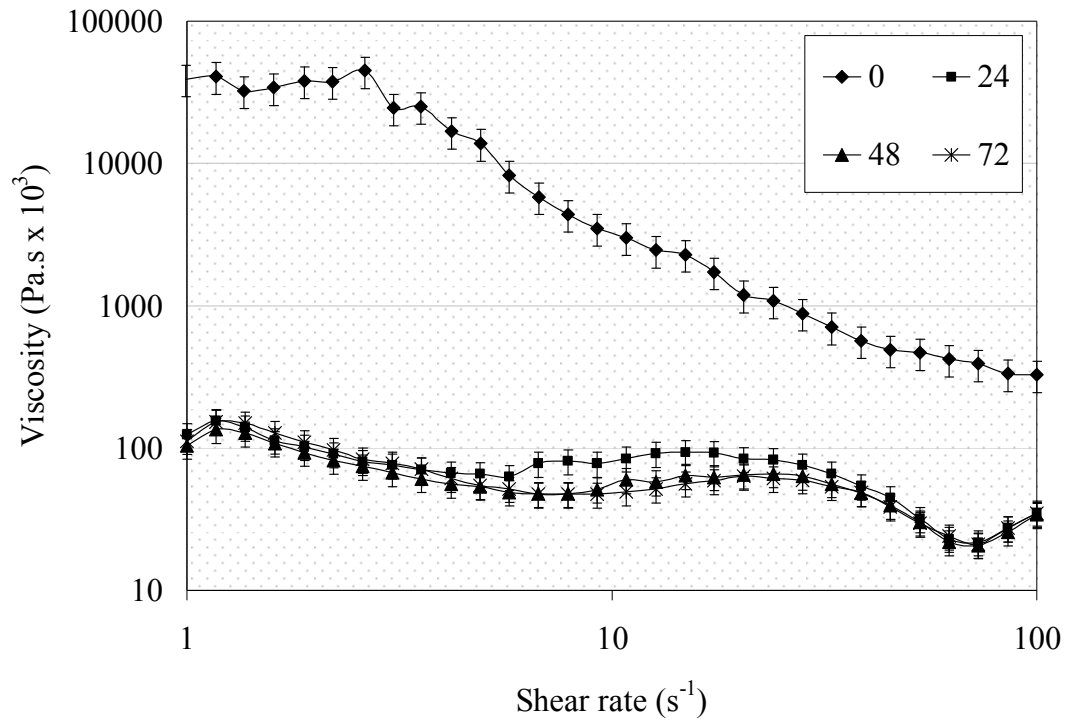


Figure A7. Viscosity vs. shear rate at different times during enzymatic saccharification
(Size range: $150 \mu\text{m} < x \leq 180 \mu\text{m}$, 10% initial solids concentration).

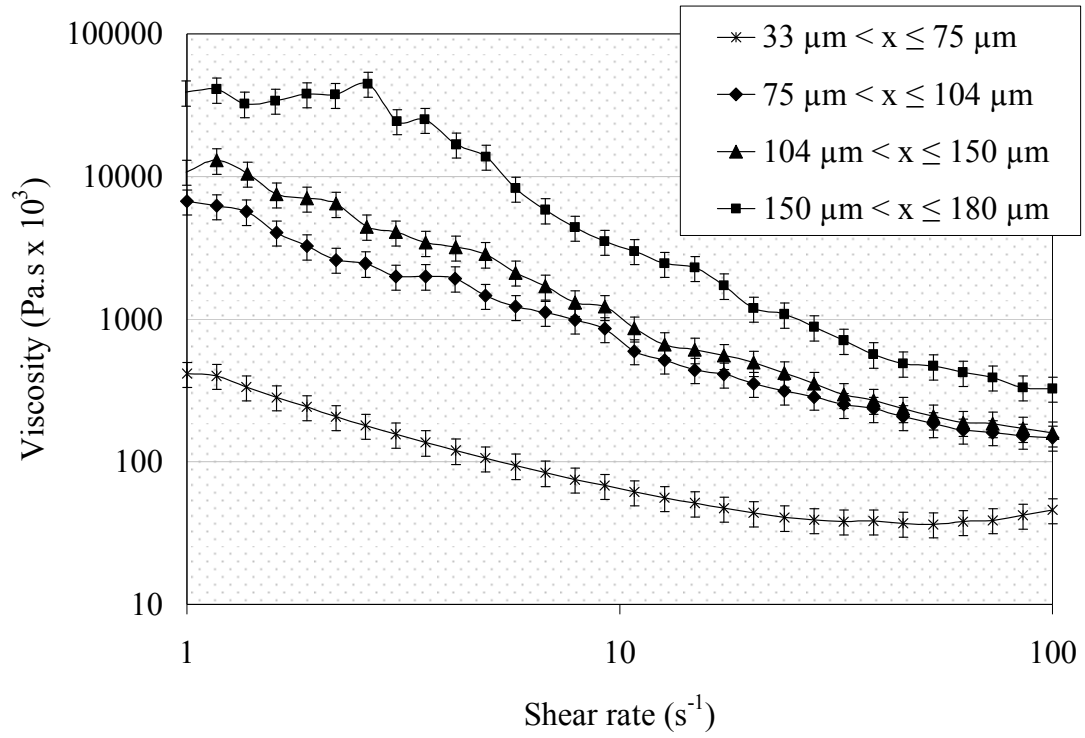


Figure A8. Viscosity vs. shear rate (t = 0 hr, 10% initial solids concentration).

Table A1

Power Law Model Parameters for Sawdust Slurries with 13% Initial Solids ($75 \mu\text{m} < x \leq 104 \mu\text{m}$) Concentration at Various

Times of Enzymatic Saccharification.

	0 hour	24 hours	48 hours	72 hours
R²	0.9903	0.9392	0.9367	0.8907
K (Pa·sⁿ x 10³)	157.5	0.273	0.275	0.222
n	-0.1973	0.5262	0.4745	0.5337

Table A2

Power Law Model Parameters for Sawdust Slurries with 13% Initial Solids ($104 \mu\text{m} < x \leq 150 \mu\text{m}$) Concentration at Various

Times of Enzymatic Saccharification.

	0 hour	2 hour	4 hour	8 hour	24 hours	48 hours	72 hours
R²	0.9935	0.9797	0.9739	0.965	0.8935	0.9154	0.914
K (Pa·sⁿ x 10³)	181.814	11.851	9.168	10.907	0.3458	0.312	0.266
n	-0.2071	0.0329	0.1276	0.1159	0.6145	0.6252	0.6064

Table A3

Power Law Model Parameters for Sawdust Slurries with 13% Initial Solids ($150 \mu\text{m} < x \leq 180 \mu\text{m}$) Concentration at Various

Times of Enzymatic Saccharification.

	0 hour	2 hour	4 hour	8 hour	24 hours	48 hours	72 hours
R²	0.9909	0.9982	0.9977	0.9893	0.8578	0.7547	0.813
K (Pa·sⁿ x 10³)	227.266	7.358	7.553	7.151	0.4373	0.362	0.444
n	-0.1506	0.0973	0.1208	0.1243	0.5007	0.6057	0.578

Table A4

Power Law Model Parameters for Sawdust Slurries with 10% Initial Solids ($33 \mu\text{m} < x \leq 75 \mu\text{m}$) Concentration at Various

Times of Enzymatic Saccharification.

	0 hour	2 hours	4 hours	8 hours	24 hours	48 hours	72 hours
R²	0.8952	0.8905	0.8643	0.8603	0.3616	0.3284	0.2063
K (Pa·sⁿ x 10³)	0.2936	0.2306	0.208	0.191	0.0352	0.027	0.227
n	0.4553	0.53	0.541	0.5581	0.8071	0.8191	0.8693

Table A5

Power Law Model Parameters for Sawdust Slurries with 10% Initial Solids ($75 \mu\text{m} < x \leq 104 \mu\text{m}$) Concentration at Various Times of Enzymatic Saccharification.

	0 hour	24 hours	48 hours	72 hours
R^2	0.9863	0.9515	0.8465	0.7411
$K (\text{Pa}\cdot\text{s}^n \times 10^3)$	5.873	0.355	0.1311	0.0803
n	0.1238	0.4387	0.5864	0.6597

Table A6

Power Law Model Parameters for Sawdust Slurries with 10% Initial Solids ($104 \mu\text{m} < x \leq 150 \mu\text{m}$) Concentration at Various Times of Enzymatic Saccharification.

	0 hour	24 hours	48 hours	72 hours
R^2	0.9874	0.779	0.7632	0.76
$K (\text{Pa}\cdot\text{s}^n \times 10^3)$	12.369	0.0762	0.067	0.069
n	-0.0278	0.6946	0.6664	0.6779

Table A7

Power Law Model Parameters for Sawdust Slurries with 10% Initial Solids ($150 \mu\text{m} < x \leq 180 \mu\text{m}$) Concentration at Various

Times of Enzymatic Saccharification.

	0 hour	24 hours	48 hours	72 hours
R²	0.9696	0.6443	0.7092	0.7806
K (Pa·sⁿ x 10³)	70.290	0.133	0.107	0.12
n	-0.2538	0.715	0.7211	0.6824

Table A8

Power Law Model Parameters for Sawdust Slurries with Various Initial Solids Concentrations at Time '0' Hour for the Particle

Size Range $33 \mu\text{m} < x \leq 75 \mu\text{m}$.

	10%	11%	12%	13%	14%	15%	16%	17%	18%	19%
R²	0.895	0.9429	0.9636	0.9668	0.946	0.949	0.975	0.984	0.992	0.994
K (Pa·sⁿ x 10³)	0.293	0.4515	0.6704	0.8266	1.88	2.93	14.23	31.23	155.84	244.5
n	0.455	0.4161	0.4324	0.4681	0.437	0.395	0.155	0.066	-0.016	0.044

APPENDIX – B

SUGAR RELEASE AND VISCOSITY DATA IN THE SSBR

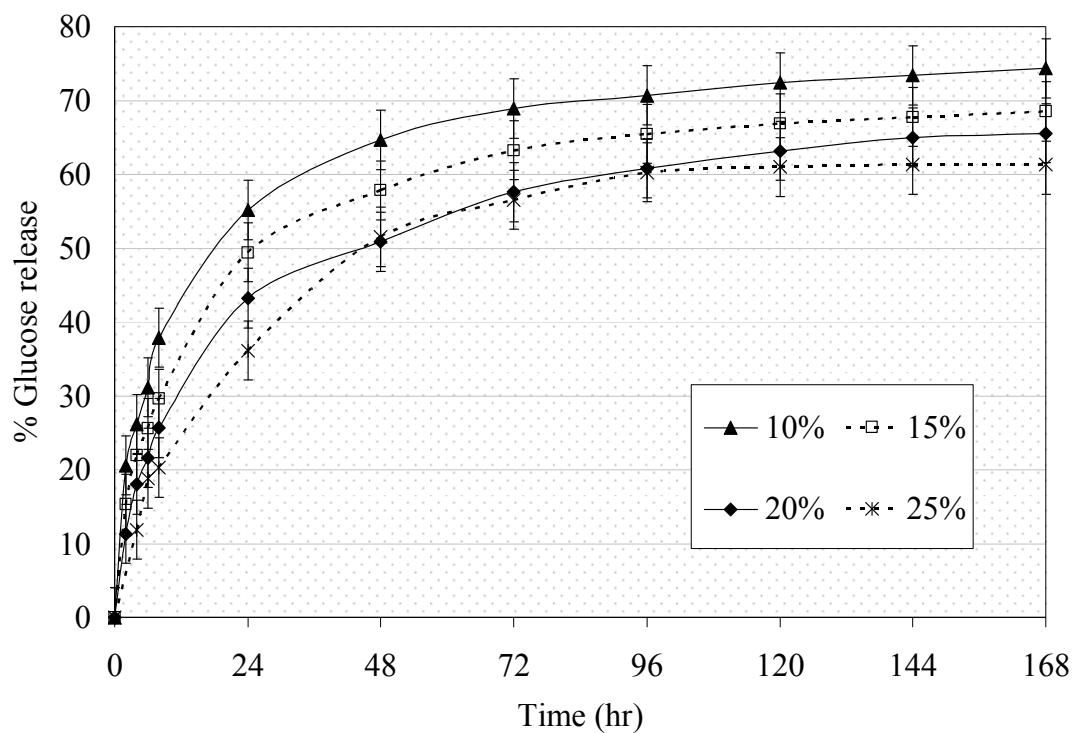


Figure B1. Glucose release during batch enzymatic saccharification in the shake flask with various initial PCS solids concentrations.

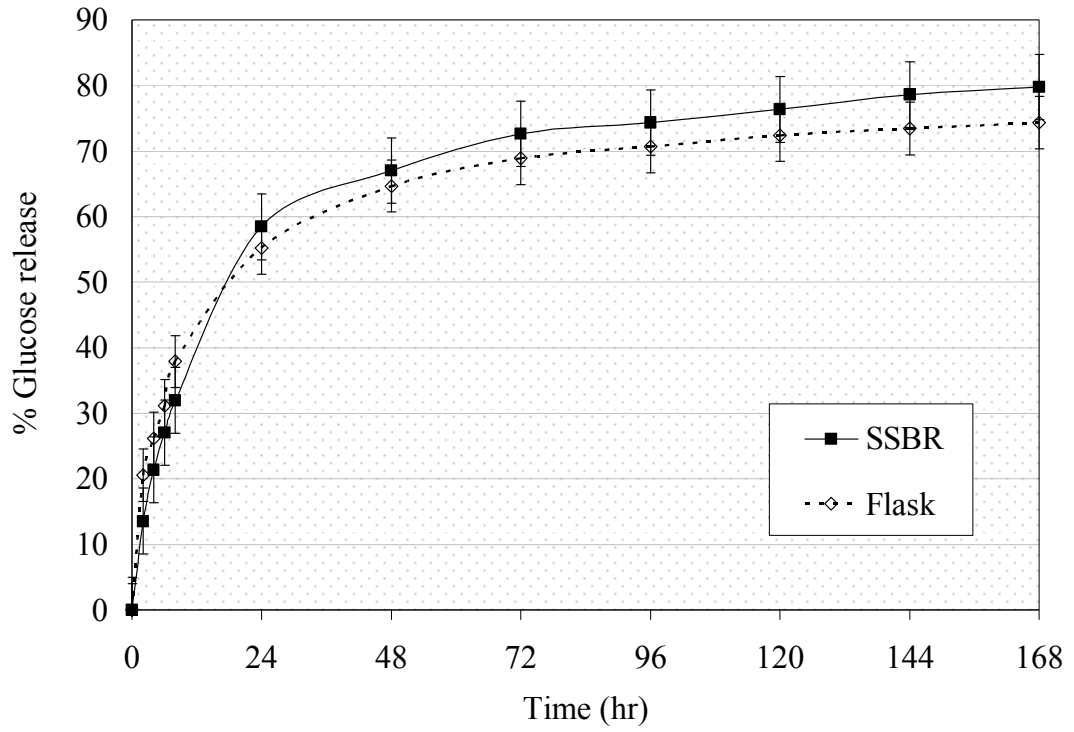


Figure B2. Comparison of glucose yields between the SSBR and the shake flask during batch enzymatic saccharification with 10% initial PCS solids concentrations.

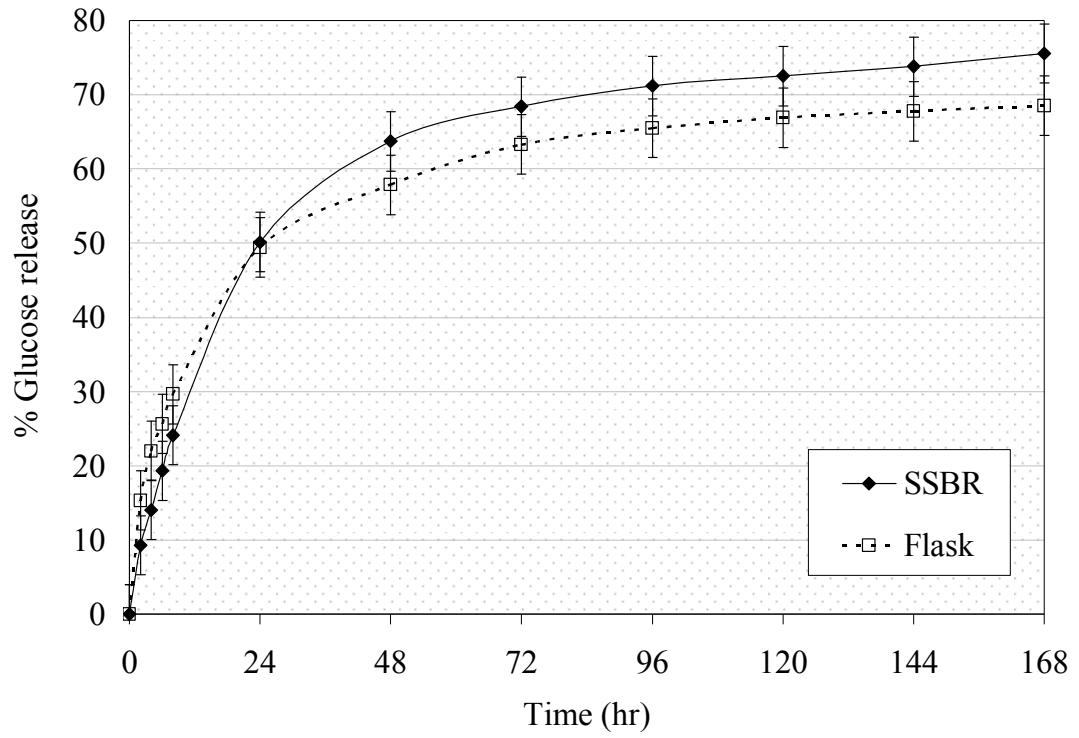


Figure B3. Comparison of glucose yields between the SSBR and the shake flask during batch enzymatic saccharification with 15% initial PCS solids concentrations.

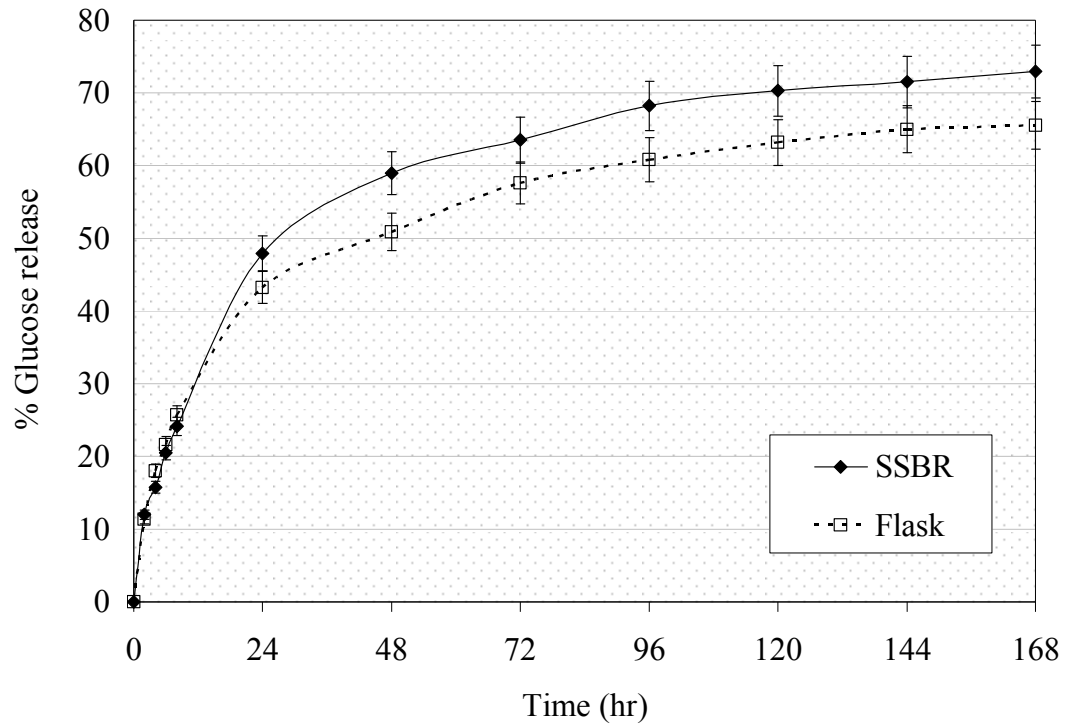


Figure B4. Comparison of glucose yields between SSBR and shake flask during batch enzymatic saccharification with 20% initial PCS solids concentrations.

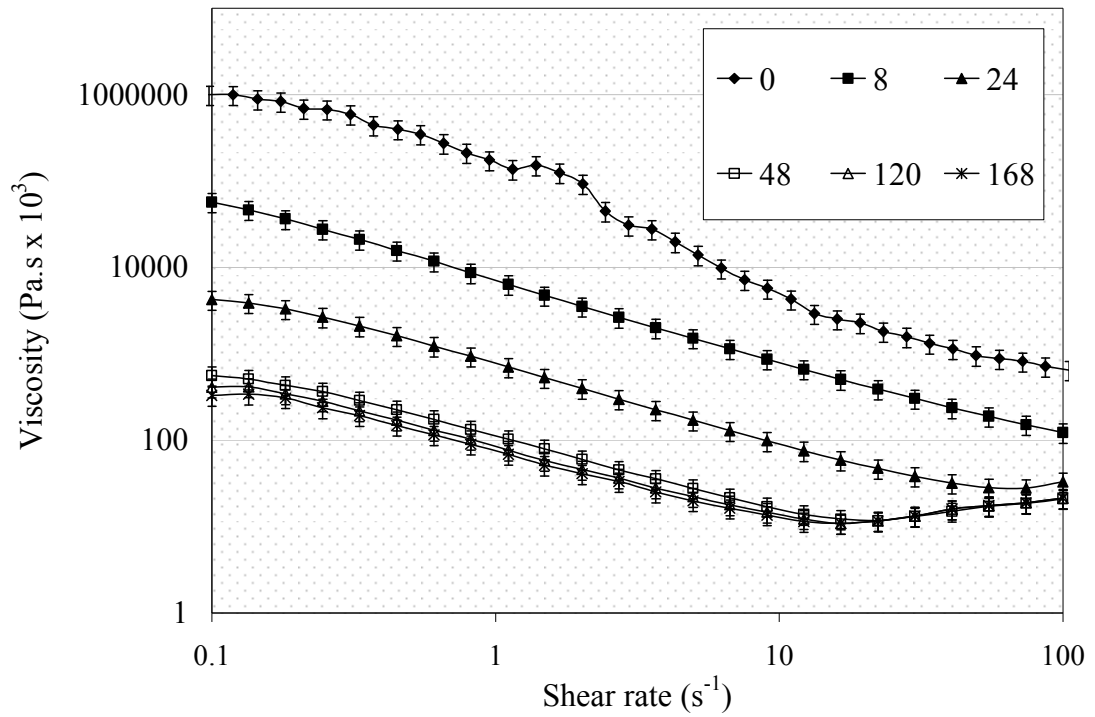


Figure B5. Viscosity changes during batch enzymatic saccharification in the SSBR for 15% initial PCS solids concentration.

Table B1

Power Law Parameters for Viscosity Data During Batch Enzymatic Saccharification of 15% Initial PCS Solids in the SSBR

Time	0	8	24	48	120	168
R²	0.9816	0.9987	0.9869	0.894	0.86	0.8427
K (Pa·sⁿ x 10³)	118.85	7.1104	0.73235	0.11433	0.09071	0.08033
n	-0.225	0.0798	0.1793	0.3966	0.4475	0.4769

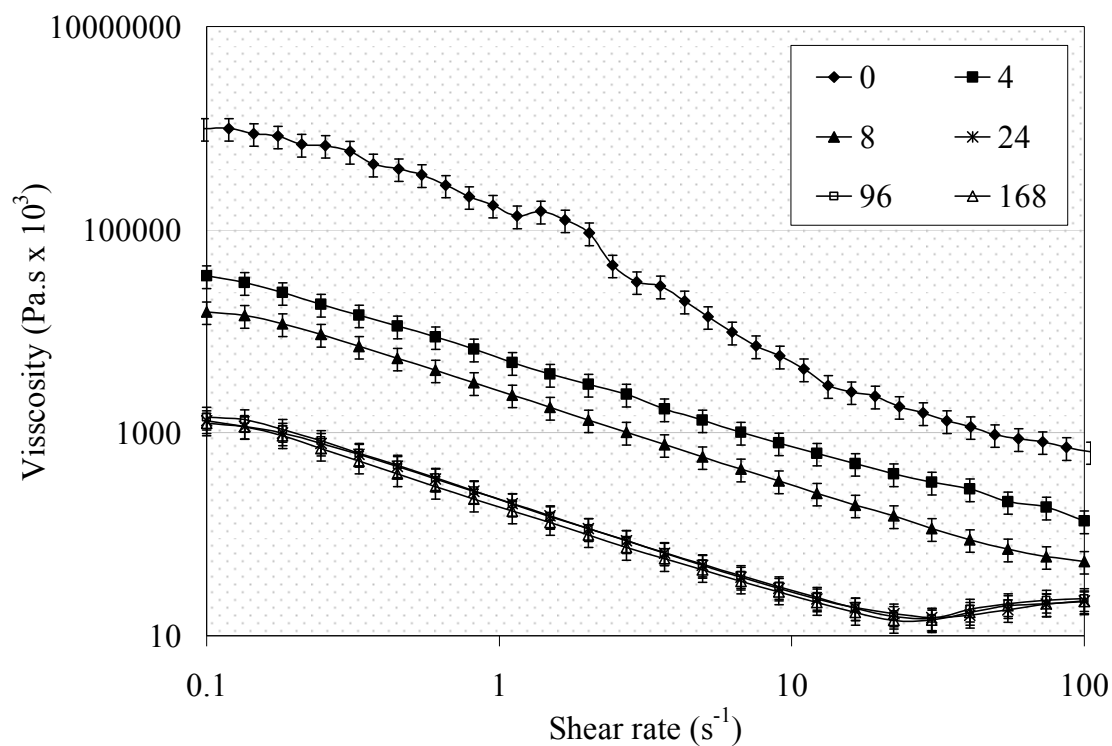


Figure B6. Viscosity changes during batch enzymatic saccharification in the shake flask for 15% initial PCS solids concentration.

Table B2

Power Law Parameters for Viscosity Data During Batch Enzymatic Saccharification of 15% Initial PCS Solids in the Shake Flask

Time	0	4	8	24	96	168
R²	0.9816	0.9981	0.9979	0.9438	0.9354	0.9309
K (Pa·sⁿ x 10³)	118.85	5.4892	2.4862	0.22249	0.23136	0.19925
n	-0.225	0.1728	0.118	0.2797	0.2787	0.2968

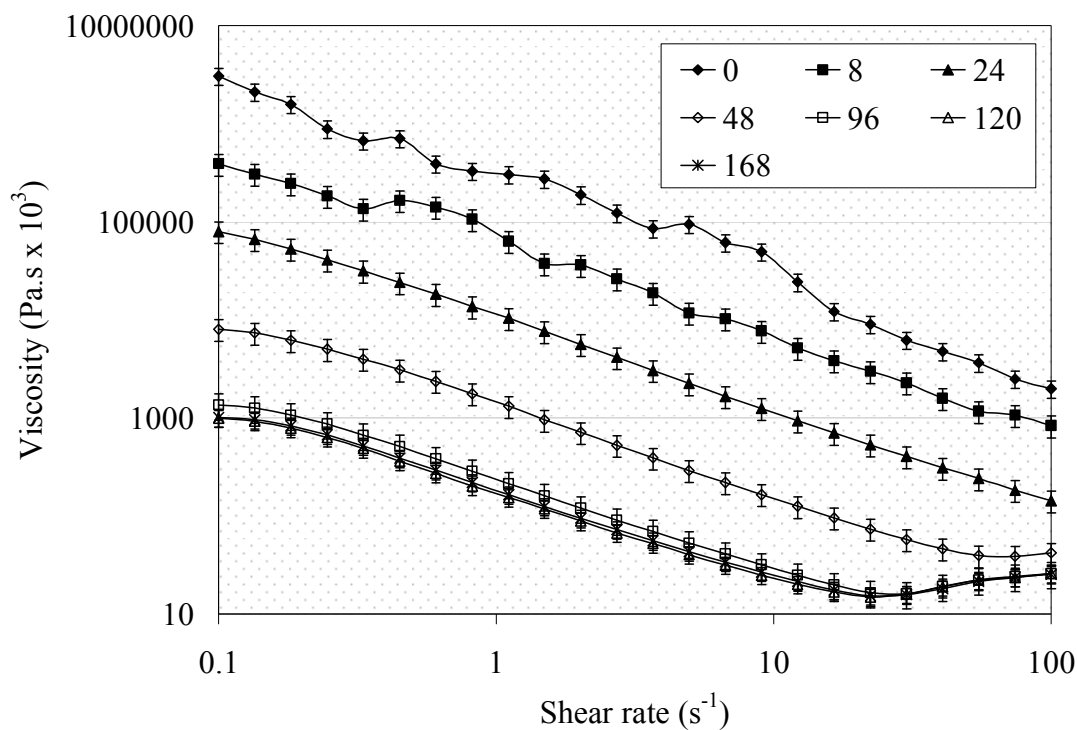


Figure B7. Viscosity changes during batch enzymatic saccharification in the SSBR for 20% initial PCS solids concentration.

Table B3

Power Law Parameters for Viscosity Data During Batch Enzymatic Saccharification of 20% Initial PCS Solids in the SSBR

Time	0	8	24	48	96	120	168
R^2	0.9848	0.9912	0.9991	0.9909	0.9326	0.9086	0.9182
K ($\text{Pa}\cdot\text{s}^n \times 10^3$)	292.293	58.73	10.572	1.3241	0.23907	0.17994	0.18983
n	-0.0506	0.0622	0.0521	0.1278	0.2902	0.3419	0.3322

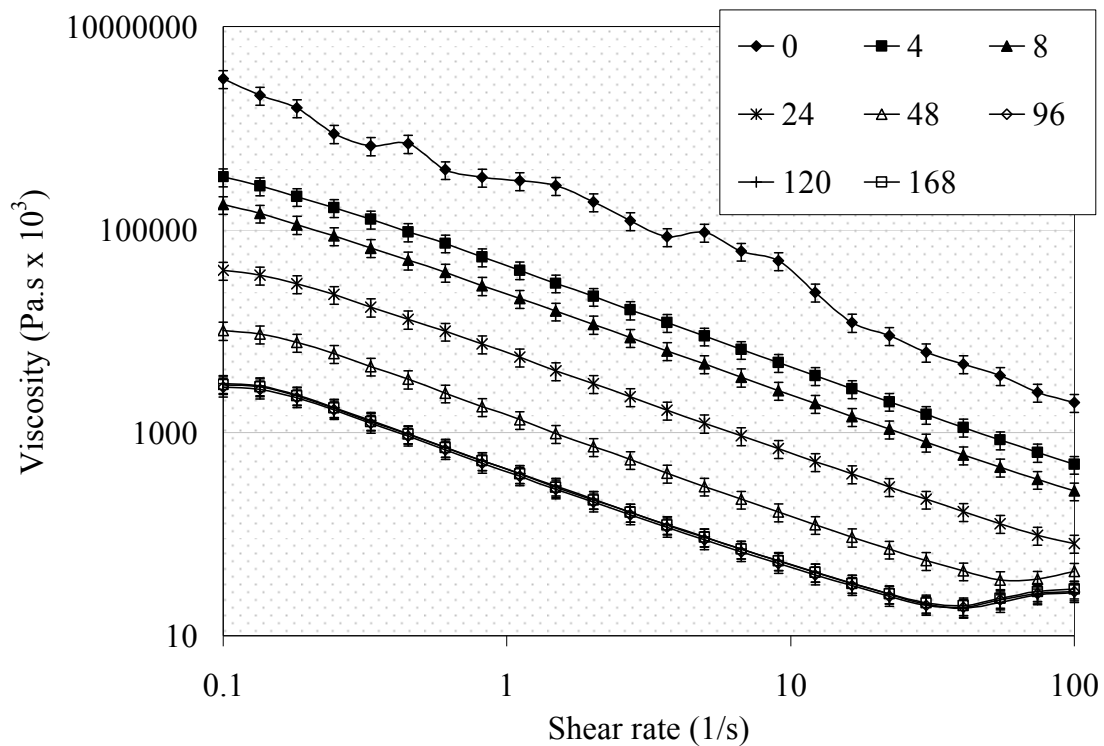


Figure B8. Viscosity changes during batch enzymatic saccharification in the shake flask for 20% initial PCS solids concentration.

Table B4

Power Law Parameters for Viscosity Data During Batch Enzymatic Saccharification of 20% Initial PCS Solids in the Shake

Flask

Time	0	4	8	24	48	96	120	168
R²	0.9848	0.9994	0.9996	0.9988	0.9903	0.9623	0.9676	0.963
K (Pa·sⁿ x 10³)	292293	41933	22174	5750.7	1444.5	425.35	449.45	445.92
n	-	0.0321	0.0359	0.0553	1.9121	0.1943	0.1819	0.1943

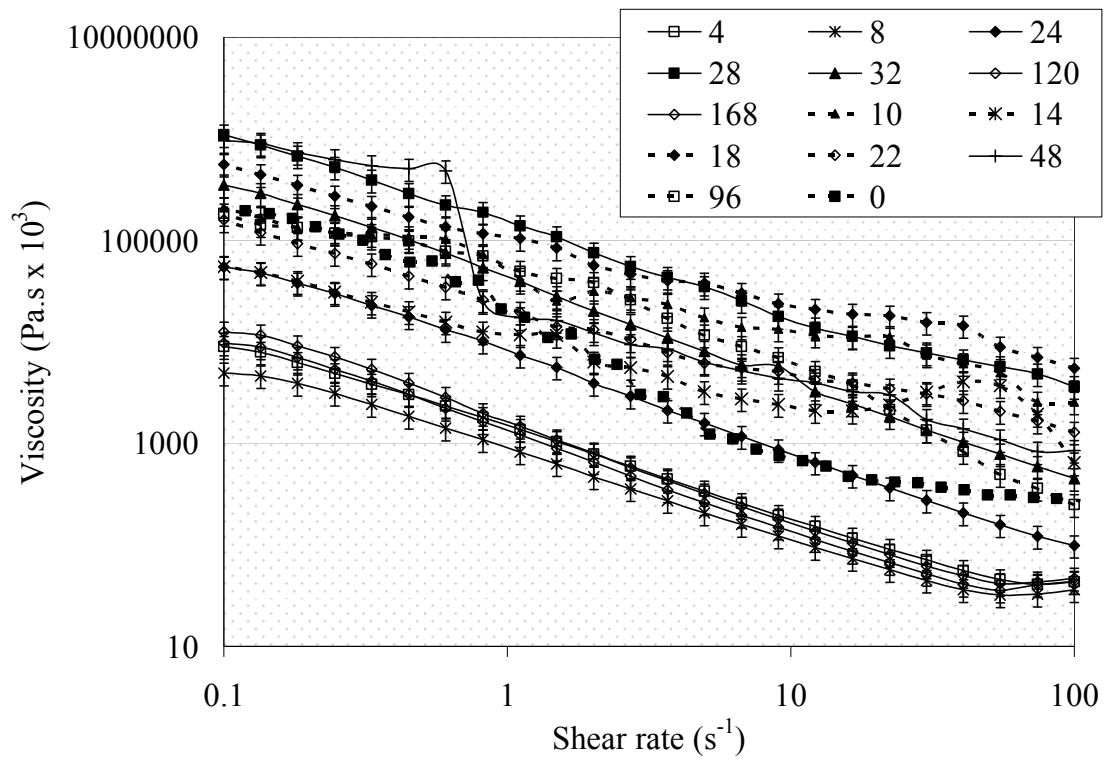


Figure B9. Viscosity changes during semi-batch enzymatic saccharification in the shake flask for 25% final equivalent PCS solids concentration.

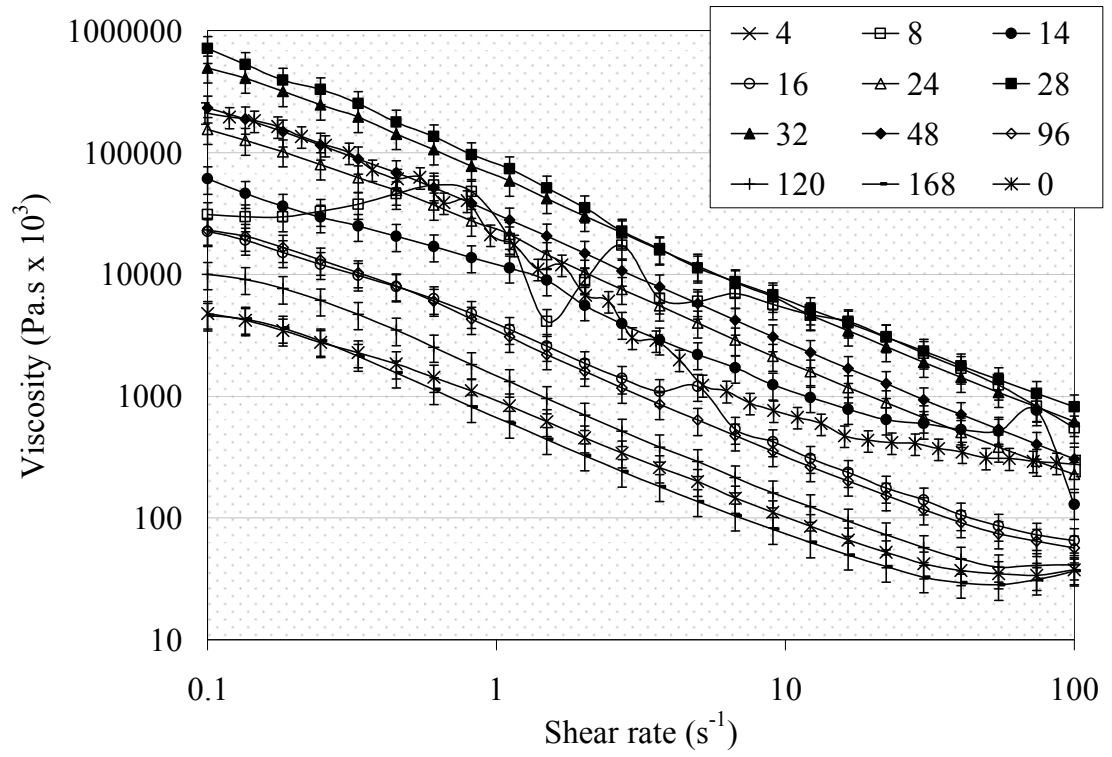


Figure B10. Viscosity changes during semi-batch enzymatic saccharification in the SSBR for 25% final equivalent PCS solids concentration.

Table B5

Power Law Parameters for Viscosity Data During Semi-Batch Enzymatic Saccharification of 25% Equivalent Final PCS

Solids in the Shake Flask

Time	0	4	8	10	14	18	22	28	32	48	120	168
R²	0.9612	0.9958	0.9898	0.9765	0.8867	0.9902	0.982	0.9949	0.9988	0.9139	0.9892	0.987
K (Pa·sⁿ x 10³)	18189	1417.6	864.63	52494	12481	108343	25065	145909	41733	68698	1649.1	1316
n	-0.129	0.1508	0.1802	0.3833	0.4695	0.3693	0.3283	0.1466	0.0058	-0.127	0.0792	0.1012

Table B6

Power Law Parameters for Viscosity Data During Semi-Batch Enzymatic Saccharification of 25% Equivalent Final PCS

Solids in the SSBR

Time	0	4	8	14	24	28	32	48	120	168
R²	0.9612	0.9859	0.8623	0.9731	0.9982	0.997	0.9992	0.999	0.9894	0.9727
K (Pa·sⁿ x 10³)	18189	824.1	16408	9695.7	19932	72299	59331	28469	1436.3	683.45
n	-0.129	0.1889	0.4006	0.1864	0.015	-0.0135	0.0002	0.0091	0.0959	0.1656

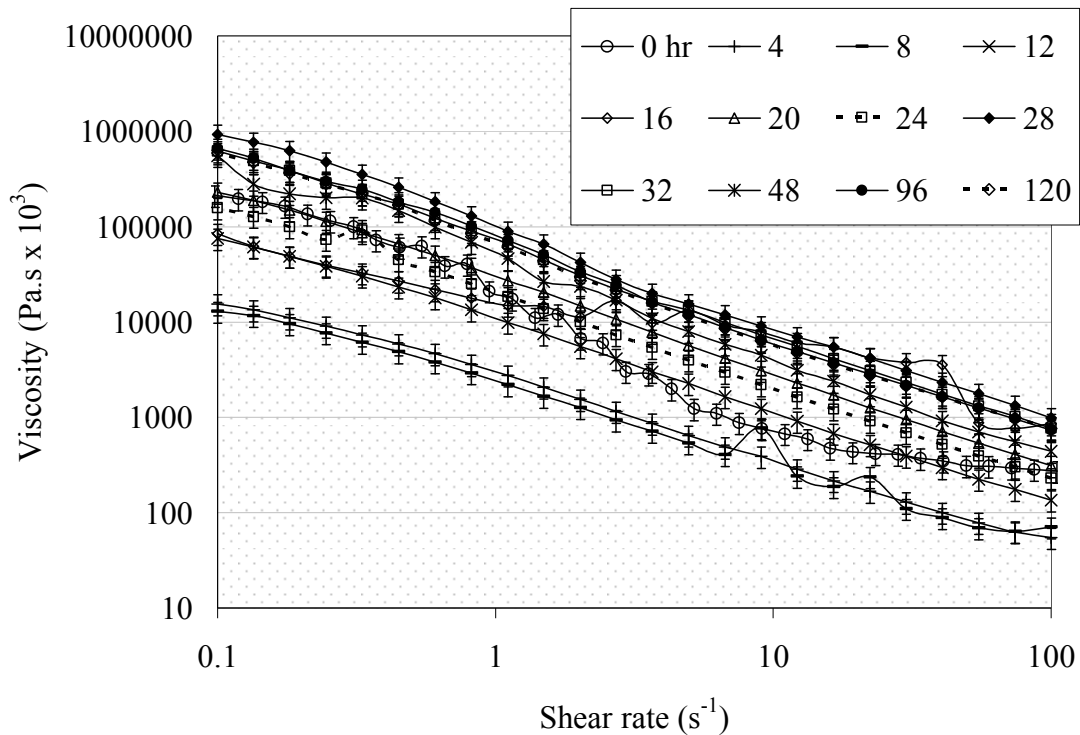


Figure B11. Viscosity changes during semi-batch enzymatic saccharification in the shake flask for 30% final equivalent PCS solids concentration.

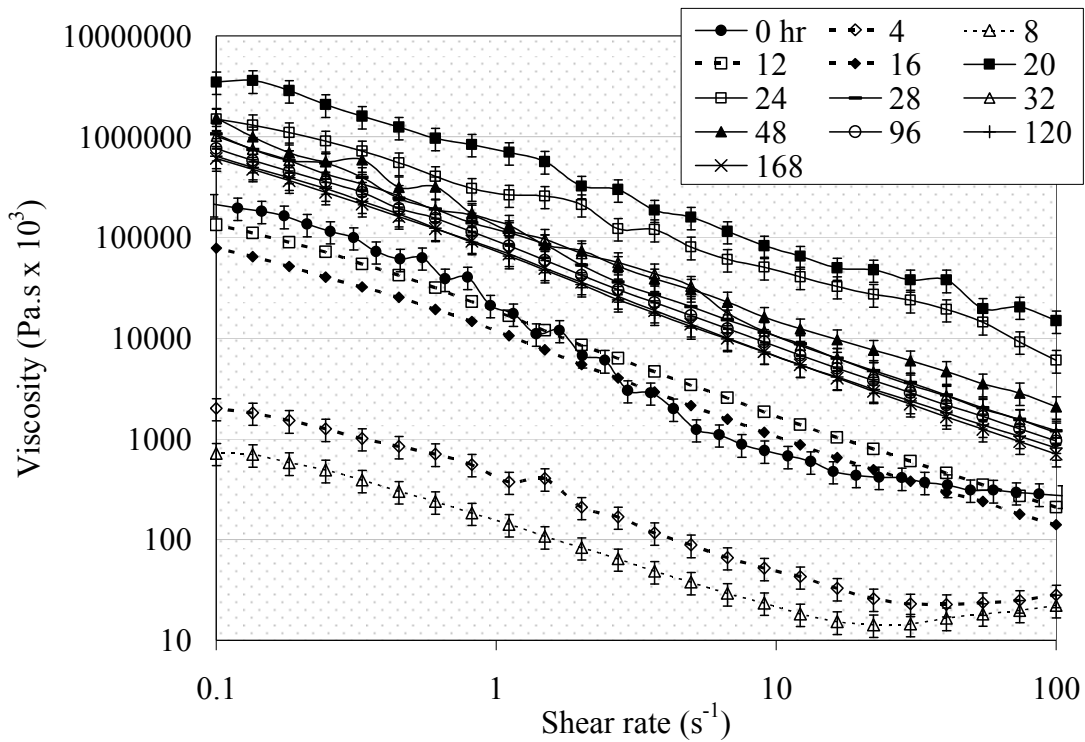


Figure B12. Viscosity changes during semi-batch enzymatic saccharification in the SSBR for 30% final equivalent PCS solids concentration.

Table B7

Power Law Parameters for Viscosity Data During Semi-Batch Enzymatic Saccharification of 30% Equivalent Final PCS Solids in the

Shake Flask

Time	0	8	12	16	20	24	28	32	48	96	168
R²	0.9612	0.9855	0.999	0.9244	0.9992	0.9972	0.9966	0.9989	0.9955	0.9976	0.9314
K (Pa·sⁿ x 10³)	18189	2308.9	10169	19880	28133	19856	97974	68430	47356	70966	55432
n	-0.129	0.1733	0.0543	0.4163	0.0131	0.0201	-0.0283	0.0058	-0.0506	-0.0236	-0.1985

Table B8

Power Law Parameters for Viscosity Data During Semi-Batch Enzymatic Saccharification of 30% Equivalent Final PCS Solids in the

SSBR

Time	0	8	12	16	20	24	28	32	48	96	168
R²	0.9612	0.923	0.9986	0.9981	0.9938	0.9947	0.9984	0.9949	0.9962	0.9993	0.9994
K (Pa·sⁿ x 10⁵)	18189	152.45	17111	10444	633296	291053	110995	118392	150324	85556	68991
n	-0.129	0.3638	0.0241	0.0422	0.1651	0.2229	-0.0055	-0.003	0.0436	0.008	-0.0012

Table B9

Power Law Parameters for Viscosity Data During Semi-Batch Enzymatic

Saccharification of 25% Equivalent Final PCS Solids in the Shake Flask with Hand-

Mixing

Time	0	8	12	24	48	72	144	168
R ²	0.9612	0.98	0.99	0.9986	0.9987	0.9912	0.981	0.979
K (Pa·s ⁿ × 10 ³)	18189	767	3878	7031	5850.1	1823.7	961.1	987
n	-0.1289	0.18	0.09	0.0351	0.0423	0.074	0.1228	0.124

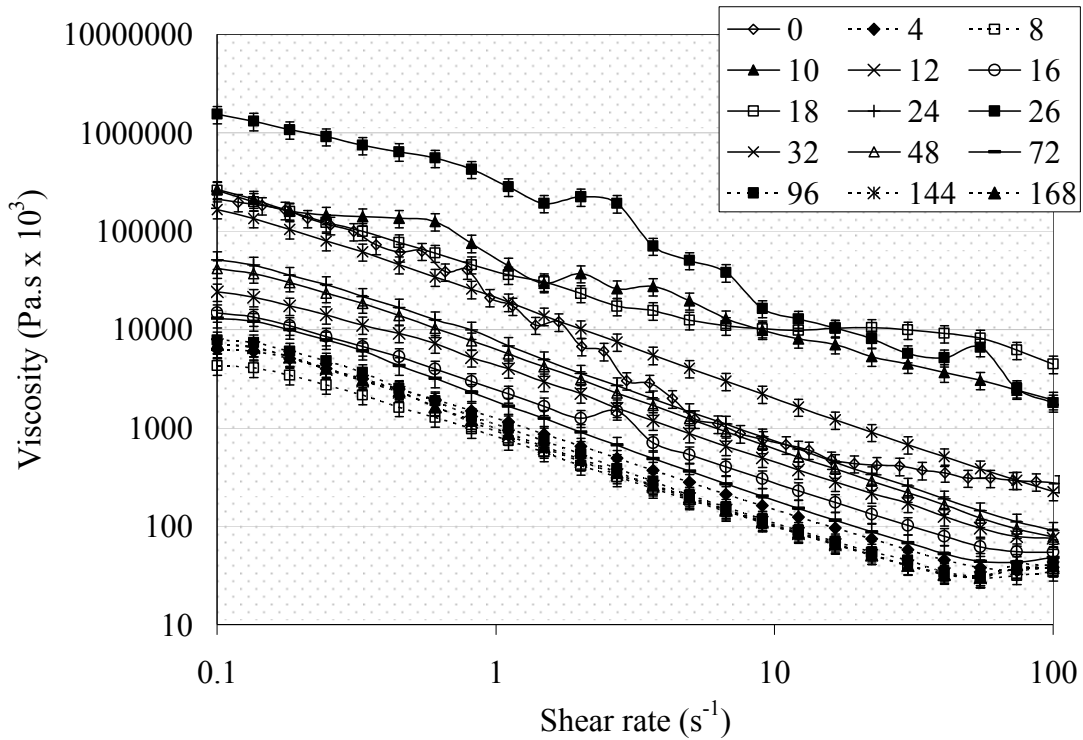


Figure B13. Viscosity changes during semi-batch enzymatic saccharification of 25% equivalent final PCS solids in the shake flask with hand-mixing.

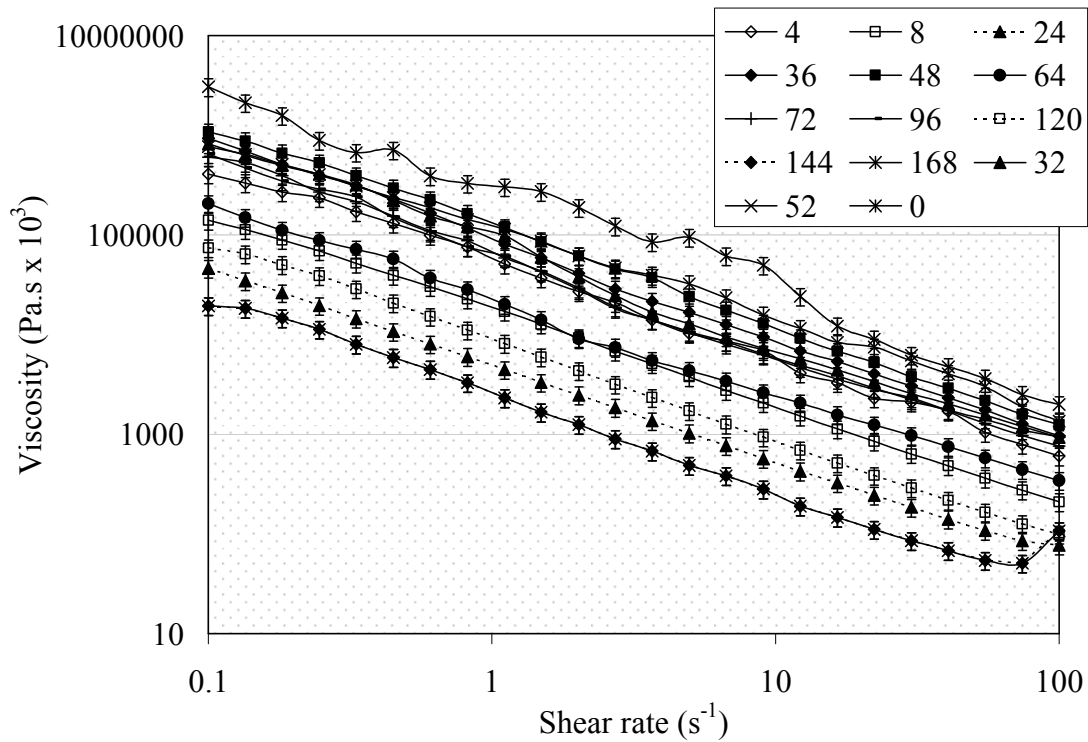


Figure B14. Viscosity changes during semi-batch enzymatic saccharification of 30% equivalent final PCS solids in the shake flask with the 2nd type of feeding.

Table B10

Power Law Parameters for Viscosity Data During Semi-Batch Enzymatic Saccharification of 30% Equivalent Final PCS Solids in the

Shake Flask with 2nd Type Feeding

Time	0	4	8	24	36	48	64	72	96	120	168
R ²	0.9848	0.997	0.9994	0.9991	0.9988	0.9992	0.9969	0.9972	0.9946	0.9992	0.9808
K (Pa·s ⁿ x 10 ³)	292293	53.88	17.588	4.9531	91.812	123.99	22.33	64.424	63.096	8.8352	2.5463
n	-0.0506	0.026	0.0345	0.0453	-0.0078	-0.0103	0.0636	0.0002	0.0158	0.0028	0.0672

Table B11

Power Law Parameters for Viscosity Data During Semi-Batch Enzymatic Saccharification of 30% Equivalent Final PCS Solids in the

SSBR with 2nd Type Feeding

Time	0	4	8	24	36	48	72	96	120	168
R ²	0.9848	0.998	0.9986	0.9979	0.9631	0.9992	0.999	0.9991	0.9993	0.9993
K (Pa·s ⁿ x 10 ³)	292293	46269	3061	5352.3	396210	36774	65306	75721	30569	12003
n	-0.0506	0.012	0.0226	0.0642	-0.0104	0.0015	-0.0157	-0.0154	-0.0038	0.0087

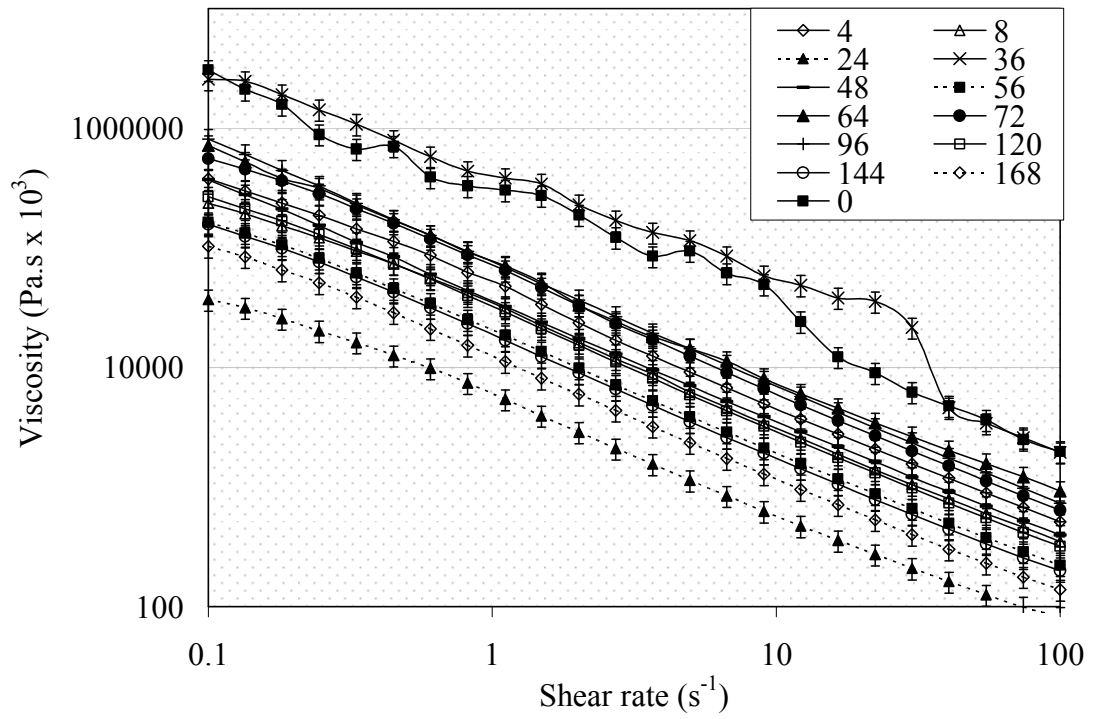


Figure B15. Viscosity changes during semi-batch enzymatic saccharification of 30% equivalent final PCS solids in the SSBR with the 2nd type of feeding.

APPENDIX – C

BATCH SCRIPT FILES FOR FLUENT SIMULATIOINS

Input File Script

```
rc /homebackup/fluentscr/Rajesh/Viscometer/USS/120/cupnvane_120.cas
rd /homebackup/fluentscr/Rajesh/Viscometer/USS/120/cupnvane_120.dat

solve 3d

5000

100

wc /homebackup/fluentscr/Rajesh/Viscometer/USS/120/cupnvane_120_final.cas
wd /homebackup/fluentscr/Rajesh/Viscometer/USS/120/cupnvane_120_final.dat

quit

exit

yes
```

Batch File Script

```
#!/bin/bash

#PBS -l nodes=1:ppn=1

#PBS -m e

#PBS -M rajesh.dasari@louisville.edu

INPUT_FILE=/homebackup/scrfluent/Rajesh/Viscometer/USS/120/inputfile_uss
```

```
OUTPUT_FILE=/homebackup/scrfluent/Rajesh/Viscometer/USS/120/outputfile  
DIM=3d  
PROG="/apps/Fluent.Inc/bin/fluent "  
PROGARGS="$DIM -g -i $INPUT_FILE"  
echo Running on:  
cat $PBS_NODEFILE  
NPROCS=`wc -l < $PBS_NODEFILE`  
echo This job uses $NPROCS processors  
hostname  
$PROG $PROGARGS > $OUTPUT_FILE 2>&1
```

APPENDIX – D
NOMENCLATURE

a	Exponent in Equation (19)
C	Amount of cellulose
D	Impeller diameter, m
D_p	Particle diameter, m
\vec{F}	External body force, N
G_t	Amount of glucose released at time 't', g/L
g	Acceleration due to gravity, 9.8 m/s^2
H	Impeller height, m
I	unit tensor
K	Flow consistency index, $\text{Pa}\cdot\text{s}^n$
K	Proportionality constant in Equation (19)
k	Dimensionless proportionality constant
K_{pq}	Exchange coefficient
L	Reactor length, m
m_q	Mass of q^{th} phase, kg
M	Torque, N.m
N	Impeller speed, rps
N_{Re}	Reynolds number

n	Flow behavior index
N_{js}	Just suspended speed, rpm
N_p	Impeller power number, dimensionless
P_0	Power number
P	Power, Watts
p	Static pressure, Pa
P_v	Specific power, Watts/m ³
R	Weight ratio of solid to liquid
R_{pq}	Interaction force between phases
S	% Initial solids concentration
S_0	Total initial solids, g/L
t	Exponent in Equation (6)
t	Time, s in Equation (8)
T	Vessel diameter, m
u_i	velocity of component 'i'
V	Volume, m ³
V_q	Volume of phase 'q', m ³
x	Direction vector
X	Fraction of cellulose in substrate
Y_t	% Glucose yield at time 't'

GREEK LETTERS

α_q	Volume fraction of the q th phase
∇	Vector differential operator
Ψ	Constant in Equation (6)
γ	Shear rate, s ⁻¹
μ	Viscosity, Pa·s
η_a	Apparent viscosity, Pa·s
ρ	Liquid density, kg/m ³
ρ_p	Particle density, kg/m ³
$\rho \vec{g}$	Gravitational force
$\hat{\rho}_q$	Effective density of phase 'q'
τ	Shear stress, Pa
$\overline{(\tau)}$	Stress tensor

CURRICULUM VITAE

NAME:

RAJESH K. DASARI

ADDRESS:

J. B. Speed School of Engineering
Chemical Engineering Department
University of Louisville
Louisville KY 40292

DOB:

Tadpatri, India – June 8, 1983

EDUCATION:

B. Tech., Chemical Engineering
Osmania University, Hyderabad, India
2000-04

Ph.D., Chemical Engineering
University of Louisville, Louisville, KY
2004-08

AWARDS

- First position in Engineers Expo, a graduate level poster event, University of Louisville, February-2006
Poster Title: The effect of biomass particle size on hydrolysis reaction rates and rheological properties.
- First prize (Group Term Project), Six Sigma, University of Louisville, December-2005

AFFILIATIONS

- American Institute of Chemical Engineers (AIChE)

PRINCIPAL PUBLICATIONS

- Dasari R. K. and Berson R. E., The ethanol buzz, *Sustain*, 15, 15-21.
- Dasari R. K. and Berson R. E., The effect of particle size on hydrolysis reaction rates and rheological properties in cellulosic slurries, accepted for publication in *Appl. Biochem. & Biotech*, 137-140, 289-299.
- Berson, R. E., Dasari R. K. and Hanley, T. R., Modeling of a continuous pretreatment reactor using Computational Fluid Dynamics, *Appl. Biochem. & Biotech*, 130(1-3), 621-630.
- Murthy, J.S.N., Dasari R. K. and Mattapelli, S., Polymer Design Catalysts – A Comprehensive Picture, *Indian Chem. Engr.*, Section B, 47(3), 168-182.

CONFERENCE PRESENTATIONS

- “Power consumption in a scraped surface bio-reactor for batch and fed-batch enzymatic hydrolysis of pretreated corn stover slurries” presented at the 29th Symposium on Biotechnology for Fuels and Chemicals, Denver, CO, U.S.A., May-2007.
- ‘The effect of particle size on hydrolysis reaction rates and rheological properties in cellulosic slurries’, poster presented at the 28th *Symposium on Biotechnology for Fuels and Chemicals*, Nashville, TN, U.S.A., May-2006.
- ‘Modeling of a continuous pretreatment reactor using Computational Fluid Dynamics’, poster presented at the 27th *Symposium on Biotechnology for Fuels and Chemicals*, Denver, CO, U.S.A., May-2005.
- ‘Optimization of medium for the selective bioleaching of Nickel using *Thiobacillus Ferrooxidans*’ presented at the International level *Indian Chemical Engineering Congress*, Bhubaneswar, OR, India, December-2003.